
GAZİ ÜNİVERSİTESİ
Gazi
1926

DESIGN, SYNTHESIS, AND INVESTIGATION OF PHOTOPHYSICAL AND THERMAL PROPERTIES OF NEW PUSH-PULL DYES FOR SECOND-ORDER NONLINEAR OPTICAL AND CHEMOSENSOR APPLICATIONS

A THESIS SUBMITTED TO
THE GRADUATE SCHOOL OF NATURAL AND APPLIED SCIENCES
OF
GAZİ UNIVERSITY

BY
Mohamed YAHYA

IN PARTIAL FULFILLMENT OF THE REQUIREMENTS
FOR
THE DEGREE OF DOCTOR OF PHILOSOPHY
IN
CHEMISTRY

JANUARY 2022

ETHICAL STATEMENT

I hereby declare that in this thesis study I prepared in accordance with thesis writing rules of Gazi University Graduate School of Natural and Applied Sciences;

- All data, information and documents presented in this thesis have been obtained within the scope of academic rules and ethical conduct,
- All information, documents, assessments and results have been presented in accordance with scientific ethical conduct and moral rules,
- All material used in this thesis that are not original to this work have been fully cited and referenced,
- No change has been made in the data used,
- The work presented in this thesis is original,

or else, I admit all loss of rights to be incurred against me.

Mohamed YAHYA

27/01/2022

İKİNCİ DERECEDEN DOĞRUSAL OLMAYAN OPTİK VE KEMOSENSÖR UYGULAMALARI İÇİN YENİ İTME-ÇEKME BOYAR MADDELERİN FOTOFİZİKSEL VE TERMAL ÖZELLİKLERİNİN TASARIMI, SENTEZİ VE ARAŞTIRILMASI

(Doktora Tezi)

Mohamed YAHYA

GAZİ ÜNİVERSİTESİ

FEN BİLİMLERİ ENSTİTÜSÜ

Ocak 2022

ÖZET

Bu araştırmada, üç seri D-π-A kromoforunun sentezi yapılmıştır. Kromoforların sentezinde kullanılacak, Diaril-1,3-bütadien, 1-disiyanometilen-2-aril-indon ve 3-amino-2,4-disiyano-1-aril-9H-floren bileşikleri başlangıç bileşiklerinden başarıyla sentezlenmiştir. 1. Seri bileşikleride, elektron veren bir grup olarak alkilamino grubunun 1,1-dicyano-2,4-diaril-1,3-bütadien temelli bileşiklerin fotofiziksel özelliklerine olan etkisi ayrıntılı olarak incelenmiştir. 2. Seri bileşiklerde ise, 1-disiyanometilen-2-aril-indon temelli bileşiklerin spesifik anyonları tespit etmek için kemosensör adayı olup olmadıkları araştırılmış ve bileşiklerin fotofiziksel özellikleri üzerine sübstitüentlerin etkisi incelenmiştir. 3.seride, aril 3-amino-2,4-disyano-1-aril-9H-floren ve 1-disiyanometilen-2-aril-indon türevlerini içeren bileşikler tek kap, çok aşamalı, ve mikrodalga ışıması (MDI) gibi sentez yöntemleri kullanılarak sentezlenmiş ve bu bileşikler için en uygun yöntem ortaya koyulmuştur. Elde edilen tüm bileşiklerin karakterizasyonları için FT-IR, ^{1}H NMR, ^{13}C NMR ve HRMS ve X-ışını kristalografisi gibi spektroskopik yöntemler kullanılmıştır. Sentezlenen kromoforların fotofiziksel özelliklerini araştırmak için UV-GB ve floresan spektroskopisi yöntemleri kullanılmıştır. 1. ve 2. seri bileşiklerin ikinci dereceden doğrusal olmayan optik özellikleri elektrik alanı kaynaklı ikinci harmonik üretim (EFISH) yöntemi kullanılarak tespit edilmiştir.

Bilim Kodu	: 20114
Anahtar Kelimeler	: Allilidenemalononitril, Floren türevleri, itme-çekme kromoforları, Kemosensör, Anyon tespiti, UV-vis, Floresan.
Sayfa No	: 144
Danışman	: Prof. Dr. Zeynel SEFEROĞLU

DESIGN, SYNTHESIS, AND INVESTIGATION OF PHOTOPHYSICAL AND THERMAL PROPERTIES OF NEW PUSH-PULL DYES FOR SECOND-ORDER NONLINEAR OPTICAL AND CHEMOSENSOR APPLICATIONS

(Ph.D. Thesis)

Mohamed YAHYA

GAZİ UNIVERSITY

GRADUATE SCHOOL OF NATURAL AND APPLIED SCIENCES

January 2022

ABSTRACT

In this research, the synthesis of three series of D-π-A chromophores based on 1,1-dicyano-2,4-diaryl-1,3-butadiene, 1-dicyanomethylene-2-aryl-indone, and 3-amino-2,4-dicyano-1-aryl-9*H*-fluorene was successfully obtained. The influence of the alkylamino group as an electron-donating group on the photophysical properties of the series based on 1,1-dicyano-2,4- diaryl -1,3-butadiene was studied. The compounds based on 1-dicyanomethylene-2-aryl-indone were used as chemosensors to detect specific anions. The influence of group substitution was also investigated. The compounds containing various aryl 3-amino-2,4-dicyano-1-aryl-9*H*-fluorene and 1-dicyanomethylene-2-aryl-indone derivatives were synthesized via various routes and synthesis methods: one-pot, multi-step, and microwave irradiation (MWI). Furthermore (*E*)-2-(2-(anthracen-9-ylmethylene)-2,3-dihydro-1*H*-inden-1-ylidene) malononitrile (2b) compound, was obtained a crystal structure. Spectroscopic methods such as FT-IR, ^{1}H NMR, ^{13}C NMR, and HRMS, as well as X-ray analysis, were used to characterize all the obtained compounds. The UV-vis and fluorescence spectroscopic methods were used to investigate the photophysical properties of the synthesized chromophores. Finally, the electric field-induced second harmonic generation (EFISH) method evaluated the second-order nonlinear optical properties.

Science Code : 20114
Key Words : Allylidenemalononitrile, Fluorene derivatives, push-pull chromophores, Chemosensor, Anions detection, UV-vis, Fluorescence.

Page Number : 144
Supervisor : Prof. Dr. Zeynel SEFEROĞLU

ACKNOWLEDGMENT

This dissertation would not have been possible without the help and guidance of numerous persons who, in one way or another, contributed to making this dream a reality. First and foremost, I would like to express my deepest gratitude and appreciation to Prof. Dr. Zeynel SEFEROĞLU for his guidance, precious advice, moral support, and enlightening my academic vision during my Ph.D. thesis. There is no question that Prof. Dr. Zeynel SEFEROĞLU is one of the most influential people in my life. I most appreciate the exciting and challenging environment he presented to follow my own research ideas. Thank you very much. I learned a lot from you.

I would like to thank the Turkish Government Scholarship (YTB) for providing me with a scholarship to pursue a Ph.D. program at Gazi University. My thanks also go to the Ministry of National Education, Vocational Training, Higher Education and Scientific Research Kingdom of Morocco for offering me the "Scholarships for Study Abroad."

I would like to express my appreciation to my thesis examination committee members Prof. Dr. Barış TEMELLİ and Prof. Dr. Ebru AKTAN. My thanks go to the members of the jury.

The work presented in this Ph.D. thesis is the fruit of genuine collaboration. I am thankful to Dr. Alberto BARSELLA from Strasbourg University for his experimental work relating to EFISH measurements and Assoc. Prof. Dr. Sylvain ACHELLE from Rennes University, for his contribution to this work.

Many thanks to all the professors who were a part of my education. I will always be grateful for all the knowledge you gave me during my years of studies. My thanks also go to all the members of the Synthesis Group of Target Organic Molecules (SYNGTOM).

I would like to thank Dr. Asmae BOUZIANI from Middle East Technical University for her help and collaboration.

None of this would happen without the support of my family. First and foremost, my mother Fatima and Father Abdessalam, for their moral support and prayers. I am here today because of your faith in me. To my sister: Bahia, thank you for always being there for me, and finally, my little brother Ismail for his support.

TABLE OF CONTENTS

Page

ÖZET IV

ABSTRACT V

ACKNOWLEDGMENT VI

TABLE OF CONTENTS VII

LIST OF TABLES X

LIST OF FIGURES XI

LIST OF ABBREVIATIONS XV

1. GENERAL INTRODUCTION 1

2. BIBLIOGRAPHICAL REVIEW 5

2.1. Photophysical Background 5

2.1.1. Luminescence 5

2.1.2. Solvatochromism 10

2.2. Optical Chemosensors 10

2.2.1. Colorimetric chemosensors 10

2.2.2. Fluorometric chemosensors 11

2.2.3. Applications of fluorescent chemosensors 16

2.3. Second-Order Nonlinear Optical Chromophores 17

2.3.1. Overview of nonlinear optical materials 17

2.3.2. Push-pull chromophores 18

2.3.3. Second order NLO response measurements 19

2.3.4. Application of NLO materials 20

2.4. Organic Molecules Containing Fluorene Derivatives 21

2.4.1. Fluorene hybrid chromophore 21

2.4.2. Aggregation-caused quenching 22

2.4.3. Aggregation-induced emission 23

2.4.4. Application of fluorene and its derivatives 24

3. MATERIALS AND METHODS 25

Page

3.1. Chemicals 25
3.2. Instrumentation 25
3.3. Synthesis of Compounds 27
3.3.1. Synthetic procedures of π–conjugated push-pull chromophores 27
3.3.2. Synthesis of 1-dicyanomethylene-2-aryl-indone derivatives 31
3.3.3. Synthetic procedures of inden-1-ylidene and fluorene 34

4. RESULTS AND DISCUSSION 39

4.1. Push-Pull Chromophores Type π–Conjugated 39
4.1.1. Introduction 39
4.1.2. Synthesis and characterization 39
4.1.3. Photophysical properties 42
4.1.4. Second order NLO properties 48
4.1.5. Thermal stability 48
4.2. 1-Dicyanomethylene-2-aryl-indone Derivatives For Chemosensing 49
4.2.1. Introduction 49
4.2.2. Synthesis and photophysical properties of the chemosensors 6a-f 50
4.2.3. Anions-chemosensing interaction study in organic medium 56
4.2.4. Anion interaction in partial aqueous medium for selectivity 60
4.2.5. Tap water experiment 62
4.2.6. Sensing mechanism 65
4.2.7. Reversibility properties in aqueous medium DMSO/H_2O 67
4.2.8. pH-dependent study 73
4.2.9. Limit of detection and limit of quantification for cyanide ion in partial aqueous medium 78
4.2.10. Sensitivity study of organic amines 79
4.2.11. Thermal stability 82
4.3. Inden-1-ylidene and Fluorene 83
4.3.1. Introduction 83
4.3.2. Synthesis and characterization 84
4.3.3. Photophysical properties 86
4.3.4. Thermo-gravimetric analysis (TGA) 92

Page

5. CONCLUSION 95

REFERENCE 97

ANNEXES 107

ANNEX-1. FT-IR, 1H-NMR, 13C-NMR, and HR-MS spectra of compound 3a-d 108

ANNEX-2. FT-IR, ^{1}H-NMR, ^{13}C-NMR, and HR-MS spectra of compound 6a-f 115

ANNEX-3. FT-IR, ^{1}H-NMR, ^{13}C-NMR, and HR-MS spectra of compounds 7a-c and 8a-c 128

ANNEX-4. Calibration curve of [CN^-] for 6a-f 142

CURRICULUM VITAE 143

LIST OF TABLES

Table **Page**

Table 2.1. WHO and EU drinking water standards for anions..... 17
Table 4.1. UV-Vis absorption and photoluminescence (PL) data of compounds 3a-d in $CHCl_3$ solution..... 42
Table 4.2. Emission solvatochromism of compounds 3a-d in various aprotic solvents. . 44
Table 4.3. Results for EFISH measurements for compounds 3a-d..... 48
Table 4.4. Photophysical properties of 6a-f..... 55
Table 4.5. Changes in chemical shifts as a result of the interaction of 6d with CN^- and F^-..... 67
Table 4.6. Values of LOD and LOQ of the chemosensors 6a-f 79
Table 4.7. Yields of compounds according to the methods used..... 85
Table 4.8. UV-Vis and photoluminescence (PL) data of compounds 7 and 8 in DCM.. 87
Table 4.9. Emission solvatochromism of compounds 8 in various solvents..... 88
Table 4.10. Thermal decomposition values of compounds 7a-c and 8a-c. 93

LIST OF FIGURES

Figure **Page**

Figure 1.1. Synthesis route and Structures of synthesized compounds within the scope of this study. 3
Figure 2.1. Range of electromagnetic radiation in optical studies and photochemistry ... 6
Figure 2.2. Light-induced phenomena 6
Figure 2.3. Illustration of Beer-Lambert law..... 7
Figure 2.4. The Jablonski diagram(Lakowicz, 2006) 8
Figure 2.5. Steady-state measurement..... 9
Figure 2.6. Fluorescence sensing (a) A spaced model (b) An integrated model. 12
Figure 2.7. Molecular orbital diagram of the photo-induced electron transfer process .. 13
Figure 2.8. Schematic representation of PET chemosensor in the sensing process 13
Figure 2.9. Schematic representation of ICT chemosensor in the sensing process 14
Figure 2.10. Schematic representation of excited-state intramolecular proton transfer.. 15
Figure 2.11. Schematic representation of FRET chemosensor in the sensing process. ... 16
Figure 2.12. Schematic presentation of second-harmonic generation 18
Figure 2.13. Schematic representation of a push-pull molecule composed of the model (D-π-A) with examples for each component. 19
Figure 2.14. Different applications of NLO. 20
Figure 2.15. The structure of Fluorene..... 21
Figure 2.16. ACQ and AIE effect enhanced fluorescence with water ratio increase 24
Figure 4.1. Synthesis of 1,1-dicyano-2,4-diaryl-1,3-butadiene derivatives (3a-d).(i) malononitrile, NH_4OAc/AcOH, MWI (ii) Ar-CHO, ethanol, piperidine..... 40
Figure 4.2. The plausible mechanism for the synthesis of 1,1-dicyano-2-aryl-propene.. 41
Figure 4.3. Normalized absorption (solid lines) and emission (dashed lines) spectra of compounds 3a-d in chloroform solution. 43
Figure 4.4. $CHCl_3$ solution of 3a-d (from left to right) under white light (part a) and under UV lamp irradiation (part b) (c = 3-6 10^{-4} M) 43
Figure 4.5. Normalized emission spectra of 3a in different aprotic solvents 45
Figure 4.6. Solution of 3b (from left to right: toluene, 1,4-dioxane, $CHCl_3$, DCM and MeCN under white light (part a) and under UV lamp irradiation (part b) (c = 1.9 10^{-5} M)..... 45

Figure **Page**

Figure 4.7. Compound 3b emission spectra in different aprotic solvents (c = 5.10^{-6} M). 46
Figure 4.8. Compound 3c emission spectra in different aprotic solvents (c = 5.10^{-6} M). 46
Figure 4.9. Emission spectra of compound 3d in various aprotic solvents (c = 5.10^{-6}M) 47
Figure 4.10. Normalized solid-state (powder) spectra of compounds 3a-d. 47
Figure 4.11. Emission of compounds **3a** and **3c** in solid-state (powder). The photograph was taken in the dark upon irradiation with a hand-held UV lamp (λ_{em} = 366 nm)..... 48
Figure 4.12. TGA curves of chromophores 3a-d under nitrogen gas in the temperature range of 25-600°C at a heating rate of 10 °C min^{-1}. 49
Figure 4.13. Synthesis routes of the chemosensors 6a-f (i) cyclohexane/piperidine..... 51
Figure 4.14. The possible Mechanism for the Synthesized of 1-dicyanomethylene-2-aryl-indone..... 52
Figure 4.15. The normalized absorption spectra of 6a-f (30 μM) in various solvents..... 53
Figure 4.16. The normalized emission spectra of 6d (30 μM) in various solvents..... 54
Figure 4.17. a) Absorption spectra (10 μM);(b) Emission spectra (25 μM) of compounds 6a in DMSO after adding 20 equiv. of the anions. Insets: Photographs of Color (ambient light) and fluorescence change after adding 20 equiv. of anions..... 56
Figure 4.18. a) Absorption spectra (10 μM);(b) Emission spectra (25 μM) of compounds 6b-f in DMSO after adding 20 equiv.of the anions. Insets: Photographs of Color (ambient light) and fluorescence change after adding 20 equiv. of anions..... 57
Figure 4.19. Chemosensor 6a-f (10 μM) UV-vis titration spectra with CN^- anion 0-20 equiv. in DMSO..... 59
Figure 4.20. a) Absorption spectra (10 μM); (b) Emission spectra (20 μM) of compounds 6a in (DMSO/ H_2O, 1/1:v/v) after addition of 20 equiv. of the anions..... 60
Figure 4.21. a) Absorption spectra (10 μM);(b) Emission spectra (20 μM) of compounds 6b-f in (DMSO/ H_2O, 1/1:v/v) after addition of 20 equiv. of the anions.. 61
Figure 4.22. a) Absorption spectra (10 μM);(b) Emission spectra (20 μM) of compounds 6a in (DMSO/ tap water, 1/1:v/v) after addition of 20 equiv. of anions .. 63
Figure 4.23. a) Absorption spectra (10 μM);(b) Emission spectra (20 μM) of compounds 6b-f in (DMSO/ tap water, 1/1:v/v) after addition of 20 equiv. of anions . 63

Figure **Page**

Figure 4.24. The plausible sensing mechanisms..... 65
Figure 4.25. ^{1}H NMR spectral changes of 6d (10 mM) in the absence (a) and presence of 0.5 equiv. (b) and 1 equiv. (c) of TBACN in DMSO-d_6..... 66
Figure 4.26. ^{1}H NMR spectral changes of 6d (10 mM) in the absence (a) and presence of 0.5 equiv. (b) and 1 equiv. (c) of TBAF in DMSO-d_6 67
Figure 4.27. Deprotonation and reverse protonation process. 68
Figure 4.28. Absorption (a) (c) and emission spectra (b) (d) of 6a in the absence of CN^- and OH^- upon addition of TFA (1 M) into the (DMSO/H_2O, 1/1:v/v) Insert: photographs of 6a upon the addition of CN^-, OH^- and TFA under ambient light (a) (c) and UV light (b) (d)..... 69
Figure 4.29. Absorption and emission spectra (10 μM) of 6b-c in the absence of CN^- and OH^- upon addition of TFA (1M) into the (DMSO/H_2O, 1/1:v/v) Insert: Photographs of 6b-f upon the addition of CN^-, OH^- and TFA under ambient light. 70
Figure 4.30. Absorption spectra (a) and (b), Emission spectra (c) and (d) of 6a (10 μM) in DMSO/PBS buffer in the absence and presence of CN^- at different pH. Insert: photographs of 6a in different pH values under ambient light (a) and UV light (b). After addition of 20 equiv CN^- anion ambient light (c), UV light (365nm) (d)..... 74
Figure 4.31. Absorption spectra (a) and (b), Emission spectra (c) and (d) of 6b-f (10 μM) in DMSO/PBS buffer in the absence and presence of CN^- at different pH. Insert: Photographs of 6b-f in different pH values under ambient light (a) and UV light (b). After addition of 20 equiv CN^- ambient light (c) , UV light (365nm) (d)..... 75
Figure 4.32. a) Absorption spectra (10 μM);(b) Emission spectra (20 μM) of compounds 6a in DMSO after addition of 20 equiv. of different organic bases in DMSO. Insert: photographs of 6a under ambient light (a) and UV light (b).After the addition of 20 equiv. of different organic bases. 80
Figure 4.33. a) Absorption spectra (10 μM);(b) Emission spectra (20 μM) of compounds 6b-f in DMSO after addition of 20 equiv. of different organic bases in DMSO. Insert: photographs of 6b-f under ambient light (a) and UV light (b). After the addition of 20 equiv. of different organic bases 80

Figure **Page**

Figure 4.34. TGA curves of 6a-f under nitrogen gas in the temperature range of 50-600°C at a heating rate of 10°C min^{-1} 83
Figure 4.35. Synthetic routes for compounds 7a-c and 8a-c 85
Figure 4.36. Plausible Mechanism for 3-amino-2,4-dicyano-1-aryl-9*H*-fluorene..... 86
Figure 4.37. Normalized absorption (dashed lines) and emission (solid lines) spectra of compounds 8a-c in DCM. Insert: photographs of DCM solution taken in the dark upon irradiation with hand-held UV lamp (λ_{em} = 366 nm)..... 87
Figure 4.38. Absorption spectra of compounds 7a-c in DCM..... 88
Figure 4.39. Normalized emission spectra of compound 8a in various solvent 89
Figure 4.40. Normalized emission spectra of compound 8b in various solvent..... 89
Figure 4.41. Normalized emission spectra of compound 8c in various solvent 90
Figure 4.42. Emission spectra of compound 8a in THF/water mixture (c = 1.5 10^{-5} M, λ_{ext} = 379 nm) Insert: photographs of solution with 100:0 10:90 3:97 THF/water ratio taken in the dark upon irradiation with hand-held UV lamp (λ_{em} = 366 nm)..... 91
Figure 4.43. Emission spectra of compound 8b in THF/water mixture (c = 1.5 10^{-5} M, λ_{ext} = 360 nm) Insert: photographs of solution with 100:0 50:50 10:90 THF/water ratio taken in the dark upon irradiation with hand-held UV lamp (λ_{em} = 366 nm) 91
Figure 4.44. Emission spectra of Compound 8c in THF/water mixture (c = 1.5 10^{-5} M, λ_{ext} = 360 nm) Insert: photographs of solution with 100:0, 50:50, 10:90 THF/water ratio taken in the dark upon irradiation with hand-held UV lamp (λ_{em} = 366 nm)..... 92
Figure 4.45. TGA curves of chromophores 7a-c and 8a-c under nitrogen atmosphere in the temperature range of 40-700°C at a heating rate of 10°C min^{-1} 93

LIST OF ABBREVIATIONS

The abbreviation used in this thesis are presented below with explanations.

Abbreviation	Explanations
A	Absorbance
λ_{abs}	Maximum absorption wavelength
λem	Maximum fluorescence wavelength
MeCN	Acetonitrile
AcOH	Acetic acid
AIE	Aggregation-induced emission
ACQ	Aggregation-caused quenching
J	Coupling constants
$CDCl_3$	Deutero Chloroform
$CHCl_3$	Chloroform
C, mol/L	Concentration
D-π-A	Donor-π-acceptor
DEA	Diethylamine
DPA	Diphenylamine
ETOH	Ethanol
DCM	Dichloromethane
DMSO-d_6	Dimethyl sulfoxide- d_6
EFISH	Electric Field Induced Second- Harmonic Generation
ESIPT	Excited-state intramolecular proton transfer
X-Ray	X-radiation
EI	Electron ionization
λ_{em}	Emission maximum
EL	Electroluminescence
FRET	Fluorescence Resonance Energy Transfer

Abbreviation	Explanations
HCl	Hydrochloric Acid
HRMS	High-Resolution Mass Spectrometry
h	Hour
Hz	Hertz
HOMO	Highest occupied molecular orbital
ICT	Intramolecular charge transfer
IR	Infrared
LUMO	Highest unoccupied molecular orbital
LOD	The limit of detection
LOQ	The limit of quantification
mL	Milliliter
m.p	Melting point
MeOH	Methanol
MWI	Microwave Irradiation
M	Molarity/ Molar concentration
NMR	Nuclear Magnetic Resonance
NLO	Nonlinear Optical
NIR	Near-infrared
nm	Nanometer
OLED	Organic Light-Emitting Devices
OS	Oscillator forces
PL	Photoluminescence
Ph	Phenyl
PET	Photo-induced electron transfer
ppm	Part per million
pH	Potential of hydrogen
Φ_F	Quantum yield
rt	Room Temperature
PhMe	Toluene
TLC	Thin layer chromatography
TMS	Tetramethylsilane

Abbreviation	Explanations
TGA	Thermal Gravimetric Analysis
TEA	Triethylamine
TFA	Trifluoroacetic acid
THF	Tetrahydrofuran
TBA	Tetrabutylammonium
Td	Temperature of decomposition
UV	Ultraviolet
UV-vis	Ultraviolet-visible
W	Watt
WHO	World Health Organization

1. GENERAL INTRODUCTION

Humankind has a long history of using organic compounds. Many small organic molecules are used as drugs, dyes, food additives, etc. More lately, large assemblies of organic molecules called materials have reached a leading significance position in science. This interest is mainly due to the easiness of tuning the organic materials to enhance their properties. Among all organic molecular materials, push-pull systems are more promising because of the intramolecular charge-transfer process. They usually contain an electron-donor (D) and an electron-acceptor (A) group linked via a π-conjugated system. In their excited states, charge transfer and separation in these materials provide them with exclusive optical and electrical properties. Molecular systems based on donor-linker-acceptor (D-π-A) design have found applications in several technological research fields. Lately, D-π-A systems have been applied in electroactive and photoactive materials, biochemical fluorescent technology, environmental sensing, photovoltaic cells, and nonlinear optics. The main advantage of these systems is the easiness of tuning their physical properties over large scales via suitable chemical alteration of the structures of D-π-A. Among such organic chromophores, carbazole, triphenylamine, and indanone-based compounds are being progressively used in a variety of fields, such as nonlinear optics and chemosensors. They have displayed several promising results and ought to be further investigated.

Hence, we were interested in designing, synthesizing, and studying various donor-acceptor compounds' photophysical properties and applications. The outcomes of our studies will help research chemists and applied chemists to construct and create improved push-pull materials for applications in nonlinear optics (NLO) and Chemosensing.

The central part of this dissertation is the design and synthesis of the push-pull D-π-A system based on Indone and triphenylamine. It was organized into three chapters. The first chapter is a bibliographical review covering the molecular fluorescence and an overview of the optical sensor followed by second-order NLO chromophores and their applications, and finally, a summary regrouping the organic compounds based on Fluorene (Figure 1.1). The second chapter covers the materials and methods used to fulfill this thesis, the synthesis of the target molecules, UV-vis measurements, and others.

The third chapter is divided into three subtitles:

- Push-pull chromophores type π-conjugated is discussed. The synthesis, photophysical, and NLO responses are reported.
- 1-dicyanomethylene-2-aryl-indone derivatives for Chemosensing are reported. First, the synthesis and photophysical properties are considered. The investigation of the anions sensing abilities of the obtained compounds both in organic and in partial aqueous media are conducted.
- inden-1-ylidene and Fluorene: reported the synthesis of compounds based on Fluorene via numerous methods such as di/three-component one pot. The photophysical properties are reported.

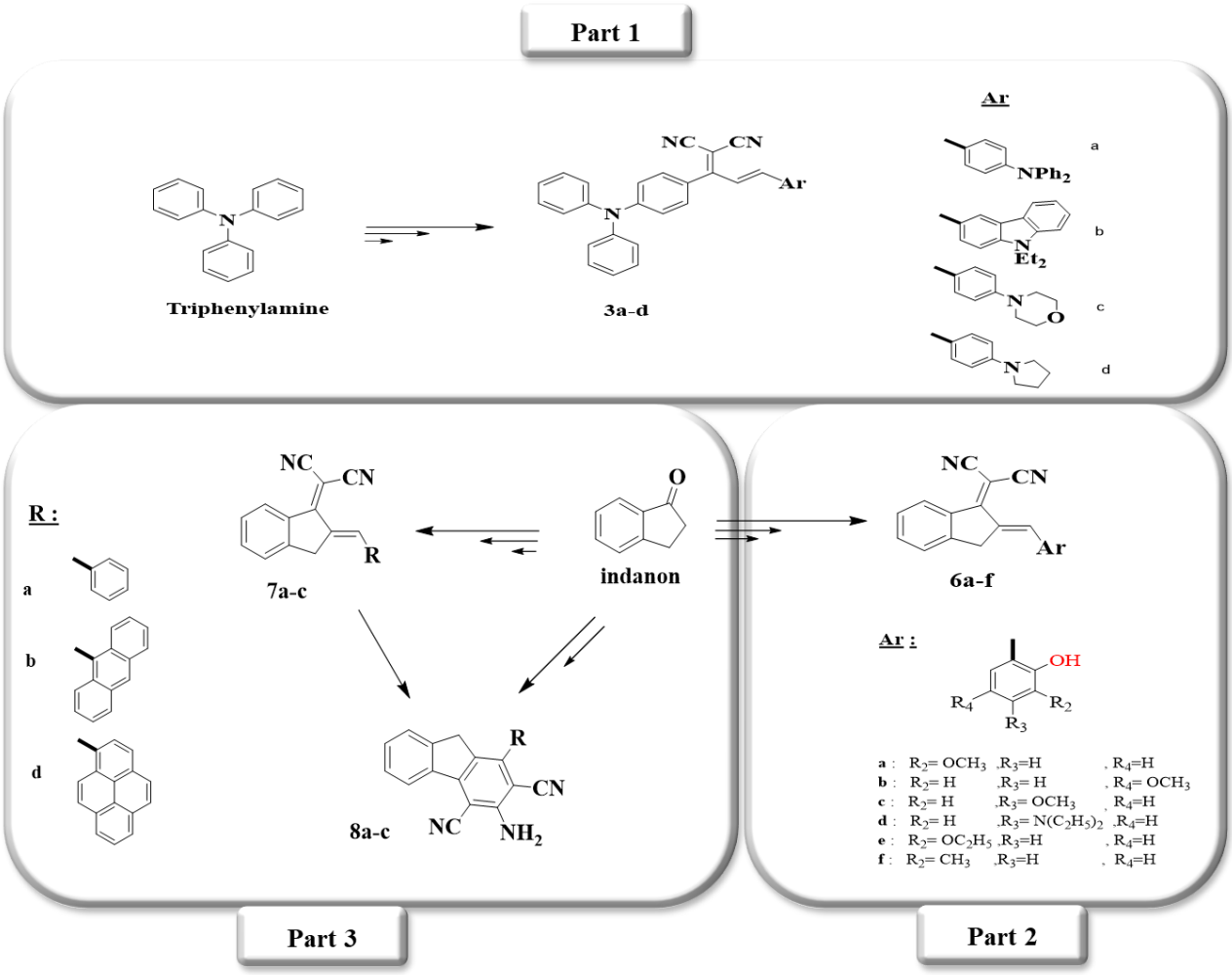

Figure 1.1. Synthesis route and Structures of synthesized compounds within the scope of this study.

Objectives of this thesis

This dissertation's overall scientific goal is to design and synthesize three novel series of organic chromophores containing a donor-acceptor system (D-π-A) and their application in different fields.

The specific objectives are:

- Synthesis of a Serie based on 1,1-dicyano-2,4-diaryl-1,3-butadiene derivatives 3a-d and substituted by various amino groups on both sides. The obtained compounds will be investigated for second-order NLO properties.
- A second synthesized series based on 1-dicyanomethylene-2-aryl-indanone derivatives 6a-f is tested as chemosensors to detect several anions. Additionally, numerous factors were studied, such as pH, solvent, substitution, and others.
- A third series is based on 1-dicyanomethylene-2-aryl-indones 7a-c and 3-amino-1-aryl-9*H*-fluorene-2,4-dicarbonitriles 8a-c is synthesized via by di/three-component one-pot method. Phenyl, anthracen-9-yl, and pyren-1-yl groups will be aromatic fragments to enhance the photoluminescence (PL) properties. The photophysical of these compounds were studied in various solvents with different polarities.

2. BIBLIOGRAPHICAL REVIEW

2.1. Photophysical Background

2.1.1. Luminescence

Luminescence is defined as the process of light quanta emission after an extern energy excitation, which can be chemical (chemiluminescence), thermal (thermoluminescence), mechanical action on a solid (mechanoluminescence), light (photoluminescence), which is the main interest of this study.

Photoluminescence is known as the optical property of a substance that can absorb photons from its excited state as radiative energy (Bernard Valeur, 2012; Demchenko, 2015). The chemical entities that absorb ultraviolet (UV) or visible light are denoted as chromophores. Colored compounds are an indicator of visible light absorption.

Photoluminescence is categorized as fluorescence and phosphorescence, depending on the nature of the excited state. A fluorophore is a molecule that has the capacity to fluoresce. Due to the color property, a fluorophore is generally labeled as a dye (Braslavsky, 2007; Lakowicz, 2006).

Absorption of Light (Excitation)

Light

Light is defined as electromagnetic radiation labeled in terms of a "wave-particle duality" notion. Accurately, light is a photon characterized by its energy (E, eV) and a wave described by its wavelength (λ, nm) or wavenumber (σ, cm^{-1}) as described in Eq.2.1,

$$E = h\nu = \mathrm{h}\frac{\mathrm{c}}{\lambda} \quad and \quad \sigma = \frac{1}{\lambda} \tag{2.1}$$

Where c and h are the speed of light and Planck's constant, respectively.

Photochemistry and optical studies are carried out in the range of electromagnetic radiations displayed in Figure 2.1 and characterized by E and λ (Bernard Valeur, 2012; Lakowicz, 2006).

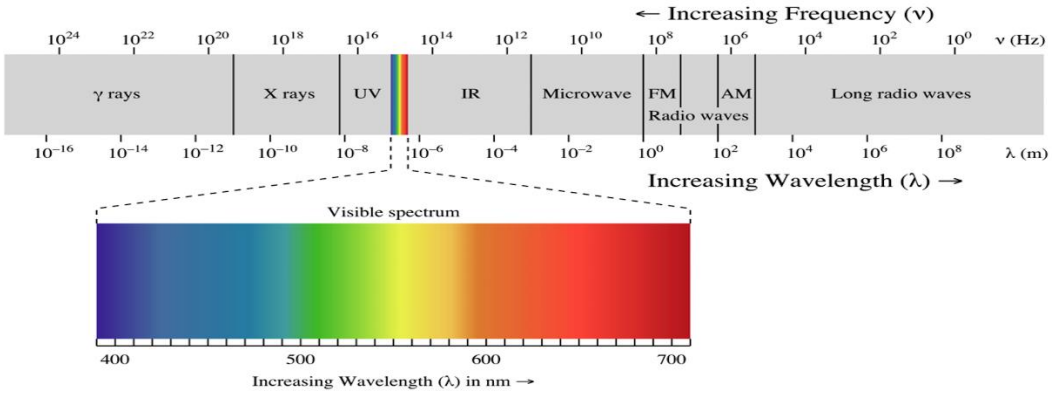

Figure 2.1. Range of electromagnetic radiation in optical studies and photochemistry

Absorption

In the absenteeism of any exterior sources of perturbation, the organic molecule exists in the ground state (S_0, singlet by multiplicity), where two electrons are present in the highest occupied molecular orbital (HOMO), whereas the lowest unoccupied molecular orbital (LUMO) is free. However, when the molecule is subjected to extreme-ultraviolet radiation (λ_{max} < 200 nm), ionization occurs by explicating one of its electrons. Though, subjecting the molecule to UV/visible irradiation (200-800 nm) leads to an electron transition from HOMO to LUMO, triggering an excited electronic state (S_1, singlet by multiplicity). An intersystem crossing can occur in the excited state, as displayed in Figure 2.2 (Bernard Valeur, 2012; Braslavsky, 2007).

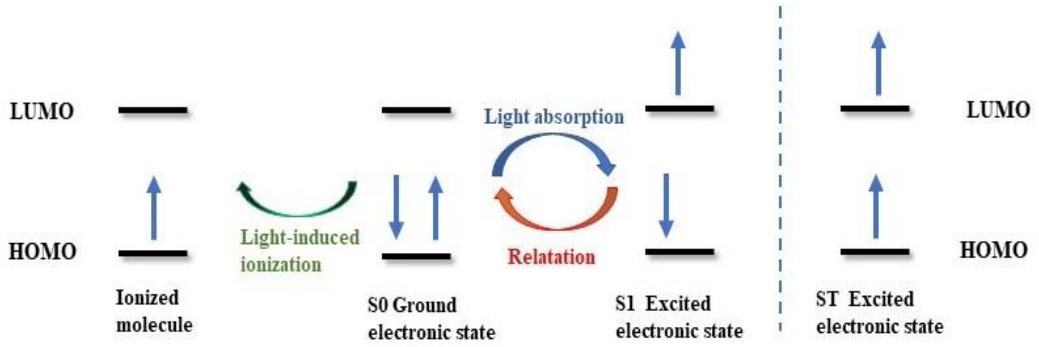

Figure 2.2. Light-induced phenomena

The Beer-Lambert Law

On a spectrophotometer, the absorbance (A) calculated at any wavelength is relational to the dye concentration (*c*, mol/L) and the light path length in a sample (1 cm) (Figure 2.3). In this relation, the molar absorption coefficient (ε) is the proportionality coefficient, as shown in Eq.2.2.

$$A = \varepsilon . c . L \qquad (2.2)$$

Occasionally deviation from Beer-Lambert law occur, and the fluorophore absorbs light nonlinearity. Several factors can cause this deviation: inner filter effect, broadband illumination, turbidity of biological samples, and molecular aggregation. The latter is a self-association that enhances the size of the particle triggering more light scattering or shift in the absorption maximum. If the fluorophore is concentrated or insoluble, aggregation is observed (Lakowicz, 2006).

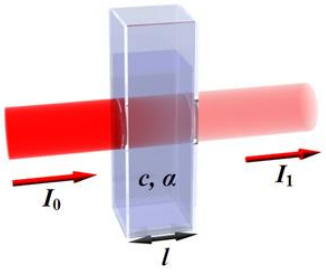

Figure 2.3. Illustration of Beer-Lambert law

Molar absorptivity or absorption coefficient

The possibility of an electronic transition from the ground to an excited state at a given wavelength is defined as extinction coefficient or molar absorptivity (ε).

- If $\varepsilon > 10^5$ $M^{-1}.cm^{-1}$: the transition is entirely permitted.
- If $\varepsilon < 10^2$ $M^{-1}.cm^{-1}$: the transition is prohibited.
- If $10^2 < \varepsilon < 10^5$ $M^{-1}.cm^{-1}$: the transition is partly permitted.

Mainly, ε increases with the size of the fluorophore (Dziuba, 2011).

Fluorescence emission

In a Jablonski diagram (Jablonski, 1933), displayed in Figure 2.4, the horizontal lines correspond to the vibrational levels of the electronic states, and the vertical axis is the energy. The electronic transition occurs from the lowest vibrational level of the ground state to various excited states' vibrational levels. The arrows present the numerous possible transition process. Eventually, the excited molecules go back to the relaxed state after undergoing a vibrational relaxation (10^{-10}-10^{-12} s). The molecule could also go through an intersystem crossing causing an alteration in the electron spin multiplicity from a singlet (S1) to a triplet

state (T1). A T1 to S0 transition emits light as phosphorescence (10^{-1}-10^{-4} s) (Braslavsky, 2007). Kasha's rule states that the luminescence emission has a significant yield only from the excited state's lowest vibrational level (Kasha, 1950).

The model of energy transition processes associated with the absorption of light and the return to the ground state is complicated and might involve the relaxation of the solvent, delayed fluorescence, and several non-radiative processes and phenomena (Lakowicz, 2006).

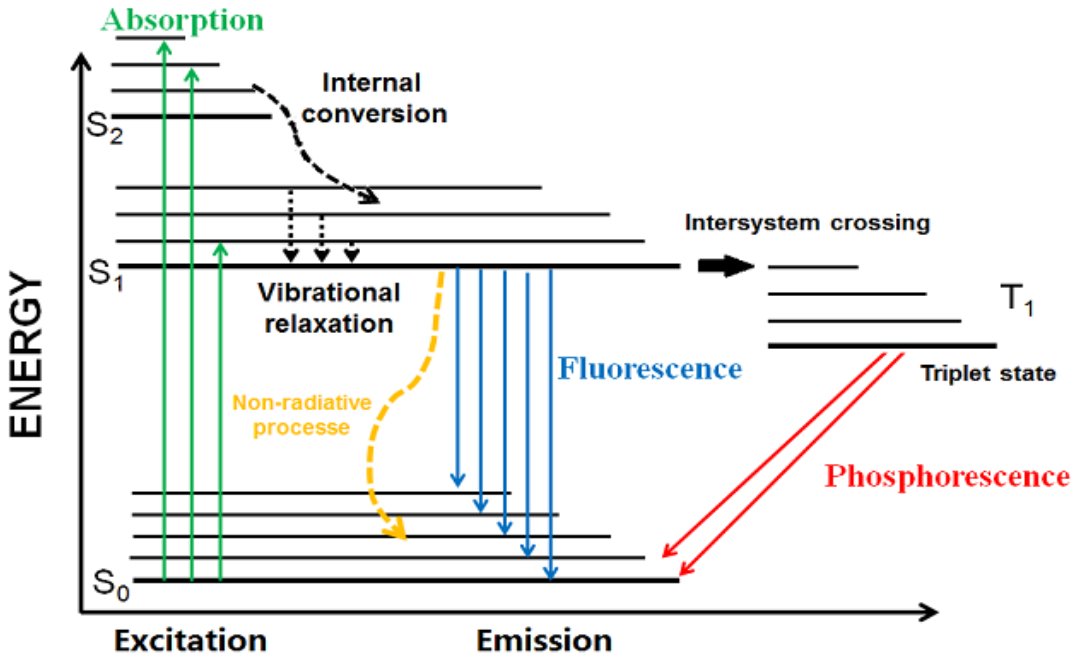

Figure 2.4. The Jablonski diagram(Lakowicz, 2006)

Steady-state measurement

The steady-state measurements were conducted by subjecting the sample to a continuous beam of light (Figure 2.5). The essential optical characteristic is: "Stokes shift" in tribune to the British physicist Stokes and the fluorescence quantum yield (Lakowicz, 2006).

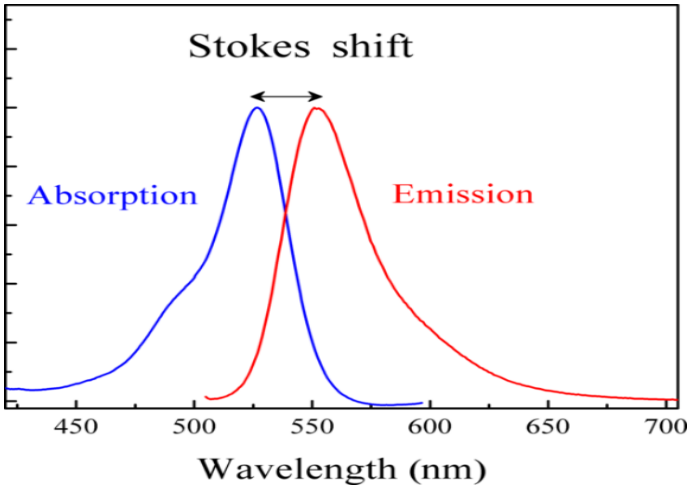

Figure 2.5. Steady-state measurement

Quantum yield

The quantum yield (ϕ) is defined as the ratio of the number of photons emitted and the number of photons absorbed (Eq.2.3). It recognizes the fluorescence process's efficiency vs. the other decay pathways of the excited species (Weber & Teale, 1957).

$$\Phi = \frac{\text{emitted photons}}{absorbed\ photons} = \frac{k_r}{k_r + k_{nr}} \tag{2.3}$$

Stokes shift

Absorption maximum (λ_{abs}) and emission maximum (λ_{em}) are the most important properties identifying a fluorophore. Generally, the fluorescence emission shifts to the lower energy side compared to the absorption ($\lambda_{em} > \lambda_{abs}$) because of the dissipated energy absorbed in non-radiative relaxation. The variation between the position of the maximum band of absorption and emission spectra of the same electronic transition is defined as the Stokes shift ($\Delta\lambda_{SS}$) (Figure 2.5). Furthermore, it can be measured using Eq.2.4, typically expressed in wavenumber units. Wavelength units are also applied for ease (Lakowicz, 2006).

$$\Delta\lambda_{ss}(nm) = \lambda_{em} - \lambda_{abs} \tag{2.4}$$

Relative brightness

Relative brightness can be determined from the product of ε and ϕ. Consequently, considering both the absorption and the fluorescence efficiency.

2.1.2. Solvatochromism

Solvatochromism refers to the shift of the solute's electronic absorption band upon alteration of the polarity of the solvent. It results from a difference in the solvation of the ground and the first excited state of the light-absorbing molecule or its chromophore (Marini et al., 2010). The solvatochromism of a molecule in a solution is seen via UV/Visible spectroscopy. Typically, two types of solvatochromism are observed:

- Negative Solvatochromism: This phenomenon is unusual, contrary to the positive solvatochromism exhibited by thousands of dyes. Negative solvatochromism or hypsochromic shift corresponds to an emission band dislocation to a shorter wavelength (blue shift) when the solvent polarity increases. A hypsochromic shift is noticed if the dye's first excited state is less polar than the ground state (Marini et al., 2010; Reichardt, 1994).
- Positive Solvatochromism: Most dyes display variations in the emission band to a longer wavelength (red-shift) when the solvent polarity increases. This is identified as a "bathochromic shift." In the following sections, solvatochromism discussions will describe this main class of dyes with bathochromic shifts (Marini et al., 2010; Reichardt, 1994).

2.2. Optical Chemosensors

Optical sensors are investigation techniques that detect light intensity. They modify the receptor's photophysical properties upon analyte (guest) binding to the receptor. Depending on the type of sensor, the characterization of these modifications is detected in UV-visible and fluorescence spectroscopy instruments. The chemosensors can be classified into colorimetric chemosensors and fluorometric chemosensors or fluorescent chemosensors.

2.2.1. Colorimetric chemosensors

Colorimetric chemosensor is defined as the color change that occurs after the receptor's binding with a specific analyte (M. Wang et al., 2014). After the binding between the receptor and the analyte, the chemosensor's signaling unit shows a color change (Kaur et al., 2009). Colorimetric chemosensors have attracted significant interest due to the possibility of obtaining qualitative and quantitative data via the naked eye (Dong et al., 2016) without referring to any complex techniques (G. J. Park et al., 2016).

2.2.2. Fluorometric Chemosensors

General principle: design of chemosensor

One of the most valuable response methods for optical readout is fluorescence. The fluorescence chemosensors have attracted considerable interest due to their sensitivity, selectivity, quick response time, on-site and real-time detection, straightforward performance, flexibility, and present low molar estimate of the analyte. In the case of fluorometric chemosensors, the binding of the analyte to the receptor leads to a change in fluorescence behavior (J. H. Wang et al., 2020). In 1867 Goppelsroder reported the first fluorescent chemosensor to detect aluminum ions via the formation of a morin chelate which is strongly fluorescent.

The use of fluorescent chemosensor allows the detection at the picomolar scale; however, the colorimetric sensors can only detect concentration at micromolar levels. The fluorometric chemosensor's advantages are mainly due to the proportionality of the emitted fluorescence to the analyte concentration. In contrast, in absorbance measurements, the concentration of the analyte and the absorbance are proportional, which is associated with the ratio between intensities measured before and after the beam passes through the sample.

The essential parts of the fluorescent chemosensors are the recognition and signaling moieties, as given in Figure 2.6. Accordingly, a fluorescent chemosensor is developed by connecting a receptor (ionophore) to a fluorophore responsible for converting the recognition into the photophysical signal (like spectra, fluorescence quantum yield, and lifetime).

The alteration of the photophysical properties can occur by binding a particular analyte to the receptor, leading to a fluorescence signal, with either an enhancement or quenching of fluorescence. The binding of the analyte to the receptor leads to an enhanced fluorescence intensity called turn-on chemosensor (A. Gupta & Kumar, 2016; Zeng et al., 2019), whereas the analyte bounding to the fluorophore results in a decrease of fluorescent intensity quenching called turn-off chemosensor (Riis-Johannessen et al., 2010; Wu et al., 2017).

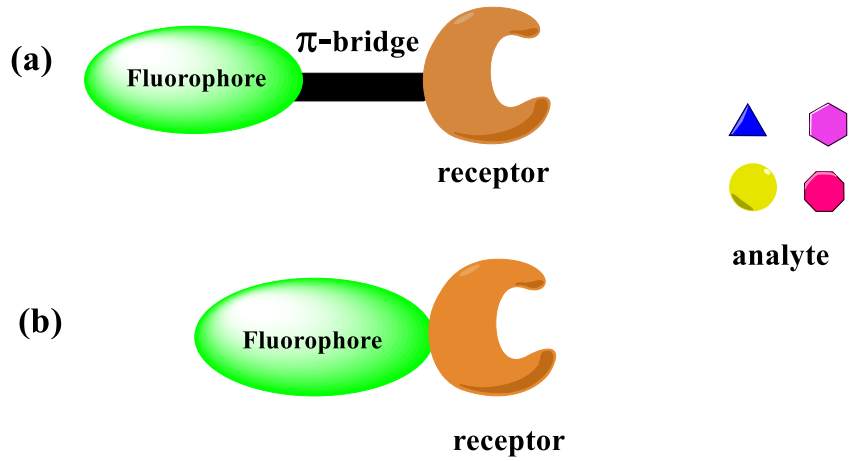

Figure 2.6. Fluorescence sensing (a) A spaced model (b) An integrated model.

Depending on the connection of fluorophore and receptor, two models of fluorescent chemosensors can be defined: spaced (Figure 2.6 (a)) and integrated model (Figure 2.6 (b)). The spaced model offers a design where the fluorophore is connected to the receptor via spacer and signaling moieties that prevent conjugations. In the integrated model, the fluorophore and receptor are conjugatively connected to each other; in this model, the receptor is a part of the π-electron system of the fluorophore.

Photo-induced electron transfer

The fluorescence quenching is due to a photo-induced electron transfer (PET); the normal state returns when a non-luminescent process follows the PET process (De Silva et al., 1997). The PET process could explain the "on-off" switching of fluorescent chemosensors based on the molecular orbital theory. The basic design of the florescent chemosensors based on PET is a fluorophore- spacer- receptor. This model has a spacer separating the fluorophore from the receptor, consequently electronically disconnecting the π-electron systems from the fluorophore and receptor. The PET process is divided into 2 types: reductive PET and oxidative PET, depending on the electron acceptor or donor links to the fluorophore and receptor (Boens et al., 2012). However, in this study, only the reductive PET will be investigated. The design of the fluorescent chemosensors is given in Figure 2.7. The reductive PET is defined as the system where the fluorophore is reduced, whereas the receptor is oxidized. In this type of PET process, the fluorophore provides an electron acceptor, and the receptor serves as an electron donor. The electron photo-excitation from HOMO to LUMO occurs through the reductive PET process. Consequently, the fluorophore

and the analyte react and cause the occurrence or elimination HOMO and LUMO "adjacent" orbital, resulting in the fluorescence quenching or enhancement, respectively (Figure 2.8).

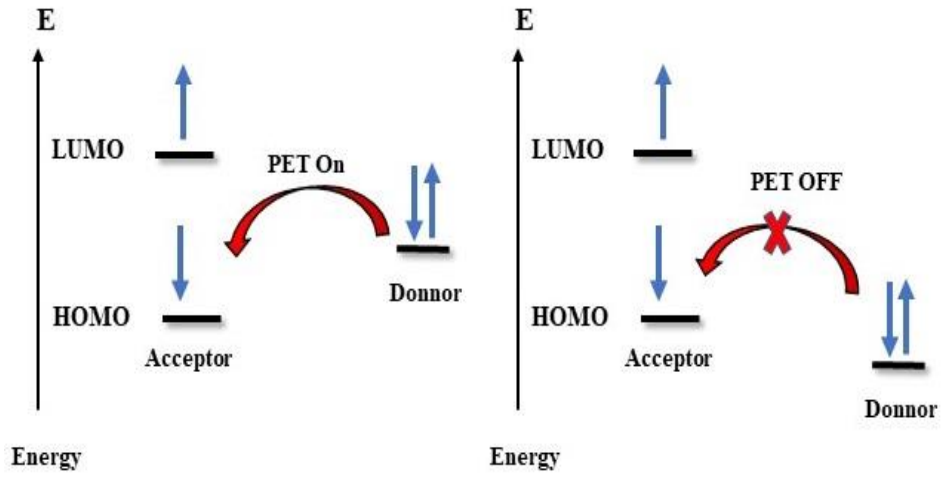

Figure 2.7. Molecular orbital diagram of the photo-induced electron transfer process (PET)

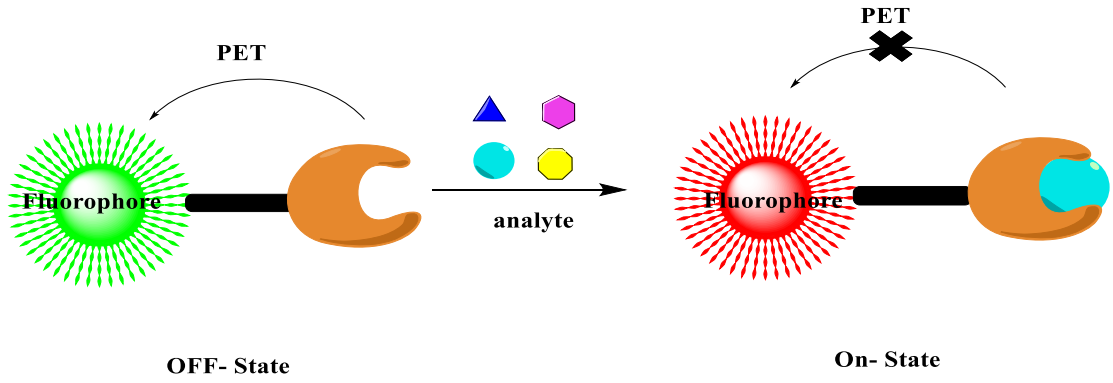

Figure 2.8. Schematic representation of PET chemosensor in the sensing process

Intra and intermolecular charge transfer

Valeur et al. were the first to introduce the intramolecular charge transfer (ICT) process for cation sensing (Valeur & Leray, 2000). ICT process is defined as an excited state where the conjugation of an electron-donating unit (such as $–NH_2$, $–NMe_2$, $–OCH_3$) to an electron-accepting (like >C=O, –CN) unit in one molecule is shown to rise a "push-pull" π- electron system (Grabowski & Dobkowski, 1983), which have been widely applied for cation sensing. A blue shift in the absorption spectrum is observed when the electron donor interacts with the analyte, decreasing the electron-donating character. However, the analyte reacts with the electron acceptor part leading to a red-shift due to a developed ICT (Figure 2.9).

Furthermore, alterations in the fluorescence lifetimes and quantum yields are also detected. Thus far, many fluorescent imaging molecules are obtained from the ICT process by modifying either the electron donor, electron acceptor capacity, or π-conjugation degree of the fluorophores to react with the target analyte.

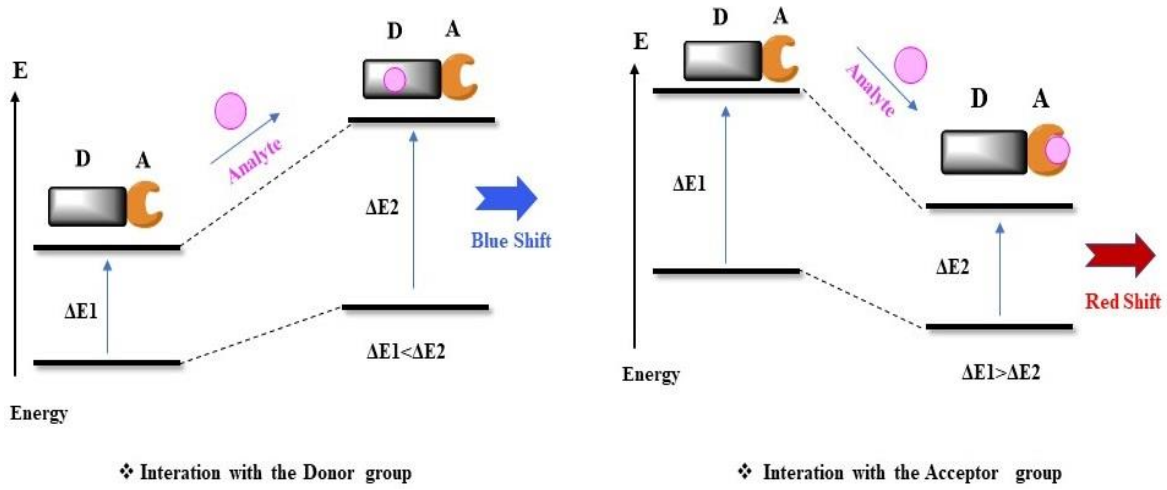

Figure 2.9. Schematic representation of ICT chemosensor in the sensing process

Excited-state intramolecular proton transfer

Excited-state intramolecular proton transfer (ESIPT) has been implemented to design fluorescent chemosensors due to their distinctive and exceptional spectral sensitivity to the environmental medium. ESIPT process is based on a proton transfer from a proton donor (hydroxyl or amino unit) to an acceptor unit (carbonyl oxygen or imine nitrogen) atom in the excited state of a fluorophore which is facilitated by an intramolecular hydrogen bond (Y. Yang et al., 2013). A graphical interpretation of the ESIPT process is illustrated in Figure 2.10.

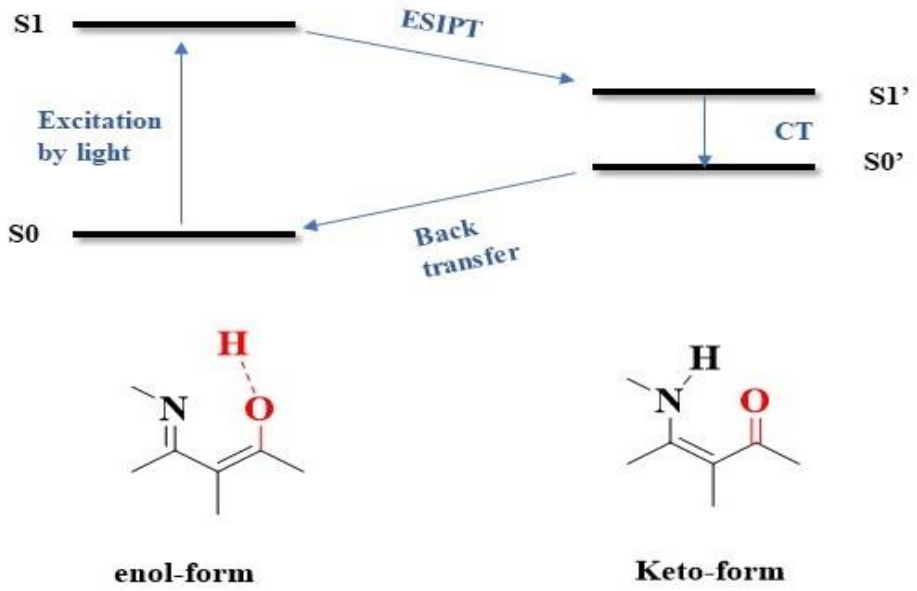

Figure 2.10. Schematic representation of excited-state intramolecular proton transfer system

Due to the change between the enol and keto form in the system based on ESIPT, the photochemical reactivity of the excited molecules is drastically reduced, leading to improved photostability. Additionally, a significant Stokes shift is observed. Hence, the ESIPT process fits the design of fluorescent chemosensors that necessitates spectral shift for selective detection.

Fluorescence resonance energy transfer

Fluorescence Resonance Energy Transfer (FRET) is another type of fluorescence modulation. FRET process is defined as a transfer of energy between a pair of fluorophores that operate as energy donors and acceptors, respectively (Fan et al., 2013; Kim & Quang, 2007). The FRET depends on the interaction distance between the electronically excited states of 2 chromophores that the excitation energy is non-radiatively relocated from a donor to an acceptor by non-radiative dipole-dipole coupling (Figure 2.11). The vibrational transitions in the donor and the acceptor are approximately equivalent. If the FRET is operative in the molecules, they are typically applied to improve the stokes shift artificially. For sensing applications, the emission of the donor at relatively short wavelengths leads to triggering the acceptor emission at longer wavelengths with a ratio of the fluorescence intensities of the donor and acceptor emissions regulated by the target analytes. Elevated FRET efficacy is obtained when the extensive spectral overlaps with the donor emission and the acceptor absorption spectrum (Y. Feng et al., 2012). Several FRET-based fluorescent

chemosensors were developed following the groundbreaking endeavors for the ratiometric detection of metal ions like Hg^{2+} [28], Zn^{2+}[29].

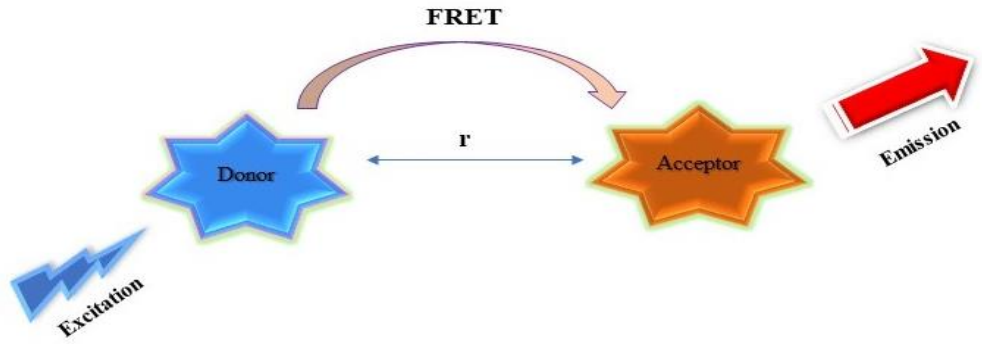

Figure 2.11. Schematic representation of FRET chemosensor in the sensing process.

2.2.3. Applications of fluorescent chemosensors

Cyanide (CN^-) and Fluoride (F^-) play an essential role in life and are deemed one of the very poisonous anions and harmful to human health. They are used in industrial activities like acrylic fiber manufacturing, metallurgy, electroplating, fibers synthesis, and gold extraction. Absorption by the lungs, exposure to the skin, food, and contaminated drinking water are all exposition methods to CN^- and F^- intoxication. Table 2.1 summarizes the World Health Organization (WHO) and European (EU) guidelines for anions in drinking water. The WHO set the provisional maximum tolerable daily intake limits to 0.07 mg/L and 1.5 mg/L for CN^- and F^-, respectively, for drinking water. It is consequently of paramount importance to be able to establish their concentration in water at such low levels precisely. The detection of anions is generally effectuated via analytic techniques such as Ionic chromatography. However, these techniques are complex and expensive, where the need to develop new techniques for anions detection that are both accurate and low cost. Recently, fluorescent chemosensors have attracted considerable attention as a promising alternative for anions sensing.

The fluorescent chemosensors have been used in numerous fields, such as biology, physiology, pharmacology, and environmental sciences. The use of fluorescent chemosensors to detect environmentally critical contaminants such as anions (CN^-, F^-) or cations (Hg^+, Pb^{2+} …) have been widely investigated. This current study will investigate the detection of anions, mainly CN^- and F^-, using chemosensors 6a-f in 4.2.

Table 2.1. WHO and EU drinking water standards for anions

Element	Symbol	WHO standards (mg/L)	EU standards (mg/L)
Cyanide	CN^-	0.07	0.05
Fluoride	F^-	1.5	1.5
Chloride	Cl^-	250	250
Hydrogen sulfate	HSO_4^-	No guideline	No guideline
Bromine	Br^-	Not mentioned	0.01
Nitrate	NO_3^-	50	50

2.3. Second-Order Nonlinear Optical Chromophores

2.3.1. Overview of nonlinear optical materials

Nonlinear optics could be defined as the study of optical phenomena instigated by the interactions between an applied electromagnetic field and a material generating the emission of a new electromagnetic field having changed photophysical properties such as frequency, phase etc.(Garcia et al., 2015; Long, 1995). The light sources generally used are lasers because of their effectiveness in altering the optical properties of the materials. The applied field ought to be very robust. The procedure of transmitting and processing signals via photons as an alternative to electrons is defined as NLO. Basically, defined, the NLO is the means for photons manipulations (Çatal et al., 2018).

NLO materials could be inorganic crystals used for several years (Gong et al., 2019). However, the low thermal stability, difficulty of tuning the optical properties, and high cost are the major drawbacks of inorganic NLO materials (J. Liu et al., 2020). Recently, organic molecules have been an appealing alternative NLO material to overcome the shortcomings of the inorganic crystals because of their easiness to tune by systematic structural and functional group modifications (Gong et al., 2019; Marder, 2009). The main advantages of organic NLO materials are high thermal stability, low cost, low dielectric constant compared to the inorganic ones, giving high sensitivity and improved performance (J. Liu et al., 2020; Suresh et al., 2012).

Among the optical phenomenon that NLO materials could exhibit, the most examined one is the second-order which is known as the second-harmonic generation (SGH), where the

input wave having a frequency ω, is converted to twice the frequency at the output wave 2 ω (Figure 2.12) (Kato, n.d.).

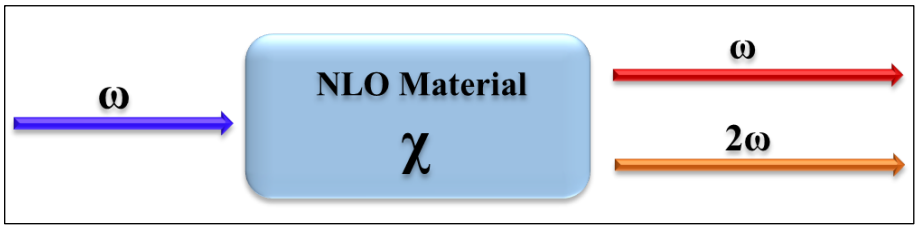

Figure 2.12. Schematic presentation of second-harmonic generation

In order to obtain materials exhibiting efficient second-order NLO, large hyperpolarizability (β) must be obtained (Ruslim & Ichimura, 2001). Designing materials exhibiting second-order NLO is now well established, and crucial requirements for displaying large hyperpolarizabilities have been found. The fundamental requirements for the molecule should possess NLO activity:

- It must be non-centrosymmetric.
- Polarizable material
- Donor-acceptor molecules, having asymmetric charge distribution.
- Pathway of π-conjugation
- Chiral center containing molecules, with Acentric crystal packing.

Among all the organic molecules that can display a second-order NLO response, linear asymmetric molecules with π-conjugated bonds, known as "push-pull," are the ones investigated in this thesis.

2.3.2. Push-pull chromophores

Push-pull π-conjugated chromophores are molecular systems containing a donor group (D) and acceptor group (A) linked via a π-conjugated spacer (D-π-A) (Figure 2.13). They display two major advantages: high dipolar moment (μ) both in the ground and excited states, and ICT process from the D to the A. Push-pull systems found applications in numerous fields because of their physicochemical properties (Gautam et al., 2017; Kundu & Kulshreshtha, 2015). So far, several D-π-A systems have been designed and synthesized via a combination of various donor/acceptor molecules with established π-spacer parts.

The first developed series D-π-A systems were designed using 4-nitrophenyl moiety as an acceptor group and *N*,*N*-dimethylanilino as an electron donor. Lately, however, the interest switched to stronger organic donor and acceptor molecules such as allylidenemalononitrile and amino-electron-donating group (Yahya, Seferoğlu, et al., 2021). Numerous studies revealed that the nature of the terminals in the donor/acceptor groups influences the optical properties of the obtained materials and the structure and length of the π-conjugation. Various conjugated spacers have been integrated into the push-pull systems, such as polyenes, stilbene, thiophene, etc. (Figure 2.13).

It is evident from the literature that push-pull systems are very investigated primarily for their NLO properties (Huo et al., 2019; Mohammed et al., 2017). Furthermore, they are used as model systems to study the PET process discussed in detail in section 2.2.1.

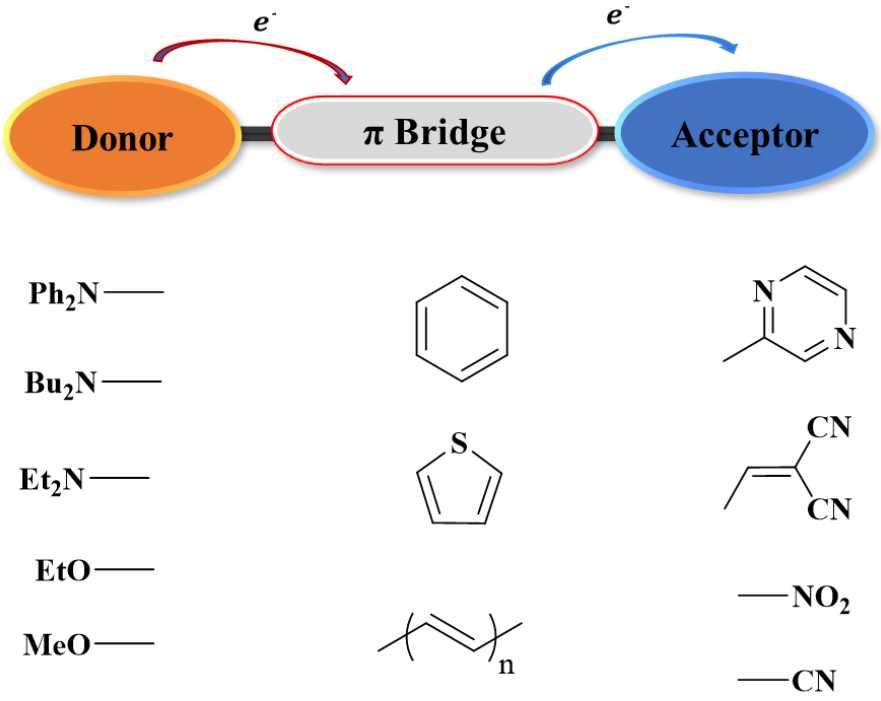

Figure 2.13. Schematic representation of a push-pull molecule composed of the model (D-π-A) with examples for each component.

2.3.3. Second order NLO response measurements

The most used technique to measure the hyperpolarizability (β) of NLO materials is the Electric Field Induced Second- Harmonic Generation (EFISH). It is an experimental method established on submitting the chromophore solution to a static electric field. The bias on the orientation average is due to an interaction between the electric field and the molecules'

permanent dipole. The intensity of light of the second-harmonic leads to the determination of the second-harmonic due to the isotropy partial removal.

The EFISH measurement provides the data about the scalar product $\mu\beta(2\omega)$ of the vector module of the first hyperpolarizability tensor β and the dipole moment vector (Levine & Bethea, 1974; Singer & Garito, 1981; Thami et al., 1992). This product is acquired from the Eq.2.5, and $\gamma_0(-2\omega,\omega,\omega,0)$, the third-order term is believed to be negligible for the push-pull dyes evaluated in the present research. This estimate is usually used for push-pull organic molecules.

$$\gamma_{EFISH} = \mu\beta/5KT + \gamma 0(-2\omega,\omega,\omega,0) \quad (2.5)$$

2.3.4. Application of NLO materials

NLO materials can be valuable for a diversity of applications (Figure 2.14) varying from commercial lasers, telecommunications, sensors, environmental monitoring, medicine, manufacturing and materials processing, the military, and in scientific instrumentation, modulation of optical signals eased by the electro-optic effect-the effect whereby the refractive index of material variations in response to an applied electric field-to microfabrication, sensing, imaging, and cancer therapy simplified by multiphoton absorption, wherein molecules simultaneously absorb two or more photons of light (R. W. Munn, 1993).

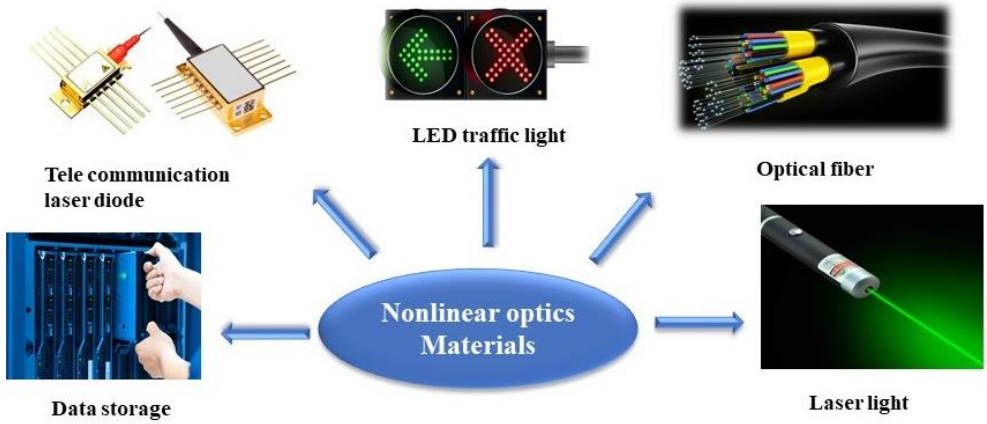

Figure 2.14. Different applications of NLO.

2.4. Organic Molecules Containing Fluorene Derivatives

2.4.1. Fluorene hybrid chromophore

Fluorene or 9*H*-fluorene is an inflexible, planar polycyclic aromatic hydrocarbon with an extensive π-electron delocalization (Figure 2.15). Fluorene structures white crystals with violet fluorescence from which its name was derived (Kurdyukova & Ishchenko, 2012).

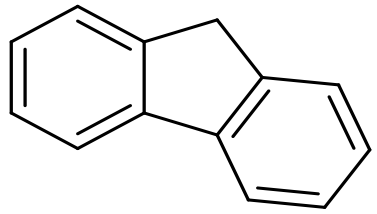

Figure 2.15. The structure of Fluorene

The fluorene displays four advantages :

- The fluorene chromophore is an aromatic, or π-conjugated, compound. This results from the cyclic conjugated nature of the two benzene constituents within the chromophore. Each benzene structure possesses six π electrons which are completely delocalized around the ring. This electron delocalization can give large molecular polarizability, which promises a strong nonlinear interaction upon excitation (Kurdyukova & Ishchenko, 2012).
- One of the significant advantages of fluorenes compared to the other traditional heterocyclic chromophores is the absence of auxochromes. Endocyclic heteroatoms in other spacers induce non-radiative deactivation of the excited states, decreasing the quantum yields (Cohanoschi et al., 2005). Auxochromes additionally enable the forbidden n-π transitions as effective channels of photodegradation (Lovell et al., 2010). Similarly, the chromophoric systems incorporating the fluorene nucleus exhibited somewhat superior thermal and photochemical stability under one and multi-photon excitation environments (Kurdyukova & Ishchenko, 2012; Ziarani et al., 2018).
- The high fluorescence efficiency is the most alluring advantage of this family. Undeniably, some fluorene derivatives fluoresce with quantum yields that approach "unity" (Cheng et al., 2011).
- The aromatic core of the fluorene chromophore has a high degree of functionality. This means several potential sites can append substituent groups onto the base molecule to

alter its structural properties. The base chromophore may be functionalized or chemically appended on the molecule's 2, 4, 7, and/or 9 positions. These positions are marked for reference in Figure 2.15.

Several researchers have grasped the benefits of mixing pyrene or anthracene with fluorene groups into one chromophore (X. Feng et al., 2015; Lavanya Devi et al., 2015; G. Ma et al., 2018; Reddy et al., 2017; Wan et al., 2013). Pyrene and anthracene belong to the polycyclic aromatic hydrocarbons family and act as electron donors and electron acceptors. Pyrene exhibits strong photoluminescence (PL) in solution (Figueira-Duarte & Müllen, 2011; S. W. Yang et al., 2005). Generally, pyrene and its derivatives produce excimers in condensed media (Ge et al., 2020; J. Wang et al., 2020). On the other hand, anthracene derivatives have drawn considerable researchers because of their exceptional PL and electroluminescence (EL) properties, wide-energy gap, and good thermal stability.

2.4.2. Aggregation-caused quenching

Aggregation-caused quenching (ACQ) is a well-known photophysical phenomenon responsible for the low emission of chromophores in the form of solid-state (e.g., in nanostructures, nano-precipitates). It is defined as the phenomenon in which fluorophores highly emissive in a dilute solution state become weakly emissive or even non-emissive in an aggregated state Figure 2.16 (A) (Birks, n.d.; Kisiel et al., 2020). ACQ is usually considered unfavorable and remains an obstacle to applying conventional fluorophores (X. Ma et al., 2016; Qi et al., 2019; Zhao et al., 2014). Any effort to lessen ACQ has turned out to be of little success due to the aggregation and natural process (Guo et al., 2012; Qi et al., 2019). The most apparent unfavorable ACQ effect is the fluorescence mitigation that frequently ends in low fluorescence (M. Huang et al., 2016). Also, the fluorescence linearity array is usually minimal due to ACQ, raising concerns of inaccuracy in molecular bioimaging (Meng et al., 2018). It must be emphasized that this process is often coupled with a noticeable variation in emission, detected without metathesis (chemical change) of the dye (also observed for poly (octylthiophene), when nanoparticles are created (Kłucińska et al., 2016; Stelmach et al., 2020)). The change in emission is caused by the reorganization of chromophore groups (molecules) in space, resulting in reduced interactions, favoring emission. The ACQ effect is one of the main blockages that hinder the efficient development of these fluorine-based materials. Hence the need to modify the compound based on Fluorene in order to develop a compound displaying an aggregation-induced emission (AIE).

2.4.3. Aggregation-induced emission

Aggregation-induced emission (AIE) is another photophysical phenomenon combined with chromophore aggregation Figure 2.16 (B). Contrary to ACQ, AIE chromophores display low or insignificant emission in solution, although in the solid-state, the emission is intense (Y. Chen et al., 2019). The dissolution of chromophores having an AIE results in a dramatic consummation of the excitation energy by the active intramolecular rotations and vibrations, which leads to a facilitated non-radiative decay. After aggregation, these intramolecular AIE chromophores' movement is considerably restricted, changing the consumption from non-radiative relaxation to radiative decay. Besides, the π-π in ACQ chromophores is hindered in AIE chromophores due to the molecules' nonplanarity. Currently, the emission wavelength of numerous described AIE chromophores already covers the whole visible spectrum and is broadening to the near-infrared (NIR) range (Mei et al., 2015, 2018; Qi, Chen, et al., 2018; Qi, Sun, et al., 2018; Würthner, 2020; Zheng et al., 2018). Meanwhile, natural luminous with AIE properties are also known to enhance AIE chromophores' molecular library (Gu et al., 2018; He et al., 2018). As indicated by the fast-increasing publications of AIE in the past decade, the usage of AIE chromophores for biomedical applications embodies a new research edge, which creates new vitality and vigor for exploring several advanced biological systems.

Recently, numerous technologies have been using the AIE properties (Mei et al., 2018). The molecules' AIE aggregation is tuned by several parameters (electrostatic interaction, coordination interaction, hydrophobic interaction, steric hindrance, polarity, viscosity etc.), resulting in the generation of turn-on probes. Furthermore, fluorene is known to display weak emission in the solution. However, an intense emission and fluorescence color change are observed after aggregation.

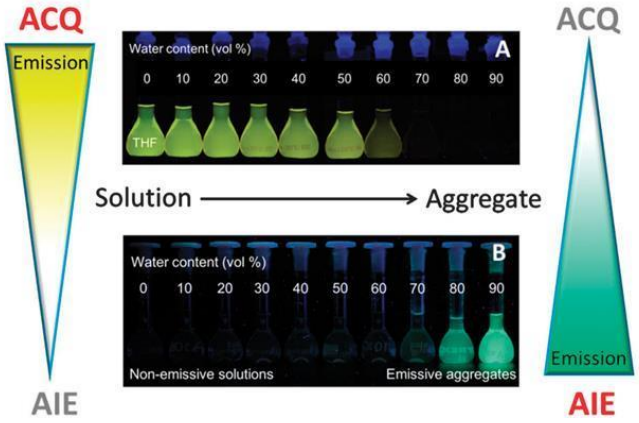

Figure 2.16. ACQ and AIE effect enhanced fluorescence with water ratio increase (Hu et al., 2014)

2.4.4. Application of Fluorene and its derivatives

Many studies have investigated Fluorene-based molecules for application in numerous fields such as electronic devices, medical fields, and optics (Kurdyukova & Ishchenko, 2012).

- ✓ Optical data storage: The usage of dyes in the optical recording is based on converting excitation energy into thermal via non-radiative degeneration. Basically, the discs are coated with fluorene dyes as recording films (Gu et al., 2018; He et al., 2018).
- ✓ Organic Light-Emitting Devices (OLEDs): The emissive flat panel displays are generally used in OLEDs. The advantage of using fluorene is the thermal, photo stability, improved packaging, and solubility. The UV or deep blue light emissions are the most alluring properties for blue light-emitting diodes application (G. Chen et al., 2021; Lucas et al., 2020; Peng et al., 2017).
- ✓ Dye-sensitized solar cells (DSSCs): The use of fluorene as photosensitizers in DSSCs leads to the injection of an electron into the conduction band resulting in the separation of charges which are transported to a charge collector (R. Y. Huang et al., 2020; Karuppasamy et al., 2018; Xu et al., 2018).
- ✓ NLO dyes in telecommunication: The transmission of data is effective through infrared laser radiation. Hence, using fluorene that displays a high 2PA cross-section leads to the energy doubling and converting the IR to visible radiation, letting more straightforward signals detection (Huo et al., 2019; F. Liu et al., 2020).

3. MATERIALS AND METHODS

3.1. Chemicals

All the chemicals used for the synthesis were purchased from Aldrich Chemical Company (USA) and Merck, and no further purification was applied. All solvents used were of analytical grade. The TLC was used to follow the reactions' progress and control the purity of the synthesized compounds. It was conducted on Merck silica gel (60 F254) plates (0.25 mm) and revealed under UV light. Melting points were determined in open capillary tubes in an Electrothermal 9200 melting point apparatus and were uncorrected.

3.2. Instrumentation

Infrared Spectroscopy (IR)

Thermo Scientific Nicolet IS 5 spectrophotometer (at Gazi University Department of Chemistry) (ν, in cm^{-1}) ATR-FTIR was used to document the spectra.

^{1}H and ^{13}C nuclear magnetic resonance spectrometer

^{1}H NMR and ^{13}C spectra were recorded on Bruker ASCEND 600 (^{1}H: 600 MHz, ^{13}C: 151 MHz) spectrometer (Sanko Tekstil Is¸letmeleri Sanayi ve Ticaret A. S. Isko Sb, Bursa, Turkey) and Bruker Avance 300 (^{1}H NMR: 400 MHz, ^{13}C: 100 MHz) spectrometer (Gazi University Department of Chemistry, Turkey) in DMSO-d_6 and $CDCl_3$. Chemical shifts are expressed in δ units (ppm) with tetramethylsilane (TMS) as the internal reference. Coupling constants (J) are given in hertz (Hz). Signals are abbreviated as follows: singlet, s; doublet, d; doublet-doublet, dd; triplet, t; multiplet, m.

Mass spectrometer

High-Resolution Mass Spectrometry (HRMS) was recorded at Gazi University, Faculty of Pharmacy, using electron ionization (EI) mass spectrometry (Waters-LCT-Premier-XELTOF (TOF-MS) instruments; in m/z (rel. %).

UV-Vis / fluorescence spectrophotometer

Ultraviolet-visible (UV-vis) absorption spectra were recorded on a SHIMADZU UV-1800 Spectrophotometer (Gazi University, Department of Chemistry, Turkey) at the maximum absorption wavelength (λ_{max}, in nm) using UV Probe 2.42 software. Fluorescence spectra were recorded on HITACHI F- 7000 FL Spectrofluorophotometer using the software FL Solutions 4.0.

Microwave irradiation (MWI)

The microwave syntheses were performed in a Milestone Start microwave reaction system.

Thermal Gravimetric Analysis (TGA)

Thermal analyses were performed using a Shimadzu DTG-60H system. The heating was carried out from 25 up to 600 ^{o}C with a rate of 10 ^{o}C per min under a dynamic nitrogen atmosphere (15 mL min^{-1}).

X-Ray Powder Diffraction Spectroscopy

A four-circle Rigaku R-AXIS RAPID-S diffractometer (equipped with a two-dimensional area IP detector) was used for crystal characterization. Graphite-monochromated Mo-Kα radiation (λ= 0.71073 Å) and oscillation scans technique with Δw = 5° for one image were used for data collection. The lattice parameters were determined by the least-squares methods based on all reflections with F2 > 2σ (F2). Integration of the intensities, correction for Lorentz and polarization effects, and cell refinement were performed using CrystalClear (Rigaku/MSC Inc., 2005) software. The structures were solved by direct methods using SHELXS-97 (Sheldrick, 2008). This allowed for most of the heaviest atoms, with the remaining non-hydrogen atoms being located from different Fourier maps calculated from successive full-matrix least-squares refinement cycles on F2 using SHELXL-97.

Electric field-induced second harmony (EFISH) measurement

The EFISH technique in chloroform was carried out at Université de Strasbourg in the Département d'Optique ultrarapid et Nanophotonique, France .to measure the second-order NLO response of the synthesized dyes, and the non-resonant wavelength was equal to 1907 nm. The second harmonic at 953 nm remains clear of the absorption bands of the

chromophores. The measurements of the EFISH were conducted following the details provided in the bibliography section (3.3).

3.3. Synthesis of Compounds

3.3.1. Synthetic procedures of π–conjugated push-pull chromophores

Synthesis of amino- substituted1,1-dicyano-2,4-diaryl-1,3-butadiene

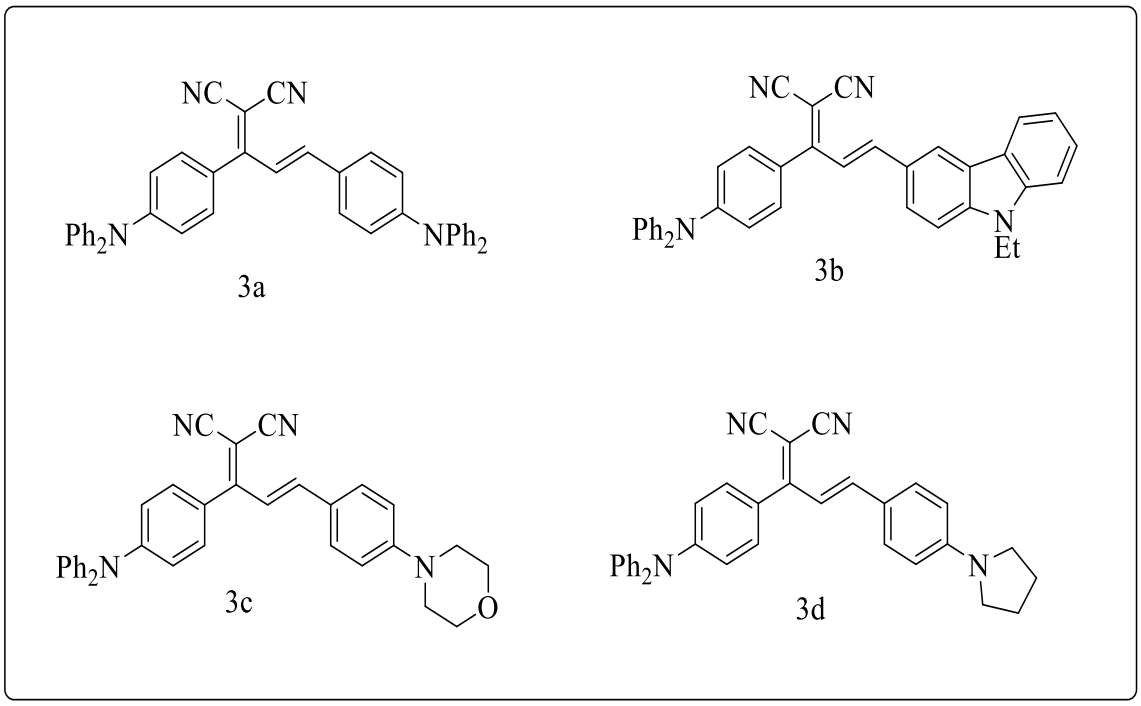

1-(4-(diphenylamino)phenyl)ethan-1-one (1)

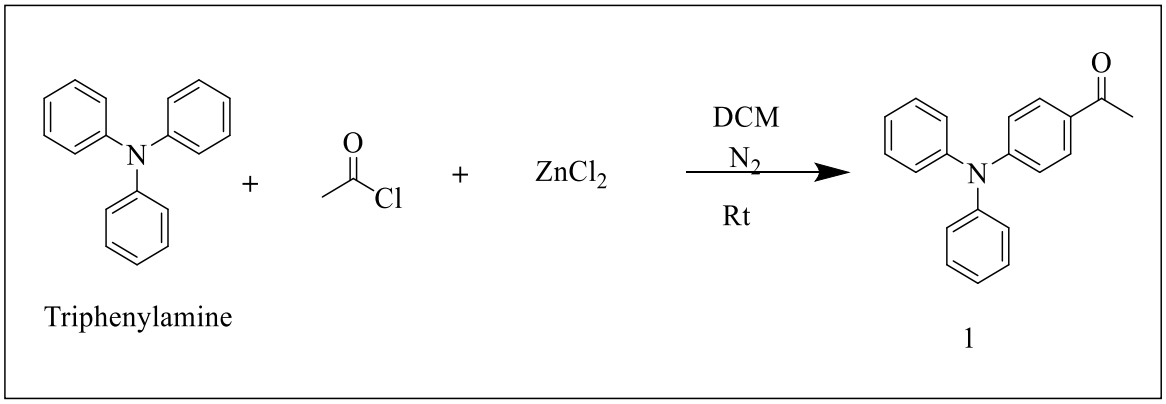

The starting compound 1 was synthesized according to the literature (H. L. Wang et al., 2007). A yellow crystal was obtained, with a high yield (5.3 g 91%). m.p =143-145°C.

Triphenylamine (5 g, 1 mol), zinc chloride (2.78 g, 1 mol), and dichloromethane (36 mL) were added slowly to a solution of acetyl chloride (1.60 g, 1.45 mL, 1 mol) in dichloromethane (4 mL) with vigorous stirring at room temperature over 5 min. The mixture was refluxed for 20 h. After cooling the mixture to room temperature, it was poured into aqueous HCl (2 M, 150 mL). The dichloromethane layer was separated and washed with water to pH 7. The dichloromethane was removed using a rotary evaporator, and the residue was purified by column chromatography over a silica gel column using petroleum ether/chloroform (v/v, 3:1) as eluent to afford (1).

2-(1-(4-(diphenylamino)phenyl)ethylidene)malononitrile (2)

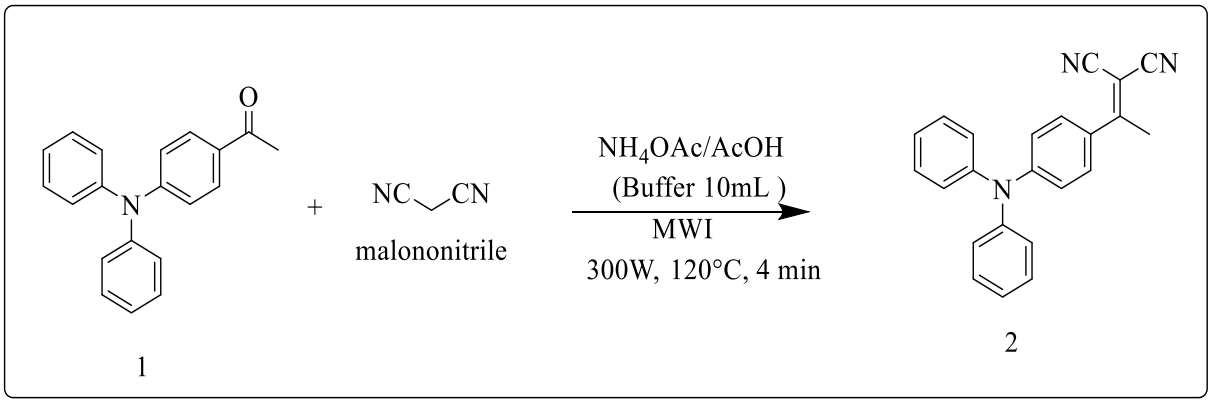

A mixture of 1 (1 mmol) and malononitrile (1 mmol) in an $NH_4OAc/AcOH$ buffer (10 mL) were irradiated in a microwave at 120°C, 300 W for 4 min. Then the mixture was cooled in an ice bath. The crude was recrystallized and washed several times with ethanol to remove acetic acid and obtain (2).

Orange crystals , Yield : (1,1 g. 94%). m.p =163-165°C. FTIR (KBr,υ cm^1): 3047,2216,1585, 1557,1489, 1318,1263,1189,1071 ^{1}H NMR (400 MHz, DMSO-d_6) δ 7.66 (d, J = 8.7 Hz, 2H), 7.42 (t, J = 7.5 Hz, 4H), 7.22 (dd, J = 17.5, 7.5 Hz, 6H), 6.86 (d, J = 8.7 Hz, 2H), 3.34 (s, 3H). ^{13}C NMR (100 MHz, DMSO-d_6) :174.9, 151.8, 145.9, 130.5, 126.8, 125.0, 118.4, 114.4, 114.7, 79.0, 23.0.

General procedure for the preparation of dyes 3a-d

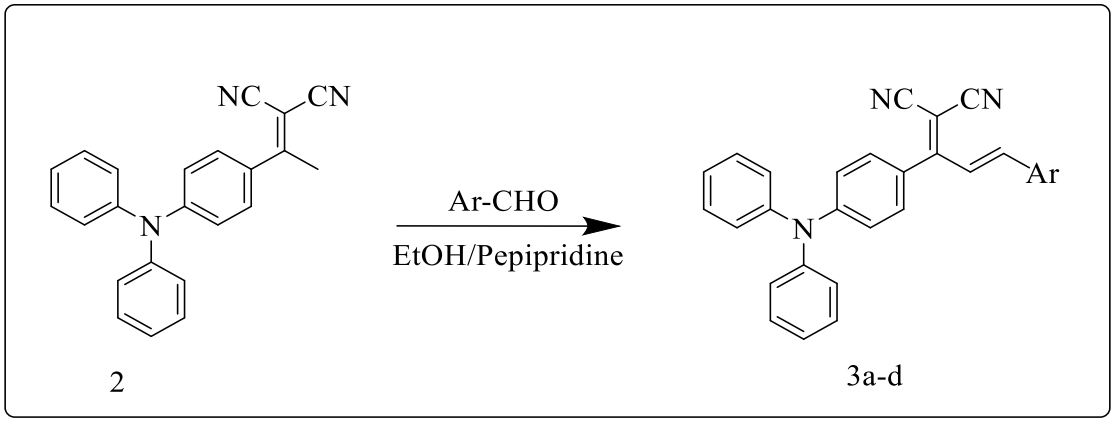

A mixture consisting of **2** (0.6 mmol) and an aldehyde (0.6 mmol) was dissolved in ethanol (10 ml), piperidine (0.1 mL) was then added, and this mixture was allowed to stir at room temperature for 12 hours under nitrogen. After 12 hours, the reaction was checked for completion by TLC. After completion of the reaction, the mass was poured over water to give a crude product. The crude mass was filtered, washed with a small volume of ethanol, and dried. This crude product was further purified by column chromatography using silica gel (120-200 mesh) with toluene as eluent.

(*E*)-2-(1,3-bis(4-(diphenylamino)phenyl)allylidene)malononitrile (3a)

Dark Red solid , Yield : (418 mg, 71%). m.p =176-178 °C. FTIR (KBr, υ cm^{-1}): 3033,2210,1573,1480,1330,1276, ^{1}H NMR (400 MHz, DMSO-d_6) δ 7.59 (d, *J* = 7.9 Hz, 2H), 7.45 – 7.35 (m, 10H), 7.31 (d, *J* = 15.3 Hz, 2H), 7.21 (d, *J* = 6.9 Hz, 7H), 7.14 (d, *J* = 7.2 Hz, 3H), 7.01 (d, *J* = 16.5 Hz, 2H), 6.93 (d, *J* = 7.6 Hz, 2H), 6.86 (d, *J* = 7.4 Hz, 2H) .^{13}C NMR (100 MHz, DMSO-d_6)146.3, 136.2, 132.5, 131.6, 131.2, 130.2, 126.5, 126.2, 120.4, 120.3 HRMS (m/z), $(M+H)^+$: $C_{42}H_{30}N_4$, calculated: 591.2543 ; found: 591.2547

(*E*)-2-(4-(diphenylamino)phenyl)-(9-ethyl-9*H*-carbazol-3-yl)allylidene)malononitrile (3b)

Red orange solid , Yield : (313 mg,69%). m.p =180-182°C. FTIR (KBr,υ cm^{-1}): 3041,2969,2216,1580,1484,1329,1099. ^{1}H NMR (400 MHz, DMSO-d_6) δ 8.58 (s, 1H), 8.24 (d, *J* = 7.7 Hz, 1H), 7.89 (d, *J* = 8.6 Hz, 1H), 7.69 (dd, *J* = 16.4, 8.5 Hz, 2H), 7.59 – 7.39 (m, 8H), 7.33 – 7.15 (m, 8H), 6.98 (d, *J* = 8.1 Hz, 2H), 4.48 (dd, *J* = 13.9, 6.9 Hz, 2H), 1.32 (t,

J = 6.8 Hz, 3H). ^{13}C NMR (100 MHz, DMSO-d_6):171.6, 151.2, 150.6, 146.3, 141.9, 140.6, 131.67, 130.4, 127.0, 126.5, 125.3, 123.3, 122.6, 121.5, 120.4, 119.3, 115.5, 110.1, 76.1, 37.8, 14.2 HRMS (m/z), $(M+H)^+$: $C_{38}H_{28}N_4$, calculated: 541.2387; found: 541.2375

(*E*)-2-(4-(diphenylamino)phenyl)-3-(4-morpholinophenyl)allylidene)malononitrile (3c)

brown solid , Yield : (300 mg,59%). m.p =165-167 °C. FTIR (KBr, υ cm^{-1}): 3031, 2841, 2215, 1577,1472.^{1}H NMR (400 MHz, $CDCl_3$) δ 7.59 (d, *J* = 8.6 Hz, 2H), 7.47 – 7.34 (m, 6H), 7.29 (d, *J* =15.3 Hz, 1H), 7.21 (d, *J* = 7.5 Hz, 6H), 7.00 (dd, *J* =11.9, 8.4 Hz, 3H), 6.95 (d, *J* = 8.7 Hz, 2H), 4.36 (t, *J* = 5.0 Hz, 2H), 3.72 (s, 2H), 3.47 – 3.41 (m, 2H), 1.05 (t, *J* = 7.0 Hz, 2H).^{13}C NMR (100 MHz,DMSO-d_6):170.6, 153.1, 150.0, 149.2, 145.8, 131.0, 129.9, 125.9, 124.0, 119.5, 118.8, 115.2, 113.8, 74.67, 65.7, 56.0, 46.6, 18.5 HRMS(m/z),$(M+H)^+$: $C_{34}H_{28}N_4O$, calculated: 509.2336; found:509.2324.

(*E*)-2-(4-(diphenylamino)phenyl)-3-(4-(pyrrolidin)phenyl)allylidene)malononitrile (3d)

Bronze solid , Yield : (450 mg,92%). m.p =150-152 °C. FTIR (KBr, υ cm^{-1}): 3000,2868, 2204 , 1569,1474,12776,1168. ^{1}H NMR (400 MHz, DMSO-d_6) δ 7.55 (d, *J* = 8.8 Hz, 2H), 7.41 (t, *J* = 7.8 Hz, 4H), 7.34 (d, *J* = 8.6 Hz, 2H), 7.24 – 7.16 (m, 7H), 6.97 (dd, *J* = 15.1, 12.1 Hz, 3H), 6.61 (d, *J* = 8.8 Hz, 2H), 3.31 (s, 4H),1.97 (s, 4H).^{13}C NMR (100 MHz,DMSO-d_6) 170.5, 150.6, 146.0, 131.7, 130.8, 129.9, 125.7, 124.8, 121.4, 119.1, 112.2, 47.5 HRMS (m/z), $(M+H)^+$: $C_{34}H_{28}N_4$, calculated: 493.2387; found:493.2369.

3.3.2. Synthesis of 1-dicyanomethylene-2-aryl-indone derivatives

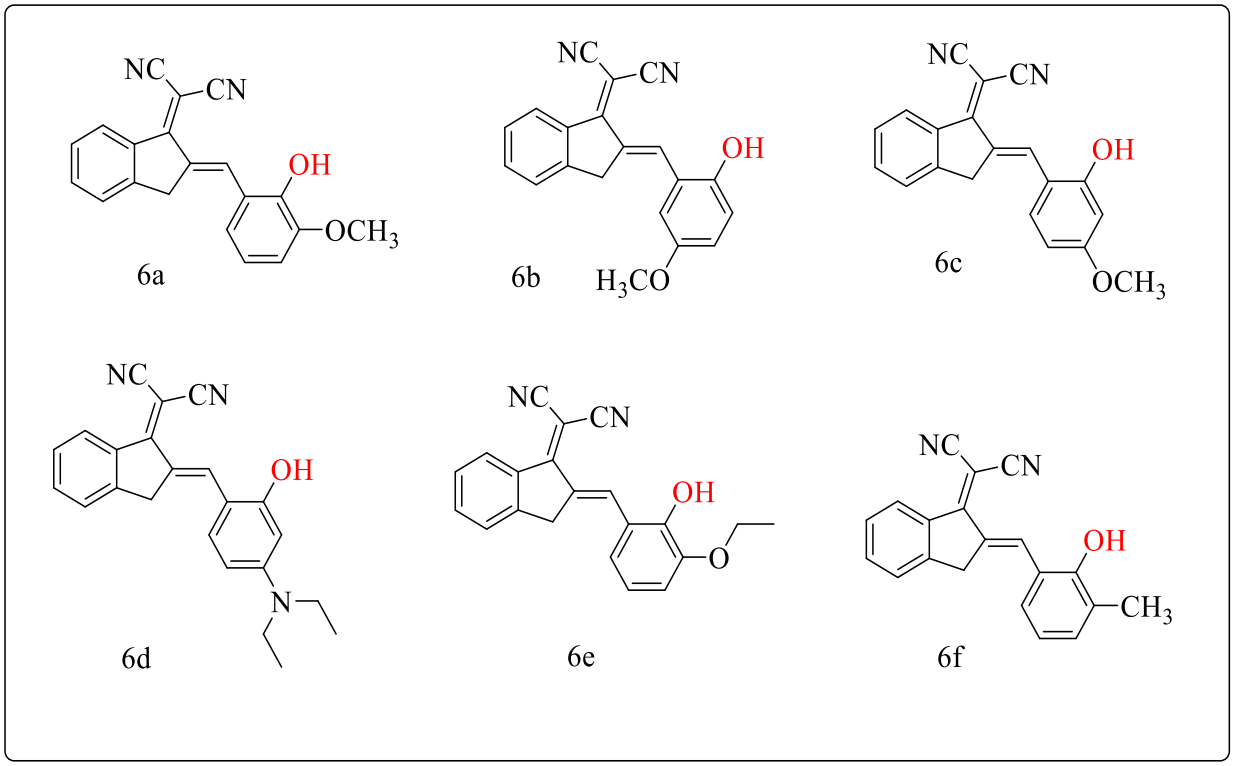

2-(2,3-dihydro-1*H*-inden-1-ylidene)malononitrile (5)

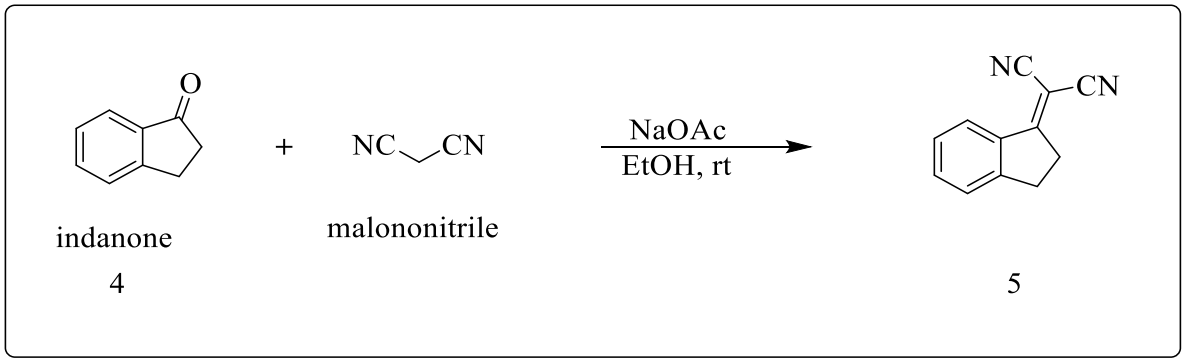

5 was synthesized according to the literature procedure (Yalçin et al., 2018b).

Anhydrous sodium acetate (6.5 g, 0.076 mol) was added to a stirred solution of 1-indone (4) (10 g, 0.075 mol) and malononitrile (5.1 g, 0.75 mol) in absolute ethanol (100 ml) at 25 °C. The reaction mixture was stirred for 2 h, diluted with water, and acidified to pH 3–4 with hydrochloric acid. The solid formed was filtered off and washed with water, followed by a small amount of ethanol. The crude product was recrystallized from ethanol to give (5) as an off-white powder.

Yield: 42%; m.p: 147-148°C (lit: 146-148°C), ^{1}H NMR (600 MHz, DMSO-d_6, δ ppm) δ 8.23 (d, *J* = 8.0 Hz, 1H), 7.72 (t, *J* = 7.5 Hz, 1H), 7.63 (d, *J* = 7.7 Hz, 1H), 7.54 (t, *J* = 7.6 Hz, 1H), 3.29 (dd, *J* = 6.2, 4.1 Hz, 2H), 3.18–3.13 (m, 2H).

General procedure for the preparation of dyes 6a-f

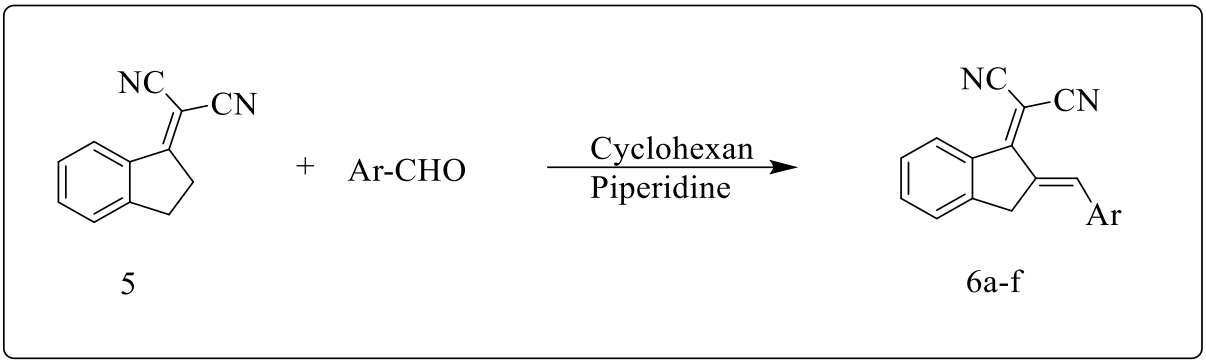

1-(dicyanomethylene)indan (180 mg, 1mmol) and appropriate salicylaldehyde (1mmol) were dissolved in cyclohexane. A few drops of piperidine were added under stirring. After adding piperidine, the reaction mixture becomes reddish. After refluxing for 3-4 h, the mixture was cooled then recrystallized using the same solvent.

(*E*)-2-(2-(2-hydroxy-3-methoxybenzylidene)-2,3-dihydro-inden-1-ylidene)malononitrile (6a)

Orange solid , Yield : (226 mg, 71%). m.p =194-197°C. FTIR (cm^{-1}): 3300.3085. 2991. 2839. 2217.1600.1578.1437. ^{1}H NMR (400 MHz, DMSO-d_6) δ 9.61 (s, 1H), 8.62 (s, 1H), 8.40 (d, *J* = 8.1 Hz, 1H), 7.68 (dt, *J* =13.7, 7.0 Hz, 1H), 7.55 (t, *J* =7.4 Hz, 2H), 7.30 (d, *J* = 7.7 Hz, 1H), 7.10 (d, *J* =8.0 Hz, 1H), 6.92 (t, *J* = 8.0 Hz, 1H), 4.07 (s, 2H), 3.84 (s, 3H).^{13}C NMR (100 MHz, DMSO-d_6)167.4, 148.5, 147.9, 146.7, 136.0, 135.8, 134.6, 131.7, 128.0, 125.9, 124.9, 122.2, 121.6, 119.2, 115.6, 113.9, 67.0, 56.1, 37.0 HRMS (m/z), (M+H)$^{+}$: $C_{20}H_{15}N_2O_2$, calculated: 315.1148; found : 315.1134.

(*E*)-2-(2-(2-hydroxy-5-methoxybenzylidene)-2,3-dihydro-inden-1-ylidene)malononitrile (6b)

Red solid , Yield : (295 mg, 94%). m.p =216-219 °C FT-IR (cm^{-1}) 3303, 2952, 2836, 2203, 1595, 1510, 1430, 1353. ^{1}H NMR (400 MHz, DMSO-d_6) δ 9.95 (s, 1H), 8.56 (s, 1H), 8.39 (d, *J* = 8.1 Hz, 1H), 7.74–7.62 (m, 2H), 7.54 (t, *J* = 7.4 Hz, 1H), 7.17 (d, *J* = 2.5 Hz, 1H), 6.96 (dd, *J* = 8.9, 2.2 Hz, 1H), 6.88 (d, *J* = 8.9 Hz, 1H), 4.10 (s, 2H), 3.77 (s, 3H). ^{13}C NMR (100 MHz, DMSO-d_6) 167.9, 152.2, 151.6, 148.4, 136.0, 135.9, 134.7, 131.7, 128.0, 126.0, 124.6, 122.1, 118.8, 116.8, 115.8, 115.3, 113.9, 66.9, 55.8, 36.6 HRMS (m/z), $(M+H)^+$: $C_{20}H_{15}N_2O_2$, calculated: 315.1129 found: 315.1134.

(*E*)-2-(2-(2-hydroxy-4-methoxybenzylidene)-2,3-dihydro-inden-1-ylidene)malononitrile (6c)

Dark red solid , Yield : (206 mg, 65,61%). m.p =212-215 °C FT-IR (cm^{-1}) : 3328, 3010, 2933, 2215, 1593, 1579, 1504, 1460. ^{1}H NMR (400 MHz, DMSO-d_6) δ 10.59 (s, 1H), 8.67 (s, 1H), 8.41 (d, *J* = 8.0 Hz, 1H), 7.80-7.61 (m, 3H),7.55 (t, *J* = 7.4 Hz, 2H), 6.59 (dd, *J* = 8.8, 2.2 Hz, 1H), 6.50 (d, *J* = 2.2 Hz, 1H), 4.07 (s, 2H), 3.79 (s, 3H). ^{13}C NMR (100 MHz, DMSO-d_6) 167.4, 163.1, 159.7, 148.2, 136.1, 134.2, 132.7, 131.6, 128.0, 126.1, 124.5, 116.0, 115.3, 106.8, 100.3, 64.8, 55.2, 37.0 HRMS (m/z), $(M+H)^+$: $C_{20}H_{15}N_2O_2$, calculated: 315.1133; found: 315.1134.

(*E*)-2-(2-(4-(diethylamino)-2-hydroxybenzylidene)-2,3-dihydro-inden-1-ylidene) malononitrile (6d)

Grey solid, Yield: (313 mg, 88.16%). m.p =223-226 °C FT-IR(cm^{-1}) : 3256, 2974, 2209, 1606, 1584, 1488, 1344, 1272. ^{1}H NMR (400 MHz, DMSO-d_6) δ 10.26 (s, 1H), 8.82 (s, 1H), 8.41 (d, *J* = 8.1 Hz, 1H), 7.68 – 7.60 (m, 3H), 7.51 (td, *J* = 8.3, 4.0 Hz, 1H), 6.40 (dd, *J* = 9.2, 2.1 Hz ,1H) , 6.19 (d, *J* = 2.1 Hz, 1H), 4.01 (s, 2H), 3.41 (q, *J* = 6.9 Hz, 4H), 1.15 (t, *J* = 7.0 Hz, 6H) .^{13}C NMR (100 MHz, DMSO-d_6) 166.0, 160.7, 152.1, 149.3, 147.8, 137.1, 133.7, 133.2, 132.0, 128.48, 127.9 , 125.6, 124.1, 117.5, 111.3, 105.5, 96.7, 59.5, 44.4, 37.1, 12.7 HRMS (m/z), $(M+H)^+$: $C_{23}H_{22}N_3O$, calculated: 356.1770; found : 356.1763.

(*E*)-2-(2-(3-ethoxy-2-hydroxybenzylidene)-2,3-dihydro-inden-1-ylidene)malononitrile (6e)

Orange solid , Yield : (230 mg, 70.12%). m.p =211-214°C FT-IR(cm^{-1}) : 3381, 2975, 2882, 2213, 1606, 1517, 1466, 1385. ^{1}H NMR (400 MHz, DMSO-d_6) δ 9.41 (s, 1H), 8.64 (s, 1H), 8.40 (d, *J* = 8.1 Hz, 1H), 7.74–7.61 (m, 2H), 7.55 (t, *J* = 7.4 Hz, 1H), 7.29 (d, *J* = 8.0 Hz, 1H), 7.08 (d, *J* = 8.0 Hz, 1H), 6.90 (t, *J* = 8.0 Hz, 1H), 4.09 (dd, *J* = 12.4, 4.7 Hz, 4H), 1.36 (t, *J* = 6.9 Hz, 3H). ^{13}C NMR (100 MHz, DMSO-d_6) 167.5, 148.6, 147.0, 146.7, 135.9, 135.9, 135. 7, 134.6, 131.6, 127.9, 126.1, 124.9, 122.3, 121.6, 119.3, 115.6, 115.4, 115.3, 67.4, 64.4, 36.9, 14.6 HRMS (m/z), $(M+H)^+$: $C_{21}H_{17}N_2O_2$ calculated: 329.1283 ; found : 329.1290.

(*E*)-2-(2-(2-hydroxy-3-methylbenzylidene)-2,3-dihydro-inden-1-ylidene)malononitrile (6f)

Orange solid, Yield: (250 mg, 83.39%). m.p=185-188°C FT-IR(cm^{-1}): 3288, 2994, 2835, 2221, 1606, 1579, 1484, 1438. ^{1}H NMR (400 MHz, DMSO-d_6) δ 9.32 (s, 1H), 8.66 (s, 1H), 8.41 (d, *J* = 8.0 Hz, 1H), 7.76 – 7.62 (m, 2H), 7.56 (t, *J* = 7.8 Hz, 2H), 7.24 (d, *J* = 7.2 Hz, 1H), 6.91 (t, *J* = 7.6 Hz, 1H), 4.07 (s, 2H), 2.22 (s, 3H). ^{13}C NMR (100 MHz, DMSO-d_6) 167.7, 155.2, 148.4, 135.9, 134.5, 133.0, 128.1, 127.7, 126.0, 125.5, 124.7, 122.9, 120.0, 115.7, 115.4, 66.8, 36.6, 16.5 HRMS (m/z), $(M+H)^+$: $C_{20}H_{15}N_2O$, calculated: 299.1170; found : 299.1184.

3.3.3. Synthetic procedures of inden-1-ylidene and fluorene

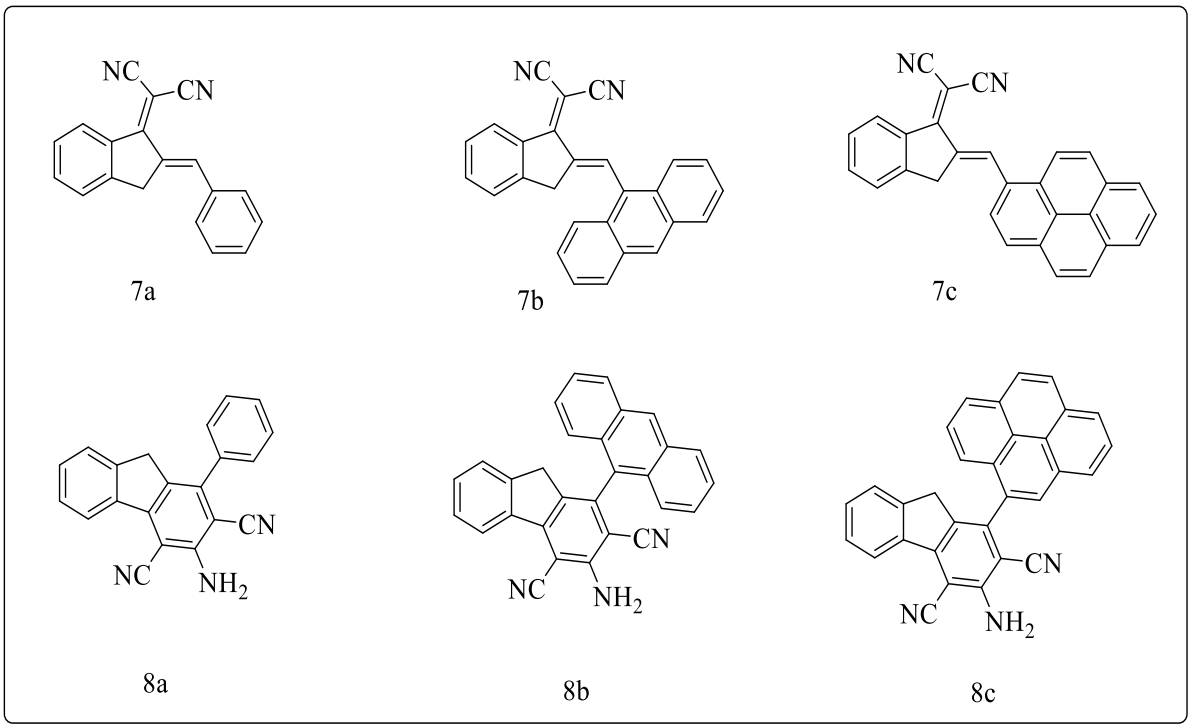

Synthesis of 1-dicyanomethylene-2-aryl-indone (7a-c)

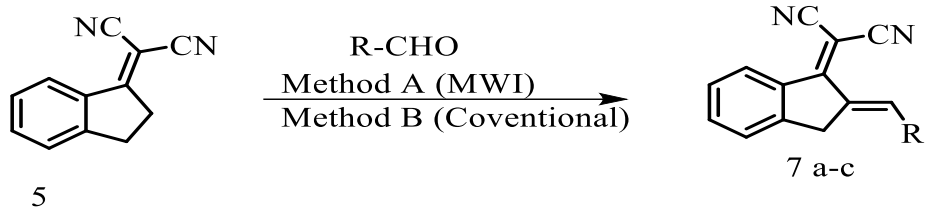

5 7 a-c

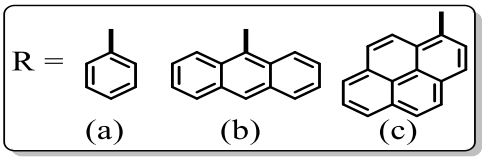

Method A-Microwave procedure: Compound 5 (1.00 mmol) and proper aldehyde (1.00 mmol) were dissolved in 10 mL ethanol. Piperidine was added as a catalyst. An MWI (300 W) heating was applied to the mix for 5 min. Then the mixture was cooled to room temperature, and the obtained precipitate was filtered and washed with ethanol.

Method B-Conventional procedure: Compound 5 (1.00 mmol) and proper aldehyde (1.00 mmol) were dissolved in cyclohexane (10 ml). Under continuous stirring, piperidine was added dropwise. Upon piperidine addition, the reaction mixture turns reddish. Next, the refluxing was carried out for ~ 3 – 4 h. Then the reaction mixture was cooled to room temperature. Finally, the obtained precipitate was filtered and recrystallized from ethanol.

(*E*)-2-(2-benzylidene-2,3-dihydro-1*H*-inden-1-ylidene)malononitrile (7a): Obtained according to Method B, Yield: (260 mg, 97%), yellow solid m.p.: 180-182 ºC (lit. m.p.: 175-177ºC) (Tao et al., 2005) FT-IR (ATR, cm^{-1}): 3069 (C-H Aromatic), 2940 (C-H Aliphatic), 2219 (CN), 1616 (C=C), ^{1}H NMR (600 MHz, DMSO-d_6, δ ppm) 8.40 (d, J = 8.1 Hz, 1H), 8.20 (s, 1H), 7.74–7.70 (m, 3H), 7.67 (d, J = 7.6 Hz, 1H), 7.60–7.53 (m, 3H), 7.53 –7.49 (m, 1H), 4.15 (s, 2H), ^{13}C NMR (151 MHz, DMSO-d_6, δ ppm) 167.5, 148.4, 137.5, 136.3, 134.9, 134.7, 130.7, 130.4, 129.2, 128.2, 126.1, 124.8, 115.4, 115.0, 36.8. HRMS m/z calculated for $C_{19}H_{13}N_2$: 269.1079, found 269.1071 $(M+H)^+$.

(*E*)-2-(2-(anthracen-9-ylmethylene)-2,3-dihydro-1*H*-inden-1-ylidene)malononitrile (7b): Obtained according to method B, Yield: (158 mg, 43%), Orange solid , m.p.: 253 - 254 ºC, FT-IR (ATR, cm^{-1}): 3049 (C-H Aromatic), 2942 (C-H Aliphatic), 2216 (CN), 1603 (C=C), ^{1}H NMR (600 MHz, DMSO-d_6, δ ppm) 8.95 (d, J = 0.8 Hz, 1H),

8.76 (s, 1H), 8.45 (d, *J* = 8.2 Hz, 1H), 8.28 – 8.10 (m, 4H), 7.64 (dd, *J* = 11.5, 4.1 Hz, 1H), 7.62 – 7.55 (m, 5H), 7.41 (d, *J* = 7.6 Hz, 1H), 3.34 (s, 2H), ^{13}C NMR (151 MHz, DMSO-d_6, δ ppm) 165.5, 147.7, 142.5, 136.3, 134.9, 133.8, 130.9, 129.0, 128.8, 128.6, 128.4, 128.2, 127.0, 126.1, 125.8, 125.4, 124.9, 114.9, 108.9, 70.1, 36.1, HRMS m/z calculated for $C_{27}H_{17}N_2$: 369.1392, found 369.1388 $(M+H)^+$.

(*E*)-2-(2-(pyren-1-ylmethylene)-2,3-dihydro-1*H*-inden-1-ylidene)malononitrile (7c):

Obtained according to Method B, Yield: (204 mg, 52%)**,** purple solid **,**m.p.: 280–281°C, FT-IR (ATR, cm^{-1}): 3043 (C-H Aromatic), 2992 (C-H Aliphatic), 2216 (CN), 1603 (C=C), ^{1}H NMR (600 MHz, DMSO-d_6, δ ppm) 9.24 (s, 1H), 8.60 (d, *J* = 9.5 Hz, 1H), 8.52 (d, *J* = 8.2 Hz, 1H), 8.47 (d, *J* = 8.8 Hz, 1H), 8.44 (d, *J* = 8.5 Hz, 1H), 8.43 – 8.37 (m, 3H), 8.33 (d, *J* = 9.3 Hz, 1H), 8.29 (d, *J* = 8.2 Hz, 1H), 8.16 (t, *J* = 7.6 Hz, 1H), 7.72 (t, *J* = 7.2 Hz, 1H), 7.66 (d, *J* = 8.0 Hz, 1H), 7.61 (t, *J* = 7.7 Hz, 1H), 3.86 (s, 2H). ^{1}H NMR (600 MHz, $CDCl_3$, δ ppm) δ 9.34 (s, 1H), 8.66 (d, *J* = 7.6 Hz, 1H), 8.39 (d, *J* = 9.0 Hz, 1H), 8.29–8.21 (m, 5H), 8.18 (d, *J* = 8.7 Hz, 1H), 8.11 (d, *J* = 8.6 Hz, 1H), 8.07 (t, *J* = 7.6 Hz, 1H), 7.58 (t, *J* = 7.3 Hz, 1H), 7.48 (t, *J* = 8.0 Hz, 1H), 7.44 (d, *J* = 7.1 Hz, 1H), 4.05 (s, 2H). ^{13}C NMR (151 MHz, $CDCl_3$, δ ppm) 147.8, 138.7, 136.9, 135.4, 135.4, 134.7, 134.6, 134.5, 132.8, 131.3, 131.0, 130.5, 129.9, 129.3, 129.3, 128.4, 127.6, 127.4, 126.9, 126.7, 126.5, 126.4, 126.4, 125.5, 124.9, 124.7, 123.3, 118.7, 37.4. HRMS m/z calculated for $C_{29}H_{17}N_2$: 393.1392, found 393.1384 $(M+H)^+$.

Synthesis of 3-amino-1-aryl-9*H*-fluorene-2,4-dicarbonitrile (8a-c)

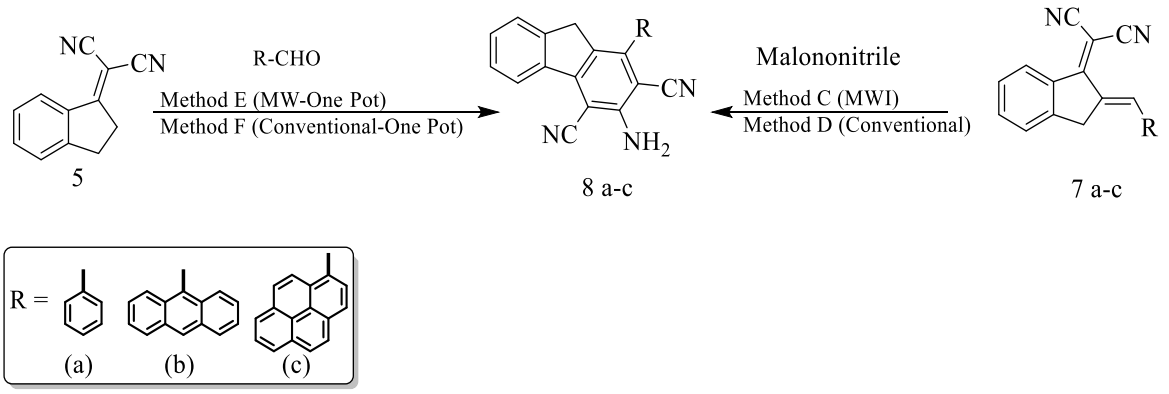

Method C-Microwave procedure: Compound 7a-c (1.00 mmol) and malononitrile (1.50 mmol) were dissolved in acetonitrile (10 mL). Pyrrolidine (1.20 mmol) as a catalyst was gradually added. MWI (300 W) was used to heat the mixture to 78°C for 5 min. The reaction

mixture was then chilled to room temperature, and the obtained precipitate was filtered and washed with ethanol.

Method D-Conventional procedure: Compound 7a-c (1.00 mmol) and malononitrile (1.50 mmol) were dissolved in acetonitrile (10 ml). Pyrrolidine (1.20 mmol) as a catalyst was gradually added. The solution was kept under stirring at ambient temperature for 45. The obtained precipitate was filtered and washed with ethanol.

Method E- Microwave one-pot procedure: Compound 5 (1.00 mmol), appropriate aldehyde (1.50 mmol), and malononitrile (1.50 mmol) were dissolved in (15 mL) acetonitrile. Pyrrolidine (1.20 mmol) was gradually added. MWI (300 W) was used to heat the mixture to 78^{o}C for 5 min. The reaction mixture was then cooled to ambient temperature, and the obtained precipitate was filtered and washed with ethanol.

Method F- Conventional one-pot procedure: Compound 5 (1.00 mmol), proper aldehyde (1.50 mmol), and malononitrile (1.50 mmol) were dissolved in acetonitrile. Pyrrolidine (1.20 mmol) was gradually added. The solution was kept under stirring for 45 min at ambient temperature. The obtained precipitate was filtered and washed with ethanol.

3-amino-1-phenyl-9*H*-fluorene-2,4-dicarbonitrile (8a): Obtained according to Method F, the compound was purified by column chromatography with toluene as an eluent. Yield: (126 mg, 41%), golden solid m.p.: 299-300^{o}C (lit. m.p.: 303-305°C) (Mirek & Milart, 1986), FT-IR (ATR, cm^{-1}): 3478 (N-H), 3373 (N-H), 3058 (C-H Aromatic), 2996 (C-H Aliphatic), 2204 (CN), 1627(C=C), ^{1}H NMR (600 MHz, DMSO-d6, δ ppm) 8.37–8.31 (m, 1H), 7.62 (dt, J = 6.4, 2.3 Hz, 1H), 7.59-7.56 (m, 4H), 7.56-7.52 (m, 2H), 7.50 (td, J = 7.3, 1.4 Hz, 1H), 6.72 (s, 2H), 3.68 (s, 2H), ^{13}C NMR (151 MHz, DMSO-d_6, δ ppm) 153.5, 146.7, 146.5, 146.3, 137.6, 136.4, 130.4, 129.8, 129.1, 128.7, 128.6, 127.4, 125.6, 121.9, 116.3, 115.9, 94.4, 87.2, 35.3, HRMS m/z calculated for $C_{21}H_{14}N_3$: 308.1188, found 308.1175 $(M\text{-}H)^{+}$.

3-amino-2,4-dicyano-1-(anthracen-9-yl)-9*H*-fluorene (8b) : Obtained according to method F, the compound was purified by column chromatography with toluene as an eluent .Yield: (130mg, 32%), light red solid m.p.: 367 - 368 ^{o}C, FT-IR (ATR, cm^{-1}): 3481 (N-H), 3373 (N-H), 3055 (C-H Aromatic), 2990 (C-H Aliphatic), 2210 (CN), 1630 (C=C), ^{1}H NMR (600 MHz, DMSO-d_6, δ ppm) 8.85 (s, 1H), 8.43 (d, J = 8.0 Hz, 1H), 8.25 (d, J = 8.5 Hz, 2H), 7.61-7.55 (m, 3H), 7.53 (d, J = 8.5 Hz, 2H), 7.51-7.41 (m, 4H), 6.91 (s, 2H), 3.14 (s,

2H).[13]C NMR (151 MHz, DMSO-d_6, δ ppm) 153.7, 147.1, 145.8, 143.7, 137.8, 132.1, 130.9, 129.9, 129.9, 128.8, 128.5, 128.4, 127.6, 127.2, 125.8, 125.7, 124.7, 122.1, 115.9, 115.8, 96.5, 88.3, 34.8, HRMS m/z calculated for $C_{29}H_{18}N_3$: 408.1501, found 408.1494 $(M-H)^+$.

3-amino-2,4-dicyano-1-(pyren-1-yl)-9*H*-fluorene (8c): Obtained according to method F, the compound was purified by column chromatography with toluene as an eluent . Yield: (129 mg, 30%), brown solid m.p.: 327 - 328 °C, FT-IR (ATR, cm^{-1}): 3484 (N-H), 3393 (N-H), 3037 (C-H Aromatic), 2890 (C-H Aliphatic), 2213 (CN), 1618 (C=C), ^{1}H NMR (600 MHz, DMSO-d_6, δ ppm) 8.48 (d, J = 7.8 Hz, 1H), 8.42 (t, J = 8.3 Hz, 2H), 8.35 (d, J = 7.7 Hz, 1H), 8.32 (dd, J = 3.5, 1.5 Hz, 2H), 8.22-8.08 (m, 3H), 7.75 (d, J = 9.2 Hz, 1H), 7.57 (dd, J = 7.9, 5.7 Hz, 1H), 7.48 (s, 2H), 6.89 (s, 2H),[13]C NMR (151 MHz, DMSO-d_6, δ ppm) 153.5, 146.8, 146.1, 145.6, 137.8, 131.8, 131.3, 131.3, 130.8, 130.3, 129.8, 128.7, 128.2, 127.6, 127.5, 127.3, 126.7, 126.6, 125.9, 125.7, 125.0, 124.0 123.9, 123.8, 122.1, 120.0, 116.1, 101.1, 95.9, 87.8, 35.2. HRMS m/z calculated for $C_{31}H_{18}N_3$: 432.1501 found 432.1489 $(M-H)^+$.

4. RESULTS AND DISCUSSION

4.1. Push-Pull Chromophores Type π–Conjugated

4.1.1. Introduction

Push-pull compounds have attracted considerable attention due to their optoelectronic properties. They are compounds containing an electron donor group (D) connected to an electron acceptor group (A) through a (π) -conjugated bridge (D-π-A). The majority of push-pull structures display fluorescence properties in solution. The modification of D π or A can lead to the tunning of the emission properties. The red-shift in both absorption and emission is due to the ICT increase. However, in solid-state face-to-face π-π intermolecular interactions also the non-radiative processes frequently lead to aggregation caused quenching (ACQ). The D-π-A chromophores rich in nitrile and Triphenylamine are well established as good solid-state fluorophores, finding application in OLEDs and solid-state lasers luminescent sensors. Furthermore, the majority of chromophores exhibiting second-order NLO have a push-pull structure. The second-order NLO compounds are primarily applied in second-harmonic generation, allowing the red light to change to blue/green laser. The second-order NLO response can explain the optical signal process and data storage application. However, for D-π-A structures, the ICT is responsible for the NLO phenomena. It is well established that compounds containing 1,1-dicyano-2,4-diaryl-1,3-butadiene scaffold display a bright, intense color favorable for textile coloring. These compounds' substitution by an electron-donor group results in an exciting NLO response. Sekar and coworkers reported substituting 2 amino groups in the para position of phenyls in 1,1-dicyano-2,4-diphenyl-1,3-butadiene. The ICT occurs from amino acids group of phenyl in C4 to cyano groups. In this part, the photophysical properties, in both solid and liquid state emission, of a series of 1,1-dicyano-2,4-diaryl-1,3-butadiene derivatives 3a-d that various amino groups substitute on both sides will be reported.

4.1.2. Synthesis and characterization

3a-d synthetic routes are presented in Figure 4.1. First, 1-(4-(diphenylamino)phenyl)ethan-1-one (1) was converted to 2-(1-(4-(diphenylamino)phenyl)ethylidene)malononitrile (2) in the presence of NH_4OAc/AcOH via microwave irradiation (MWI) by enhanced synthetic methods with higher yield (Raikwar et al., 2019). Final products (3a-d) were obtained by the

piperidine-catalyzed condensation reaction of 2 and corresponding aldehydes in boiling ethanol. The mechanism for the formation of malononitriles is presented in Figure 4.2.

FTIR, NMR, and mass spectroscopic techniques were used to verify the synthesized dyes' structures. The ^{1}H NMR spectra proved that all compounds have a vinylic coupling constant (J_{HH} =15-16 Hz) of the olefinic protons, proving that only the formation of *E* stereoisomer could be identified.

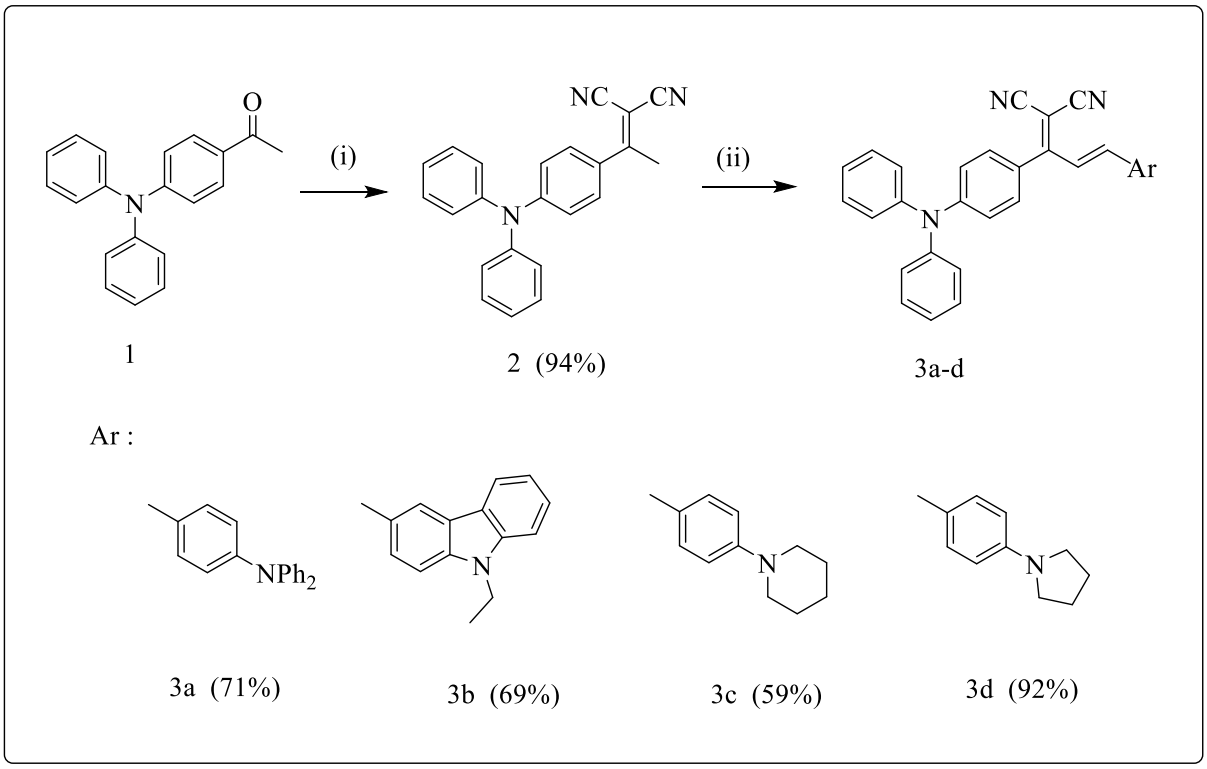

Figure 4.1. Synthesis of 1,1-dicyano-2,4-diaryl-1,3-butadiene derivatives (3a-d).(i) malononitrile, NH_4OAc/AcOH, MWI (ii) Ar-CHO, ethanol, piperidine.

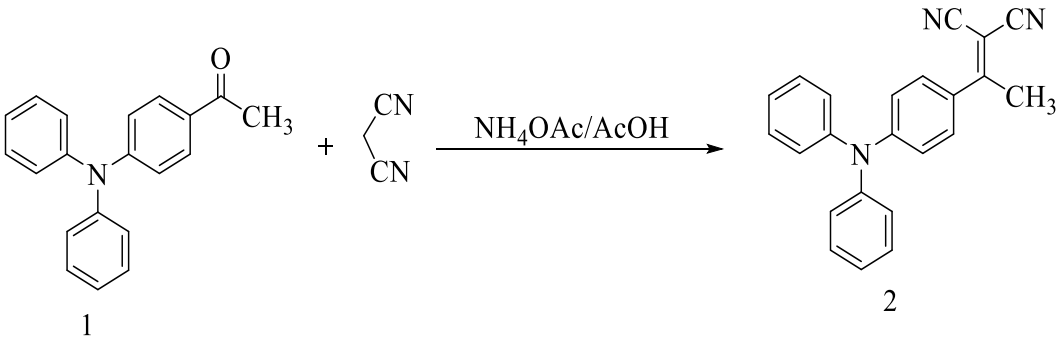

1

2

Mechanism :

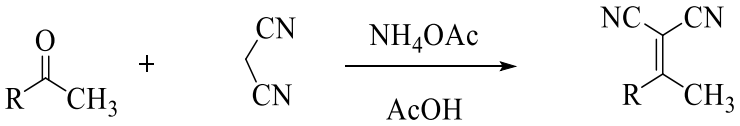

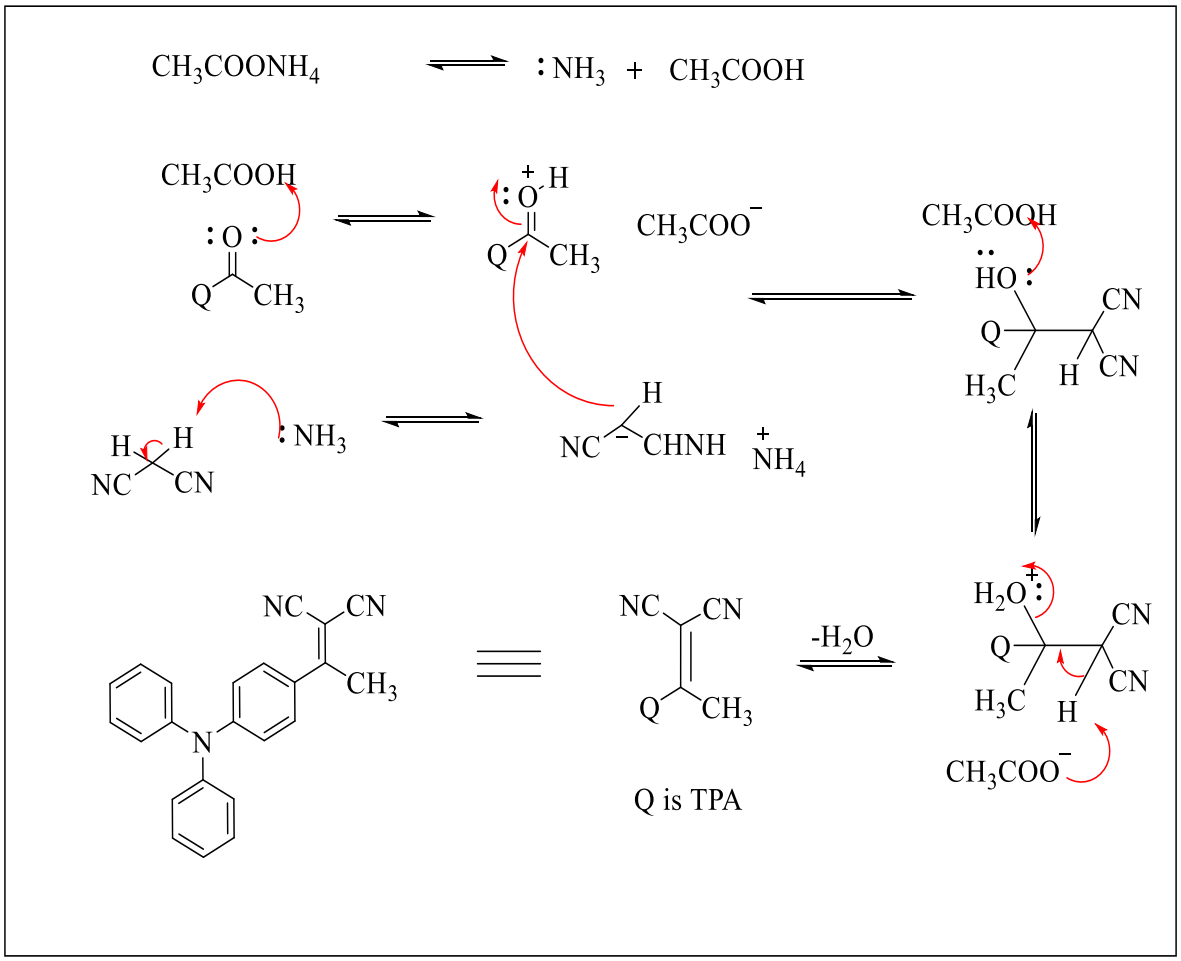

Figure 4.2. The plausible mechanism for the synthesis of 1,1-dicyano-2-aryl-propene (2)

4.1.3. Photophysical properties

3a-d UV/Vis and photoluminescence (PL) spectroscopic data were measured in $CHCl_3$ at room temperature. The obtained results are given in Table 4.1, and normalized UV/Vis and PL spectra are shown in Figure 4.3. Two absorption bands are detected for all chromophores, first at 300 nm and the second at 450-510 nm range ascribed to charge transfer π-π* transition. The presence of diphenylamino and pyrrolidinyl derivatives in 3a and 3d resulted in high red-shifted absorption compared to carbazole and morpholine substituted compounds 3b and 3c. 3d displays a considerable hyperchromism for the charge-transfer band, also ε value was 2-1.5 times high compared to 3a-c. An orange-red emission was observed for 3a-d in chloroform solution, and the quantum yield was < 0.10. Furthermore, 3d exhibited blue-shift emission spectra compared to 3a-c. Hence, the low steric hindrance with the pyrrolidine fragment leads to a downward stokes shift for 3d, decreasing the amino group's torsional twist in the ground state. The diphenylamino derivative 3a (Φ_F = 0.10) displays the highest quantum yield. Agreeing to the literature data, the analog of 3a without NPh_2 substituent on phenyl ring in the C2 position (V. D. Gupta et al., 2013). It seems that this diphenylamino group generates a blue shift in absorption (9 nm) but a redshift (25 nm) in emission (Figure 4.4).

Table 4.1. UV-Vis absorption and photoluminescence (PL) data of compounds 3a-d in $CHCl_3$ solution.

Compound	λ_{abs} (nm)	ε (mM^{-1} cm^{-1})	λ_{em} (nm)	Φ_F	Stokes Shift (cm^{-1})	Brightness (mM^{-1} cm^{-1})
3a	304, 493	40.5, 49.0	644	0.10	4760	4.9
3b	297, 456	31.7, 36.1	654	0.046	6640	1.7
3c	299, 461	24.4, 36.2	659	0.044	6520	1.6
3d	303, 507	40.4, 72.2	594	0.023	2890	1.7

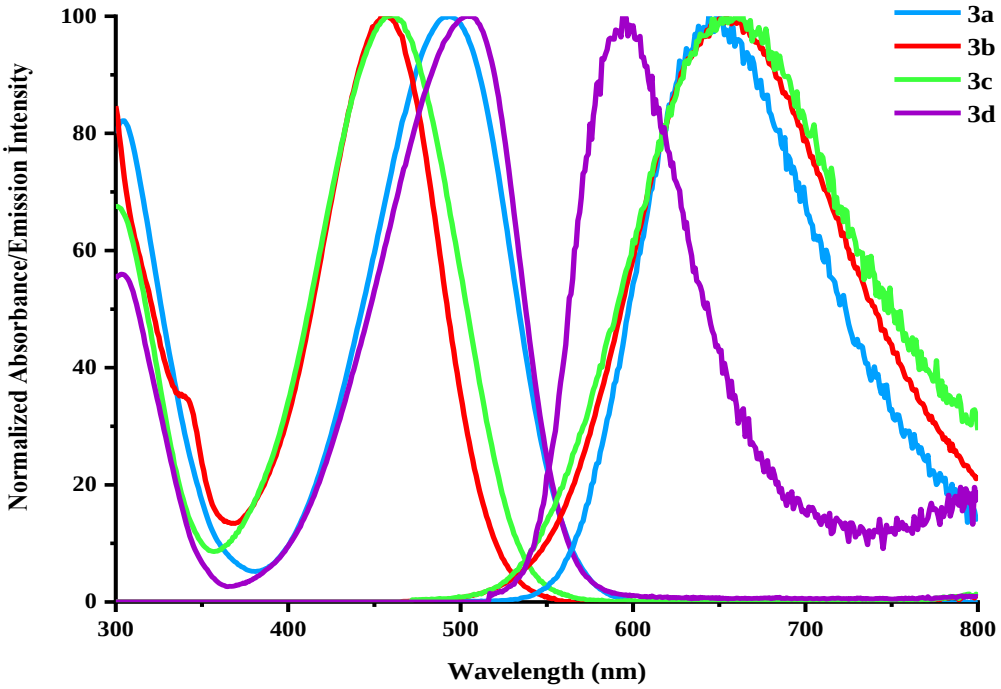

Figure 4.3. Normalized absorption (solid lines) and emission (dashed lines) spectra of compounds 3a-d in chloroform solution.

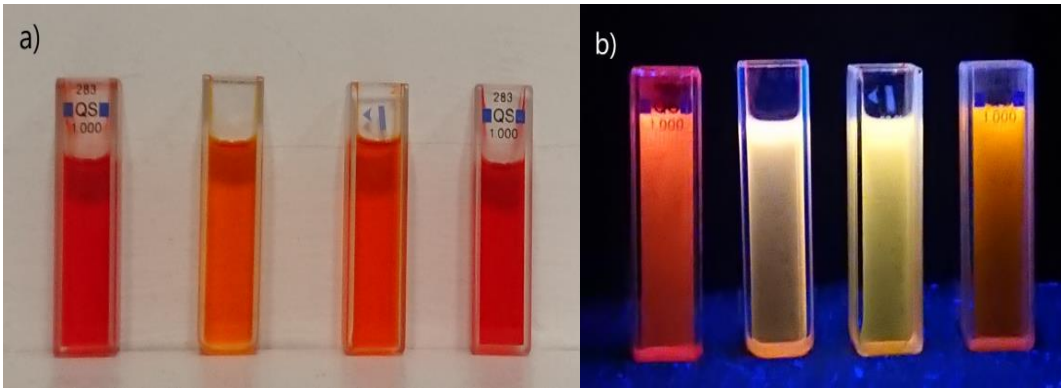

Figure 4.4. $CHCl_3$ solution of 3a-d (from left to right) under white light (part a) and under UV lamp irradiation (part b) (c = 3-6 10^{-4} M)

It is well known that fluorophores displaying ICT present strong positive solvatochromism, while their absorption spectra are less impacted by the solvent (Fecková et al., 2018). Indeed highly polar excited states of push-pull chromophores are stabilized by polar solvents. Therefore, the emission spectra of compounds 3a-d were recorded in a series of aprotic solvents of increasing polarity. The results are presented in Table 4.2. The normalized

spectra of compound 3a are shown in Figure 4.5. As anticipated, a considerable positive emission solvatochromism is seen for all compounds.

It should be noted that in the case of compounds 3a-c**,** the emission is fully quenched in a solvent of higher polarity than DCM. However, emission in acetone and MeCN can be seen in the case of compound 3d. For all compounds in chlorinated solvents ($CHCl_3$ or DCM), the emission intensity is the highest (Figure 4.7, Figure 4.8, and Figure 4.9)

Table 4.2. Emission solvatochromism of compounds 3a-d in various aprotic solvents.

Compound	*n*-heptane	Toluene	1,4-dioxane	THF	$CHCl_3$	DCM	Acetone	MeCN	Solid State
E_T30 (kcal/mol)	30.9	33.9	36.0	37.4	39.1	40.7	42.2	45.6	(powder)
3a	555	589	606	650	644	673	-[a]	-[a]	657
3b	550	587	620	667	654	694	-[a]	-[a]	663
3c	538	580	602	607	659	697	-[a]	-[a]	688
3d	539	567	577	605	594	607	623	628	706

[a]no emission detected

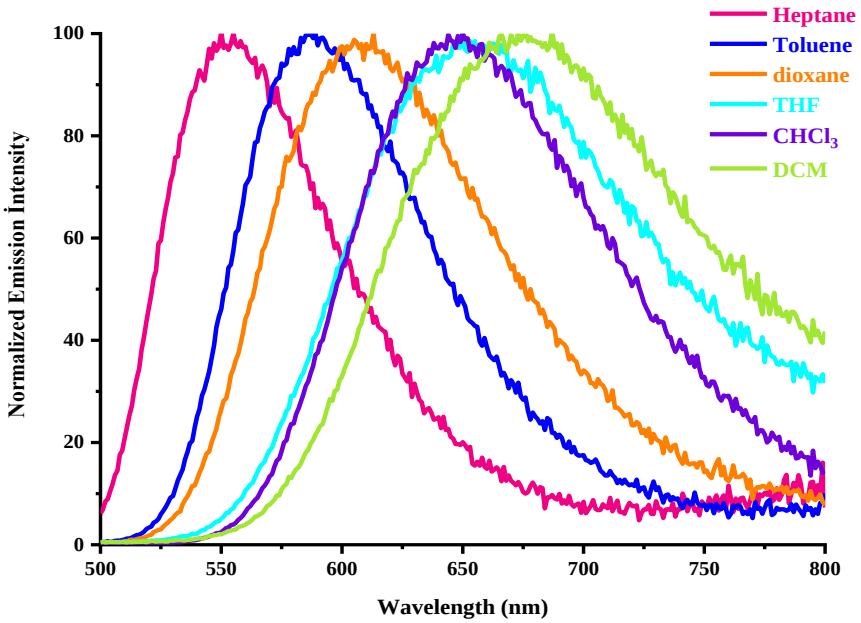

Figure 4.5. Normalized emission spectra of 3a in different aprotic solvents

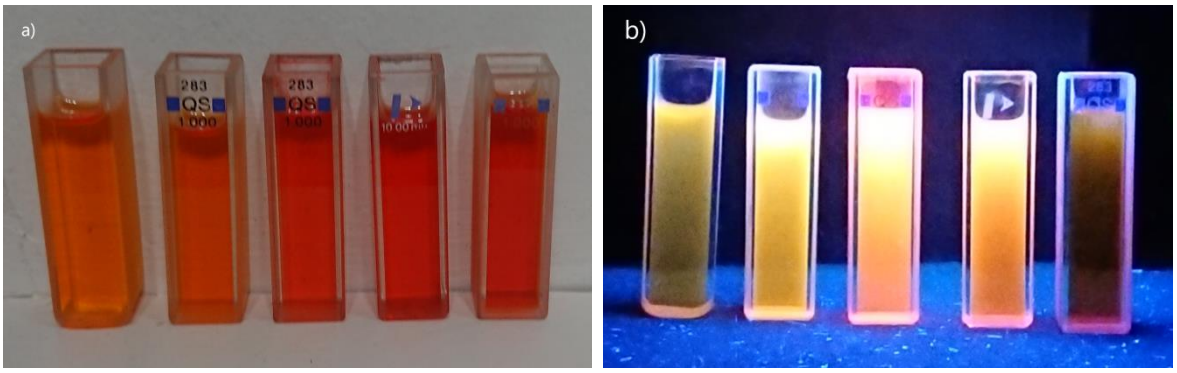

Figure 4.6. Solution of 3b (from left to right: toluene, 1,4-dioxane, $CHCl_3$, DCM and MeCN under white light (part a) and under UV lamp irradiation (part b) (c = 1.9 10^{-5} M)

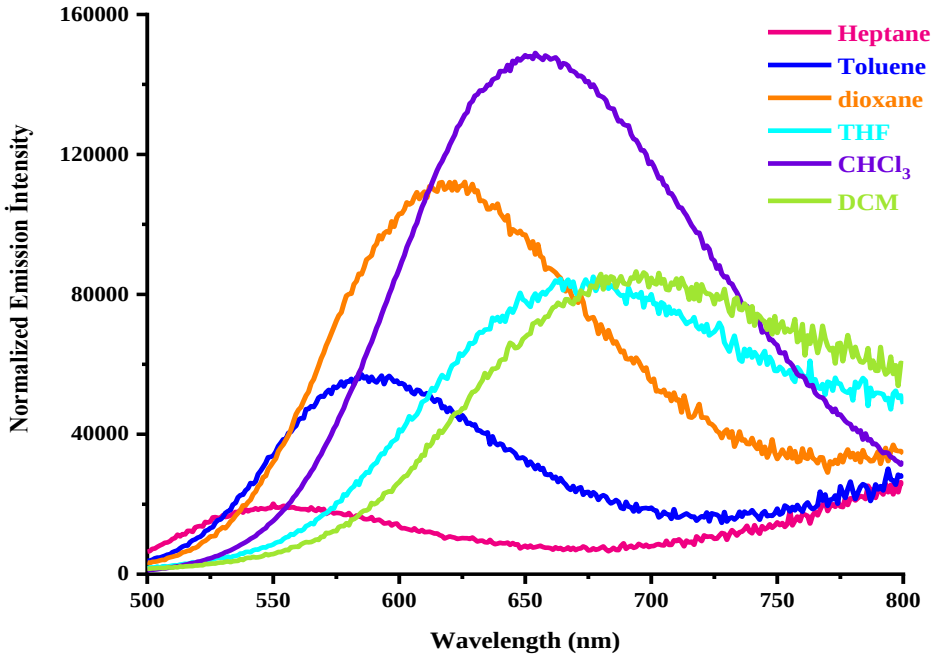

Figure 4.7. Compound 3b emission spectra in different aprotic solvents (c = 5.10^{-6} M)

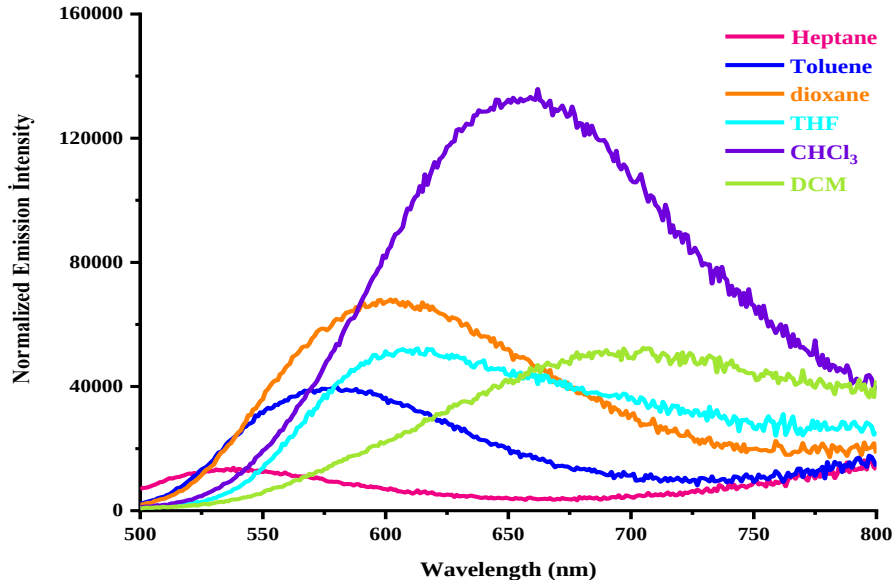

Figure 4.8. Compound 3c emission spectra in different aprotic solvents (c = 5.10^{-6} M)

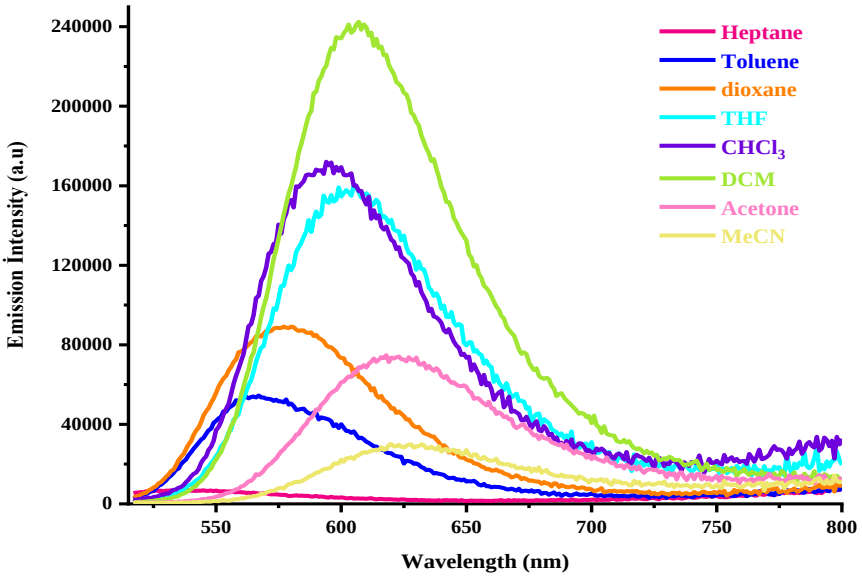

Figure 4.9. Emission spectra of compound 3d in various aprotic solvents (c = 5.10^{-6} M)

Strong red-near IR emission was displayed in the solid-state (powder) for all compounds Figure 4.10 and Figure 4.11. The most red-shift emission was displayed by **3d** with λ_{em} = 706 nm. 3b and 3c emission spectra were considerably wider and presented a full half-width maximum (FHWM) around 3500 cm^{-1} in both cases.

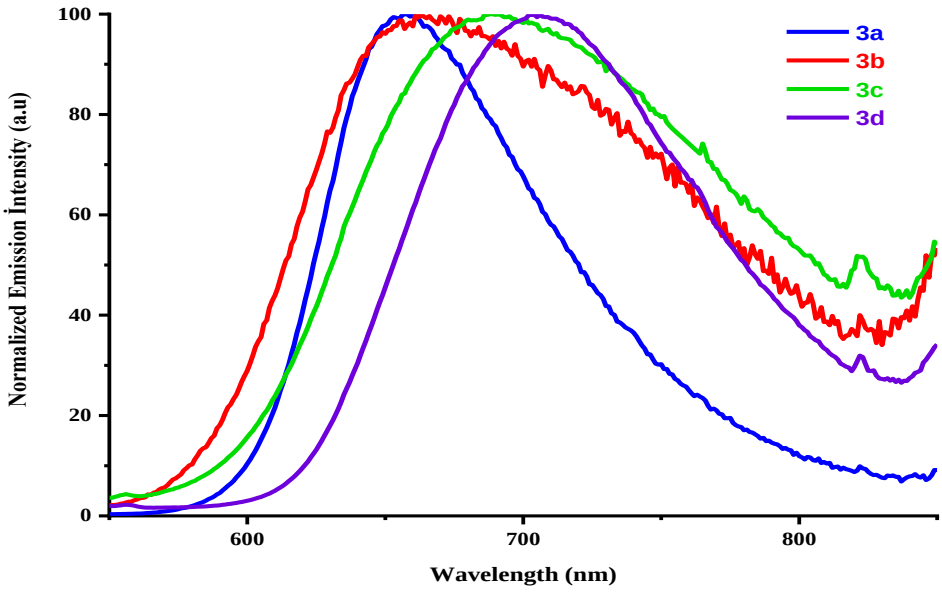

Figure 4.10. Normalized solid-state (powder) spectra of compounds 3a-d.

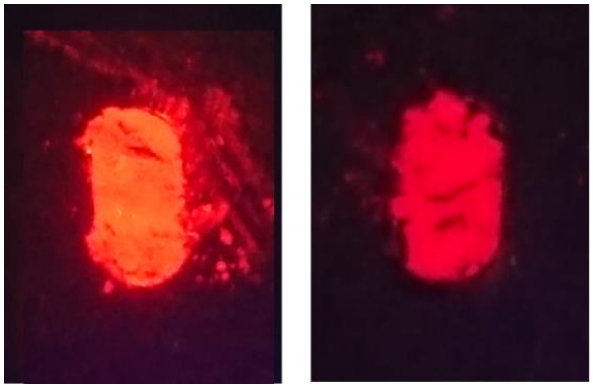

Figure 4.11. Emission of compounds **3a** and **3c** in solid-state (powder). The photograph was taken in the dark upon irradiation with a hand-held UV lamp (λ_{em} = 366 nm)

4.1.4. Second order NLO properties

The electric field-induced second harmonic generation (EFISH) method was used at a non-resonant incident wavelength of 1907 nm to investigate the second-order NLO properties in chloroform. Hence, the second harmonic absorption band of the chromophores was at λ= 953 nm. The calculation for $\mu\beta$ values ($\mu\beta_0$) levels was also performed. Table 4.3 regroups the obtained results. The ground and excited states are both polarized in the same direction, and also the excited state is more polarized compared to the ground state. These results are in accord with the positive results obtained from the emission solvatochromism. High values of $\mu\beta_0$ are noted for all the obtained chromophores. In agreement with the red-shifted absorption maxima detected for 3d, signifying a stronger ICT, this compound demonstrates the highest NLO response.

Table 4.3. Results for EFISH measurements for compounds 3a-d.

	3a	3b	3c	3d
$\mu\beta$ (10^{-48} esu)[a]	950	900	800	1300
$\mu\beta_0$ (10^{-48} esu)[b]	650	650	580	870

[a] $\mu\beta(2\omega)$ at 1907 nm in $CHCl_3$. Molecular concentrations used for the measurements were in the range of 10^{-3} to 10^{-2} M, $\mu\beta \pm 10\%$ [b] Two level corrected $\mu\beta$ values ($\mu\beta_0$) (Ledoux & Zyss, 1982).

4.1.5. Thermal stability

The thermogravimetric analyses (TGA) were conducted to investigate the thermal stability of the obtained chromophores. As shown in Figure 4.12, all compounds exhibited no

considerable weight loss up to 300ºC. Furthermore, the onset decomposition temperature (Td) of compounds 3a-d are 347°C (96%), 340°C (97%), 352°C (95%) and 339°C (94%), respectively. These chromophores present high thermal stability, compatible with the used material fabrication process.

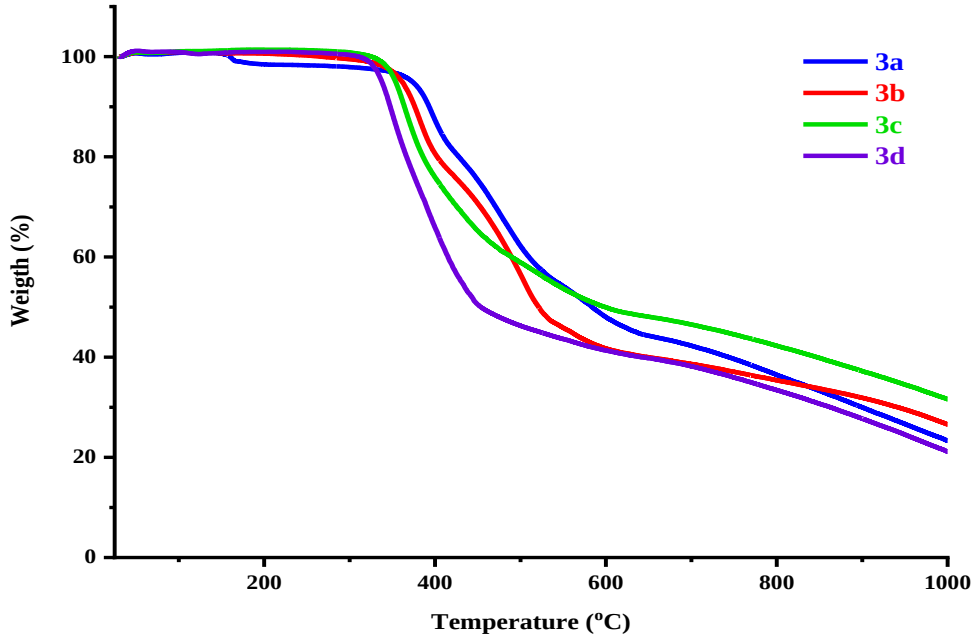

Figure 4.12. TGA curves of chromophores 3a-d under nitrogen gas in the temperature range of 25-600°C at a heating rate of 10 °C min^{-1}.

4.2. 1-dicyanomethylene-2-aryl-indone derivatives for Chemosensing

4.2.1. Introduction

Optical Chemosensors have attracted much interest as anions sensors due to their ability to change color upon detecting harmful anions (Y. Feng et al., 2018; Mahalakshmi et al., 2021; Stock et al., 2019). Furthermore, single optical molecule probes able to detect several cations or anions have been studied intensively because of the possibility of instantaneous analysis of these analytes without using analytical techniques (Chemchem et al., 2018; Lee et al., 2010). F^- and CN^- anions are among the most anions that ought to be monitored due to their crucial roles in our daily lives. Cyanide is mainly used in organic chemicals and polymer products such as nylon, acrylic plastics, and nitriles, making its usage faster. In order to ensure the safety of people in contact with cyanide, a straightforward approach for its detection is needed. Likewise, fluoride is used in dental care and osteoporosis treatment

resulting in a high dosage, which is hazardous (Chadwick, 1988; Kirk & Kirk, 1991). Chemosensors with acidic NH and OH groups have attracted much interest in F^- sensing because of the electronegativity of F^-, which results in the formation of a strong hydrogen bond. CN^- sensing was also achieved via numerous approaches like chemodosimeters, hydrogen bonding, etc. (S. Park & Kim, 2010; Saha et al., 2010).

Recently, the design and synthesis of fluorophores for CN^- sensing have attracted much interest. Donor-π- acceptor chromophores have become exceptional molecules used for anion sensing (Chemchem et al., 2018). The sensors' selectivity and sensitivity can be tuned by adding CN^- to the imine group. The design and synthesis, as well as the effect of the substitution on the sensitivity and selectivity, were reported by our group (Chemchem et al., 2018; Yahaya et al., 2019).

In this part, 1-dicyanomethylene-2-aryl-indone derivatives were synthesized. The compounds' characterization was performed using IR, UV-vis, ^{1}H NMR, ^{13}C NMR, and HRMS techniques. The obtained fluorophores were tested for anions sensing in several experimental conditions: solvents, pH, substitution, and thermal stabilities of the compounds were also studied.

4.2.2. Synthesis and photophysical properties of the chemosensors 6a-f

The chemosensors (6a-f) were easily obtained at high yields (70-95%) by coupling 1-dicyanomethyleneindane (1) and salicylaldehyde derived (a-f). The synthetic routes are dissipated in Figure 4.13. FTIR, ^{1}H-NMR, ^{13}C-NMR, and HRMS analyses were carried out to characterize the structure of the obtained chemosensors. The characterization spectra are displayed in the annex.

The obtained chemosensors are solids and can be partially dissolved in the selected solvent having different polarities: Dimethyl sulfoxide (DMSO 0.44), Methanol (MeOH 0.76), Dichloromethane (DCM 0.31), Tetrahydrofuran (THF 0.21), Chloroform ($CHCl_3$ 0.26), and Toluene (PhMe 0.099). However, chemosensors 6b was not soluble in $CHCl_3$ and PhMe, while 6d was not soluble in toluene. Nearly all the synthesized chemosensors exhibited a maximum absorption band in the visible range (Figure 4.15). The obtained results did not show the expected results with the increase of the solvents' polarity except for 6d**,** which displays a bathochromic shift (21nm). This behavior is due to the strong electron-donating

diethylamino group (NEt_2) in the 4-position of salicylidene moiety. The photophysical properties results are summarized in Table 4.4. Furthermore, all the chemosensors displayed a negligible fluorescence except for 6d**,** which displays a λ_{em} around 500 nm (Figure 4.16).

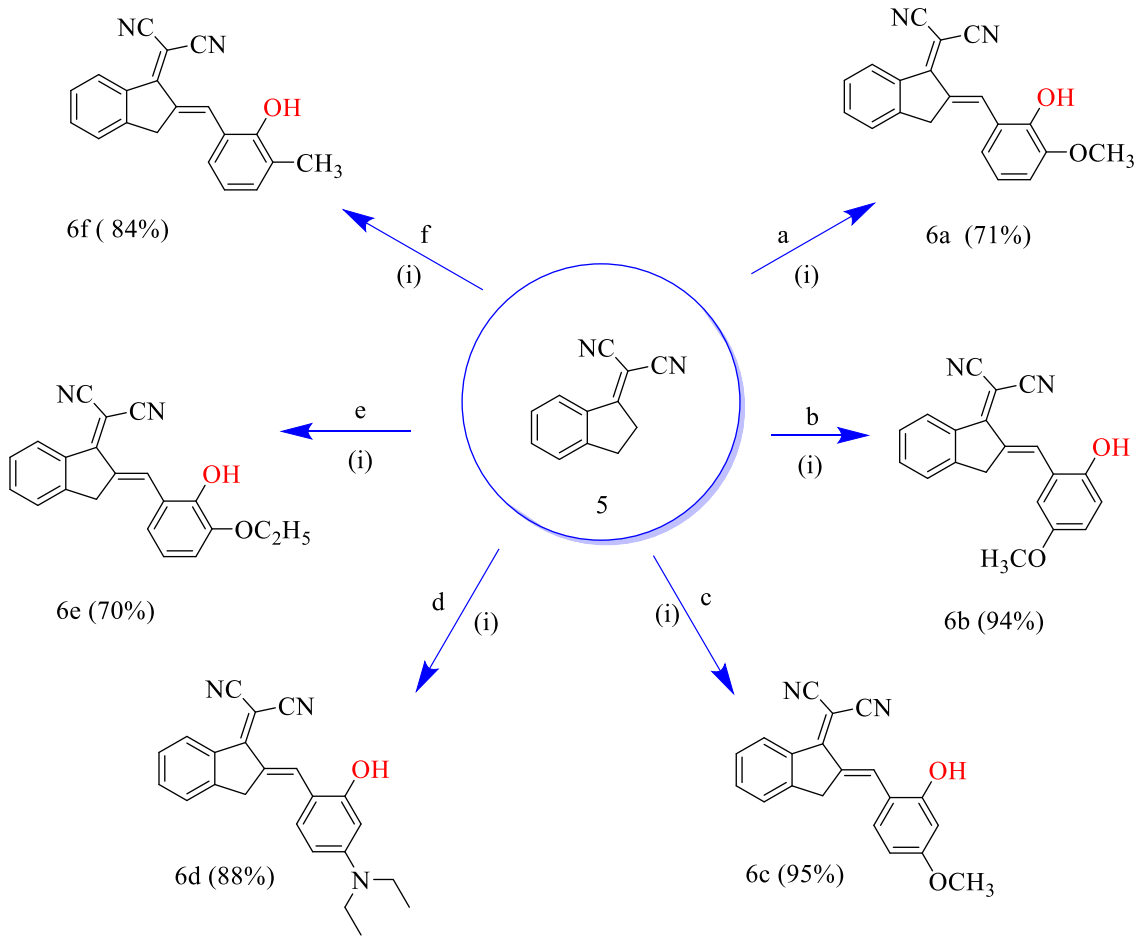

Figure 4.13. Synthesis routes of the chemosensors 6a-f (i) cyclohexane/piperidine

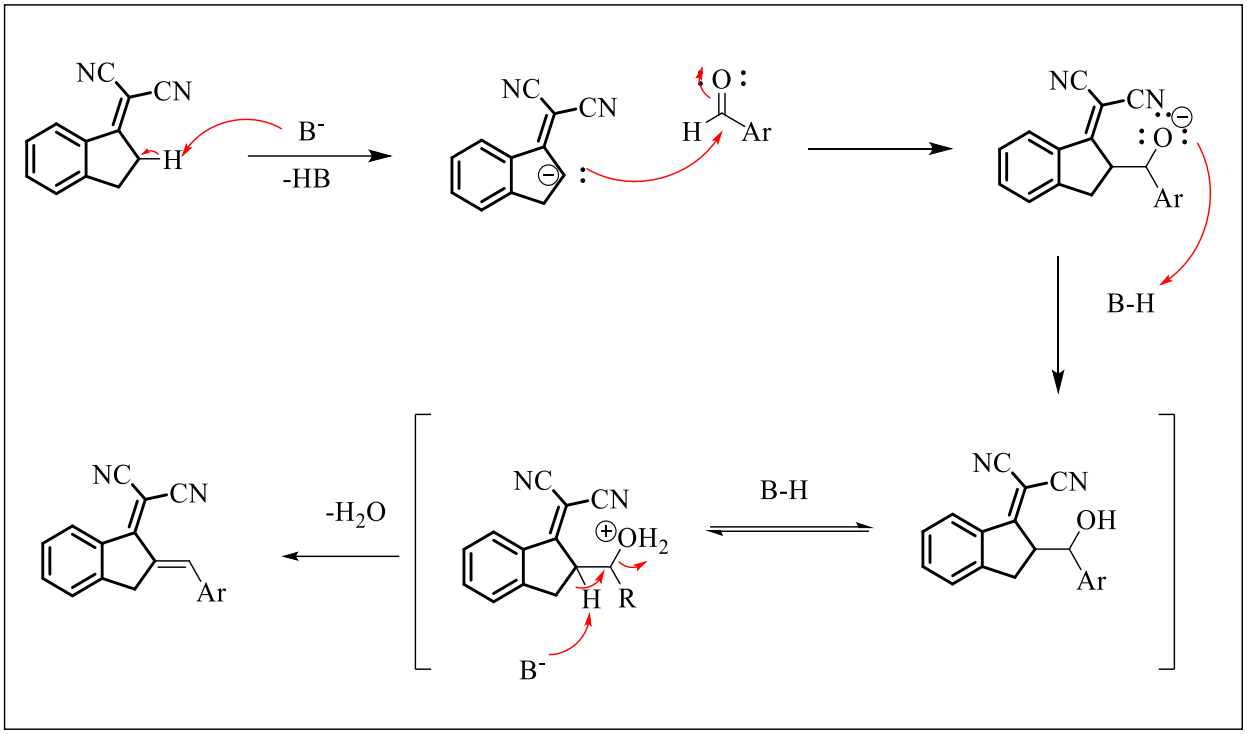

Figure 4.14. The possible Mechanism for the Synthesized of 1-dicyanomethylene-2-aryl-indone

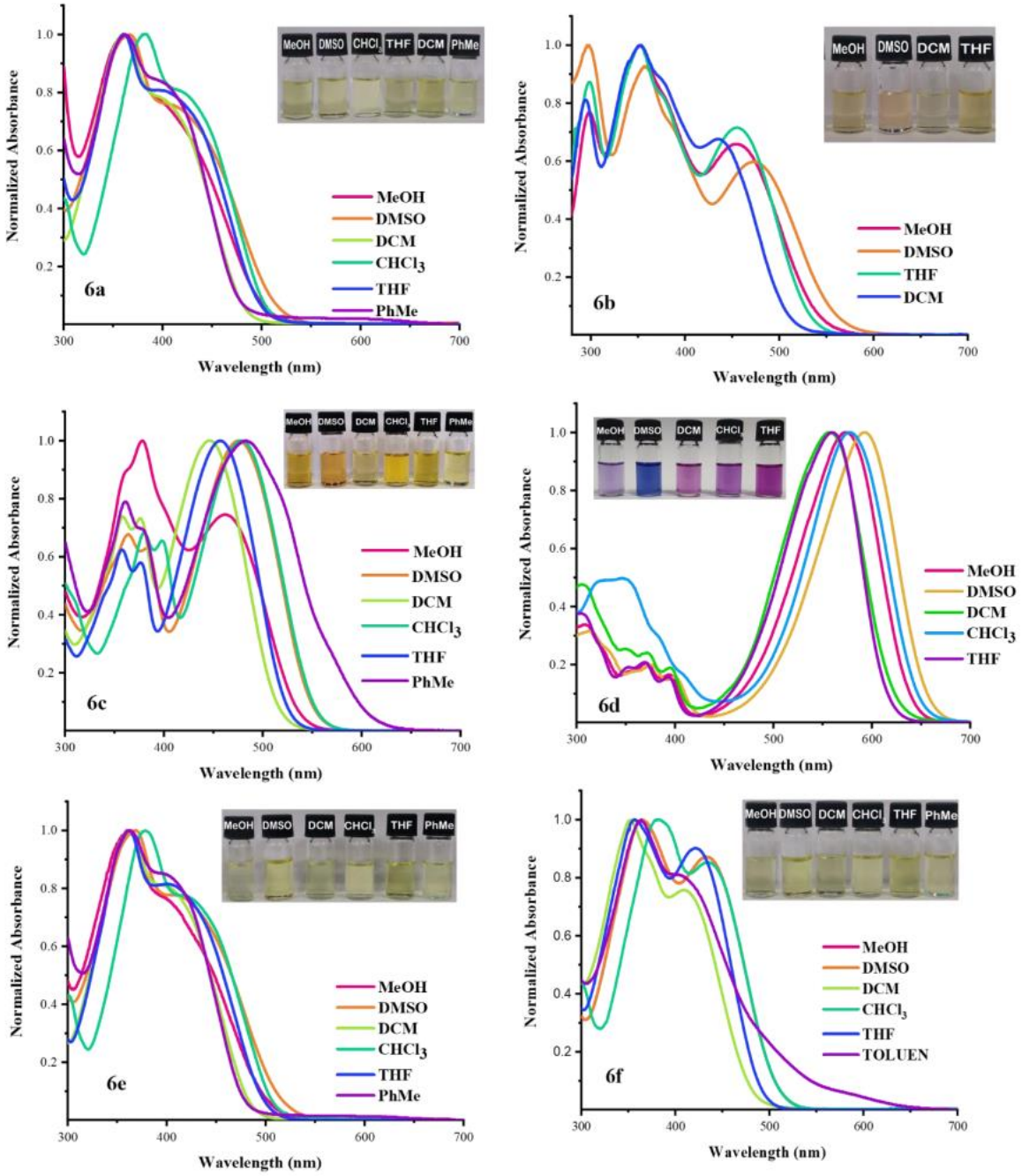

Figure 4.15. The normalized absorption spectra of 6a-f (30 μM) in various solvents

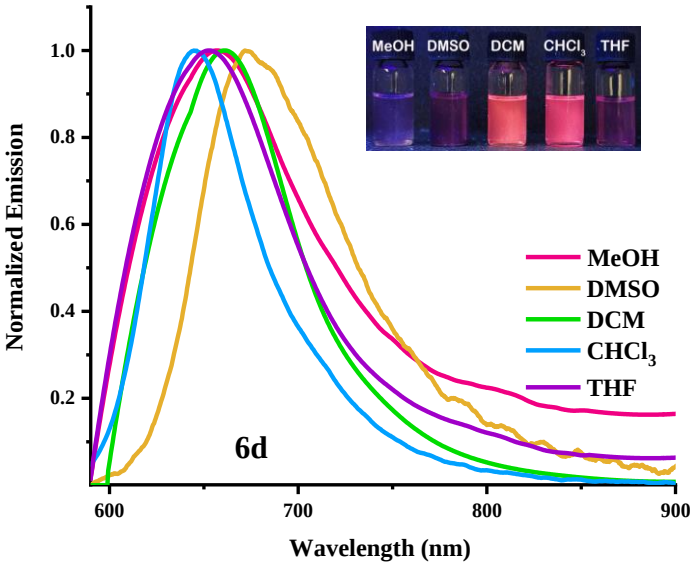

Figure 4.16. The normalized emission spectra of 6d (30 μM) in various solvents

Table 4.4. Photophysical properties of 6a-f

Dye	Solvent	λ_{abs} [a]	$\varepsilon_{abs.}$ [b]	$\lambda_{em.}$ [c]	$\varepsilon_{em.}$ [d] (10^6)	Stokes shift(cm^{-1})
6a	MeOH	361	18732	-[e]	-[e]	-[e]
	DMSO	367	17601	-[e]	-[e]	-[e]
	DCM	362	30664	-[e]	-[e]	-[e]
	$CHCl_3$	361	42011	-[e]	-[e]	-[e]
	THF	361	23197	-[e]	-[e]	-[e]
	PhMe	362	20195	-[e]	-[e]	-[e]
6b	MeOH	454/352/299	18318/26718/19544	-[e]	-[e]	-[e]
	DMSO	473/356/296	7684/12105/9293	-[e]	-[e]	-[e]
	DCM	434/353/294	22278/31203/21436	-[e]	-[e]	-[e]
	$CHCl_3$	-	-	-[e]	-[e]	-[e]
	THF	455/353/298	16092/23051/18858	-[e]	-[e]	-[e]
	PhMe	-	-	-[e]	-[e]	-[e]
6c	MeOH	461/378	16805/23691	-[e]	-[e]	-[e]
	DMSO	475/382/364	19602/12582/13570	-[e]	-[e]	-[e]
	DCM	446/376/359	12424/8684/8447	-[e]	-[e]	-[e]
	$CHCl_3$	458/378	10746/7003,4	-[e]	-[e]	-[e]
	THF	457/376/358	32380/18863/20196	-[e]	-[e]	-[e]
	PhMe	482/361	12990/9548	-[e]	-[e]	-[e]
6d	MeOH	574	21790	655	10	2154
	DMSO	592	44942	672	40	2011
	DCM	557	42293	659	500	2779
	$CHCl_3$	557	1597	644	200	2425
	THF	559	43649	649	20	2481
	PhMe	-	-	-[e]	-[e]	-[e]
6e	MeOH	362/274	17008/7717	-[e]	-[e]	-[e]
	DMSO	367/284	14510/9158	-[e]	-[e]	-[e]
	DCM	363/279	71963/45703	-[e]	-[e]	-[e]
	$CHCl_3$	358	29747	-[e]	-[e]	-[e]
	THF	400/363	18359/22589	-[e]	-[e]	-[e]
	PhMe	363	14911	-[e]	-[e]	-[e]
6f	MeOH	365/435	3614/5834	-[e]	-[e]	-[e]
	DMSO	432/365	14807/17079	-[e]	-[e]	-[e]
	DCM	409/353	20906/24504	-[e]	-[e]	-[e]
	$CHCl_3$	413,05/361,5	8616/10267	-[e]	-[e]	-[e]
	THF	422/356	23483/26118	-[e]	-[e]	-[e]
	PhMe	403/363	13689/15875	-[e]	-[e]	-[e]

[a] Long wavelength absorption maximum, in nm; c = 25 μM.
[b] ε = molar absorption coefficient ($cm^{-1}M^{-1}$).
[c] Long wavelength emission maximum, in nm; c = 20 μM.
[d] ε = molar emission coefficient ($cm^{-1}M^{-1}$).
[e] no emission detected

4.2.3. Anions-Chemosensing interaction study in organic medium

The study of the sensitivity and selectivity of the competing anions (AcO^-, Br^-, CN^-, Cl^-, F^-, $H_2PO_4^-$, NO_3^-, I^-, ClO_4^- and HSO_4^-) to the chemosensors 6a-f was conducted in 10 μM of DMSO. The signaling and selectivity of the obtained chemosensors were studied via UV-vis and fluorescence spectroscopy. 6a-f (10μM) were added into a DMSO solution, then 20 equiv. of each anion (I^-, Br^-, Cl^-, F^-, CN^-, AcO^-, $H_2PO_4^-$, NO_3^-, ClO_4^- and HSO_4^-) was added. The UV-vis spectrum corresponding to 6a is shown in Figure 4.17 (a). Upon CN^-, F^-, AcO^-, OH^- and $H_2PO_4^-$ addition, an absorption band at 700 nm was recorded. The rest of the anions (I^-, Br^-, Cl^-, NO_3^-, ClO_4^-, and HSO_4^-) showed no changes upon addition. The emission spectrum of 6a (Figure 4.17 (b)) showed a negligible band at 476 nm; however, the band's intensity increased after adding CN^-, F^-, AcO^-, OH^- and $H_2PO^-_4$. The intensity of the band increased in the following order $H_2PO_4^-$ < OH^- < AcO^- < CN^- < F^-. The competing anions addition to 6b-f demonstrated a similar performance as 6a. The obtained UV and emission spectra are given in Figures 4.18

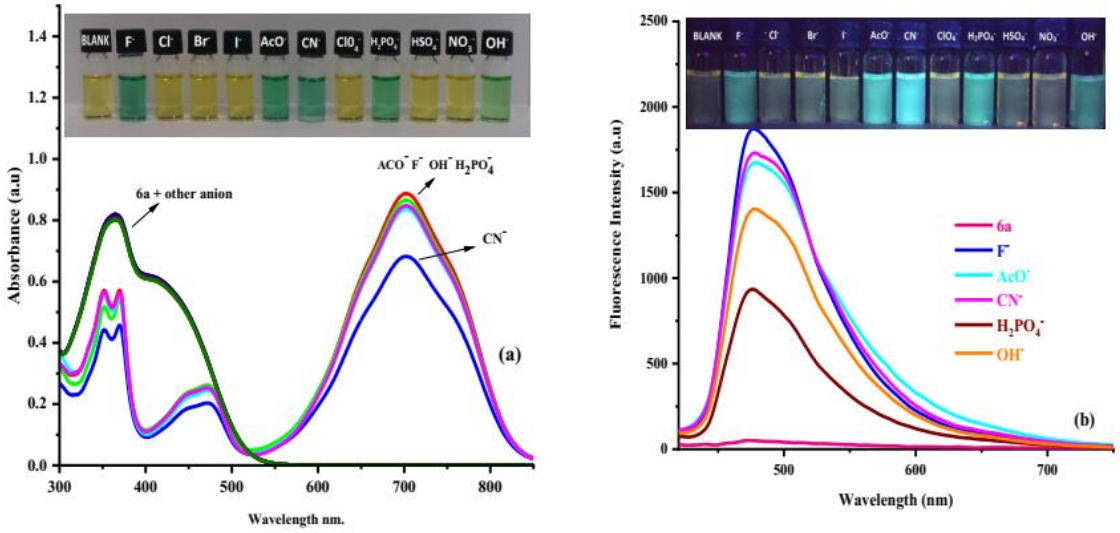

Figure 4.17. a) Absorption spectra (10 μM);(b) Emission spectra (25 μM) of compounds 6a in DMSO after adding 20 equiv. of the anions. Insets: Photographs of Color (ambient light) and fluorescence change after adding 20 equiv. of anions.

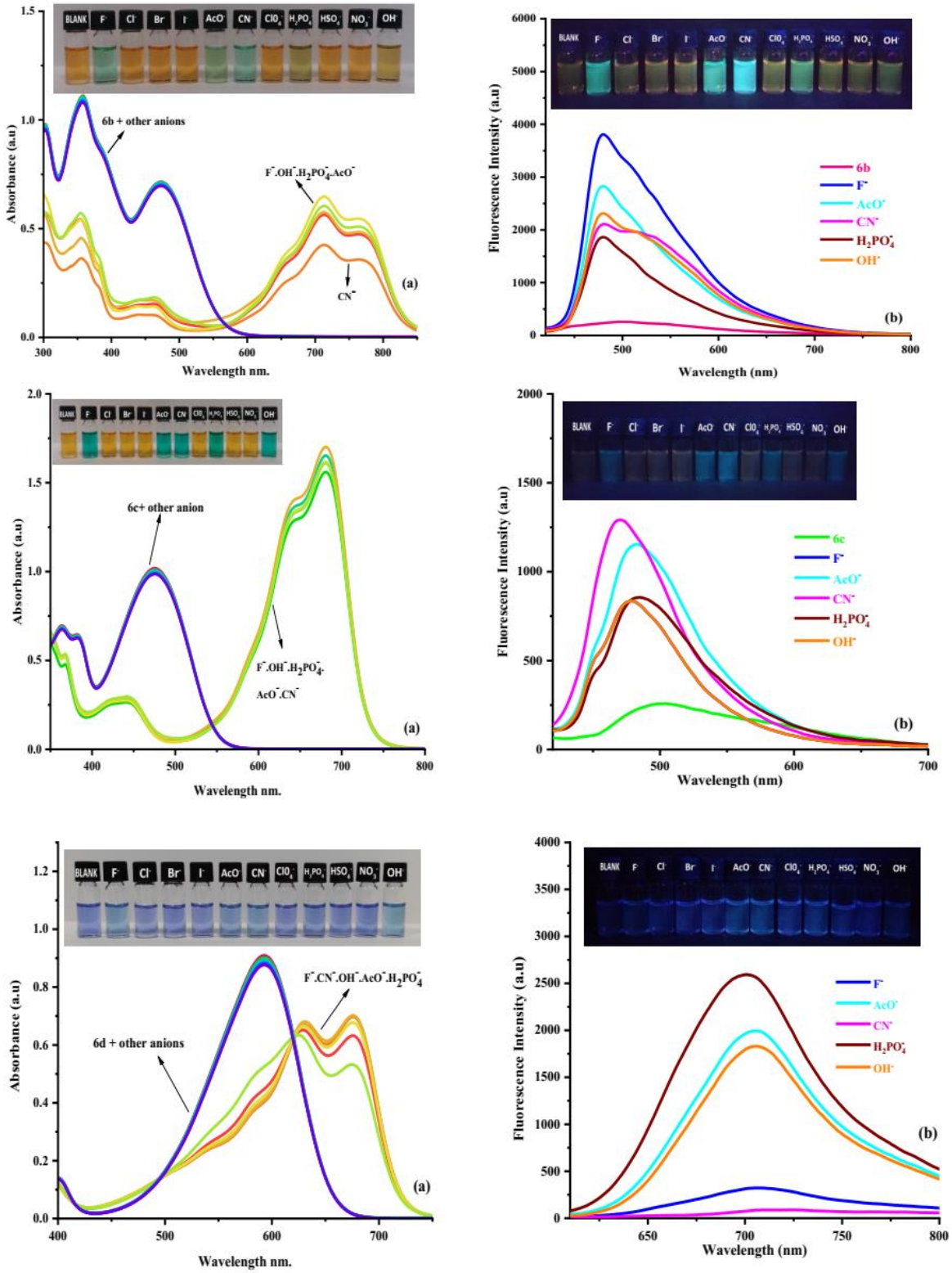

Figure 4.18. a) Absorption spectra (10 μM);(b) Emission spectra (25 μM) of compounds 6b-f in DMSO after adding 20 equiv.of the anions. Insets: Photographs of Color (ambient light) and fluorescence change after adding 20 equiv. of anions.

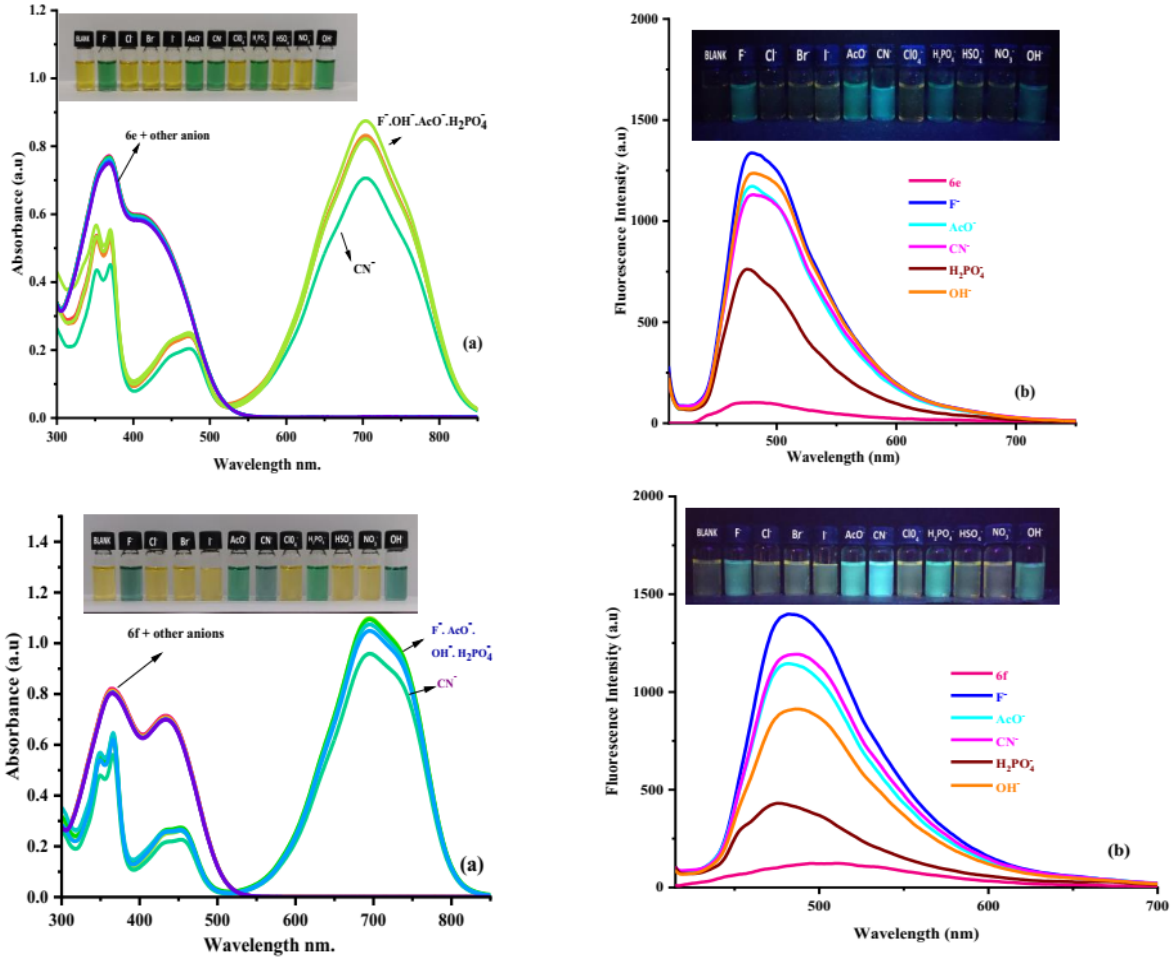

Figure 4.18. (Cont.) a) Absorption spectra (10 μM);(b) Emission spectra (25 μM) of compounds 6b-f in DMSO after adding 20 equiv.of the anions. Insets: Photographs of Color (ambient light) and fluorescence change after adding 20 equiv. of anions.

The 6a interaction with CN^- was conducted via adding 20 equiv. of cyanide anion into a solution of 6a. From the UV-vis spectrum, the apparition of two new bands at 700 nm and 471 nm can be observed after adding 20 equiv. of CN^-. Additionally, at 526 nm, an isosbestic point was observed, meaning that the reaction stoichiometry stayed unaffected through the interaction between 6a and CN^- anion. For the chemosensors 6b-f, similar investigations were carried out, and the obtained results were analogous to 6a. The UV-vis spectra are given in Figure 4.19.

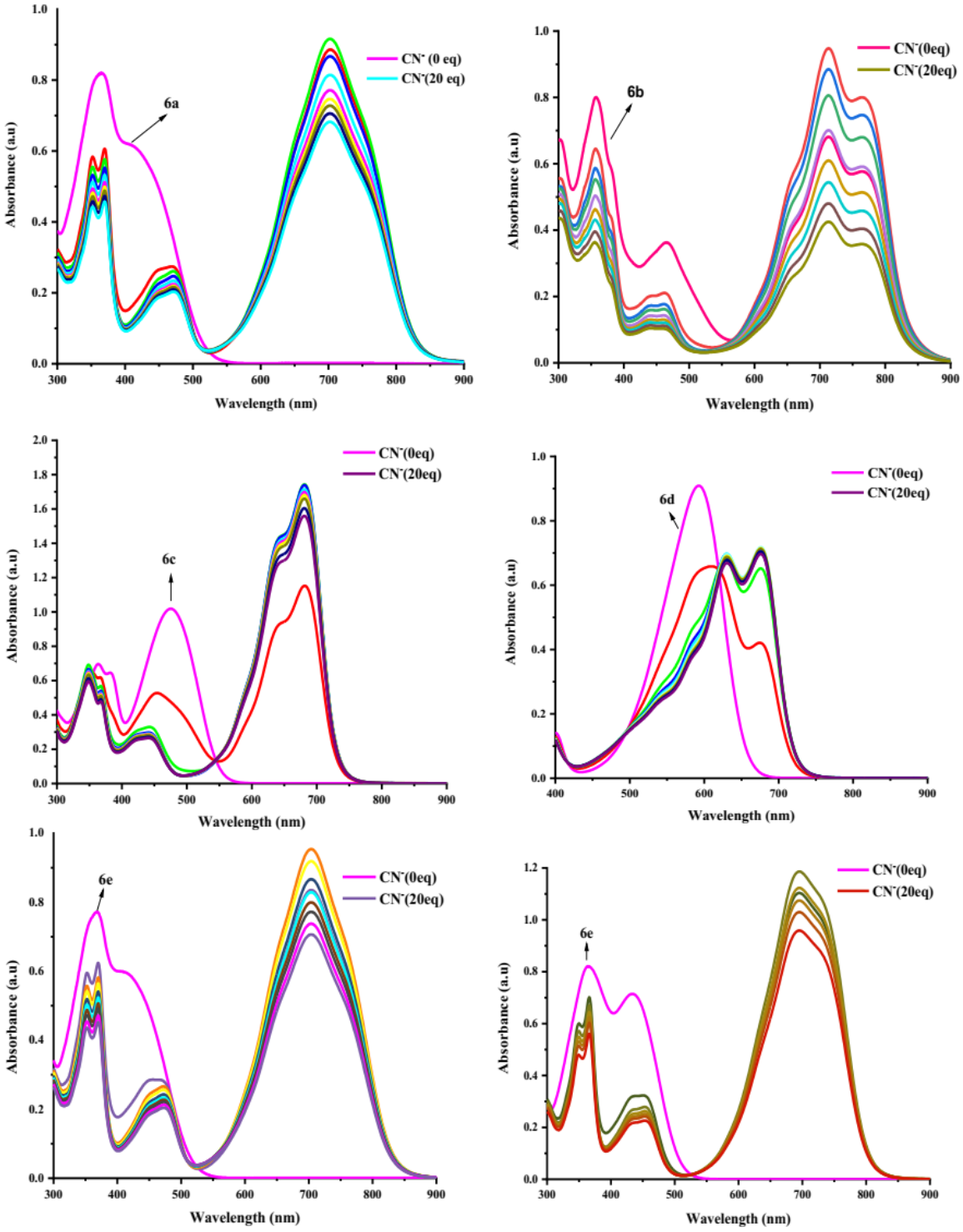

Figure 4.19. Chemosensor 6a-f (10 µM) UV-vis titration spectra with CN^- anion 0-20 equiv. in DMSO

4.2.4. Anion interaction in partial aqueous medium for selectivity

The investigation of the chemosensors 6a-f sensitivity toward the selected anions (I^-, Br^-, Cl^-, F^-, CN^-, AcO^-, $H_2PO_4^-$, NO_3^-, ClO_4^- and HSO_4^-) was conducted in a partial aqueous medium (DMSO/H_2O, 1/1:v/v). 20 equiv. of each anion was added to the chemosensors solutions. Figure 4.20 displays the interaction between 6a and all the added anions. It can be observed from the UV-vis spectra (Figure 4.21 (a)) that only CN^- and OH^- are sensitive towards 6a, which resulted in a red shift in its spectra, and a new band appeared at 646 nm. Furthermore, the emission spectra displayed in Figure 4.21 (b) showed a great increase in the fluorescence intensity after the addition of CN^- and OH^-. However, there was no visible difference in the spectral properties for the rest of the studied anions. Whereas F^-, AcO^-, and $H_2PO_4^-$ showed an interaction with 6a in an organic medium (100% DMSO), they did not display any change in the partial aqueous medium (1/1:v/v). This behavior is mainly due to the high hydration enthalpy of F^-, AcO^-, and $H_2PO_4^-$ leading to hydrogen bonds forming between those anions and water molecules (Figure 4.. IV) and causing a decrease in the basicity of the anions. However, CN- has a low hydration enthalpy, and OH- is highly basic, leading to their selective interaction with chemosensor 6a. Figure 4.20 (a) displays a band of absorption and a shoulder at 366 nm and 413 nm, respectively; however, upon adding 20 equiv. of CN^- or OH^- a new band appeared at 646 nm, and the absorbance at 366 nm decreased. The interaction between the other chemosensors 6b-f in the partial aqueous medium was also conducted. They showed selectivity towards CN^- and OH^- and were insensitive to the other anions. The obtained results are displayed in Figures 4.21.

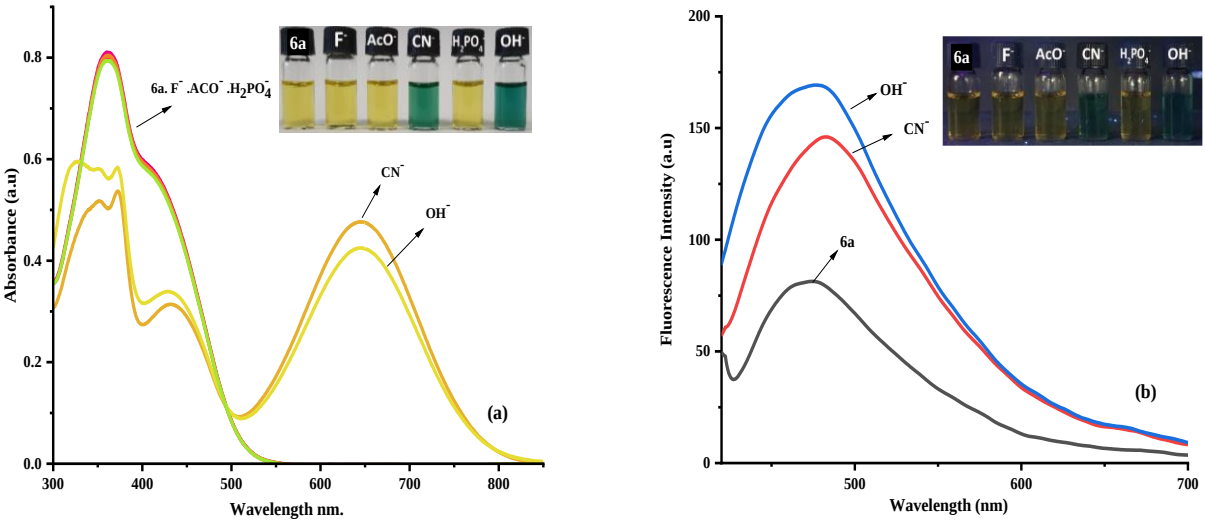

Figure 4.20. a) Absorption spectra (10 µM); (b) Emission spectra (20 µM) of compounds 6a in (DMSO/ H_2O, 1/1:v/v) after addition of 20 equiv. of the anions.

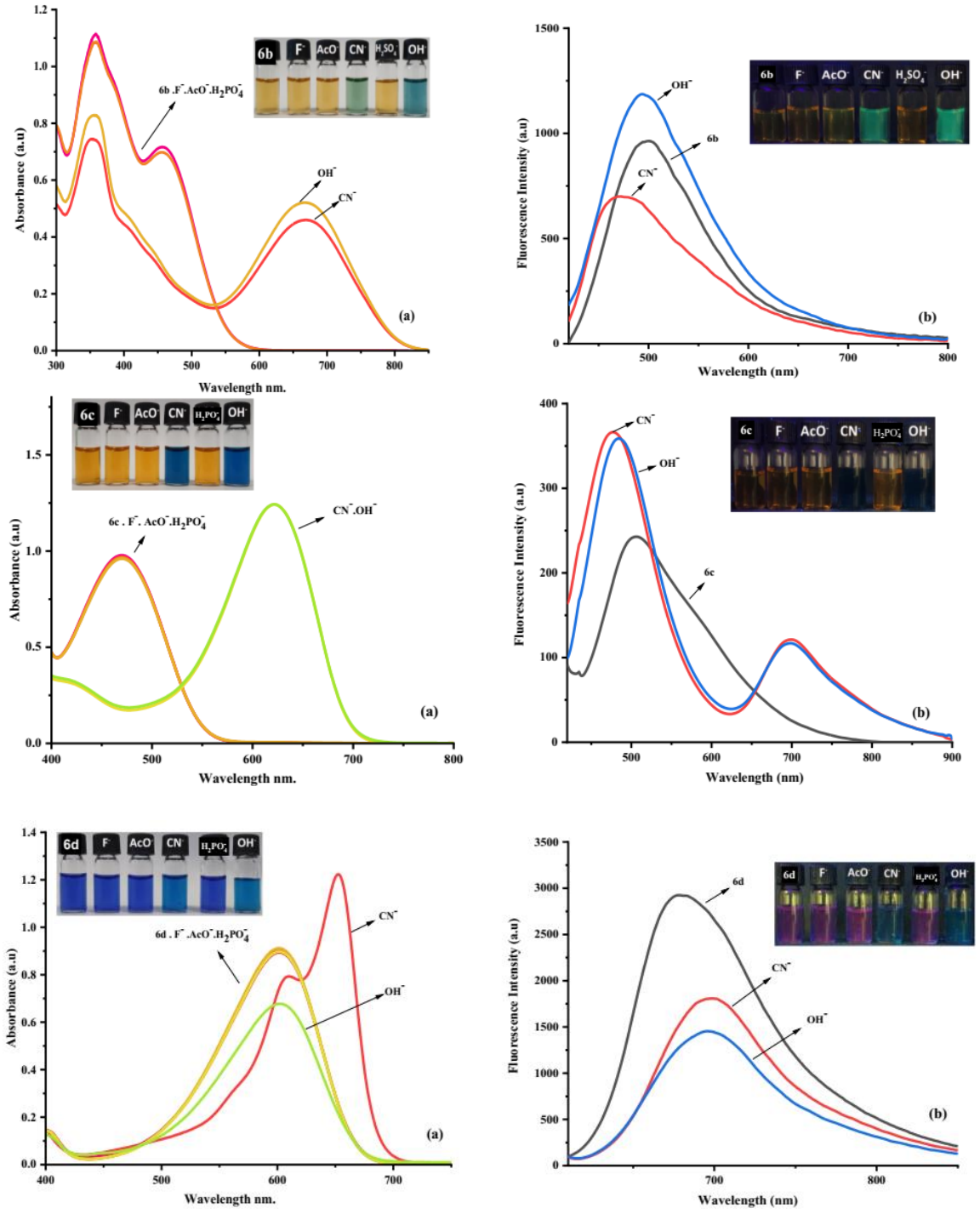

Figure 4.21. a) Absorption spectra (10 μM);(b) Emission spectra (20 μM) of compounds 6b-f in (DMSO/ H_2O, 1/1:v/v) after addition of 20 equiv. of the anions.

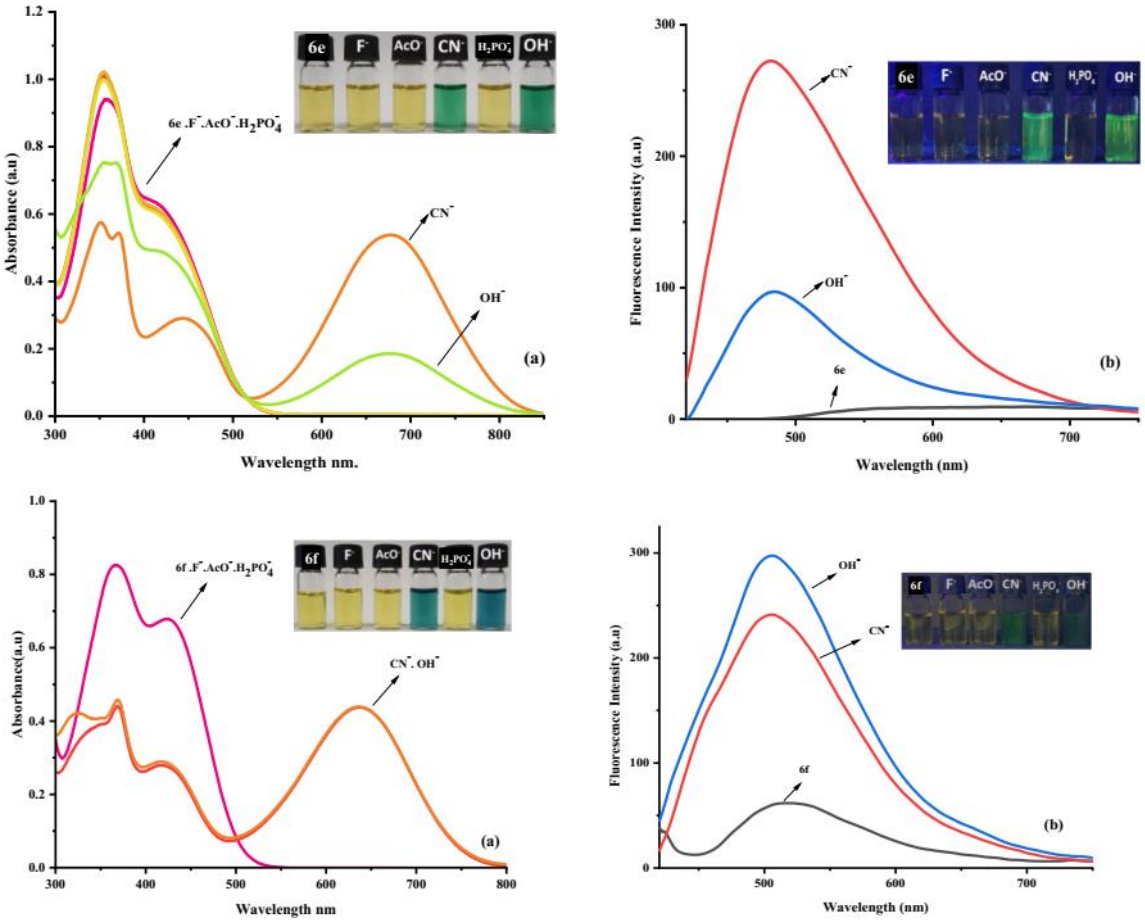

Figure 4.21. (Cont.) a) Absorption spectra (10 μM);(b) Emission spectra (20 μM) of compounds 6b-f in (DMSO/ H_2O, 1/1:v/v) after addition of 20 equiv. of the anions .

4.2.5. Tap water experiment

The study of chemosensors' selectivity towards the selected anions in tap water was performed to establish the performance of the obtained chemosensors in a natural environment. TBACN and TBAOH were dissolved in tap water (5.10^{-5} M) and used as a cyanide and hydroxyl anions source. Figure 4.22 displays the output obtained after the addition of 20 equiv. of both CN^- and OH^- to 6a. Similar results were obtained when tap water was used instead of distilled water with a new band's apparition at 646 nm in the UV-vis spectra, and the emission increased upon the addition of CN^- or OH^-. Identical results were obtained with 6b-f, and the corresponding spectra are given in Figure 4.23.

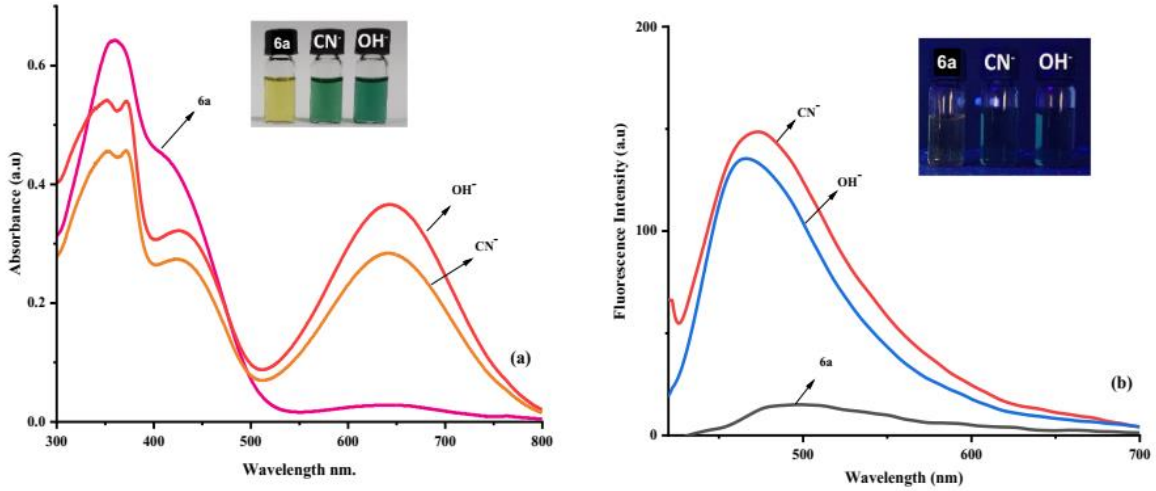

Figure 4.22. a) Absorption spectra (10 μM);(b) Emission spectra (20 μM) of compounds 6a in (DMSO/ tap water, 1/1:v/v) after addition of 20 equiv. of anions .

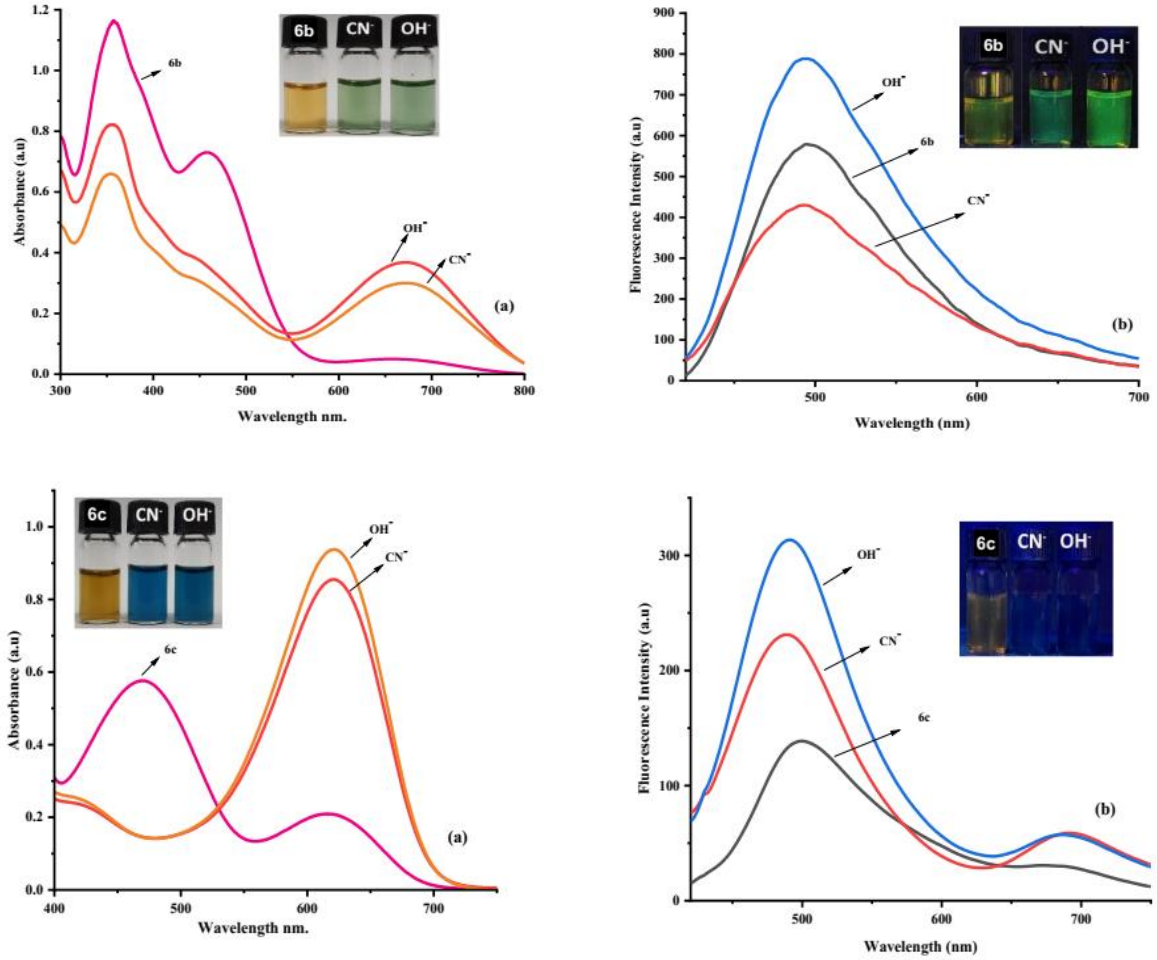

Figure 4.23. a) Absorption spectra (10 μM);(b) Emission spectra (20 μM) of compounds 6b-f in (DMSO/ tap water, 1/1:v/v) after addition of 20 equiv. of anions .

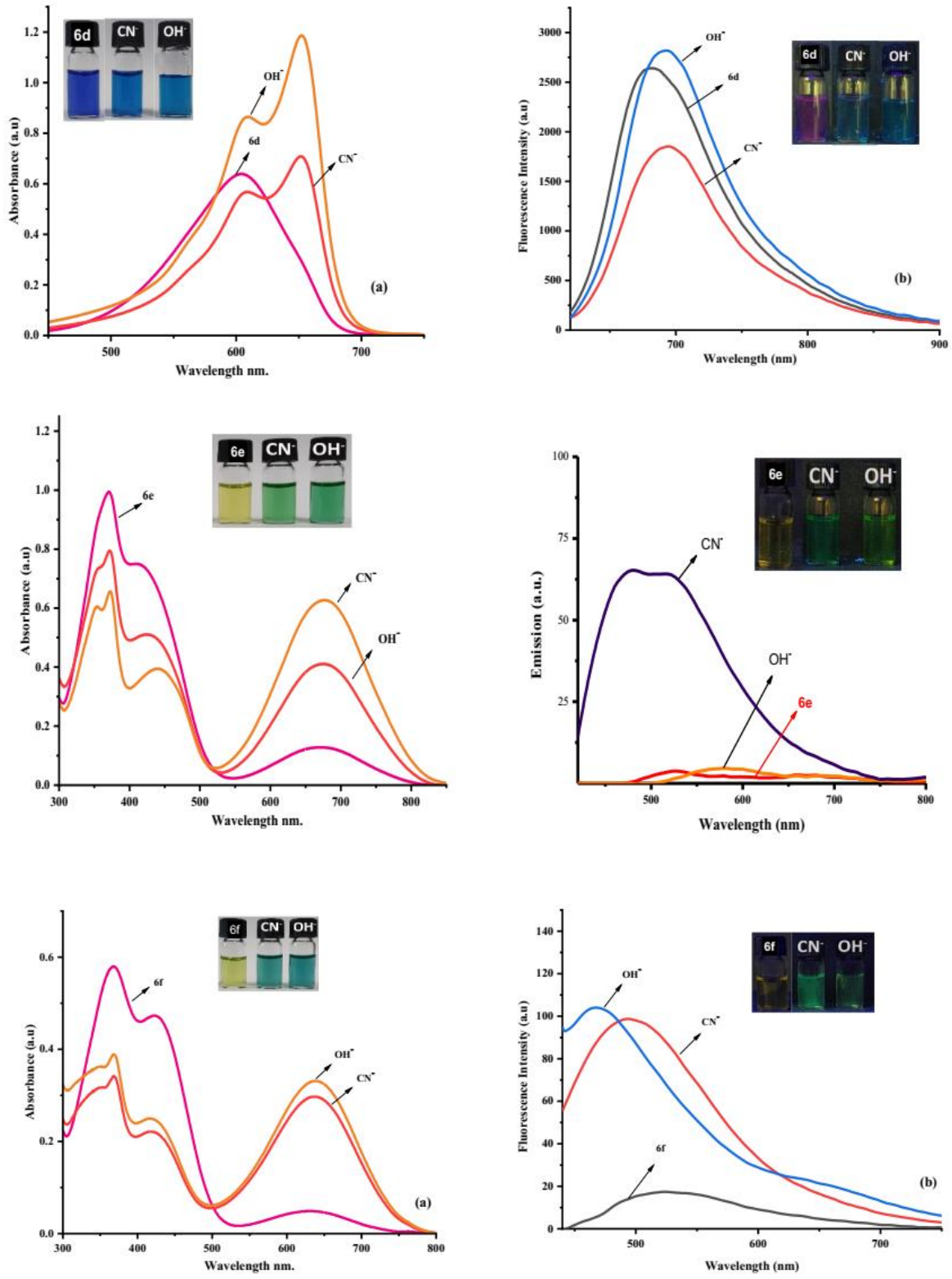

Figure 4.23. (Cont.) a) Absorption spectra (10 μM);(b) Emission spectra (20 μM) of compounds 6b-f in (DMSO/ tap water, 1/1:v/v) after addition of 20 equiv. of anions .

4.2.6. Sensing mechanism

The synthesized chemosensors (6a-f) displayed a good selectivity to F^-, AcO^-, $H_2PO_4^-$ CN^- and OH^- in the organic medium. The interaction between chemosensors and anions could happen via two possible mechanisms. The first possibility is the deprotonation of the hydroxyl hydrogen situated at phenol moiety due to the high basicity of F^-, AcO^-, $H_2PO_4^-$ CN^- and OH^- (Figure 4.. I). The new absorption bands that appeared at the bathochromic region are mainly due to the deprotonation of the hydroxyl and the formation of the phenoxide group known for their strong electron-donating properties compared to the phenol group. The second possibility is associated with the cyanide nucleophilic and basic properties, leading to the CN^- addition to the vinylic carbon. Both mechanisms are displayed in Figure 4..II

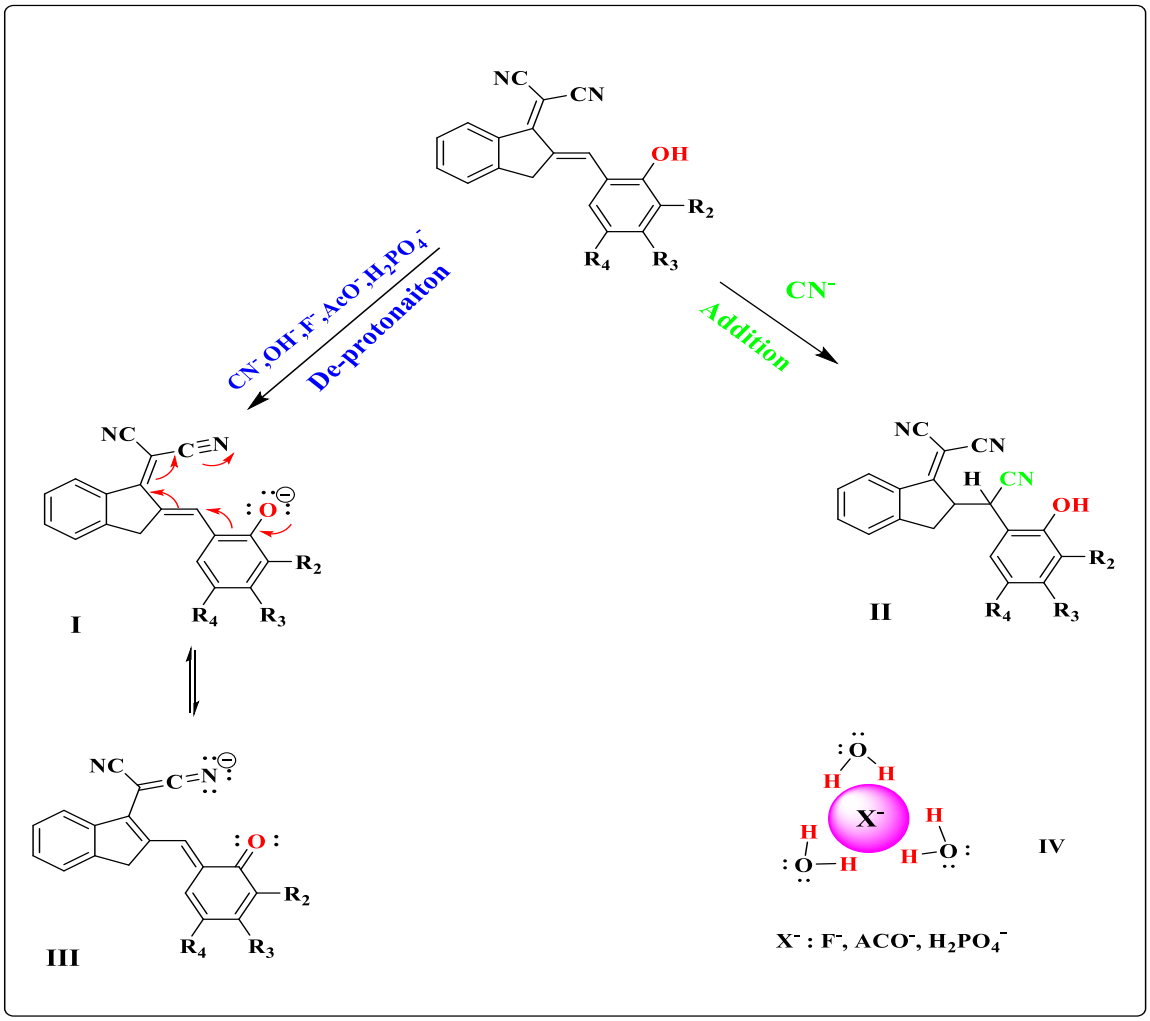

Figure 4.24. The plausible sensing mechanisms.

[1]H-NMR experiment titration of chemosensor 6d

The [1]H-NMR experiment was conducted to understand the interaction mechanism of CN^- and F^- with 6d. To achieve this purpose, a DMSO-d_6 solution of 6a was titrated with CN^- and F^- up to 1 equiv. (Figures 4.25 and 4.26). Upon adding 0.5 equiv. of CN^- the OH signal (s,1H, 10.26 ppm) disappeared. Furthermore, the signals of phenyl protons (H_a, H_b and H_c), and vinyl proton (H_d) shifted somewhat to upfield. Ha and Hb signals situated at ortho and para positions of the OH group displayed the most considerable shift due to the deprotonation of OH proton leading to the redistribution of the electron in the conjugated system. After adding 1 equiv. no further change was observed in the spectrum (Figure 4.25. (c)). Similar results were observed in the [1]H-NMR titration spectrum upon addition of 0.5 and 1 equiv. of F^-. The OH signal disappeared, and the other shifted (Figure 4.26). The [1]H-NMR experiment confirmed that the sensing mechanism occurs via deprotonation of the hydroxyl hydrogen situated at phenol moiety, resulting in UV and fluorescence spectra changes. Table 4.5 displays the changes in chemical shifts resulting from the interaction of 6d with CN^- and F^-.

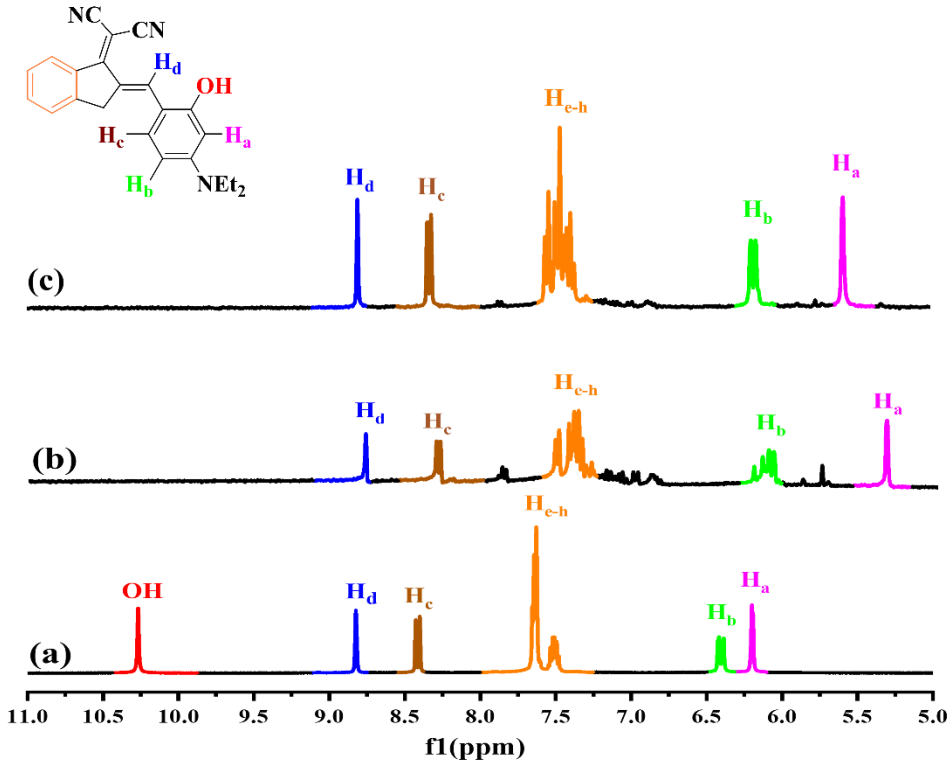

Figure 4.25. [1]H NMR spectral changes of 6d (10 mM) in the absence (a) and presence of 0.5 equiv. (b) and 1 equiv. (c) of TBACN in DMSO-d_6

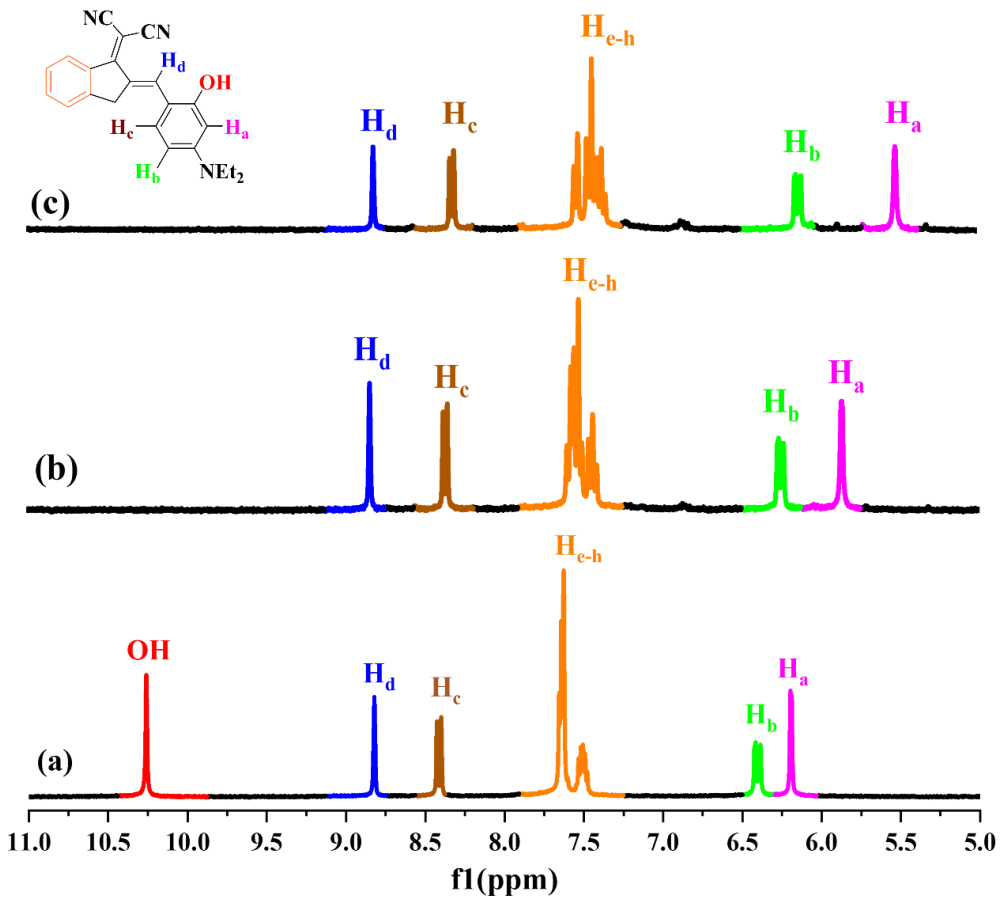

Figure 4.26. ^{1}H NMR spectral changes of 6d (10 mM) in the absence (a) and presence of 0.5 equiv. (b) and 1 equiv. (c) of TBAF in DMSO-d_6

Table 4.5. Changes in chemical shifts as a result of the interaction of 6d with CN^- and F^-

	H_a	H_b	H_c	H_d
6d	6.20	6.41	8.40	8.82
CN^-	5.57	6.15	8.31	8.80
F^-	5.51	6.11	8.30	8.81

4.2.7. Reversibility properties in aqueous medium DMSO/H_2O

The reversibility study was carried out by adding 20 equiv. CN^- and OH^- to a solution of 6a-f. The obtained absorption and emission spectra for 6a given in Figure 4.28 show that the addition of the selected anions resulted in a new band's apparition at 646 nm. However, upon addition of 20 equiv. of trifluoroacetic acid (TFA) revert to the initial maximum absorbance was observed. Furthermore, 6a displayed negligible fluorescence, but after adding 20 equiv. of CN^- or OH^- an emission band appears around 500 nm. However, after adding 20 equiv. of TFA, the emission spectra go back to the initial state. It can be concluded from the

reversibility test that only the sensing mechanism occurs via deprotonation though there was a probability of cyanide addition that can act as a nucleophile causing the CN^- to be added to the vinylic carbon (Figure 4.24). The same experiment was realized for the other chemosensors (6b-f), and similar results were found (Figures 4.29).

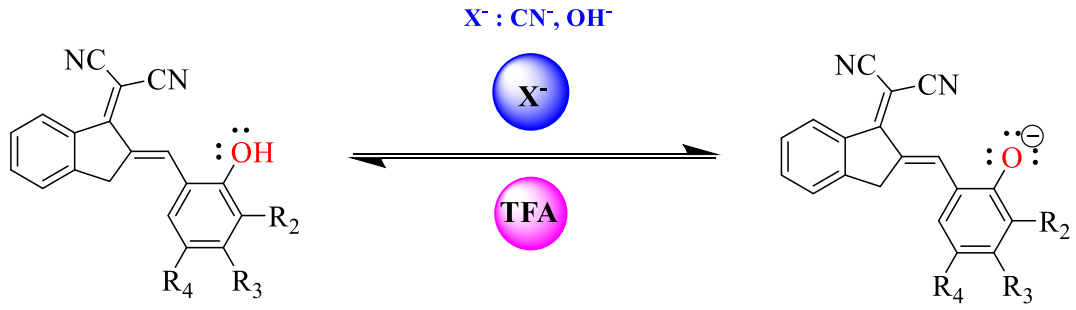

6a : R_2= OCH_3 ,R_3=H , R_4=H
6b : R_2= H ,R_3= H , R_4= OCH_3
6c : R_2= H ,R_3= OCH_3 , R_4=H
6d : R_2= H ,R_3= $N(C_2H_5)_2$,R_4=H
6e : R_2= OC_2H_5 ,R_3=H , R_4=H
6e : R_2= CH_3 ,R_3=H , R_4=H

Figure 4.27. Deprotonation and reverse protonation process.

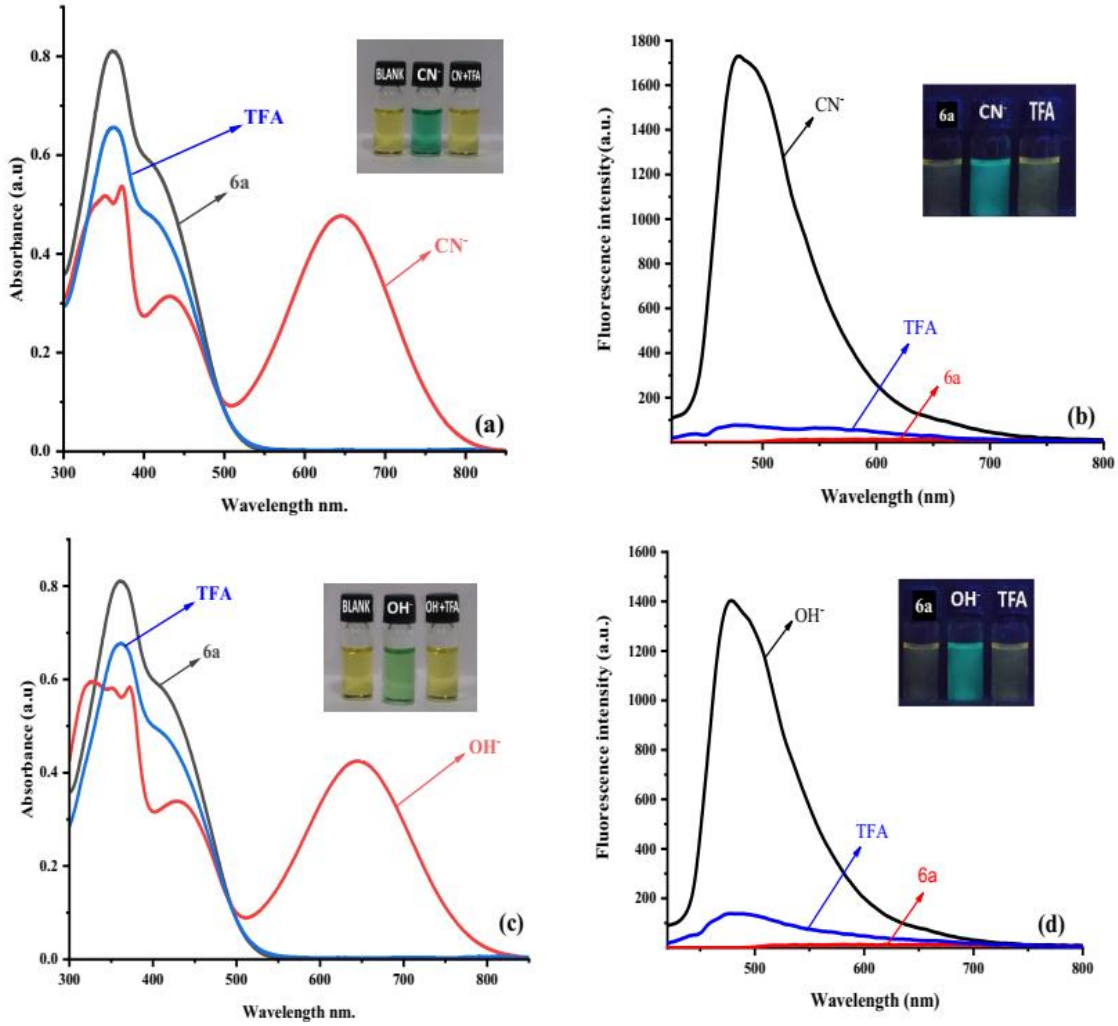

Figure 4.28. Absorption (a) (c) and emission spectra (b) (d) of 6a in the absence of CN^- and OH^- upon addition of TFA (1 M) into the (DMSO/H_2O, 1/1:v/v) Insert: photographs of 6a upon the addition of CN^-, OH^- and TFA under ambient light (a) (c) and UV light (b) (d).

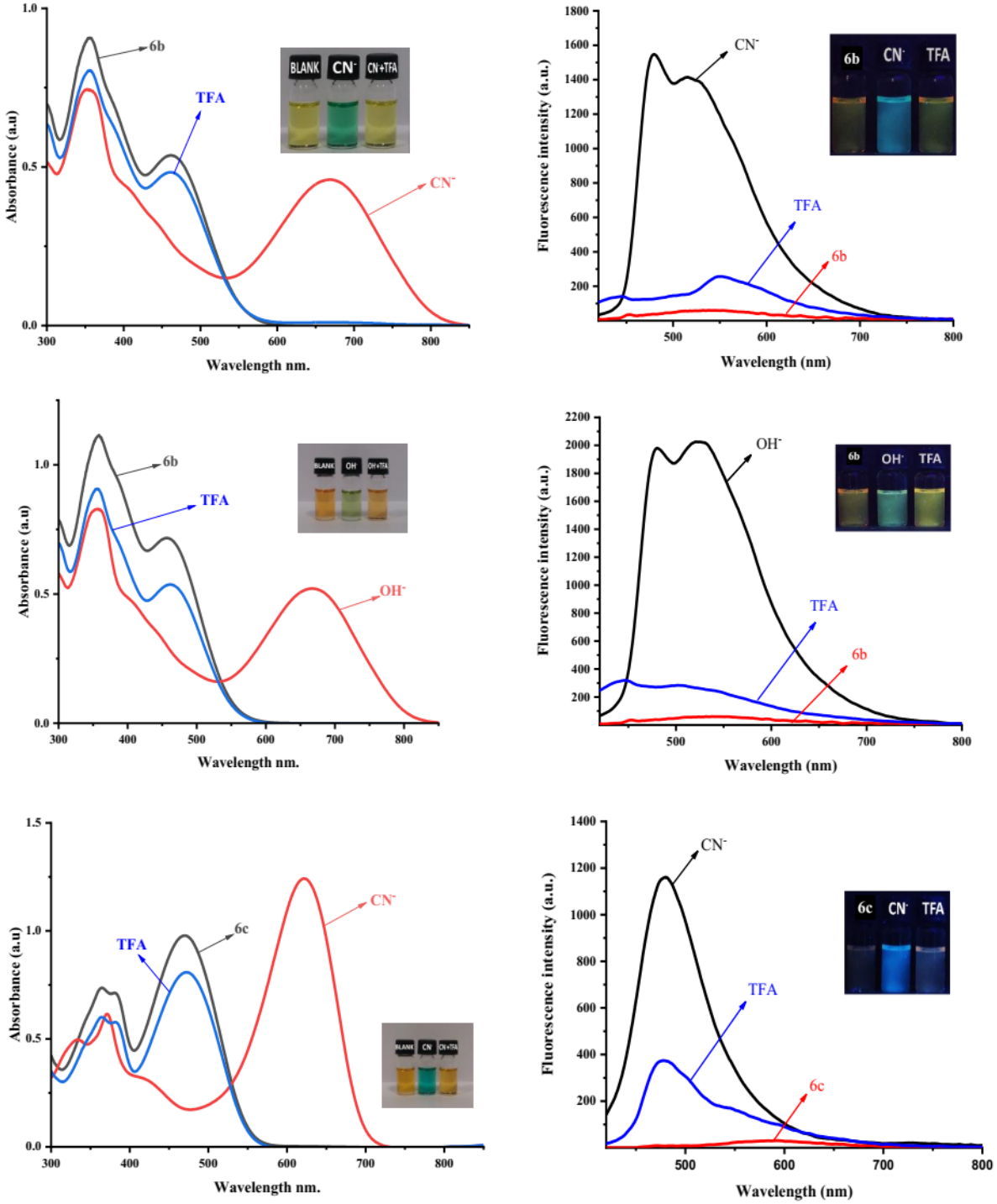

Figure 4.29. Absorption and emission spectra (10 μM) of 6b-f in the absence of CN^- and OH^- upon addition of TFA (1M) into the (DMSO/H_2O, 1/1:v/v) Insert: Photographs of 6b-f upon the addition of CN^-, OH^- and TFA under ambient light.

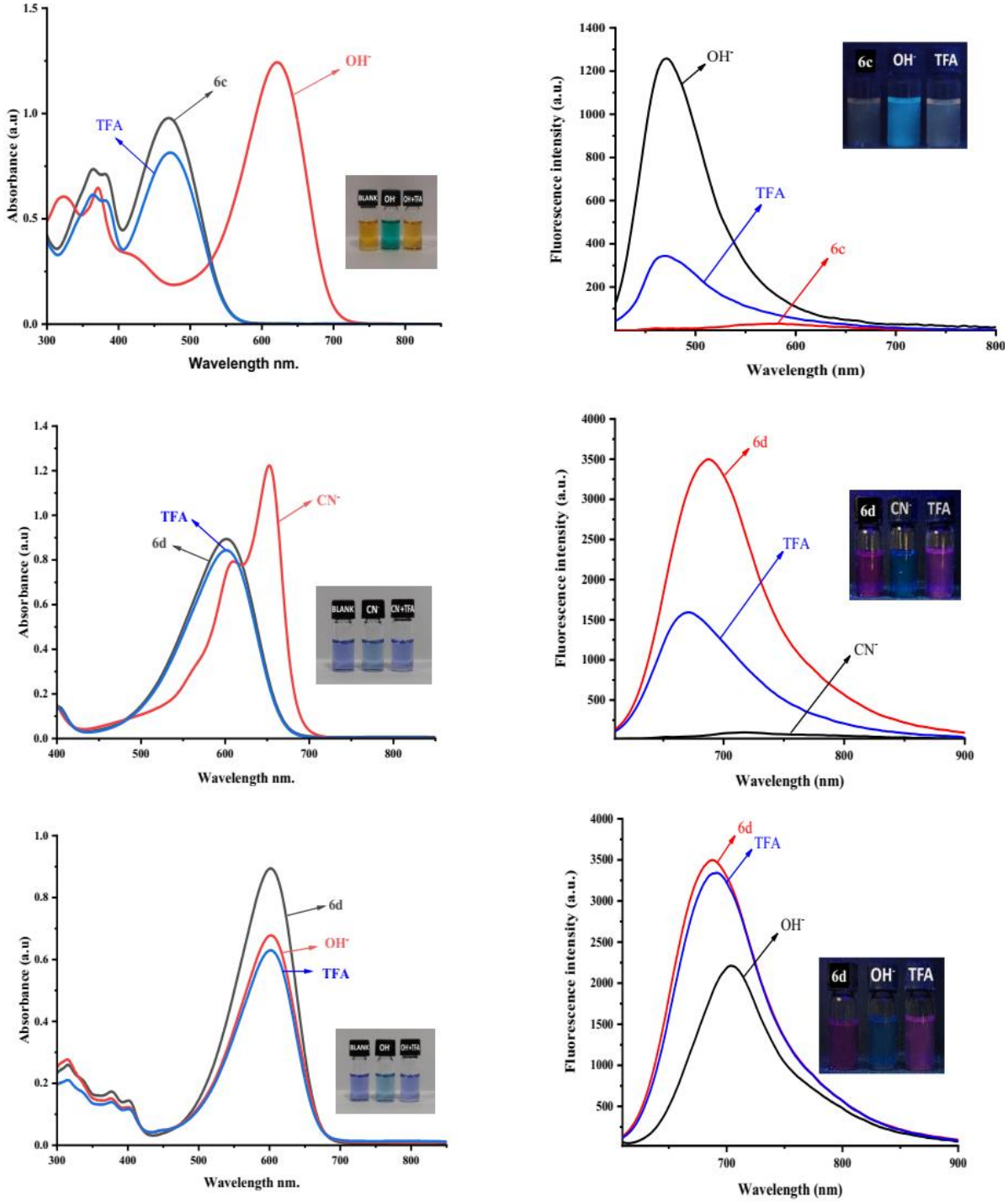

Figure 4.29. (Cont.) Absorption and emission spectra (10 μM) of 6b-f in the absence of CN^- and OH^- upon addition of TFA (1M) into the (DMSO/H_2O, 1/1:v/v) Insert: Photographs of 6b-f upon the addition of CN^-, OH^- and TFA under ambient light.

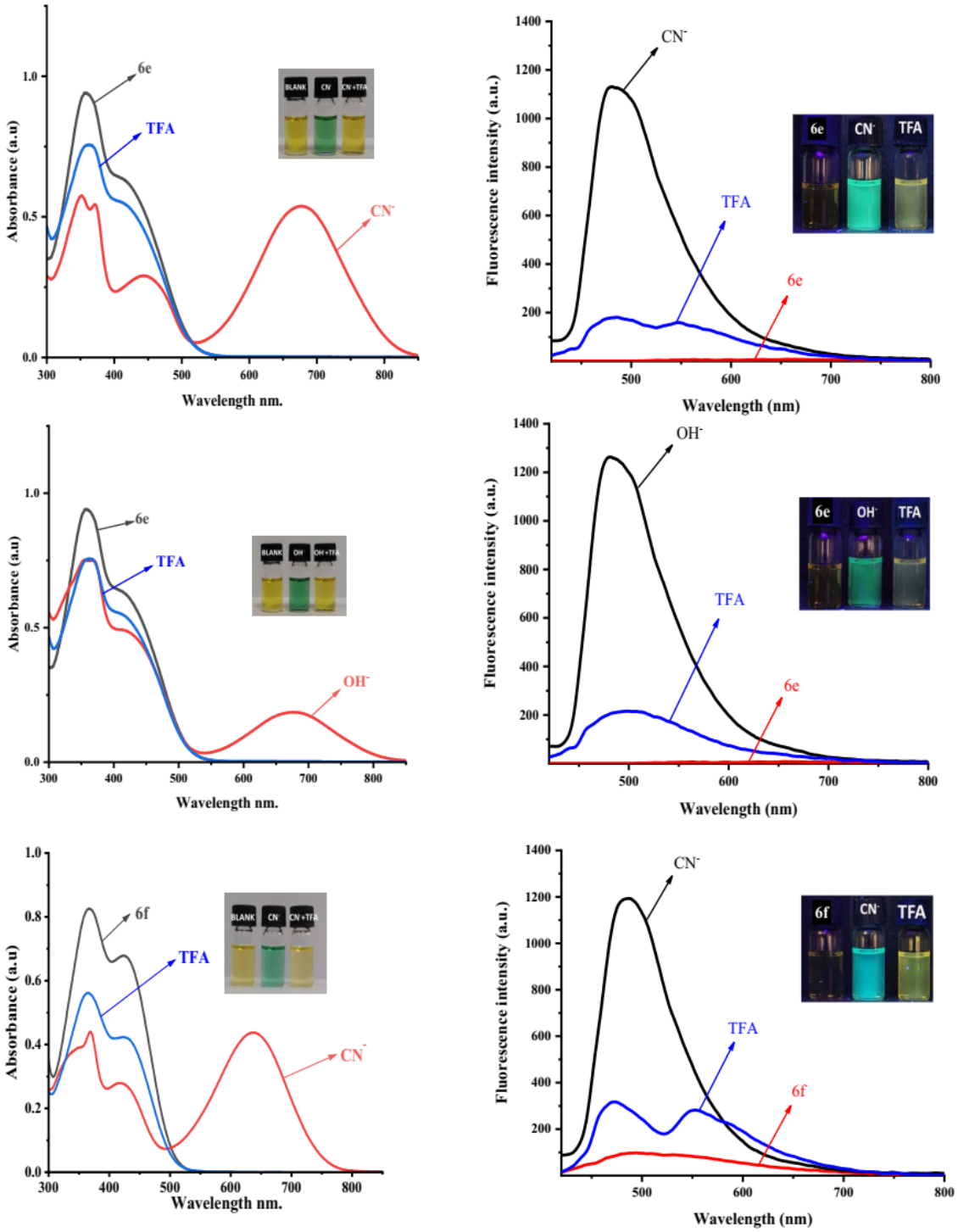

Figure 4.29. (Cont.) Absorption and emission spectra (10 μM) of 6b-f in the absence of CN^- and OH^- upon addition of TFA (1M) into the (DMSO/H_2O, 1/1:v/v) Insert: Photographs of 6b-f upon the addition of CN^-, OH^- and TFA under ambient light.

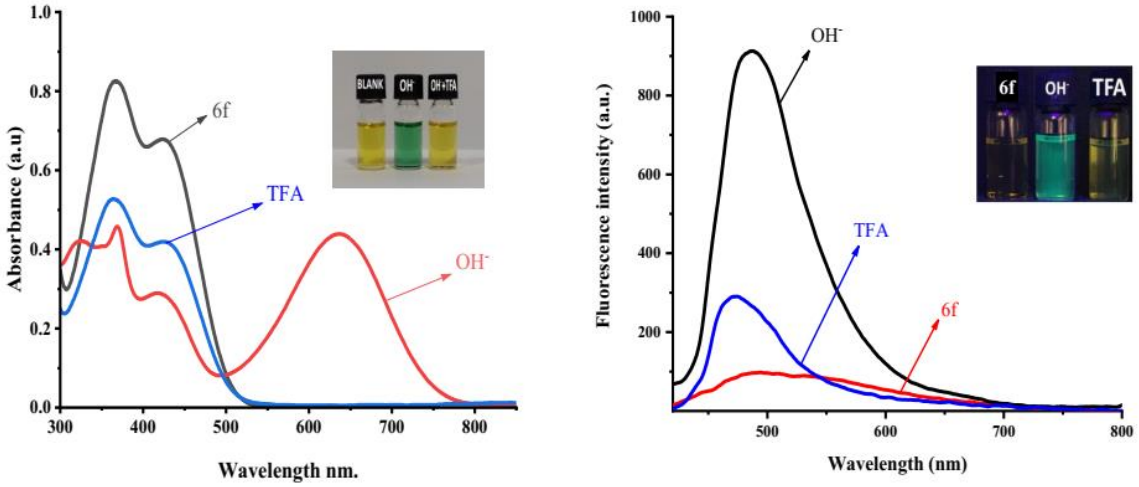

Figure 4.29. (Cont.) Absorption and emission spectra (10 μM) of 6b-f in the absence of CN^- and OH^- upon addition of TFA (1M) into the (DMSO/H_2O, 1/1:v/v) Insert: Photographs of 6b-f upon the addition of CN^-, OH^- and TFA under ambient light.

4.2.8 pH-dependent study

A pH-dependent study was carried out to investigate the influence of the basicity of the medium on the prepared chemosensors (6a-f). Britton Robinson buffer solution was used in addition to DMSO to prepare a solution with pH varying between 6.0 and 11.0. The obtained spectra for 6a are given in Figure 4.30. It can be observed that altering the pH from 6 to 11 leads to an increased absorbance of the band situated at 366 nm. Additionally, the shoulder at pH=6 present at 413 nm disappeared, and a new band appeared at 439nm and 646 nm when the pH reached 11. The emission spectra showed no significant changes in the fluorescence intensity with the variation of pH (Figure 4.30 (c)). Furthermore, adding CN^- to chemosensors 6a at pH= 6 and pH=11 did not significantly change the absorption band (Figure 4.30 (b)). Only an increase in the absorbance was observed, and no change in the wavelength. Likewise, the fluorescence intensity increased after adding 20 equiv. of CN^- (Figure. 4.30(d)). It can be concluded from the obtained results that at basic media, the hydroxyl groups present at the salicylidene moiety of the chemosensor 6a are deprotonated. Additionally, the resonance causes the negative charge of oxygen to delocalize into the aromatic system, increasing the electron density on the vinylic carbon and preventing the CN^- addition on the vinylic group (Figure 4.. I). The rest of the chemosensors showed similar results, and the corresponding spectral data are given in Figures 4.31.

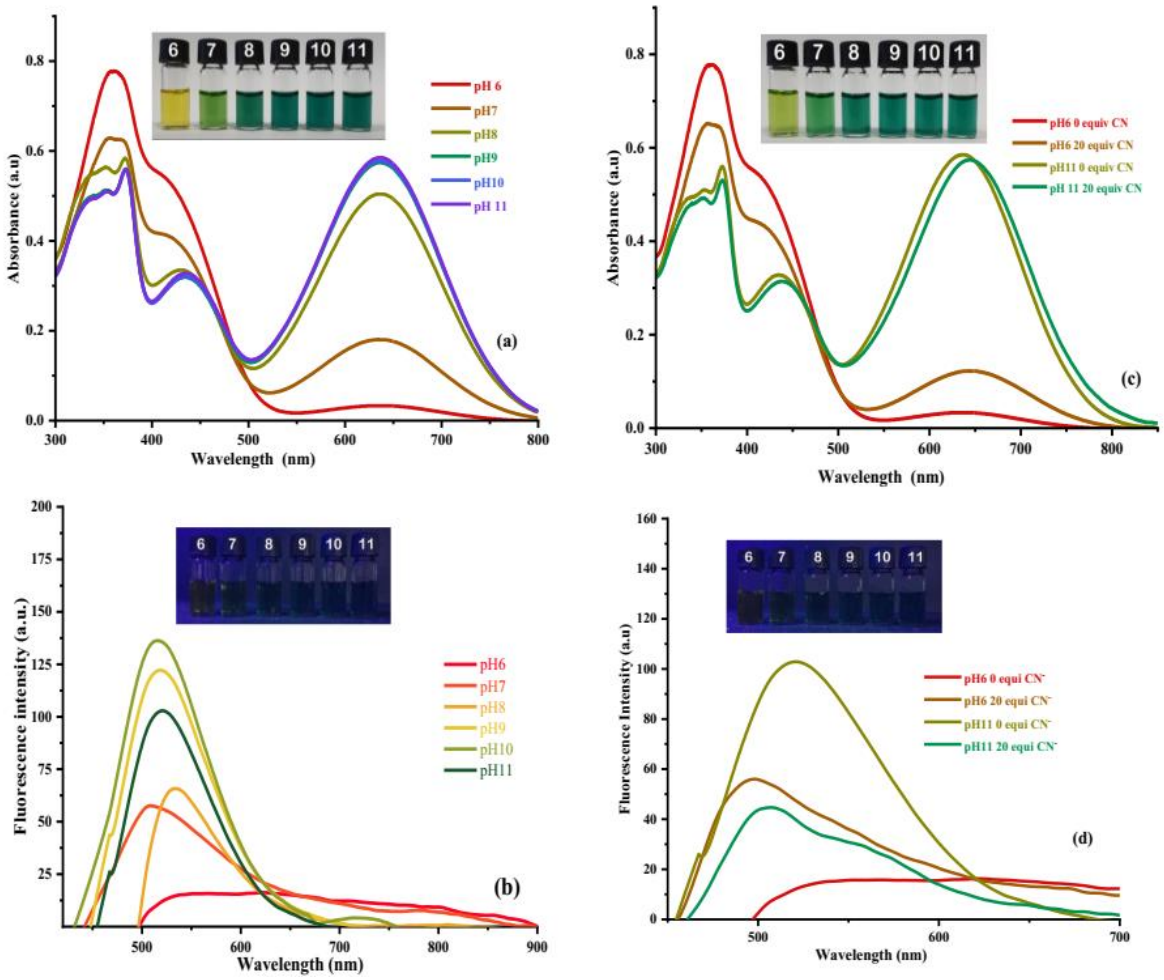

Figure 4.30. Absorption spectra (a) and (b), Emission spectra (c) and (d) of 6a (10 μM) in DMSO/PBS buffer in the absence and presence of CN^- at different pH. Insert: photographs of 6a in different pH values under ambient light (a) and UV light (b). After addition of 20 equiv CN^- anion ambient light (c) , UV light (365nm) (d).

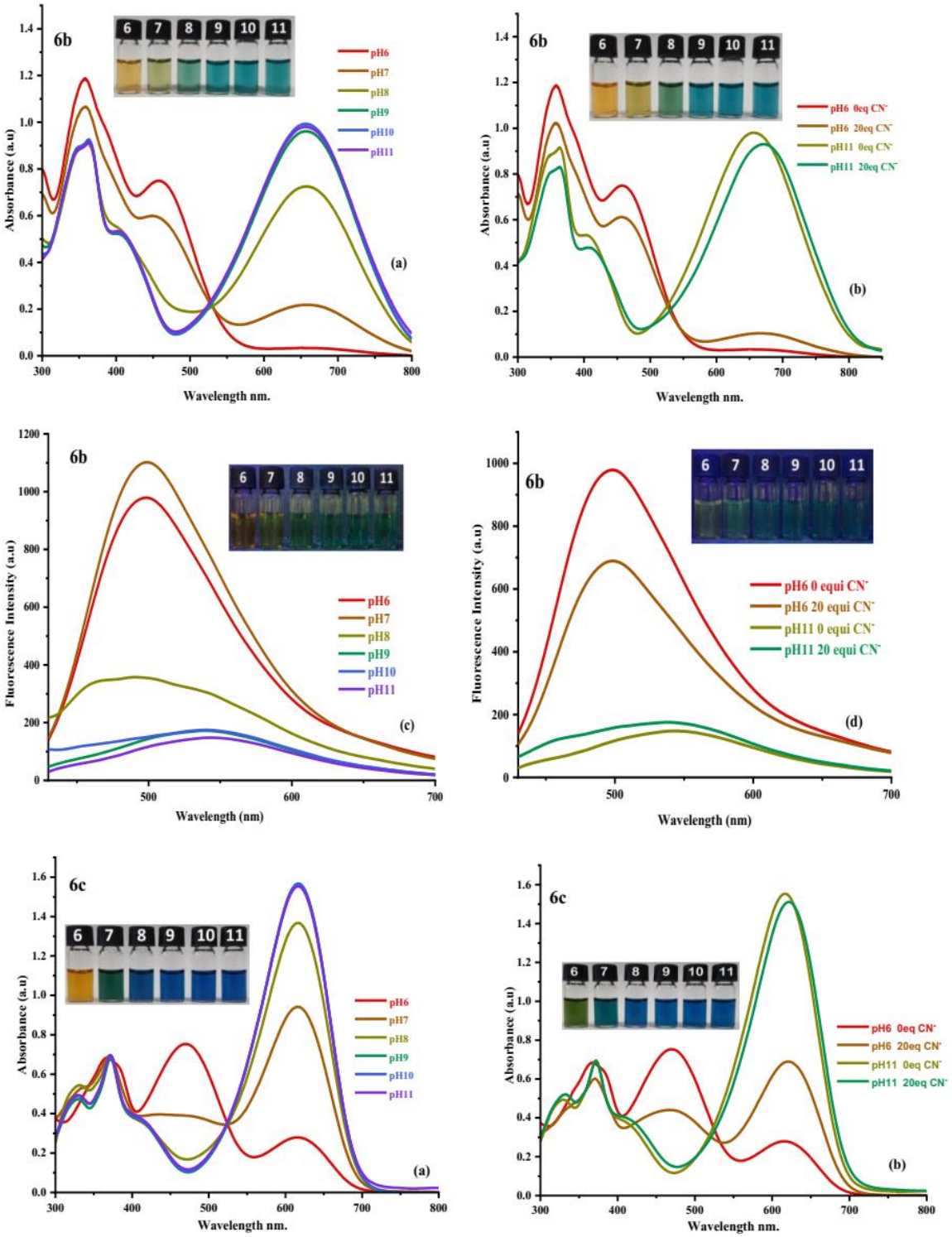

Figure 4.31. Absorption spectra (a) and (b), Emission spectra (c) and (d) of 6b-f (10 μM) in DMSO/PBS buffer in the absence and presence of CN^- at different pH. Insert: Photographs of 6b-f in different pH values under ambient light (a) and UV light (b). After addition of 20 equiv CN^- anion ambient light (c) , UV light (365nm) (d).

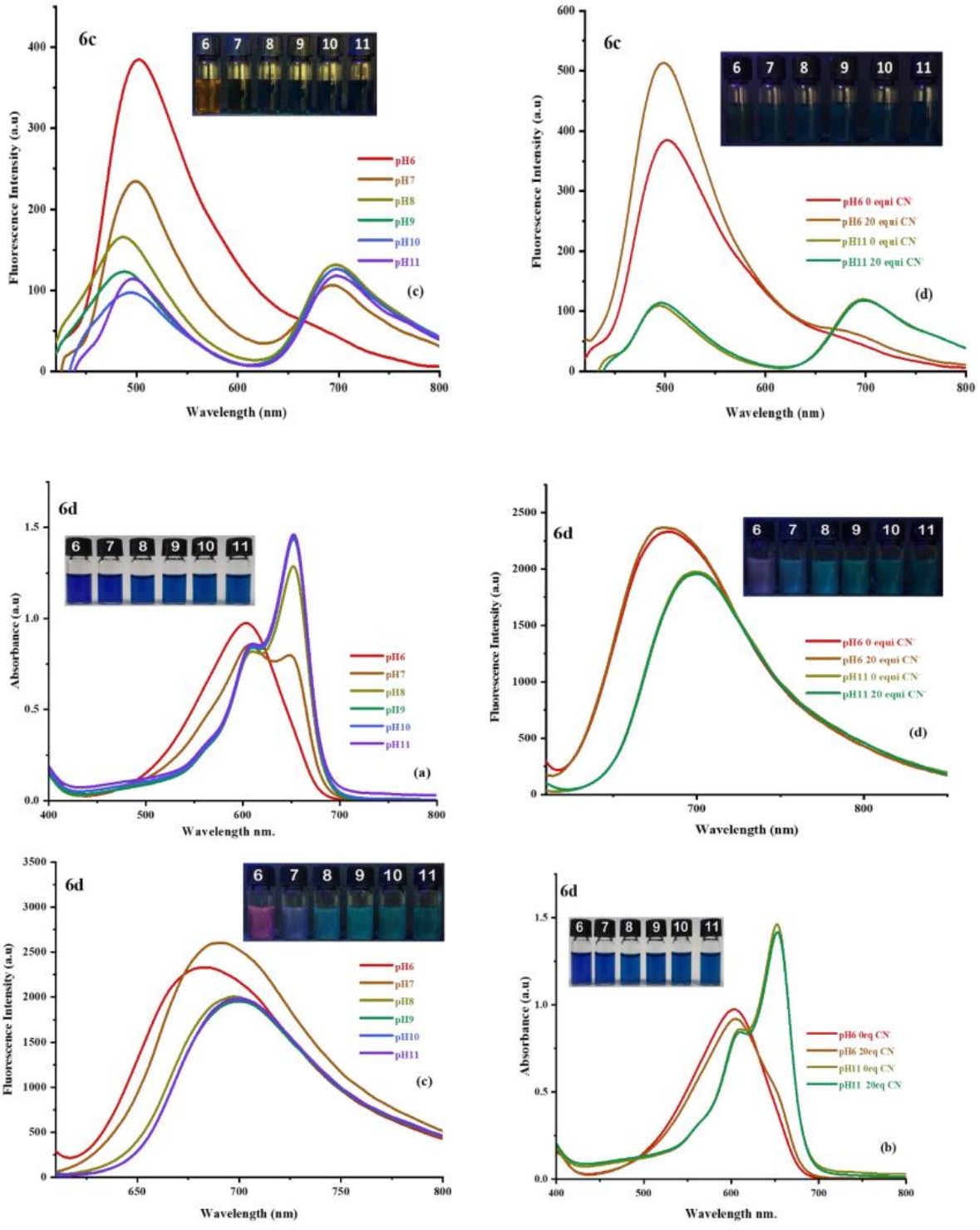

Figure 4.31. (Cont.) Absorption spectra (a) and (b), Emission spectra (c) and (d) of 6b-f (10 μM) in DMSO/PBS buffer in the absence and presence of CN^- at different pH. Insert: Photographs of 6b-f in different pH values under ambient light (a) and UV light (b). After addition of 20 equiv CN^- anion ambient light (c) , UV light (365nm) (d).

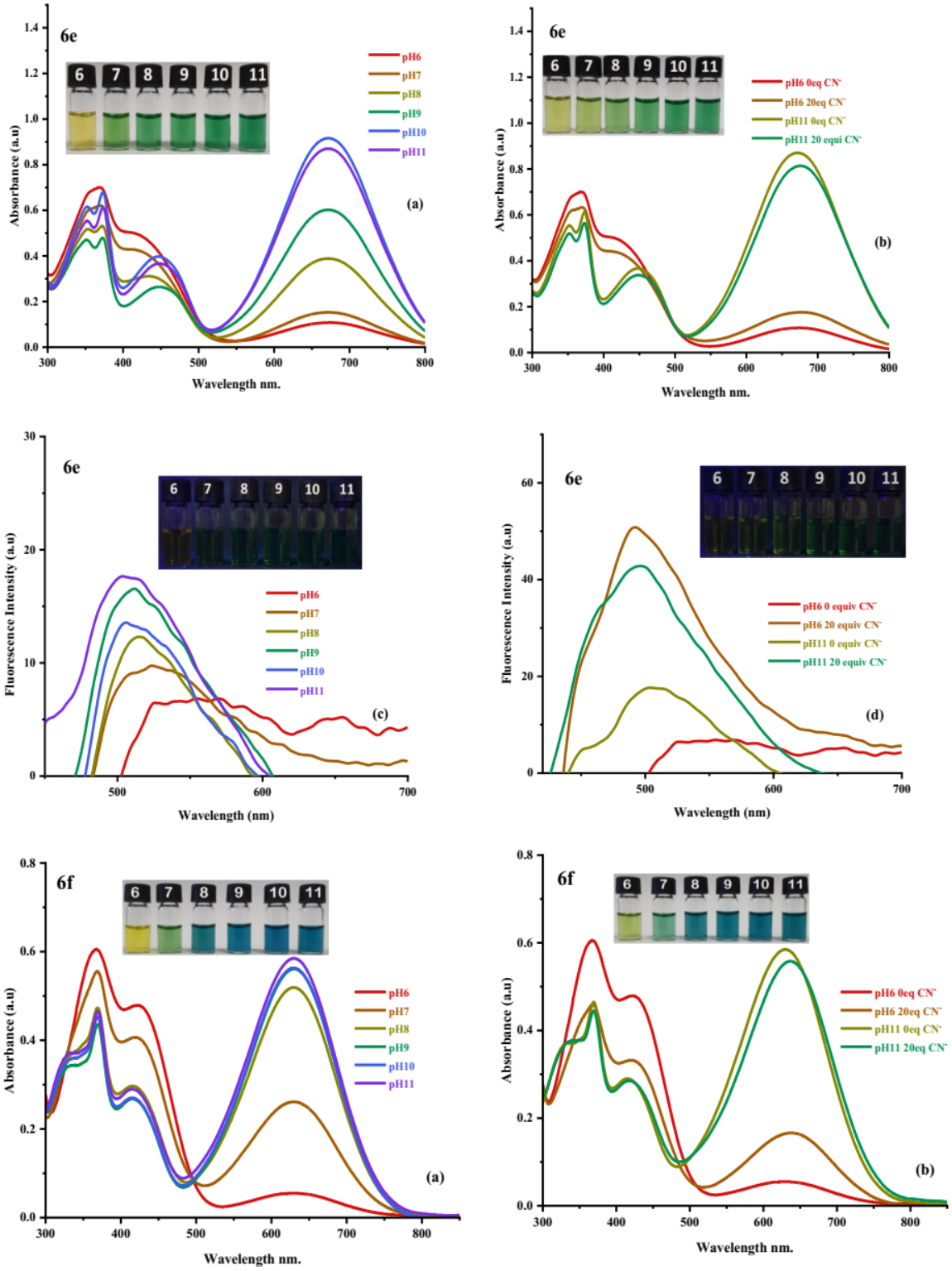

Figure 4.31. (Cont.) Absorption spectra (a) and (b), Emission spectra (c) and (d) of 6b-f (10 μM) in DMSO/PBS buffer in the absence and presence of CN^- at different pH. Insert: Photographs of 6b-f in different pH values under ambient light (a) and UV light (b). After addition of 20 equiv CN^- anion ambient light (c) , UV light (365nm) (d).

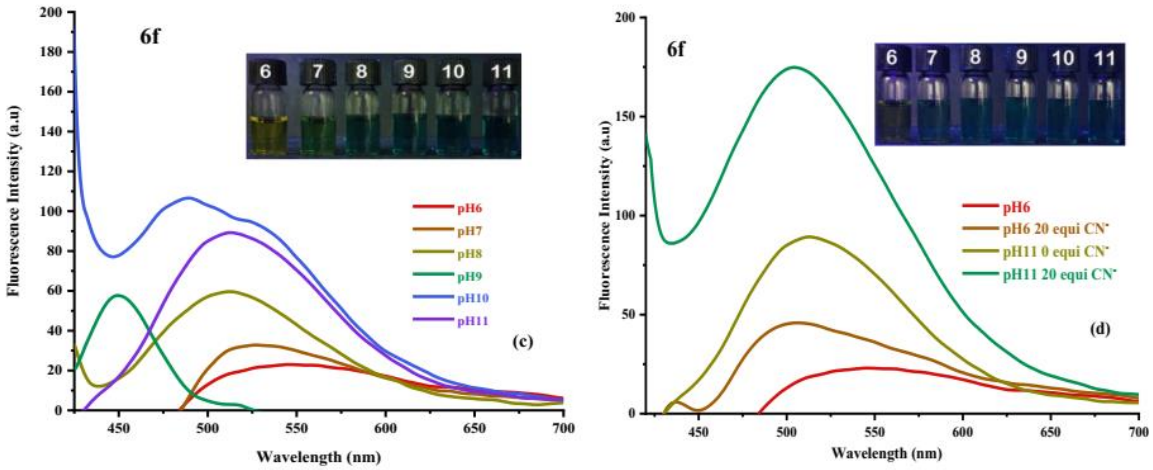

Figure 4.31. (Cont.) Emission spectra (c) and (d) of 6b-f (10 µM) in DMSO/PBS buffer in the absence and presence of CN^- at different pH. Insert: Photographs of 6f in different pH values. After addition of 20 equiv CN^- anion ambient light (c) , UV light (365nm) (d).

4.2.9. Limit of detection and limit of quantification for cyanide ion in partial aqueous medium

For method validation, the Limit of detection (LOD) and Limit of quantification (LOQ) are essential parameters. LOD and LOQ are defined as the minimal analyte concentration that an analytical technique can consistently assess. Furthermore, LOD is defined as the smallest analyte concentration detected but not essentially quantified. However, LOQ is defined as the smallest analyte concentration quantified with acceptable precision and accuracy. The LOD and LOQ are expressed as LOD= 3S/b, LOQ= 10S/b, Where S a is the standard deviation of the response, and b is the slope of the calibration curve. This method can be used in all cases, and it is generally valid when the analysis does not include background noise. It employs a variety of low values close to zero for the calibration curve, and a more homogeneous distribution will result in a more relevant evaluation. LOD and LOQ for CN^- were determined from absorbance titration experiments in an aqueous medium. The absorption calibration curve of CN^- and the results are given in Figure A.65. The results of the LOD and LOQ are presented in Table 4.6. All prepared chemosensors exhibited low LOD, especially 6b with a LOD= 1.12 µM which is lower than the WHO standards for cyanide (2.7 µM).

Table 4.6. Values of LOD and LOQ of the chemosensors 6a-f

Dyes	Calibration cuvre [a]	R^2 [b]	LOD (µM) [c]	LOQ (µM) [d]
6a	y = -1489.12x +0.0014	0.9996	2.82	9.40
6b	y =-2213.46x +0.0008	0.9999	1.12	3.75
6c	y = -1988.79x +0.0011	0.9998	1.71	5.73
6d	y =-1007.99 +0.00092	0.9996	2.75	9.18
6e	y =-1514.51x+0.0009	0.9998	1.78	5.95
6f	y = -1747.51x +0.0137	0.9997	2.35	7.83

[a] y and x refer to the signal response (S) and molar concentration (M), respectively. [b] R-squared [c] LOD: limit of detection. [d] LOQ: limit of quantification .

4.2.10. Sensitivity study of organic amines

The synthesized chemosensors were also investigated for their selectivity towards amines. They are extensive contaminants in nature, and their detection is challenging. Seven amines (pyridine, piperidine, pyrrolidine, diethylamine (DEA), Diphenylamine (DFA), triethylamine (TEA), and triphenylamine (TFA) were selected for this study; however, only four of them showed an interaction with 6a-f. The addition of piperidine, pyrrolidine, TEA, and DEA to chemosensor 6a gave a response, and a new band appeared at 702 nm. The interaction between amines and the rest of the chemosensors was like 6a. The corresponding absorption and emission spectra are given in Figure 4.32. The UV-vis spectra (Figure 4.32 a) showed a decrease in the band at 367 nm and the apparition of a new band at 700 nm upon addition of DEA, TEA, Piperidine, and pyrrolidine. Furthermore, the emission spectra displayed an increase in the fluorescence intensity upon adding the same amines (Figure 4.32 b). The interaction between chemosensors and amines is mainly due to the basicity and additional factors such as steric and conformational effects, resonance as well as induction. The high values of pKa corresponding to Piperidine (11.12), pyrrolidine (11.31), TEA (10.76), and DEA (10.84) make them more basic than DFA (0.79). However, TFA has a pKa= 10.75 but did not interact with the chemosensors; this behavior is due to the steric hindrance. The chemosensors 6b-f showed the same results. The obtained absorption and emission spectra are given in Figures 4.33.

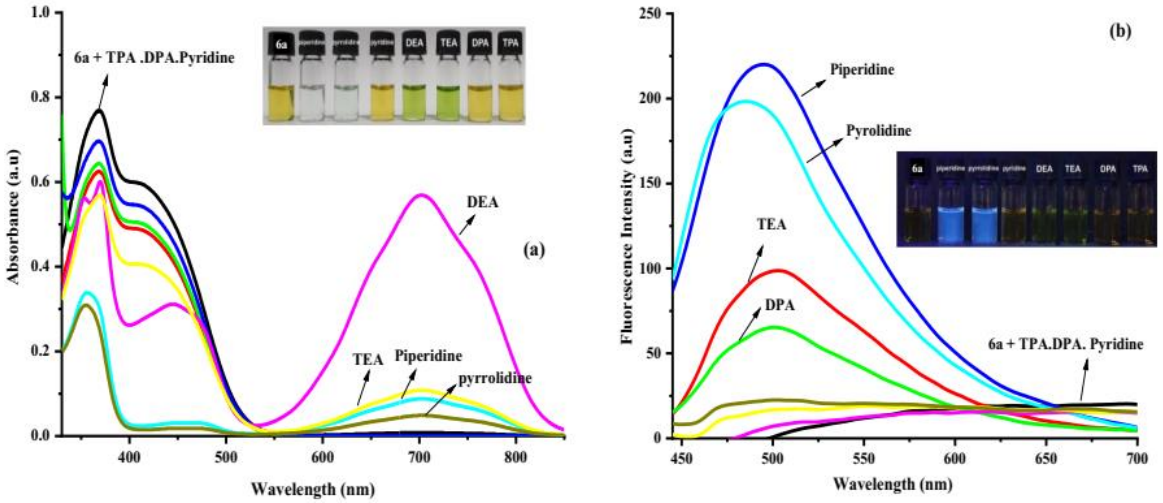

Figure 4.32. a) Absorption spectra (10 μM);(b) Emission spectra (20 μM) of compounds 6a in DMSO after addition of 20 equiv. of different organic bases in DMSO. Insert: photographs of 6a under ambient light (a) and UV light (b). After the addition of 20 equiv. of different organic bases.

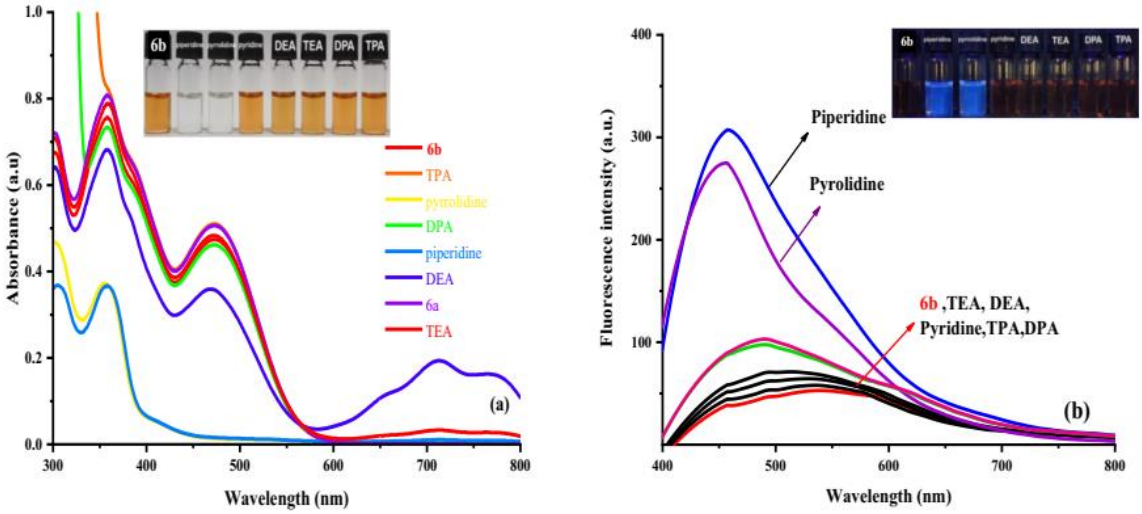

Figure 4.33. a) Absorption spectra (10 μM);(b) Emission spectra (20 μM) of compounds 6b-f in DMSO after addition of 20 equiv. of different organic bases in DMSO. Insert: photographs of 6b-f under ambient light (a) and UV light (b). After the addition of 20 equiv. of different organic bases

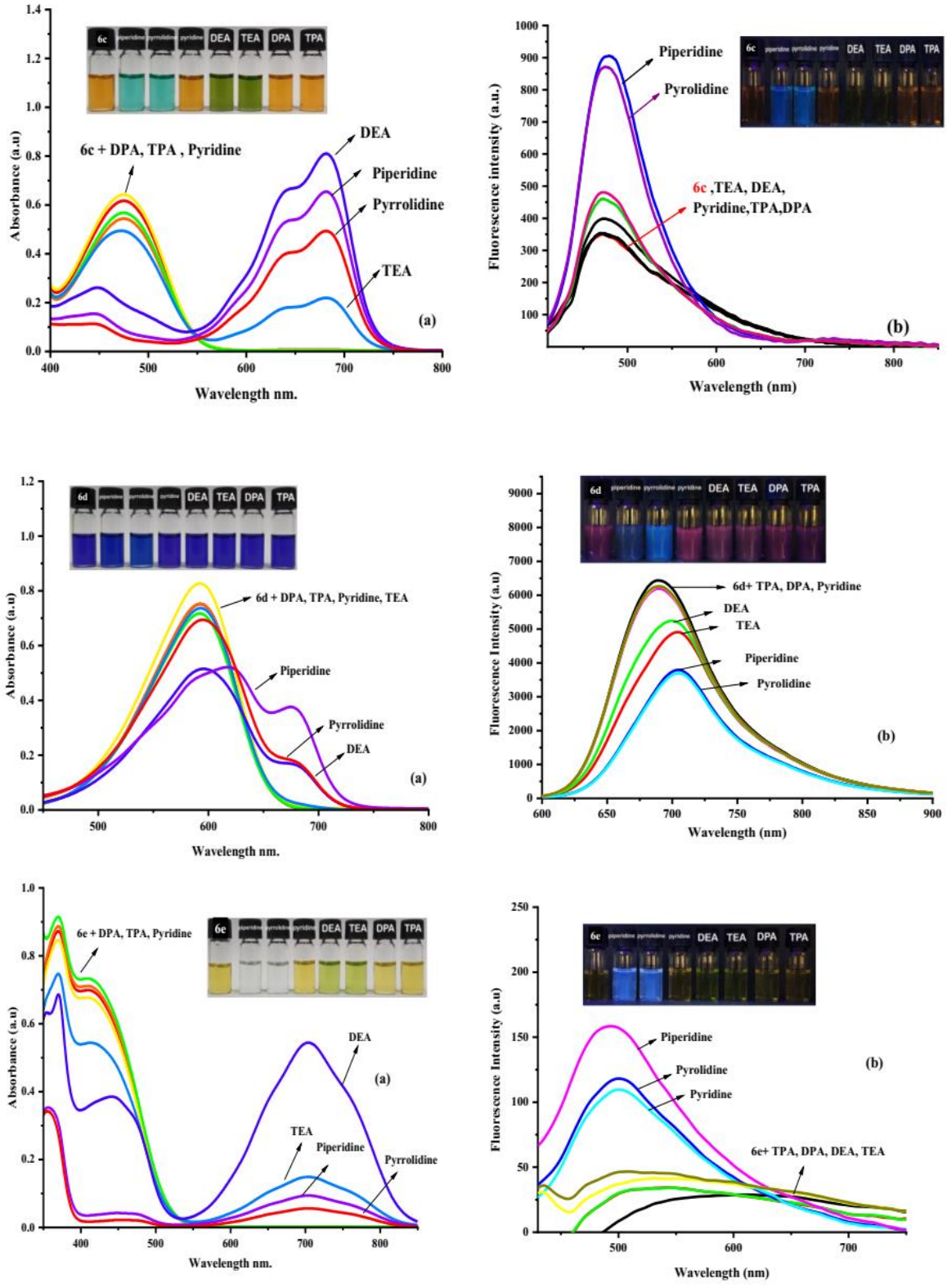

Figure 4.33. (Cont.) a) Absorption spectra (10 μM);(b) Emission spectra (20 μM) of compounds 6b-f in DMSO after addition of 20 equiv. of different organic bases in DMSO. Insert: photographs of 6b-f under ambient light (a) and UV light (b). After the addition of 20 equiv. of different organic bases

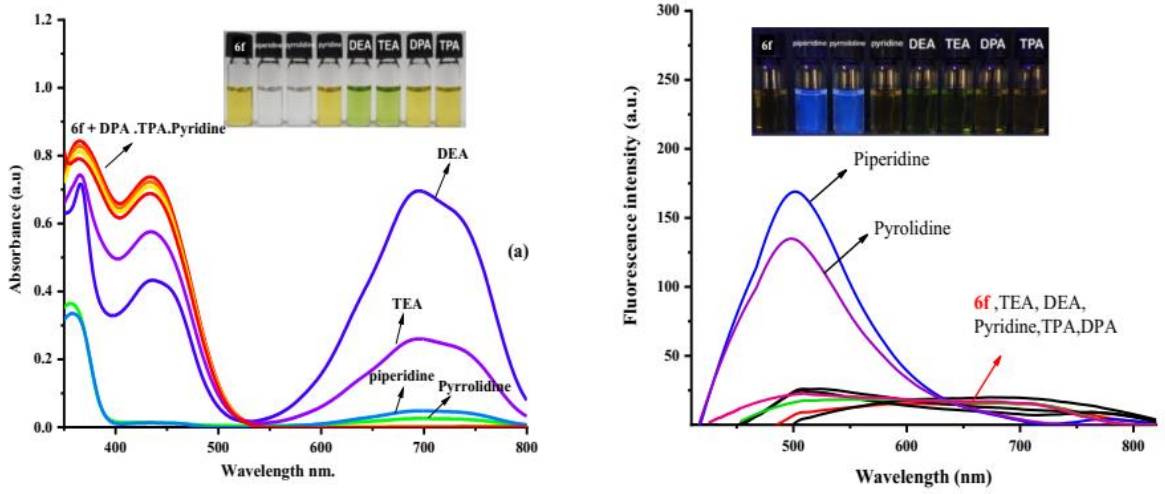

Figure 4.33. (Cont.) a) Absorption spectra (10 μM);(b) Emission spectra (20 μM) of compounds 6b-f in DMSO after addition of 20 equiv. of different organic bases in DMSO. Insert: photographs of 6f under ambient light (a) and UV light (b). After the addition of 20 equiv. of different organic bases

4.2.11. Thermal stability

In order to study the thermal stability of the prepared chemosensors, thermogravimetric analysis (TGA) was carried out. The obtained chemosensors could be used as fluorescent emitters or optical dyes. Hence the necessity of stability thermic. The synthesized compounds were submitted to TGA to study their thermic stability, and the results are shown in Figure 4.34. TGA was conducted under nitrogen gas in a temperature range of 50-600°C at a heating rate of 10°C min^{-1}. The TGA results showed that the synthesized chemosensors are stable up to 200°C. The synthesized chemosensors displayed a weight loss of less than 2% in the range of 100-200°C. The onset decomposition temperature (T_d) is 200°C, 212°C, 198°C, 203°C, 190°C and 220°C for 6a, 6b, 6c, 6d, 6e, and 6f, respectively. The results prove that the chemosensors are quite thermostable, making them an excellent potential for optical dyes applications.

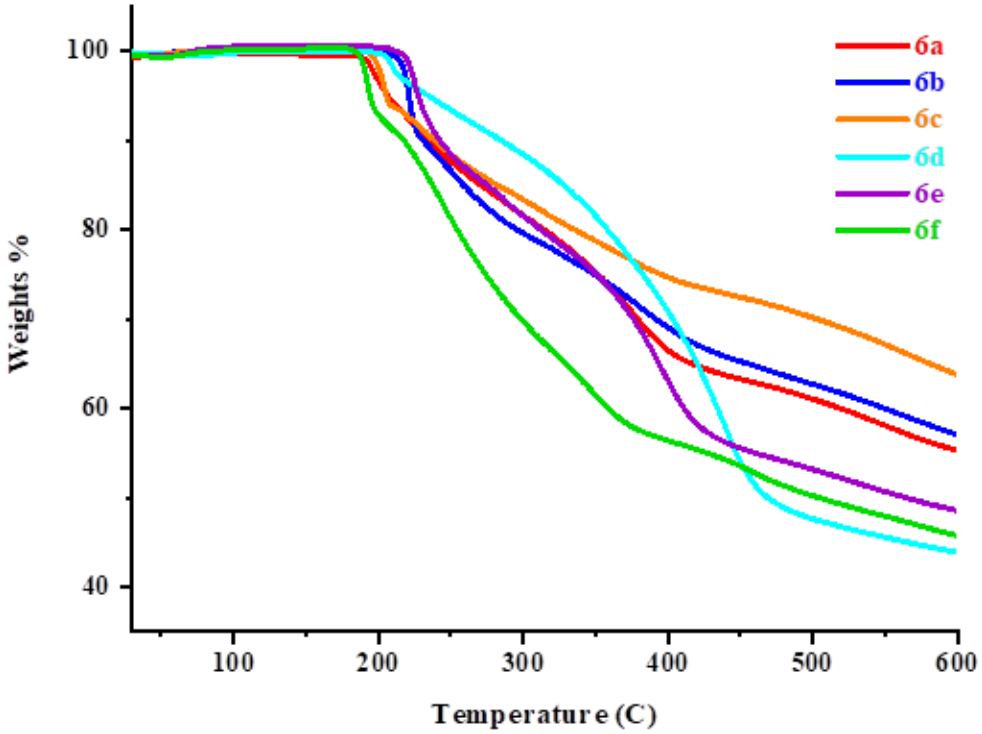

Figure 4.34. TGA curves of 6a-f under nitrogen gas in the temperature range of 50-600°C at a heating rate of 10°C min^{-1}

4.3. Inden-1-ylidene and Fluorene

4.3.1. Introduction

Due to their potential applications in optoelectronics, conjugated organic compounds have drawn immense interest. Organic materials compared to inorganic offer attractive characteristics, including good flexibility, improved transparency, and lighter weight. Flexible electronics tools originating from a flexible substrate result from organic compounds in optoelectronic devices (Kaltenbrunner et al., 2013; Liang et al., 2013; D. Liu & Kelly, 2014; Tsuyoshi Sekitani, Hiroyoshi Nakajima, Hiroki Maeda, Takanori Fukushima, Takuzo Aida, 2009). Hence, OLEDs (Li et al., 2013; Mazzio & Luscombe, 2015) and organic photovoltaic (OPV) (Gao et al., 2014; Sun et al., 2015; G. Zhang et al., 2020) have drawn immense interest. Large area and solid-state irradiation systems are the main advantages of OLEDs. Additionally, OPV offers an alternative source of energy that is renewable. Enhancing these devices' performance can be achieved by designing and tuning organic molecules' properties. In this context, Fluorene, pyrene, and anthracene have drawn considerable attention. Fluorene-based compounds found application in various areas,

including electronics, medical, and optics (Andrade et al., 2010; Knaapila & Monkman, 2013; Kozma et al., 2018; G. Ma et al., 2018; Scherf & List, 2002). The advantage of the fluorene core is the presence of a planar biphenyl unit which results in an exceptional π-conjugated core (Denneval et al., 2013; Sagan et al., 2017; Savel et al., 2014; X. Zhang et al., 2020). Besides, fluorene moiety is electron-rich, leading to enhanced absorption and reduced oxidation potential. The excimer formation, as well as a retrained aggregation, are well-established phenomena in bulky fluorene (Nijegorodov & Downey, 1994; Tao et al., 2005). Two moieties belonging to the hydrocarbons family and can act as electron donors and acceptors are Pyrene and anthracene. An intense PL is exhibited by pyrene in the solution (Figueira-Duarte & Müllen, 2011; S. W. Yang et al., 2005). The generation of excimers is generally due to pyrene and its derivatives in a condensed medium (Ge et al., 2020; J. Wang et al., 2020). Whereas the exceptional PL and EL properties, as well as the large energy gap and stability thermal of anthracene, made them very alluring for blue-emitting materials used in OLEDs (Ho et al., 2012; Qiu et al., 2020; Y. Wang et al., 2020). Several investigations have reported the benefits of pyrene or anthracene combination with fluorene compound (Yahya, Çakmaz, et al., 2021). This part reports the designing of 2 series of 1-dicyanomethylene-2-aryl-indones **7** and 3-amino-2,4-dicyano-1-aryl-9*H*-fluorenes 8 attained from a di/three-component one-pot approach. PL enhancement was achieved by adding Phenyl, anthracen-9-yl, and pyren-1-yl aromatics groups. Several media were used, and the photophysical properties of the synthesized compound were reported.

4.3.2. Synthesis and characterization

The literature has reported several approaches to synthesize fluorene core (Rong et al., 2009; X. S. Wang et al., 2007; Yalçin et al., 2018a, 2019; Zhou et al., 2011). In these approaches, the substitution of fluoren-1-yl part is merely done by small groups. While yield is good, synthesizing fluoren-1-yl using a bulky substituent is difficult. A formerly published two-step approach was used to synthesize the fluorenes 8 using 1-dicyanomethyleneindane and proper aldehydes (Figure 4.46) (Yalçin et al., 2018a). In this approach, malononitrile and pyrrolidine are used as catalysts, and corresponding fluorene 8 was obtained from the isolation and conversion of 2-arylidene-1-dicyanomethyleneindone derivatives 4. Otherwise, the one-pot approach can also give fluorene 8 (Figure 4.35) (Yalçin et al., 2018a). Hence, the two synthetic routes can be assessed. Additionally, the effects of conventional and MWI were studied, and the results are regrouped in Table 4.7.

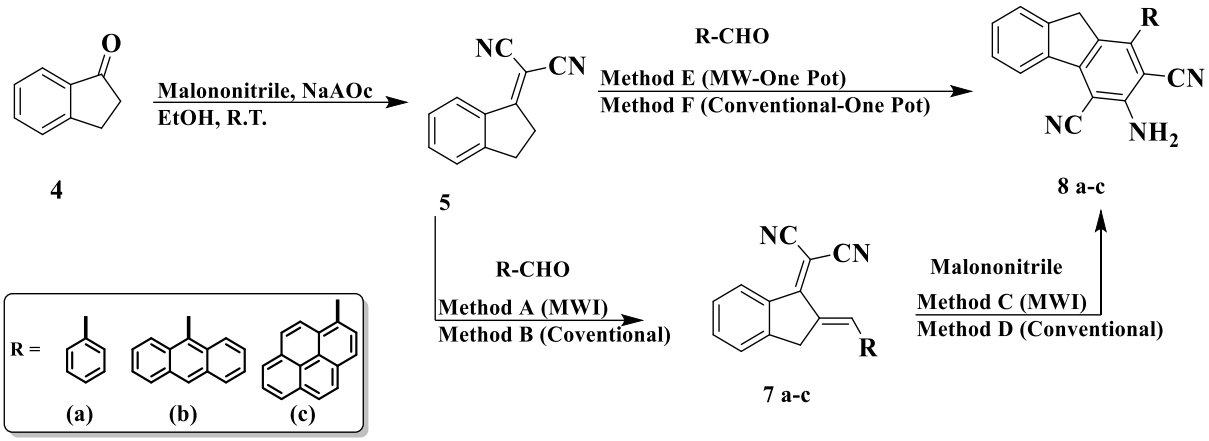

Figure 4.35. Synthetic routes for compounds 7a-c and 8a-c

Table 4.7. Yields of compounds according to the methods used.

Entry	Compound	R	Method	Yield, %
1	7a	phenyl	A	- [a]
			B	97
2	7b	anthracen-9-yl	A	43
			B	43
3	7c	pyren-1-yl	A	52
			B	43
4	8a	phenyl	C	14
			D	14
			E	31
			F	41
5	8b	anthracen-9-yl	C	- [a]
			D	- [a]
			E	23
			F	32
6	8c	pyren-1-yl	C	- [a]
			D	- [a]
			E	30
			F	30

[a]compound could not be obtained.

From Table 4.7 results, it can be concluded that regardless of the used aldehyde, the one-pot approach provides fluorene 8. Furthermore, the yields decreased when anthracen-9-yl and pyren-1-yl bulky were used as substituents, and MWI did not improve it. Additionally, only a phenyl substituent can synthesize 8a from the sequential synthesis of fluorene 8. The dicyanomethyleneindones 7b and 7c are unable to be converted to fluorene 8b and 8c, respectively (Figure 4.36). ^{1}H and ^{13}C NMR, IR spectrometry as well as HRMS were used to characterize the obtained compounds.

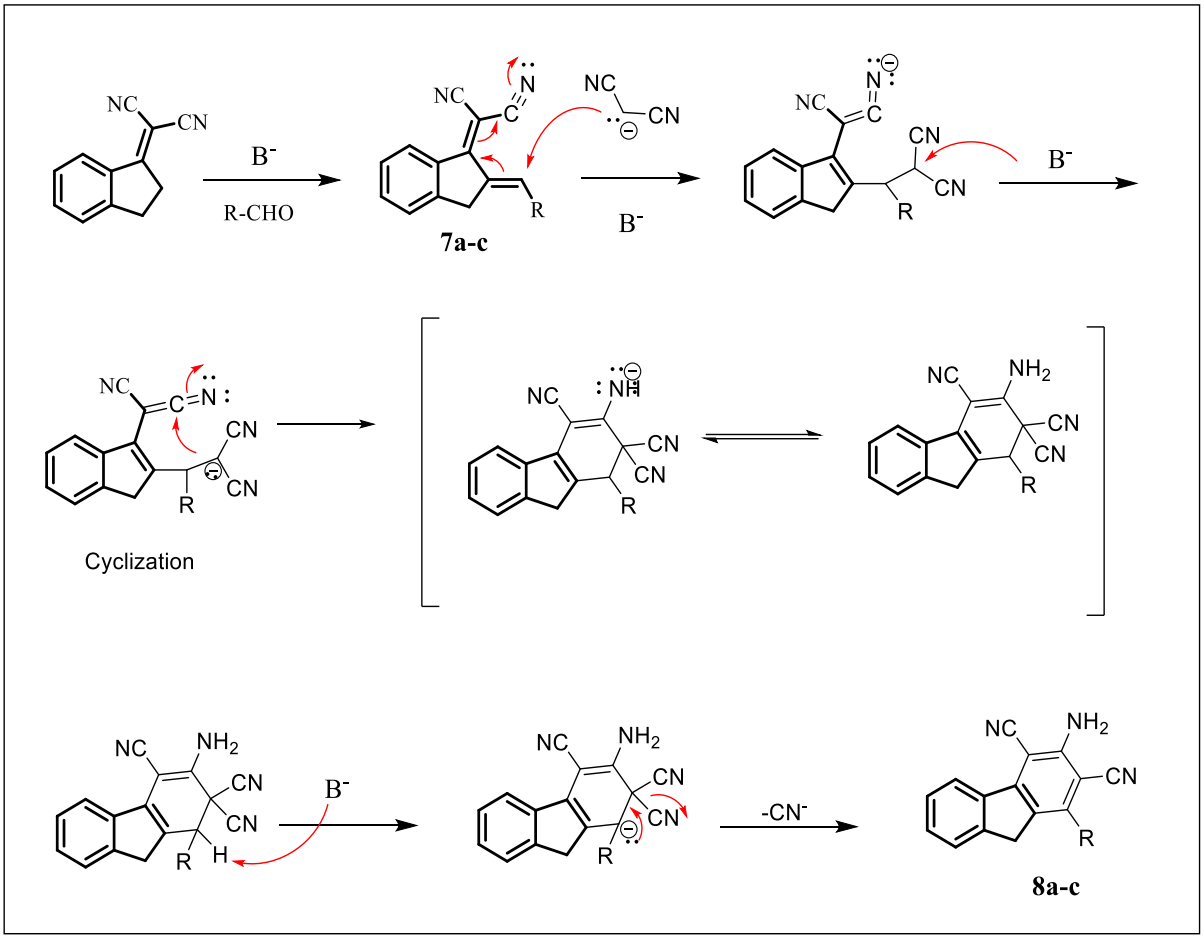

Figure 4.36. Plausible Mechanism for 3-amino-2,4-dicyano-1-aryl-9*H*-fluorene

4.3.3. Photophysical properties

The absorbance and PL investigations were carried out at an ambient temperature in DCM, and the obtained results are given in Table 4.8. Figure 4. and Figure 4. display the normalized spectra. The concentration of chromophore was low ($0.5\text{-}1.5\times10^{-5}$ M). All compounds display several absorption bands in the UV or blue range of the spectrum, apart from 8a. The dicyanometyleneindanes 7 displays a low energetic band of absorption, which is considerably more red-shifted compared to fluorene analogues 8. Fluorenes derivatives 8a, 8b, and 8c display a purple or blue emission and have moderate QY, even though Dicyanometyleneindanes 7 are not emissive. It is worth mentioning that the QY is considerably high for pyren-1-yl derivative 8c (Φ_F = 0.32) compared to the anthracen-9-yl chromophore 8b (Φ_F = 0.09).

Table 4.8. UV-Vis and photoluminescence (PL) data of compounds 7 and 8 in DCM

Compound	λ_{abs} (nm)	ε mM^{-1} cm^{-1}	λ_{em} (nm)	Φ_F	Stokes shift (cm^{-1})
7a	362/390	26.9/22.0	-[a]	-[a]	-[a]
7b	365/475	23.7/5.3	-[a]	-[a]	-[a]
7c	343/487	42.9/22.1	-[a]	-[a]	-[a]
8a	379	10.5	410	0.32	1995
8b	313/369/387	19.2/22.8/22.3	467	0.09	4426
8c	314/330/341/382	31.2/28.7/28.7/24.2	463	0.32	4580

[a]no emission detected

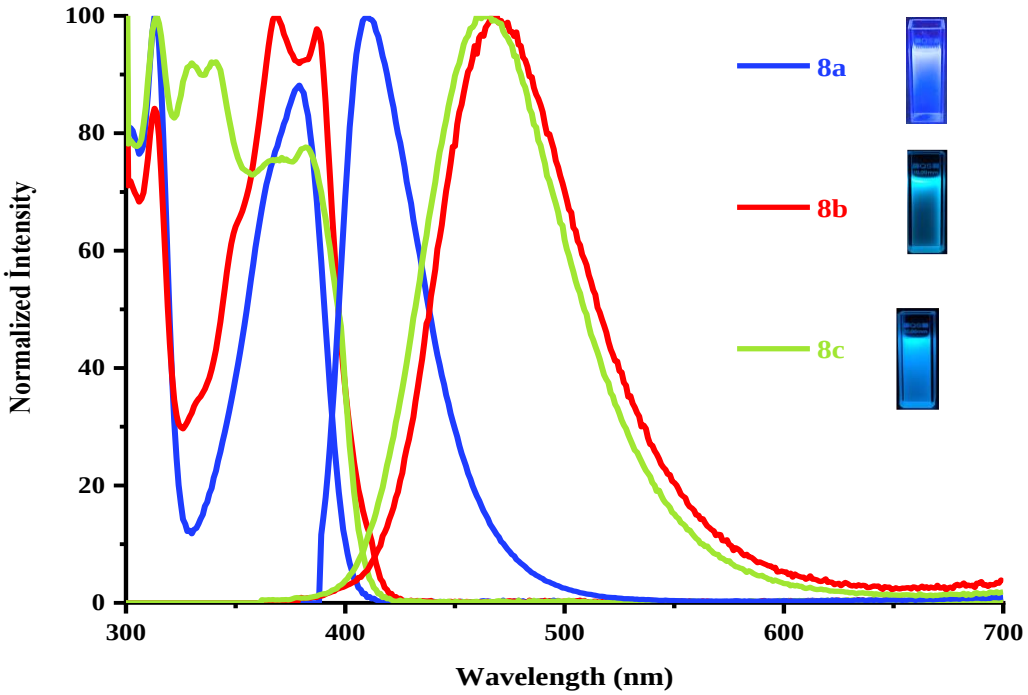

Figure 4.37. Normalized absorption (dashed lines) and emission (solid lines) spectra of compounds 8a-c in DCM. Insert: photographs of DCM solution taken in the dark upon irradiation with hand-held UV lamp (λ_{em} = 366 nm).

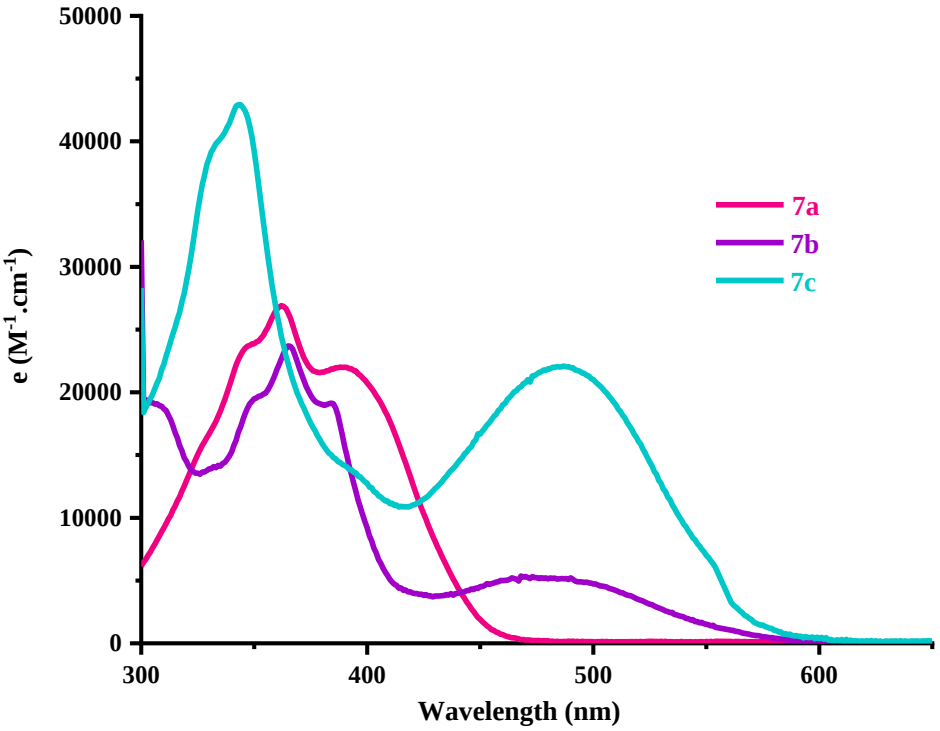

Figure 4.38. Absorption spectra of compounds 7a-c in DCM.

The emission properties of 8 were investigated in a series of solvents with increasing polarities (Table 4.9, Figures 4.39 4.40, and 4.41). The positive solvatochromic is due to the ICT (Hoffert et al., 2017; Lartia et al., 2008; Rodríguez-Aguilar et al., 2018). As anticipated, anthracen-9-yl and pyren-1-yl derivatives 8b and 8c exhibited an extended solvatochromic range because of the presence of a structure having an extended π-conjugated.

Table 4.9. Emission solvatochromism of compounds 8 in various solvents.

Compounds	*n*-heptane	Toluene	THF	$CHCl_3$	DCM	Acetone	MeCN	MeOH
	30.9[a]	33.9[a]	37.4[a]	39.1[a]	40.7[a]	42.2[a]	45.6[a]	55.4[a]
8a	402	416	428	417	410	427	423	433
8b	420	443	447	460	467	481	493	496
8c	420	431	432	450	463	468	485	481

[a] $E_T(30)$, Dimoth-Reichardt polarity parameter in kcal mol^{-1}.(Reichardt, n.d.)

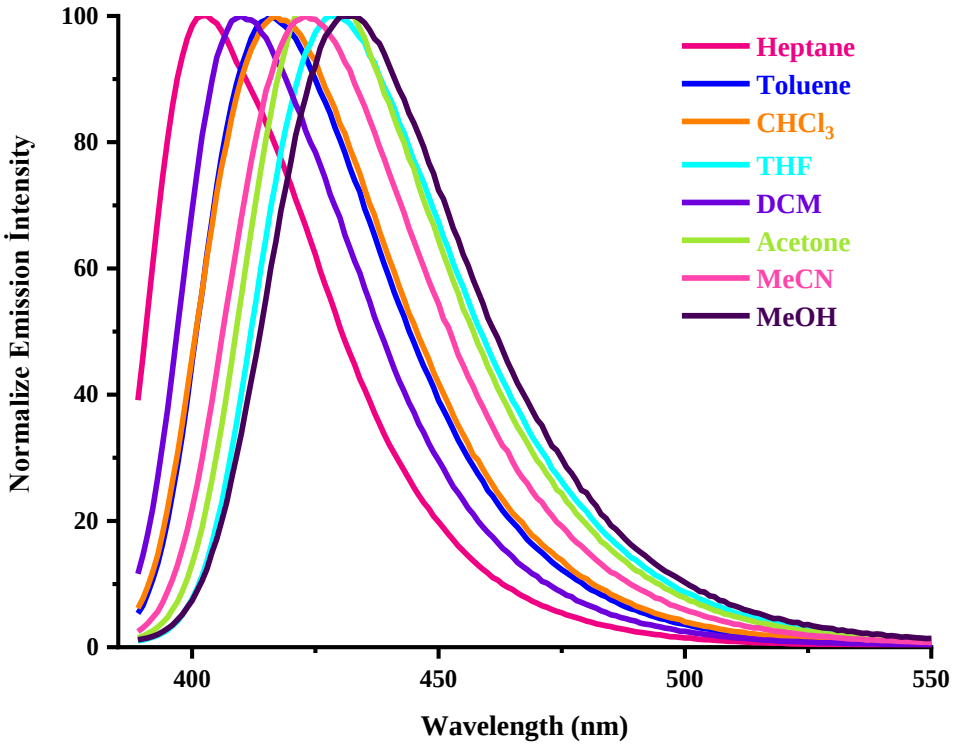

Figure 4.39. Normalized emission spectra of compound 8a in various solvent (λ_{ext} = 379 nm)

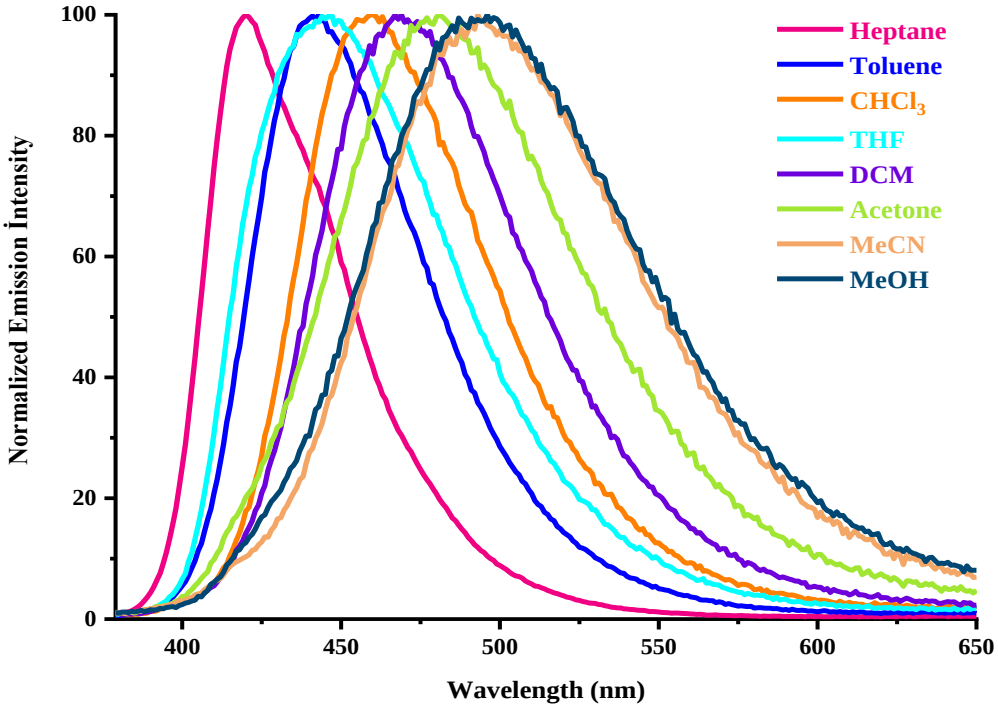

Figure 4.40. Normalized emission spectra of compound 8b in various solvent (λ_{ext} = 369 nm)

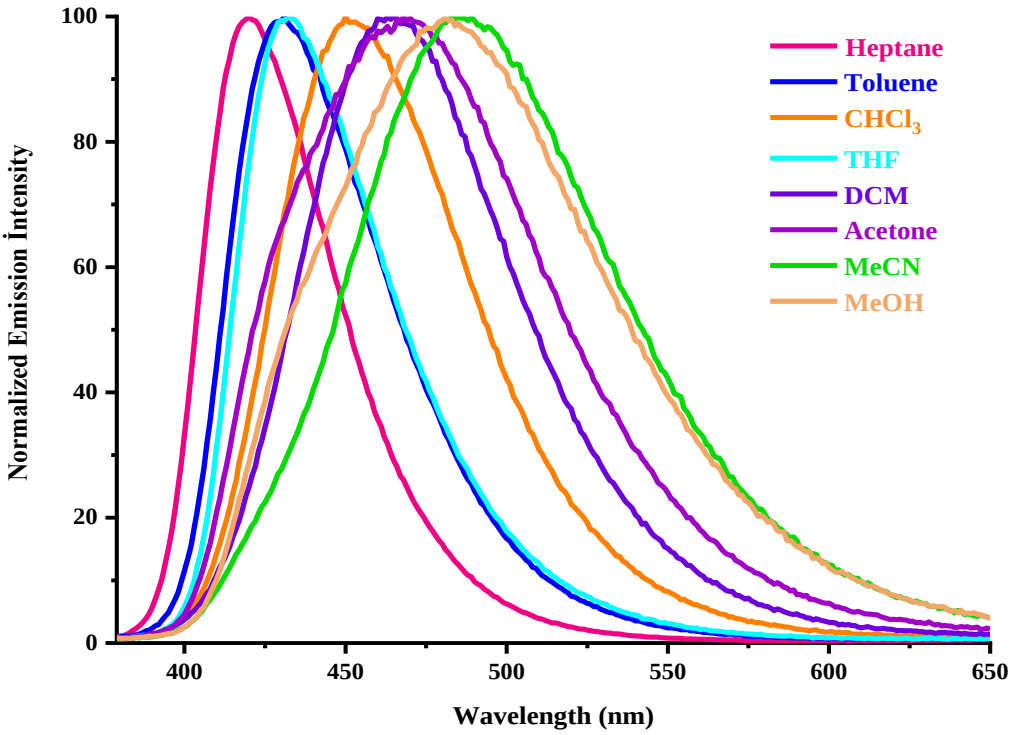

Figure 4.41. Normalized emission spectra of compound 8c in various solvent (λ_{ext} = 369 nm)

The aggregation influence on the PL properties was studied via recording emission spectra of 8 in a mixture of THF-water with various ratios. The obtained spectra are given in Figures 4.42, 4.43, and 4.44. No aggregation-induced emission (AIE) was recorded for 8b and 8c; however, 8a exhibited a different behavior. Compound 8a showed increased intensity by adding water (up to 80%) and a minor emission maximum red-shift (428 to 436 nm). This behavior is ascribed to the solvent's polarity increases. At a higher ratio of water, another band of emission having a low intensity (535 nm) was recorded, and the intensity of the maximum emission band decreased considerably. The new band apparition is credited to the J-aggregates formation. As a result, a turquoise emission is observed at a ratio of 10:90 THF/water, with a similar intensity for both bands. Furthermore, at a ratio of 3:97 THF/water, a green emission and a total quenching of the first band are seen. However, 8b and 8c presented a different behavior. Compound 8b showed a maximum emission at 447 nm in pure THF, in a range of 50% and 70% of water, the band situated at 499 nm moved to 512 nm resulting in a green emission. Adding more water leads to a total quenching of emissions. Identical behavior was recorded for 8c (Figure 4.44).

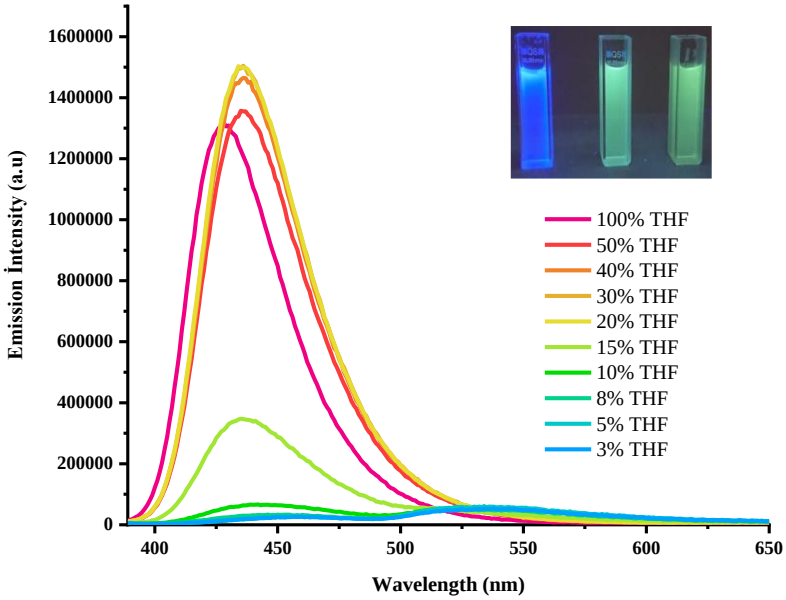

Figure 4.42. Emission spectra of compound 8a in THF/water mixture (c = 1.5 10^{-5} M, λ_{ext} = 379 nm) Insert: photographs of solution with 100:0 10:90 3:97 THF/water ratio taken in the dark upon irradiation with hand-held UV lamp (λ_{em} = 366 nm).

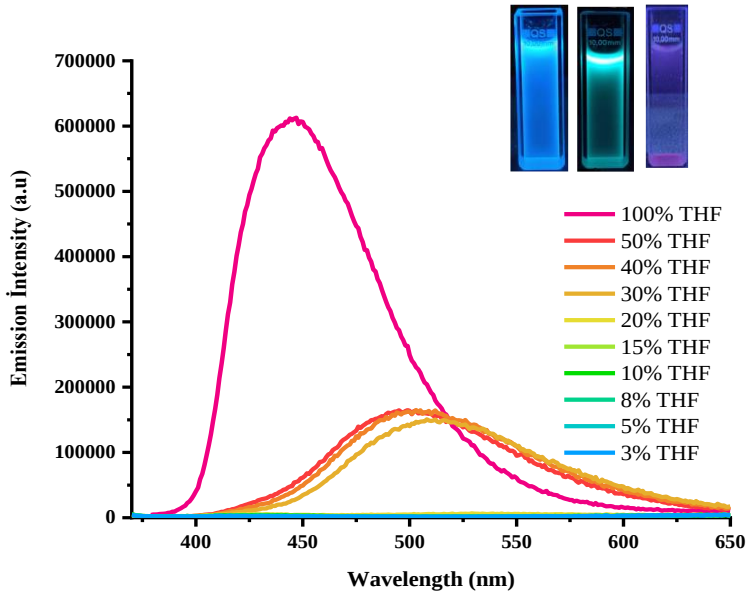

Figure 4.43. Emission spectra of compound 8b in THF/water mixture (c = 1.5 10^{-5} M, λ_{ext} = 360 nm) Insert: photographs of solution with 100:0 50:50 10:90 THF/water ratio taken in the dark upon irradiation with hand-held UV lamp (λ_{em} = 366 nm)

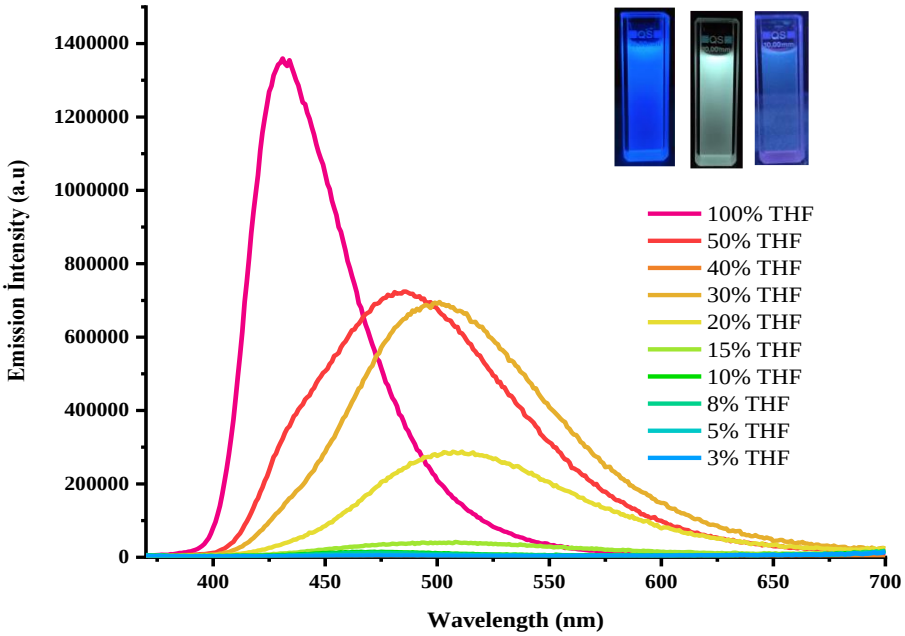

Figure 4.44. Emission spectra of Compound 8c in THF/water mixture (c = 1.5 10^{-5} M, λ_{ext} = 360 nm) Insert: photographs of solution with 100:0, 50:50, 10:90 THF/water ratio taken in the dark upon irradiation with hand-held UV lamp (λ_{em} = 366 nm).

4.3.4. Thermo-gravimetric Analysis (TGA)

TGA was conducted to investigate the thermal stability of the obtained compounds. It is worth mentioning that fluorene gave more thermal stability compared to 1-dicyanometyleneindane **7** (Table 4.10). Also, less stability was recorded for phenyl derivatives 7a and 8a. The compounds do not lose weight up to 100-150^{o}C can be explained by the lack of water or organic solvent. Considerably, 8b and 8c compounds decayed at temperatures higher than 330 ^{o}C and lost 24% and 29% of their mass (Figure 4.45), respectively, implying that 8b and 8c can be used in advanced optical fields necessitating high thermal stability.

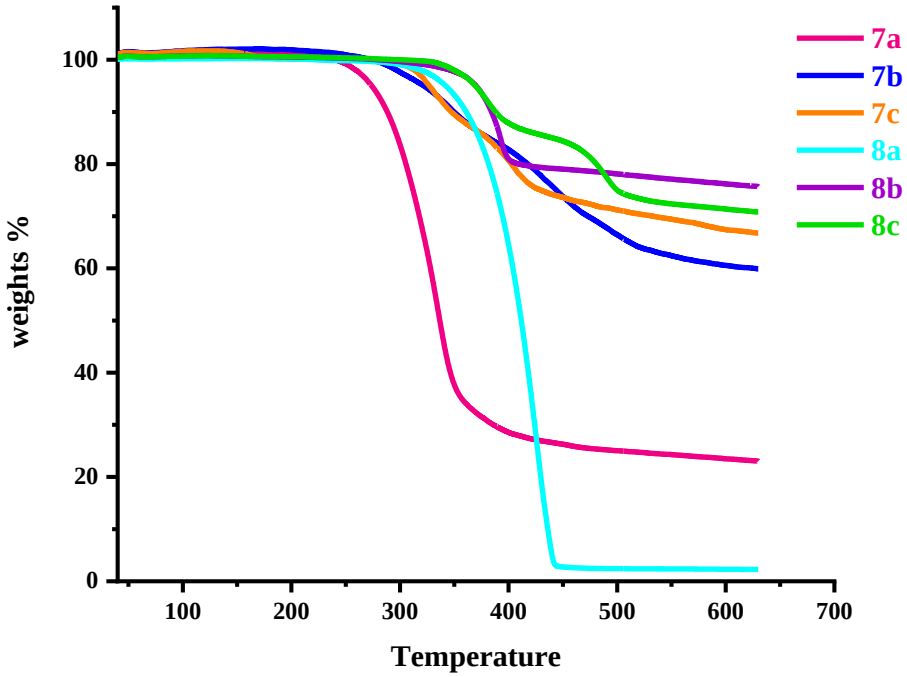

Figure 4.45. TGA curves of chromophores 7a-c and 8a-c under nitrogen atmosphere in the temperature range of 40-700°C at a heating rate of 10°C min^{-1}.

Table 4.10. Thermal decomposition values of compounds 7a-c and 8a-c.

Compound	Temperature °C
7a	246
7b	282
7c	299
8a	300
8b	327
8c	334

5. CONCLUSION

This dissertation aimed to synthesize a variety of novel Donor-π-Acceptor (push-pull) structures to use them in different applications such as NLO materials and fluorescent chemosensors. The solvatochromic properties of all the obtained compounds were also examined.

For this purpose, three systems have been established:

- The system included four 1,1-dicyano-2,4-diaryl-1,3-butadiene bearing various amino electron-donating moieties in the C4 position. These compounds presented a high stability thermic.
- Orange-red emission in solid-state and in the presence of chloroform was observed, and an intensive emission solvatochromism in aprotic solvents was detected related.
- The pyrrolidine derivative exhibited the highest red-shifted absorption band.
- The pyrrolidine derivative compound displays the highest NLO response.
- The 1-dicyanomethylene-2-aryl-indone derivatives (6a-f) were used as chemosensors to detect numerous anions in different mediums.
- Chemosensors 6a-f exhibited F^-, CN^-, AcO^-, OH^- and H_2PO_4 detection in organic and partial aqueous medium as well as tap water (to mimic the natural condition).
- The sensing of the anions (F^-, CN^-, AcO^-, OH^- and $H_2PO_4^-$) occurred via the deprotonation mechanism, confirmed via the ^{1}H-NMR titration experiment.
- The medium's pH does not affect the anions sensing at basic media because of the deprotonation of the hydroxyl groups present at the salicylidene moiety.
- All prepared chemosensors displayed low LOD, especially 6b with a LOD= 1.12 µM which is lower than the WHO standards for cyanide (2.7 µM).
- The obtained 6f presented a crystal structure characterized via the X-ray technique.
- The 3-amino-1-aryl-9*H*-fluorene-2,4-dicarbonitrile and 1-dicyanomethylene-2-aryl-indone scaffolds were investigated via numerous synthesis methods one-pot synthetic route with conventional heating was proven to be the best practical approach to get fluorene derivatives.
- The obtained compound 1-dicyanomethylene-2-anthracen-9-yl-indone 7b presented a crystal structure that was characterized via X-ray technique.
- The obtained results confirmed that the double bond was an E stereoisomery. The fluorenes derivatives displayed a stability thermic up to 300°C.

- The emission in solution was moderated, and the solvatochromism emission was characteristic of the push-pull system.
- Compound 8a-c displayed an AQE behavior; however, upon adding water to THF (50:50 to 70:30 water/THF ratio), the emission intensity of compound 8a was slightly improved.

REFERENCES

Andrade, C. D., Yanez, C. O., Rodriguez, L., & Belfield, K. D. (2010). A Series of Fluorene-Based Two-Photon Absorbing Molecules: Synthesis, Linear and Nonlinear Characterization, and Bioimaging. *The Journal of Organic Chemistry*, *75*(12), 3975–3982.

Bernard Valeur, M. N. B.-S. (2012). *Molecular Fluorescence: Principles and Applications, 2nd Edition.* Wiley-VCH.

Birks, J. B. (John B. (n.d.). *Photophysics of aromatic molecules*.

Boens, N., Leen, V., & Dehaen, W. (2012). Fluorescent indicators based on BODIPY. *Chemical Society Reviews*, *41*(3), 1130–1172.

Braslavsky, S. E. (2007). International Union Of pure and applied chemistry organic and biomolecular chemistry division title on photochemistry glossary of terms used in photochemistry 3 rd edition (IUPAC Recommendations 2006). In *Pure Appl. Chem* (Vol. 79, Issue 3).

Çatal, E., Keleş, E., Seferoğlu, N., Achelle, S., Barsella, A., Robin Le Guen, F., & Seferoğlu, Z. (2018). Triphenylamine-based allylidenemalononitrile chromophores: Synthesis, and photophysical and second-order nonlinear optical properties. *New Journal of Chemistry*, *42*(18), 15052–15060.

Chadwick, S. S. (1988). Ullmann's Encyclopedia of Industrial Chemistry. In *Reference Services Review* (Vol. 16, Issue 4, pp. 31–34). MCB UP Ltd.

Chemchem, M., Yahaya, I., Aydıner, B., Seferoğlu, N., Doluca, O., Merabet, N., & Seferoğlu, Z. (2018). A novel and synthetically facile coumarin-thiophene-derived Schiff base for selective fluorescent detection of cyanide anions in aqueous solution: Synthesis, anion interactions, theoretical study and DNA-binding properties. *Tetrahedron*, *74*(48), 6897–6906.

Chen, G., Qiu, Z., Tan, J. H., Chen, W. C., Zhou, P., Xing, L., Ji, S., Qin, Y., Zhao, Z., & Huo, Y. (2021). Deep-blue organic light-emitting diodes based on push-pull π-extended imidazole-fluorene hybrids. *Dyes and Pigments*, *184*, 108754.

Chen, Y., Lam, J. W. Y., Kwok, R. T. K., Liu, B., & Tang, B. Z. (2019). Aggregation-induced emission: Fundamental understanding and future developments. In *Materials Horizons* (Vol. 6, Issue 3, pp. 428–433). Royal Society of Chemistry.

Cheng, J. Z., Lin, C. C., Chou, P. T., Chaskar, A., & Wong, K. T. (2011). Fluorene as the π-spacer for new two-photon absorption chromophores. *Tetrahedron*, *67*(4), 734–739.

Cohanoschi, I., Belfield, K. D., & Hernández, F. E. (2005). Three-photon absorption enhancement in symmetrical charge transfer pull-pull fluorene derivatives. *Chemical Physics Letters*, *406*(4–6), 462–466.

De Silva, A. P., Gunaratne, H. Q. N., Gunnlaugsson, T., Huxley, A. J. M., McCoy, C. P., Rademacher, J. T., & Rice, T. E. (1997). Signaling recognition events with fluorescent sensors and switches. *Chemical Reviews*, *97*(5), 1515–1566.

Demchenko, A. P. (2015). Basic Principles. In *Introduction to Fluorescence Sensing* (pp. 1–37). Springer International Publishing.

Denneval, C., Moldovan, O., Baudequin, C., Achelle, S., Baldeck, P., Plé, N., Darabantu, M., & Ramondenc, Y. (2013). Synthesis and Photophysical Properties of Push-Pull Structures Incorporating Diazines as Attracting Part with a Fluorene Core. *European Journal of Organic Chemistry*, *2013*(25), 5591–5602.

Dong, X., Wang, R., Liu, G., Liu, P., & Pu, S. (2016). A novel sensitive sensor for Cu2+ and multi-switch based on a diarylethene with a 2-(2′-hydroxyphenyl)benzothiazole unit. *Tetrahedron*, *72*(22), 2935–2942.

Dziuba, D. (2011). *Synthèse de nouvelles sondes de fluorescence bicolores pour le marquage des acides nucléiques et l'étude des interactions protéines-acides nucléiques*.

Fan, J., Hu, M., Zhan, P., & Peng, X. (2013). Energy transfer cassettes based on organic fluorophores: Construction and applications in ratiometric sensing. *Chemical Society Reviews*, *42*(1), 29–43.

Fecková, M., Le Poul, P., Guen, F. R. Le, Roisnel, T., Pytela, O., Klikar, M., Bureš, F., & Achelle, S. (2018). 2,4-Distyryl- and 2,4,6-Tristyrylpyrimidines: Synthesis and Photophysical Properties. *Journal of Organic Chemistry*, *83*(19), 11712–11726.

Feng, X., Hu, J. Y., Wei, X. F., Redshaw, C., & Yamato, T. (2015). Influence of substituent position on thermal properties, photoluminescence and morphology of pyrene-fluorene derivatives. *Journal of Molecular Structure*, *1086*, 216–222.

Feng, Y., Cheng, J., Zhou, L., Zhou, X., & Xiang, H. (2012). Ratiometric optical oxygen sensing: A review in respect of material design. In *Analyst* (Vol. 137, Issue 21, pp. 4885–4901). Royal Society of Chemistry.

Feng, Y., Li, X., Ma, H., Zhang, Z., Zhang, M., & Hao, S. (2018). A simple fluorescent film probe for the detection of fluoride anion in organic solution. *Dyes and Pigments*, *153*, 200–205.

Figueira-Duarte, T. M., & Müllen, K. (2011). Pyrene-based materials for organic electronics. In *Chemical Reviews* (Vol. 111, Issue 11, pp. 7260–7314). American Chemical Society.

Gao, P., Grätzel, M., & Nazeeruddin, M. K. (2014). Organohalide lead perovskites for photovoltaic applications. In *Energy and Environmental Science* (Vol. 7, Issue 8, pp. 2448–2463). Royal Society of Chemistry.

Garcia, M. H., Mendes, P. J., Florindo, P., & Silva, T. (2015). Design and synthesis of NLO efficient organometallic molecules. *AIP Conference Proceedings*, *1642*(1), 514–517.

Gautam, P., Yu, C. P., Zhang, G., Hillier, V. E., & Chan, J. M. W. (2017). Pulling with the Pentafluorosulfanyl Acceptor in Push-Pull Dyes. *Journal of Organic Chemistry*, *82*(20), 11008–11020.

Ge, Y., Wen, Y., Liu, H., Lu, T., Yu, Y., Zhang, X., Li, B., Zhang, S. T., Li, W., & Yang, B. (2020). A key stacking factor for the effective formation of pyrene excimer in crystals: degree of π-π overlap. *Journal of Materials Chemistry C*, *8*(34), 11830–11838.

Gong, P., Liang, F., Kang, L., Chen, X., Qin, J., Wu, Y., & Lin, Z. (2019). Recent advances and future perspectives on infrared nonlinear optical metal halides. In *Coordination Chemistry Reviews* (Vol. 380, pp. 83–102). Elsevier B.V.

Grabowski, Z. R., & Dobkowski, J. (1983). Twisted intramolecular charge transfer (TICT) excited states: Energy and molecular structure. *Pure and Applied Chemistry*, *55*(2),

245–252.

Gu, Y., Zhao, Z., Su, H., Zhang, P., Liu, J., Niu, G., Li, S., Wang, Z., Kwok, R. T. K., Ni, X. L., Sun, J., Qin, A., Lam, J. W. Y., & Tang, B. Z. (2018). Exploration of biocompatible AIEgens from natural resources. *Chemical Science*, *9*(31), 6497–6502.

Guo, Z., Zhu, W., & Tian, H. (2012). Dicyanomethylene-4H-pyran chromophores for OLED emitters, logic gates and optical chemosensors. *Chemical Communications*, *48*(49), 6073–6084.

Gupta, A., & Kumar, N. (2016). A review of mechanisms for fluorescent "turn-on" probes to detect Al3+ ions. In *RSC Advances* (Vol. 6, Issue 108, pp. 106413–106434). Royal Society of Chemistry.

Gupta, V. D., Tathe, A. B., Padalkar, V. S., Umape, P. G., & Sekar, N. (2013). Red emitting solid state fluorescent triphenylamine dyes: Synthesis, photo-physical property and DFT study. *Dyes and Pigments*, *97*(3), 429–439.

He, T., Niu, N., Chen, Z., Li, S., Liu, S., & Li, J. (2018). Novel Quercetin Aggregation-Induced Emission Luminogen (AIEgen) with Excited-State Intramolecular Proton Transfer for In Vivo Bioimaging. *Advanced Functional Materials*, *28*(11), 1706196.

Ho, M.-H., Balaganesan, B., & Chen, C. H. F. (2012). Blue Fluorescence and Bipolar Transport Materials Based on Anthracene and Their Application in OLEDs. *Israel Journal of Chemistry*, *52*(6), 484–495.

Hoffert, K., Durand, R. J., Gauthier, S., Robin-le Guen, F., & Achelle, S. (2017). Synthesis and Photophysical Properties of a Series of Pyrazine-Based Push–Pull Chromophores. *European Journal of Organic Chemistry*, *2017*(3), 523–529.

Hu, R., Leung, N. L. C., & Tang, B. Z. (2014). AIE macromolecules: Syntheses, structures and functionalities. In *Chemical Society Reviews* (Vol. 43, Issue 13, pp. 4494–4562). Royal Society of Chemistry.

Huang, M., Yu, R., Xu, K., Ye, S., Kuang, S., Zhu, X., & Wan, Y. (2016). An arch-bridge-type fluorophore for bridging the gap between aggregation-caused quenching (ACQ) and aggregation-induced emission (AIE). *Chemical Science*, *7*(7), 4485–4491.

Huang, R. Y., Tsai, W. H., Wen, J. J., Chang, Y. J., & Chow, T. J. (2020). Spiro[fluorene-9,9′-phenanthren]-10′-one as auxiliary acceptor of D-A-π-A dyes for dye-sensitized solar cells under one sun and indoor light. *Journal of Power Sources*, *458*, 228063.

Huo, F., Zhang, H., Chen, Z., Qiu, L., Liu, J., Bo, S., & Kityk, I. V. (2019). Novel nonlinear optical push–pull fluorene dyes chromophore as promising materials for telecommunications. *Journal of Materials Science: Materials in Electronics*, *30*(13), 12180–12185.

Jablonski, A. (1933). Efficiency of Anti-Stokes Fluorescence in Dyes. *Nature*, *131*(3319), 839–840.

Kaltenbrunner, M., Sekitani, T., Reeder, J., Yokota, T., Kuribara, K., Tokuhara, T., Drack, M., Schwödiauer, R., Graz, I., Bauer-Gogonea, S., Bauer, S., & Someya, T. (2013). An ultra-lightweight design for imperceptible plastic electronics. *Nature*, *499*(7459), 458–463.

Karuppasamy, A., Stalindurai, K., Peng, J. De, Ho, K. C., & Ramalingan, C. (2018). Organic

dyes festooned with fluorene and fused thiazine for efficient dye-sensitized solar cells. *Electrochimica Acta*, *268*, 347–357.

Kasha, M. (1950). Characterization of electronic transitions in complex molecules. *Discussions of the Faraday Society*, *9*(0), 14–19.

Kato, N. (n.d.). *Optical second harmonic generation microscopy: application to the sensitive detection of cell membrane damage History of second harmonic generation and its application for imaging*.

Kaur, P., Kaur, S., & Singh, K. (2009). Colorimetric detection of cyanide in water using a highly selective Cu2+ chemosensor. *Inorganic Chemistry Communications*, *12*(10), 978–981.

Kim, J. S., & Quang, D. T. (2007). Calixarene-derived fluorescent probes. In *Chemical Reviews* (Vol. 107, Issue 9, pp. 3780–3799). American Chemical Society .

Kirk, K. L., & Kirk, K. L. (1991). The Halogens: Discovery, Occurrence, and Biochemistry of the Free Elements. In *Biochemistry of the Elemental Halogens and Inorganic Halides* (pp. 1–17). Springer US.

Kisiel, A., Baniak, B., Maksymiuk, K., & Michalska, A. (2020). Ion-selective reversing aggregation-caused quenching - Maximizing optodes signal stability. *Talanta*, *220*, 121358.

Kłucińska, K., Stelmach, E., Kisiel, A., Maksymiuk, K., & Michalska, A. (2016). Nanoparticles of Fluorescent Conjugated Polymers: Novel Ion-Selective Optodes. *Analytical Chemistry*, *88*(11), 5644–5648.

Knaapila, M., & Monkman, A. P. (2013). Methods for controlling structure and photophysical properties in polyfluorene solutions and gels. In *Advanced Materials* (Vol. 25, Issue 8, pp. 1090–1108). John Wiley & Sons, Ltd.

Kozma, E., Mróz, W., Andicsová Eckstein, A., Lukeš, V., Galeotti, F., Šišková, A., Danko, M., & Catellani, M. (2018). A joint experimental and theoretical study on the electro-optical properties of 1,6- and 1,7-fluorenyl disubstituted perylene diimide isomers. *New Journal of Chemistry*, *42*(2), 1061–1066.

Kundu, R., & Kulshreshtha, C. (2015). Design, synthesis and electronic properties of push-pull-push type dye. *RSC Advances*, *5*(94), 77460–77468.

Kurdyukova, I. V, & Ishchenko, A. A. (2012). Organic dyes based on fluorene and its derivatives. *Russian Chemical Reviews*, *81*(3), 258–290.

Lakowicz, J. R. (2006). Introduction to Fluorescence. In *Principles of Fluorescence Spectroscopy* (pp. 1–26). Springer US.

Lartia, R., Allain, C., Bordeau, G., Schmidt, F., Fiorini-Debuisschert, C., Charra, F., & Teulade-Fichou, M. P. (2008). Synthetic strategies to derivatizable triphenylamines displaying high two-photon absorption. *Journal of Organic Chemistry*, *73*(5), 1732–1744.

Lavanya Devi, C., Yesudas, K., Makarov, N. S., Jayathirtha Rao, V., Bhanuprakash, K., & Perry, J. W. (2015). Fluorenylethynylpyrene derivatives with strong two-photon absorption: Influence of substituents on optical properties. *Journal of Materials Chemistry C*, *3*(15), 3730–3744.

Ledoux, I., & Zyss, J. (1982). Influence of the molecular environment in solution measurements of the Second-order optical susceptibility for urea and derivatives. *Chemical Physics*, *73*(1–2), 203–213.

Lee, D. Y., Singh, N., & Jang, D. O. (2010). A benzimidazole-based single molecular multianalyte fluorescent probe for the simultaneous analysis of Cu2+ and Fe3+. *Tetrahedron Letters*, *51*(7), 1103–1106.

Levine, B. F., & Bethea, C. G. (1974). Molecular hyperpolarizabilities determined from conjugated and nonconjugated organic liquids. *Applied Physics Letters*, *24*(9), 445–447.

Li, D., Zhang, H., & Wang, Y. (2013). Four-coordinate organoboron compounds for organic light-emitting diodes (OLEDs). In *Chemical Society Reviews* (Vol. 42, Issue 21, pp. 8416–8433). Royal Society of Chemistry.

Liang, J., Li, L., Niu, X., Yu, Z., & Pei, Q. (2013). Elastomeric polymer light-emitting devices and displays. *Nature Photonics*, *7*(10), 817–824.

Liu, D., & Kelly, T. L. (2014). Perovskite solar cells with a planar heterojunction structure prepared using room-temperature solution processing techniques. *Nature Photonics*, *8*(2), 133–138.

Liu, F., Yu, C., Qin, G., Peng, M., Wang, Z., Li, Z., Wu, S., Li, C., & Zhang, M. (2020). Enhanced thermal stability and electro-optic activity from fluorene-based nonlinear optical chromophores. *Dyes and Pigments*, *183*, 108751.

Liu, J., Ouyang, C., Huo, F., He, W., & Cao, A. (2020). Progress in the enhancement of electro-optic coefficients and orientation stability for organic second-order nonlinear optical materials. In *Dyes and Pigments* (Vol. 181, p. 108509). Elsevier Ltd.

Long, N. J. (1995). Organometallic Compounds for Nonlinear Optics—The Search for En-light-enment! *Angewandte Chemie International Edition in English*, *34*(1), 21–38.

Lovell, J. F., Liu, T. W. B., Chen, J., & Zheng, G. (2010). Activatable photosensitizers for imaging and therapy. *Chemical Reviews*, *110*(5), 2839–2857.

Lucas, F., Ibraikulov, O. A., Quinton, C., Sicard, L., Heiser, T., Tondelier, D., Geffroy, B., Leclerc, N., Rault-Berthelot, J., & Poriel, C. (2020). Spirophenylacridine-2,7-(diphenylphosphineoxide)-fluorene: A Bipolar Host for High-Efficiency Single-Layer Blue Phosphorescent Organic Light-Emitting Diodes. *Advanced Optical Materials*, *8*(2), 1901225.

Ma, G., Zhao, H., Wang, J., Le, Y., Jiang, H., Deng, H., Hao, J., & Wan, W. (2018). Studies of fluorine auxochrome in C9-fluorenyl anthracenes on optoelectronic property for blue electroluminescent materials. *Dyes and Pigments*, *158*, 420–427.

Ma, X., Sun, R., Cheng, J., Liu, J., Gou, F., Xiang, H., & Zhou, X. (2016). Fluorescence Aggregation-Caused Quenching versus Aggregation-Induced Emission: A Visual Teaching Technology for Undergraduate Chemistry Students. *Journal of Chemical Education*, *93*(2), 345–350.

Mahalakshmi, G., Saravana Kumar, P., Sivaraman, G., Seenivasa Perumal, M., & Elango, K. P. (2021). A simple imine as a dual-channel chemosensor for detection of CN− and HS− ions via different mechanisms in organic and aquo-organic media. *Journal of Photochemistry and Photobiology A: Chemistry*, *406*, 113021.

Marder, S. R. (2009). Themed issue: Nonlinear optics. The evolving field of nonlinear optics - A personal perspective. In *Journal of Materials Chemistry* (Vol. 19, Issue 40, pp. 7392–7393). The Royal Society of Chemistry.

Marini, A., Muñoz-Losa, A., Biancardi, A., & Mennucci, B. (2010). What is Solvatochromism? *The Journal of Physical Chemistry B*, *114*(51), 17128–17135.

Mazzio, K. A., & Luscombe, C. K. (2015). The future of organic photovoltaics. In *Chemical Society Reviews* (Vol. 44, Issue 1, pp. 78–90). Royal Society of Chemistry.

Mei, J., Huang, Y., & Tian, H. (2018). Progress and Trends in AIE-Based Bioprobes: A Brief Overview. In *ACS Applied Materials and Interfaces* (Vol. 10, Issue 15, pp. 12217–12261). American Chemical Society.

Mei, J., Leung, N. L. C., Kwok, R. T. K., Lam, J. W. Y., & Tang, B. Z. (2015). Aggregation-Induced Emission: Together We Shine, United We Soar! In *Chemical Reviews* (Vol. 115, Issue 21, pp. 11718–11940). American Chemical Society.

Meng, F., Wang, J., Ping, Q., & Yeo, Y. (2018). Quantitative Assessment of Nanoparticle Biodistribution by Fluorescence Imaging, Revisited. *ACS Nano*, *12*(7), 6458–6468.

Mirek, J., & Milart, P. (1986). Differences between the Reaction of 2-Benzylidenecyclopentanone with Malononitrile and the Reaction of Cyclopentylidenemalononitrile with Aromatic Aldehydes; Synthesis of Strong Fluorescent o-Aminonitriles. In *Z. Naturforsch* (Vol. 41).

Mohammed, N., Wiles, A. A., Belsley, M., Fernandes, S. S. M., Cariello, M., Rotello, V. M., Raposo, M. M. M., & Cooke, G. (2017). Synthesis and characterisation of push-pull flavin dyes with efficient second harmonic generation (SHG) properties. *RSC Advances*, *7*(39), 24462–24469.

Nijegorodov, N. I., & Downey, W. S. (1994). The Influence of Planarity and Rigidity on the Absorption and Fluorescence Parameters and Intersystem Crossing Rate Constant in Aromatic Molecules. In *J. Phys. Chem* (Vol. 98).

Park, G. J., Lee, J. J., You, G. R., Nguyen, L., Noh, I., & Kim, C. (2016). A dual chemosensor for Zn2+ and Co2+ in aqueous media and living cells: Experimental and theoretical studies. *Sensors and Actuators, B: Chemical*, *223*, 509–519.

Park, S., & Kim, H. J. (2010). Highly activated Michael acceptor by an intramolecular hydrogen bond as a fluorescence turn-on probe for cyanide. *Chemical Communications*, *46*(48), 9197–9199.

Peng, F., Guo, T., Ying, L., Yang, W., Peng, J., & Cao, Y. (2017). Improving electroluminescent performance of blue light-emitting poly(fluorene-co-dibenzothiophene-S,S-dioxide) by end-capping. *Organic Electronics*, *48*, 118–126.

Qi, J., Chen, C., Ding, D., & Tang, B. Z. (2018). Aggregation-Induced Emission Luminogens: Union Is Strength, Gathering Illuminates Healthcare. *Advanced Healthcare Materials*, *7*(20), 1800477.

Qi, J., Hu, X., Dong, X., Lu, Y., Lu, H., Zhao, W., & Wu, W. (2019). Towards more accurate bioimaging of drug nanocarriers: turning aggregation-caused quenching into a useful tool. In *Advanced Drug Delivery Reviews* (Vol. 143, pp. 206–225). Elsevier B.V.

Qi, J., Sun, C., Zebibula, A., Zhang, H., Kwok, R. T. K., Zhao, X., Xi, W., Lam, J. W. Y.,

Qian, J., & Tang, B. Z. (2018). Real-Time and High-Resolution Bioimaging with Bright Aggregation-Induced Emission Dots in Short-Wave Infrared Region. *Advanced Materials*, *30*(12), 1706856.

Qiu, F., Fang, D., Bai, J., Zhang, T., Zhu, Y., Miao, J., Murtaza, I., Hu, Z., Yan, C., & Meng, H. (2020). Anthracene derivatives as highly efficient deep-blue emitters with extremely low driving voltages, Von ≤2.7 V. *Dyes and Pigments*, *180*, 108458.

R. W. Munn, C. N. I. (1993). Principles and Applications of Nonlinear Optical Materials. In C. N. I. R. W. Munn (Ed.), *Principles and Applications of Nonlinear Optical Materials*. Springer Netherlands.

Raikwar, M. M., Mathew, E., Varghese, M., Joe, I. H., & Nethi, S. N. (2019). NLOphoric Triphenylamine Derived Donor-π-Acceptor-π-Donor Based Colorants: Synthesis, Spectroscopic, Density Functional Theory and Z-scan Studies. *Photochemistry and Photobiology*, *95*(4), 931–945.

Reddy, S. M. M., Dorishetty, P., Augustine, G., Deshpande, A. P., Ayyadurai, N., & Shanmugam, G. (2017). A Low-Molecular-Weight Gelator Composed of Pyrene and Fluorene Moieties for Effective Charge Transfer in Supramolecular Ambidextrous Gel. *Langmuir*, *33*(47), 13504–13514.

Reichardt, C. (n.d.). *Solvatochromic Dyes as Solvent Polarity Indicators*.

Reichardt, C. (1994). Solvatochromic Dyes as Solvent Polarity Indicators. *Chemical Reviews*, *94*(8), 2319–2358.

Riis-Johannessen, T., Schenk, K., & Severin, K. (2010). Turn-off-and-on: Chemosensing ensembles for sensing chloride in water by fluorescence spectroscopy. *Inorganic Chemistry*, *49*(20), 9546–9553.

Rodríguez-Aguilar, J., Vidal, M., Pastenes, C., Aliaga, C., Rezende, M. C., & Domínguez, M. (2018). The Solvatofluorochromism of 2,4,6-Triarylpyrimidine Derivatives. *Photochemistry and Photobiology*, *94*(6), 1100–1108.

Rong, L., Han, H., Jiang, H., & Tu, S. (2009). Efficient and Facile Synthesis of 3-Amino-1-aryl-9 *H* -fluorene-2,4-dicarbonitrile Under Solvent-Free Conditions. *Synthetic Communications*, *39*(19), 3493–3499.

Ruslim, C., & Ichimura, K. (2001). Conformation-Assisted Amplification of Chirality Transfer of ChiralZ-Azobenzenes. *Advanced Materials*, *13*(1), 37–40.

Sagan, C., Jiang, Y., Caban, F., Snaider, J., Amell, R., Wei, S., & Florio, G. M. (2017). Oligofluorene Molecular Wires: Synthesis and Single-Molecule Conductance. *Journal of Physical Chemistry C*, *121*(45), 24945–24953.

Saha, S., Ghosh, A., Mahato, P., Mishra, S., Mishra, S. K., Suresh, E., Das, S., & Das, A. (2010). Specific recognition and sensing of CN- in sodium cyanide solution. *Organic Letters*, *12*(15), 3406–3409.

Savel, P., Akdas-Kilig, H., Malval, J. P., Spangenberg, A., Roisnel, T., & Fillaut, J. L. (2014). Metal-induced dimensionality tuning in a series of bipyrimidine-based ligands: A tool to enhance two-photon absorption. *Journal of Materials Chemistry C*, *2*(2), 295–305.

Scherf, U., & List, E. J. W. (2002). Semiconducting polyfluorenes - Towards reliable

structure-property relationships. In *Advanced Materials* (Vol. 14, Issue 7, pp. 477–487). John Wiley & Sons, Ltd.

Sheldrick, G. M. (2008). A short history of SHELX. In *Acta Crystallographica Section A: Foundations of Crystallography* (Vol. 64, Issue 1, pp. 112–122). International Union of Crystallography.

Singer, K. D., & Garito, A. F. (1981). Measurements of molecular second order optical susceptibilities using dc induced second harmonic generation. *The Journal of Chemical Physics*, *75*(7), 3572–3580.

Stelmach, E., Kaczmarczyk, B., Maksymiuk, K., & Michalska, A. (2020). Tailoring polythiophene cation-selective optodes for wide pH range sensing. *Talanta*, *211*, 120663.

Stock, R. I., Dreyer, J. P., Nunes, G. E., Bechtold, I. H., & Machado, V. G. (2019). Optical Chemosensors and Chemodosimeters for Anion Detection Based on Merrifield Resin Functionalized with Brooker's Merocyanine Derivatives. *ACS Applied Polymer Materials*, *1*(7), 1757–1768.

Sun, D., Meng, D., Cai, Y., Fan, B., Li, Y., Jiang, W., Huo, L., Sun, Y., & Wang, Z. (2015). Non-Fullerene-Acceptor-Based Bulk-Heterojunction Organic Solar Cells with Efficiency over 7%. *Journal of the American Chemical Society*, *137*(34), 11156–11162.

Suresh, S., Ramanand, A., Jayaraman, D., & Mani, P. (2012). Review on theoretical aspect of nonlinear optics] Rev. In *Adv. Mater. Sci* (Vol. 30).

Tao, S., Peng, Z., Zhang, X., Wang, P., Lee, C. S., & Lee, S. T. (2005). Highly efficient non-doped blue organic light-emitting diodes based on fluorene derivatives with high thermal stability. *Advanced Functional Materials*, *15*(10), 1716–1721.

Thami, T., Bassoul, P., Petit, M. A., Simon, J., Fort, A., Barzoukas, M., & Villaeys, A. (1992). Highly Polarizable Metallic Complexes for Nonlinear Optics. Cobaltous Complexes of Unsymmetrical Hydrazone Imine Glyoxal Derivatives. *Journal of the American Chemical Society*, *114*(3), 915–921.

Tsuyoshi Sekitani, Hiroyoshi Nakajima, Hiroki Maeda, Takanori Fukushima, Takuzo Aida, K. H. & T. S. (2009). Stretchable active-matrix organic light-emitting diode display using printable elastic conductors. *Nature Materials*, *8*, 494–499.

Valeur, B., & Leray, I. (2000). Design principles of fluorescent molecular sensors for cation recognition. *Coordination Chemistry Reviews*, *205*(1), 3–40.

Wan, W., Du, H., Wang, J., Le, Y., Jiang, H., Chen, H., Zhu, S., & Hao, J. (2013). Novel blue luminescent materials for organic light-emitting diodes based on C9-fluorenyl anthracenes. *Dyes and Pigments*, *96*(3), 642–652.

Wang, H. L., Zhang, B., Xu, W. Y., Bai, Y. Q., & Wu, H. (2007). (4-Acetylphenyl)diphenylamine. *Acta Crystallographica Section E: Structure Reports Online*, *63*(5), 2648–2649.

Wang, J. H., Liu, Y. M., Dong, Z. M., Chao, J. Bin, Wang, H., Wang, Y., & Shuang, S. M. (2020). New colorimetric and fluorometric chemosensor for selective Hg2+ sensing in a near-perfect aqueous solution and bio-imaging. *Journal of Hazardous Materials*, *382*, 121056.

Wang, J., Zhang, X., & Liu, H. B. (2020). Highly sensitive pyrene–dansyl conjugate-based fluorescent sensor for discriminative detection of water in organic solvents. *Dyes and Pigments*, *182*, 108685.

Wang, M., Leung, K. H., Lin, S., Chan, D. S. H., Kwong, D. W. J., Leung, C. H., & Ma, D. L. (2014). A colorimetric chemosensor for CU2+ ion detection based on an iridium(III) complex. *Scientific Reports*, *4*(1), 1–7.

Wang, X. S., Zhang, M. M., Li, Q., Yao, C. S., & Tu, S. J. (2007). An improved and clean procedure for the synthesis of one-donor poly-acceptors systems containing 2,6-dicyanoamine moiety in aqueous media catalyzed by TEBAC in the presence and absence of K2CO3. *Tetrahedron*, *63*(24), 5265–5273.

Wang, Y., Liu, W., Ye, S., Zhang, Q., Duan, Y., Guo, R., & Wang, L. (2020). Molecular engineering of anthracene-based emitters for highly efficient nondoped deep-blue fluorescent OLEDs. *Journal of Materials Chemistry C*, *8*(28), 9678–9687.

Weber, G., & Teale, F. W. J. (1957). Determination of the absolute quantum yield of fluorescent solutions. *Transactions of the Faraday Society*, *53*(0), 646–655.

Wu, D., Sedgwick, A. C., Gunnlaugsson, T., Akkaya, E. U., Yoon, J., & James, T. D. (2017). Fluorescent chemosensors: The past, present and future. In *Chemical Society Reviews* (Vol. 46, Issue 23, pp. 7105–7123). Royal Society of Chemistry.

Würthner, F. (2020). Aggregation-Induced Emission (AIE): A Historical Perspective. *Angewandte Chemie International Edition*, *59*(34), 14192–14196.

Xu, M., Hu, X., Zhang, Y., Bao, X., Pang, A., & Fang, J. K. (2018). Novel Organic Dyes Featuring Spiro[dibenzo[3,4:6,7]cyclohepta[1,2- b]quinoxaline-10,9′-fluorene] (SDBQX) as a Rigid Moiety for Dye-Sensitized Solar Cells. *ACS Applied Energy Materials*, *1*(5), 2200–2207.

Yahaya, I., Seferoğlu, N., & Seferoğlu, Z. (2019). Improved one-pot synthetic conditions for synthesis of functionalized fluorescent coumarin-thiophene hybrids: Syntheses, DFT studies, photophysical and thermal properties. *Tetrahedron*, *75*(14), 2143–2154.

Yahya, M., Çakmaz, D., Achelle, S., le Gall, E., Şahin, E., & Seferoğlu, Z. (2021). Synthesis, photophysical, thermal properties and X-Ray studies of novel organic dyes bearing Inden-1-ylidene and fluorene. *Journal of Photochemistry and Photobiology A: Chemistry*, *416*, 113311.

Yahya, M., Seferoğlu, N., Barsella, A., Achelle, S., & Seferoğlu, Z. (2021). Amino-substituted-1,1-dicyano-2,4-diaryl-1,3-butadiene chromophores: Synthesis and photophysical properties. *Spectrochimica Acta - Part A: Molecular and Biomolecular Spectroscopy*, *248*, 119178.

Yalçin, E., Duyar, H., Çakmaz, D., Şahin, E., & Seferoğlu, Z. (2019). The synthesis of blue emitting 3-Amino-1-hetarylfluorenes and their unprecedented alkylated derivatives. *Tetrahedron*, *75*(35), 130464.

Yalçin, E., Matković, M., Jukić, M., Obrovac, L. G., Piantanida, I., & Seferoğlu, Z. (2018a). Novel fluorene/fluorenone DNA and RNA binders as efficient non-toxic ds-RNA selective fluorescent probes. *Tetrahedron*, *74*(5), 535–543.

Yalçin, E., Matković, M., Jukić, M., Obrovac, L. G., Piantanida, I., & Seferoğlu, Z. (2018b). Novel fluorene/fluorenone DNA and RNA binders as efficient non-toxic ds-RNA

selective fluorescent probes. *Tetrahedron*, *74*(5), 535–543.

Yang, S. W., Elangovan, A., Hwang, K. C., & Ho, T. I. (2005). Electronic polarization reversal and excited state intramolecular charge transfer in donor/acceptor ethynylpyrenes. *Journal of Physical Chemistry B*, *109*(35), 16628–16635.

Yang, Y., Zhao, Q., Feng, W., & Li, F. (2013). Luminescent chemodosimeters for bioimaging. In *Chemical Reviews* (Vol. 113, Issue 1, pp. 192–270). American Chemical Society.

Zeng, S., Li, S. J., Liu, T. T., Sun, X. J., & Xing, Z. Y. (2019). A significant fluorescent "turn-on" chemosensor for Al3+ detection and application in real sample, logic gate and bioimaging. *Inorganica Chimica Acta*, *495*, 118962.

Zhang, G., Chen, X. K., Xiao, J., Chow, P. C. Y., Ren, M., Kupgan, G., Jiao, X., Chan, C. C. S., Du, X., Xia, R., Chen, Z., Yuan, J., Zhang, Y., Zhang, S., Liu, Y., Zou, Y., Yan, H., Wong, K. S., Coropceanu, V., … Cao, Y. (2020). Delocalization of exciton and electron wavefunction in non-fullerene acceptor molecules enables efficient organic solar cells. *Nature Communications*, *11*(1), 1–10.

Zhang, X., Ben Hassine, S., Richy, N., Mongin, O., Blanchard-Desce, M., Paul, F., & Paul-Roth, C. O. (2020). New porphyrin dendrimers with fluorenyl-based connectors: a simple way to improving the optical properties over dendrimers featuring 1,3,5-phenylene connectors. *New Journal of Chemistry*, *44*(10), 4144–4157.

Zhao, N., Lam, J. W. Y., Sung, H. H. Y., Su, H. M., Williams, I. D., Wong, K. S., & Tang, B. Z. (2014). Effect of the Counterion on Light Emission: A Displacement Strategy to Change the Emission Behaviour from Aggregation-Caused Quenching to Aggregation-Induced Emission and to Construct Sensitive Fluorescent Sensors for Hg^{2+} Detection. *Chemistry - A European Journal*, *20*(1), 133–138.

Zheng, Z., Zhang, T., Liu, H., Chen, Y., Kwok, R. T. K., Ma, C., Zhang, P., Sung, H. H. Y., Williams, I. D., Lam, J. W. Y., Wong, K. S., & Tang, B. Z. (2018). Bright near-infrared aggregation-induced emission luminogens with strong two-photon absorption, excellent organelle specificity, and efficient photodynamic therapy potential. *ACS Nano*, *12*(8), 8145–8159.

Zhou, Y., Wang, J., Du, R., Zhang, G., Wang, W., & Guo, C. (2011). Microwave-Assisted One-Pot Synthesis of 3-Amino-1-aryl-8-bromo-2,4-dicyano-9 *H* -fluorenes in Water. *Synthetic Communications*, *41*(21), 3169–3176.

Ziarani, G. M., Moradi, R., Lashgari, N., & Kruger, H. G. (2018). Fluorene Dyes. In *Metal-Free Synthetic Organic Dyes* (pp. 153–164). Elsevier.

ANNEXES

Annex-1. FT-IR, ^{1}H-NMR, ^{13}C-NMR, and HR-MS spectra of compound 3a-d

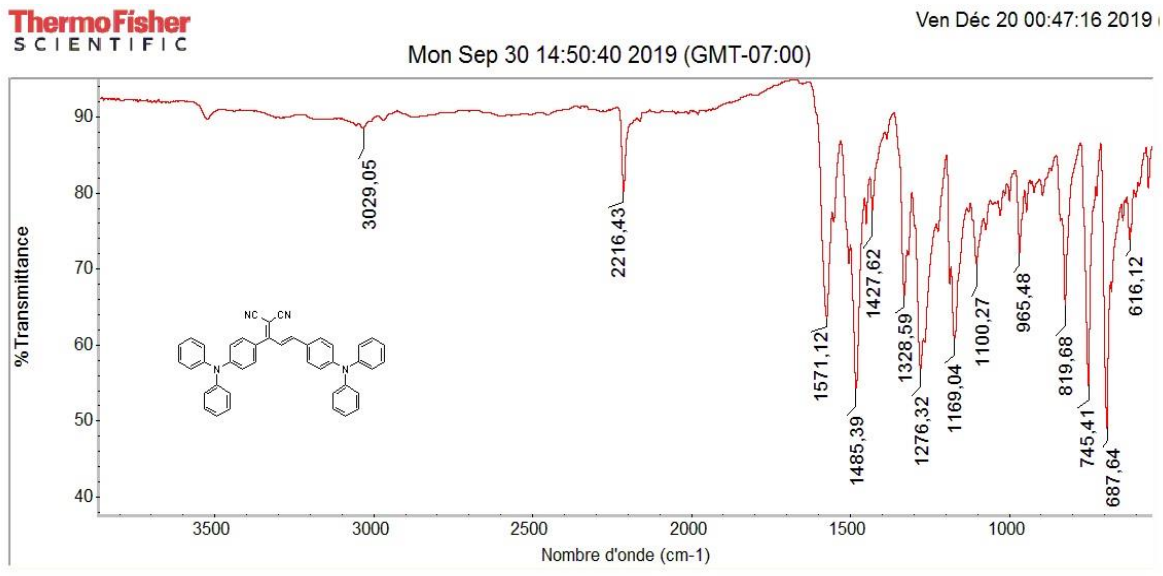

Figure 1.1. FT-IR spectra of 3a

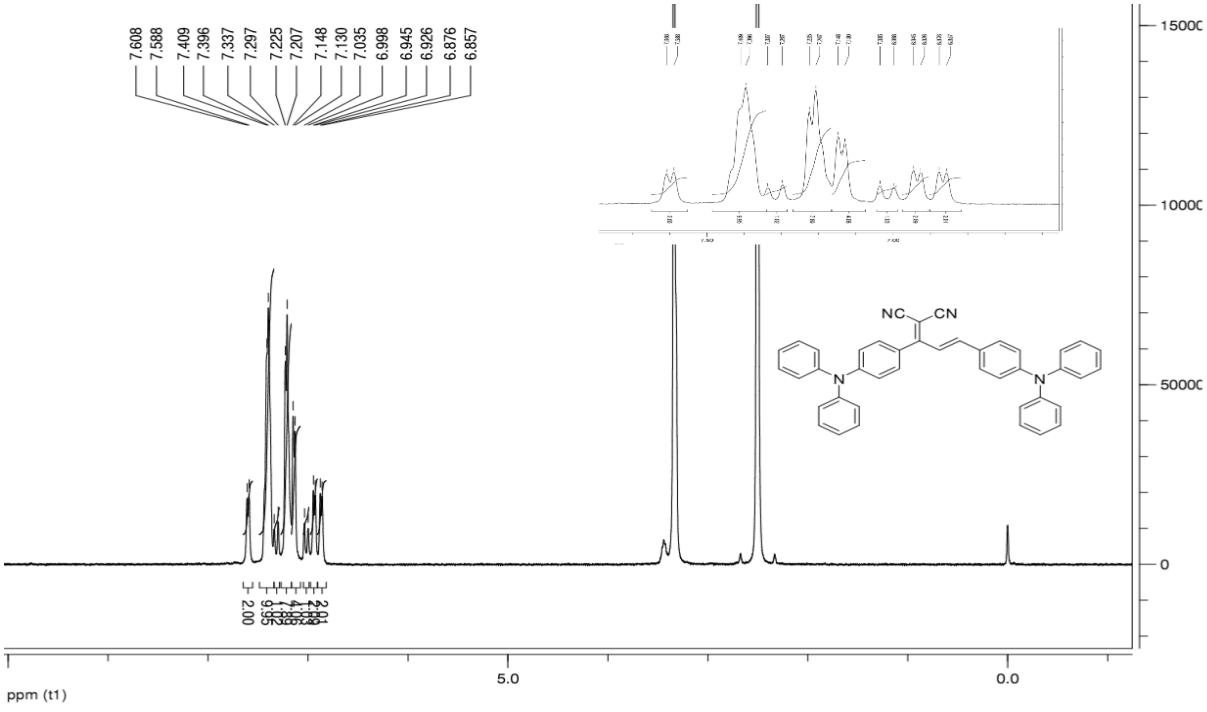

Figure 1. 2. ^{1}H NMR spectra of 3a in DMSO-d_6

Annex-1. (Cont.) FT-IR, ^{1}H-NMR, ^{13}C-NMR, and HR-MS spectra of compound 3a-d

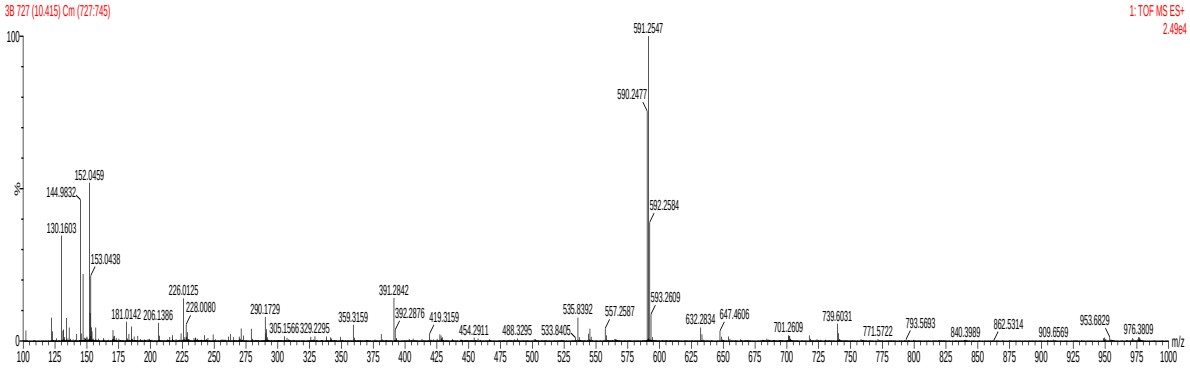

Figure 1.3. HRMS spectra of 3a

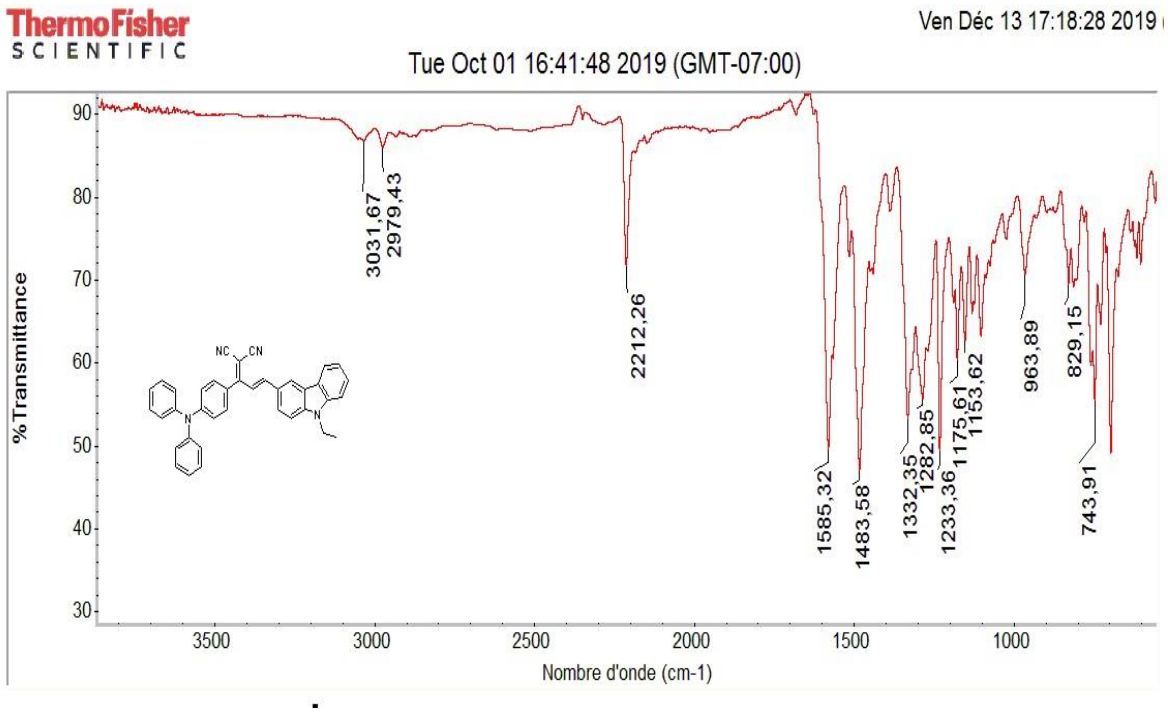

Figure 1.4. FT-IR spectra of 3b

Annex-1. (Cont.) FT-IR, ^{1}H-NMR, ^{13}C-NMR, and HR-MS spectra of compound 3a-d

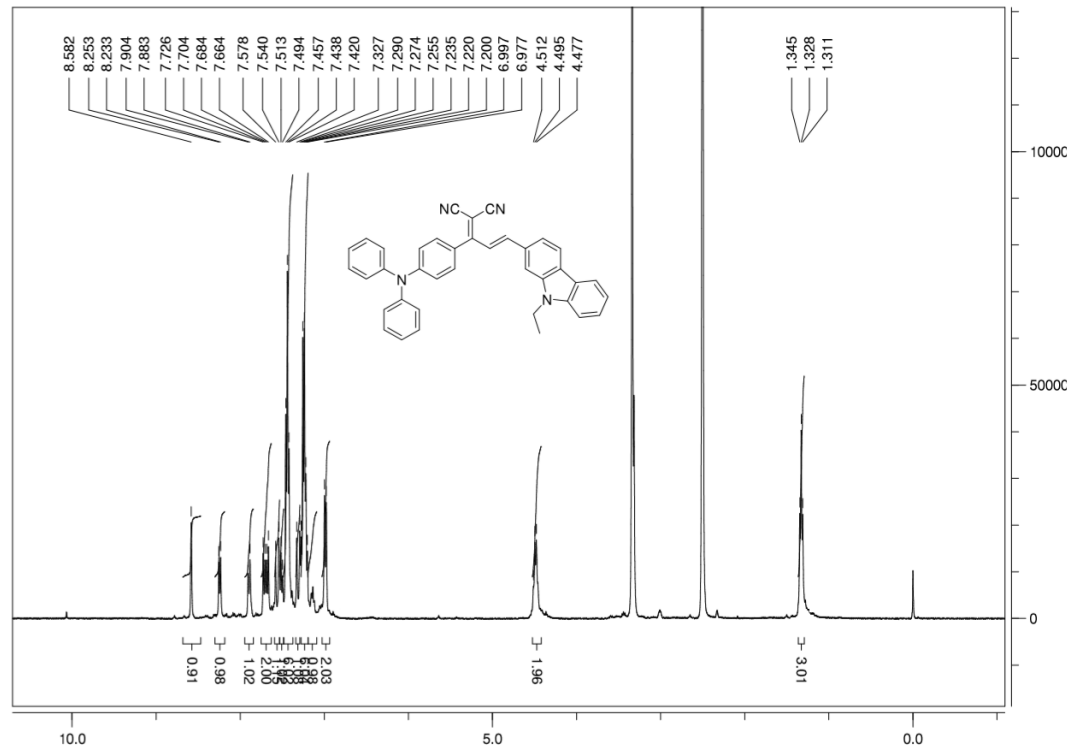

Figure 1.5. ^{1}H-NMR spectra of 3b in DMSO-d_6

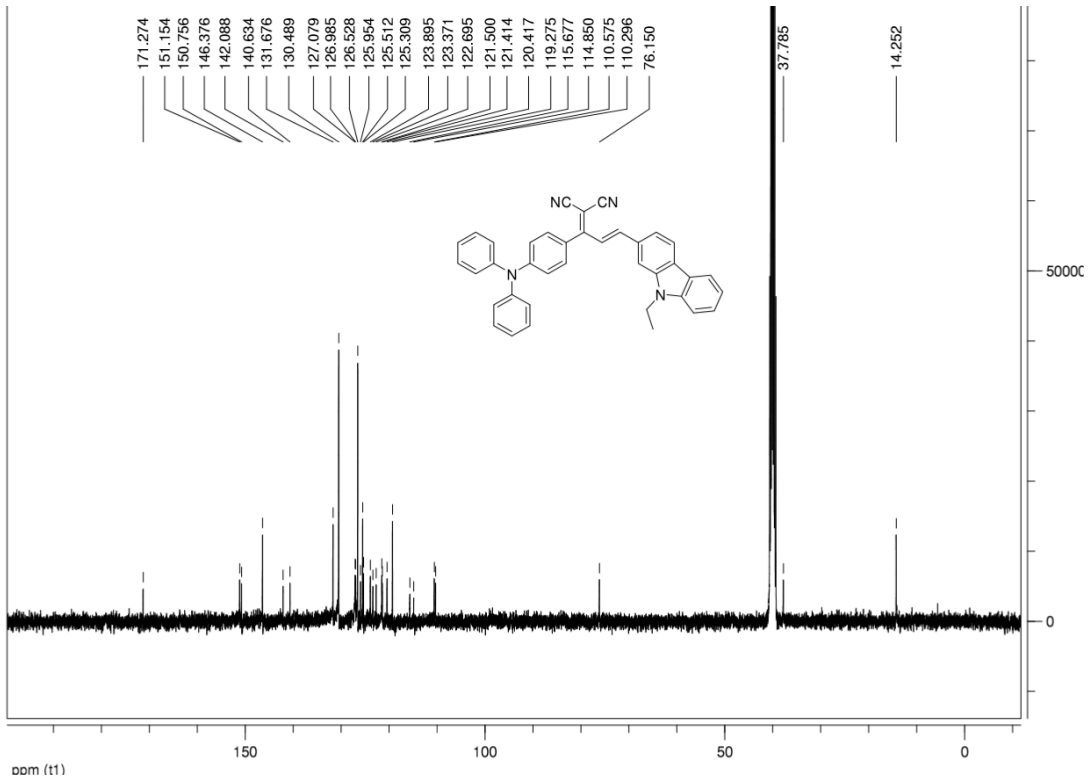

Figure 1. 6 ^{13}C-NMR spectra of 3b in DMSO-d_6

Annex-1. (Cont.) FT-IR, ^{1}H-NMR, ^{13}C-NMR, and HR-MS spectra of compound 3a-d

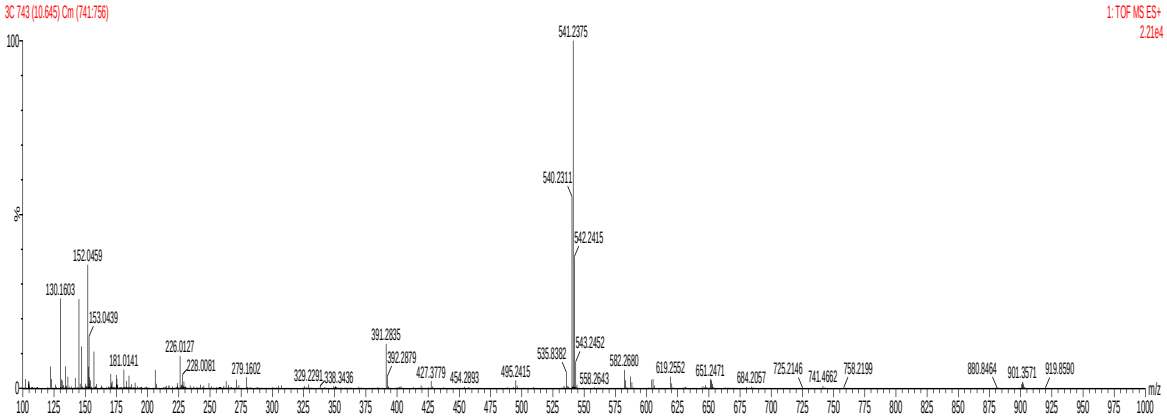

Figure 1.7. HRMS spectra of 3b

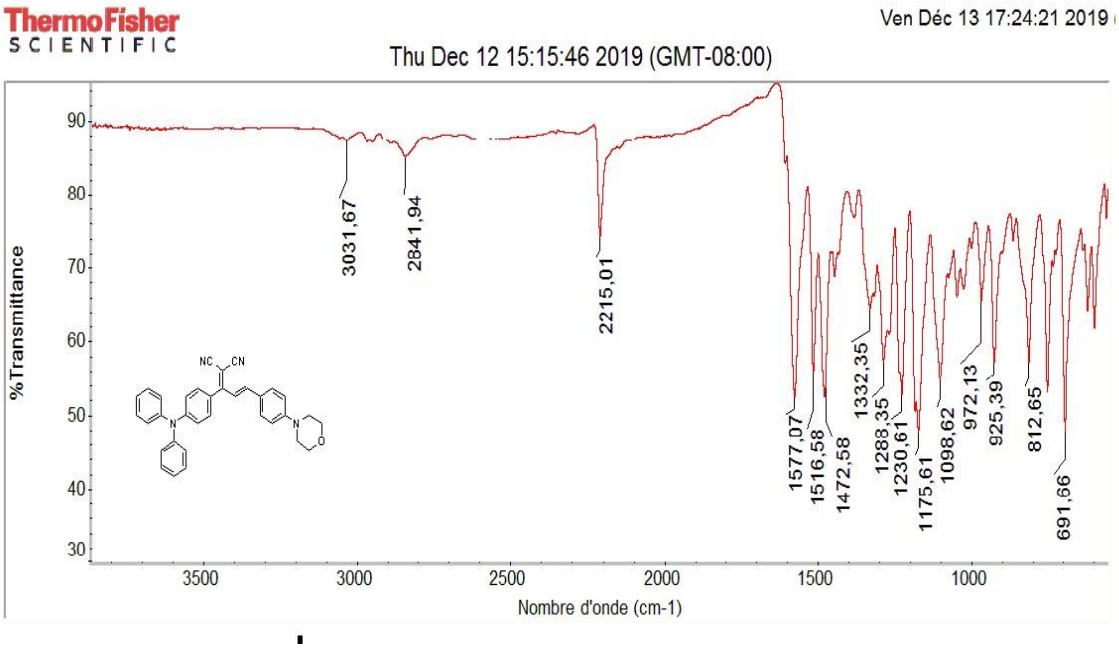

Figure 1.8. FT-IR spectra of 3c

Annex-1. (Cont.) FT-IR, ^{1}H-NMR, ^{13}C-NMR, and HR-MS spectra of compound 3a-d

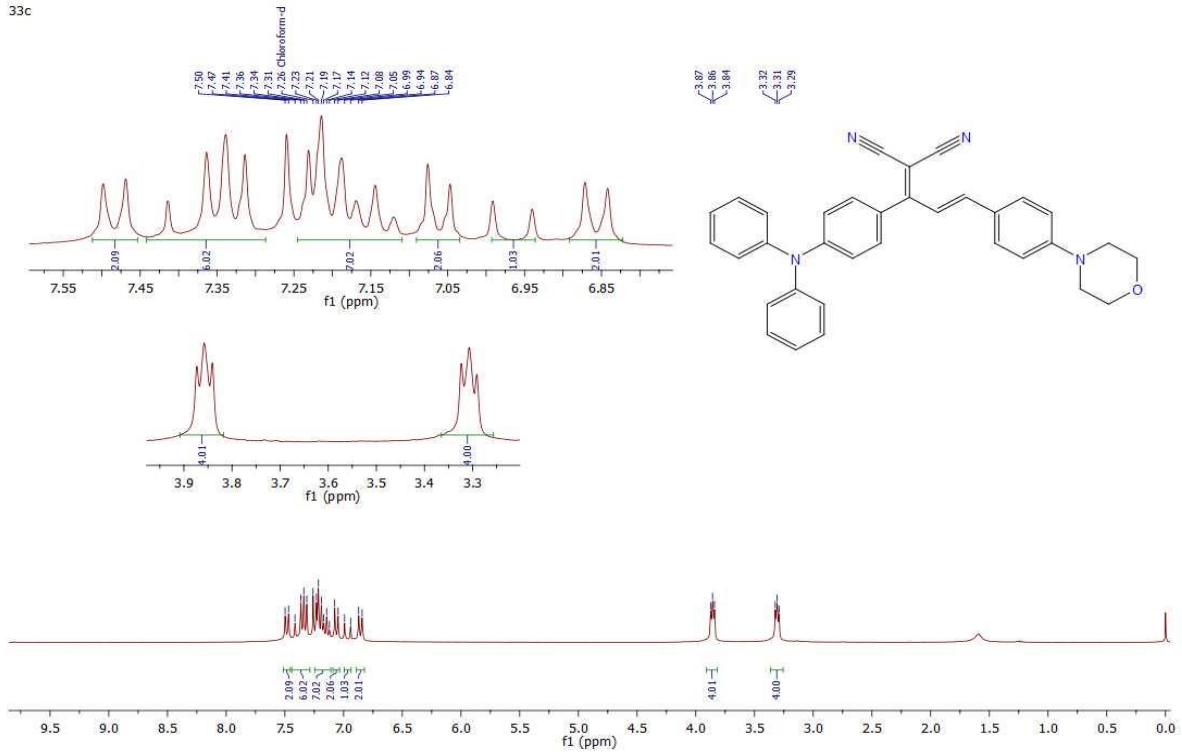

Figure 1.9. ^{1}H-NMR spectra of 3c in $CDCl_3$

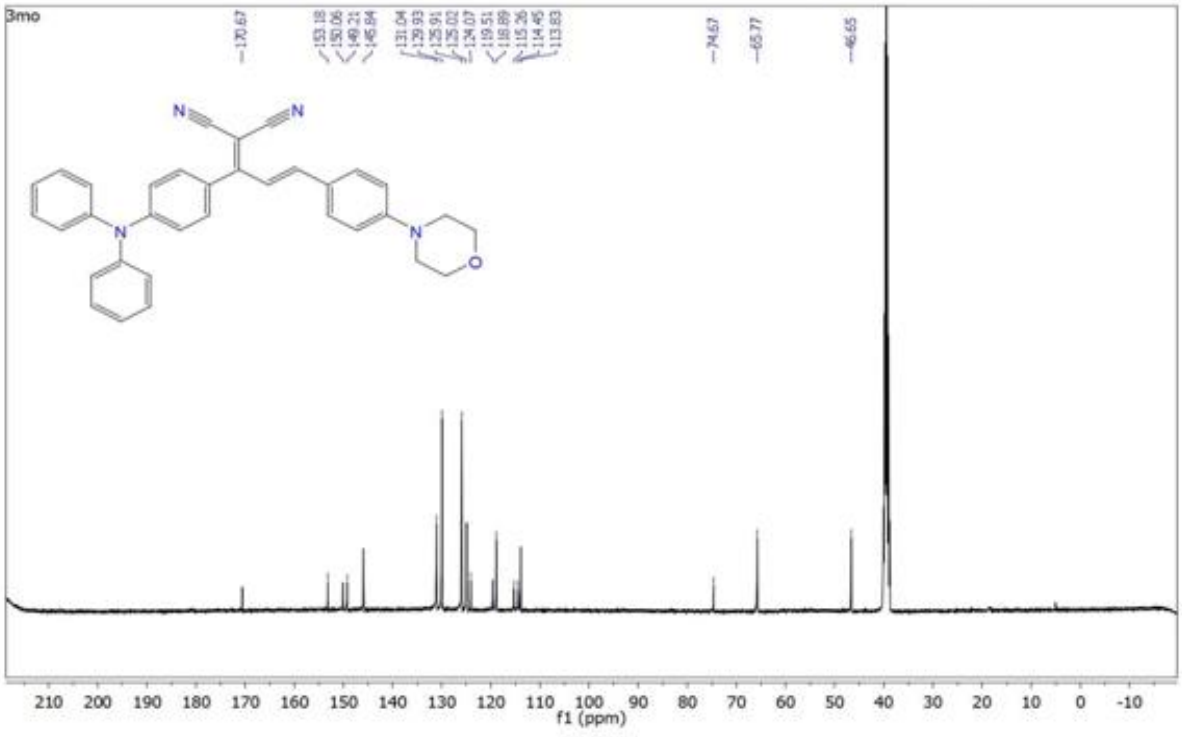

Figure 1.10. ^{13}C-NMR spectra of 3c in DMSO-d_6

Annex-1. (Cont.) FT-IR, ^{1}H-NMR, ^{13}C-NMR, and HR-MS spectra of compound 3a-d

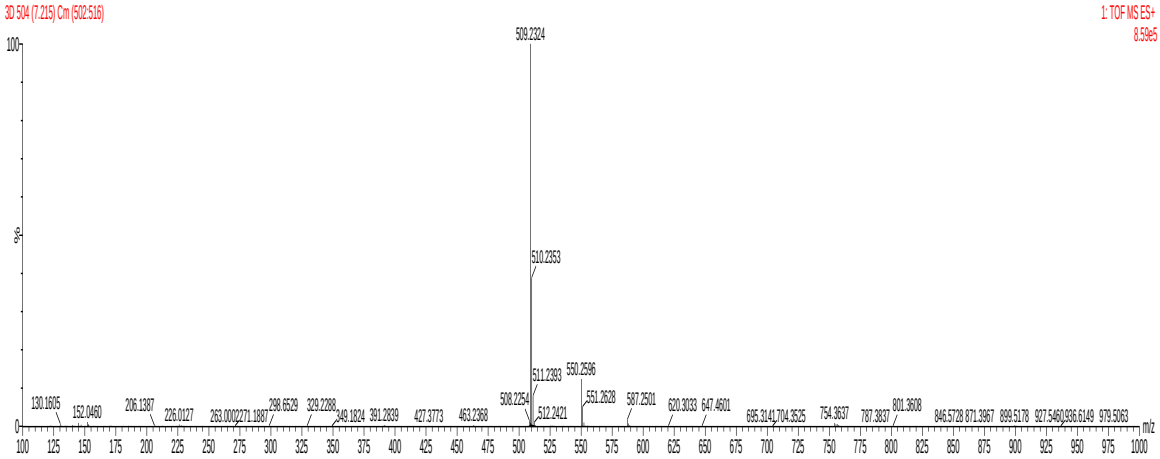

Figure 1.11. HRMS spectra of 3c

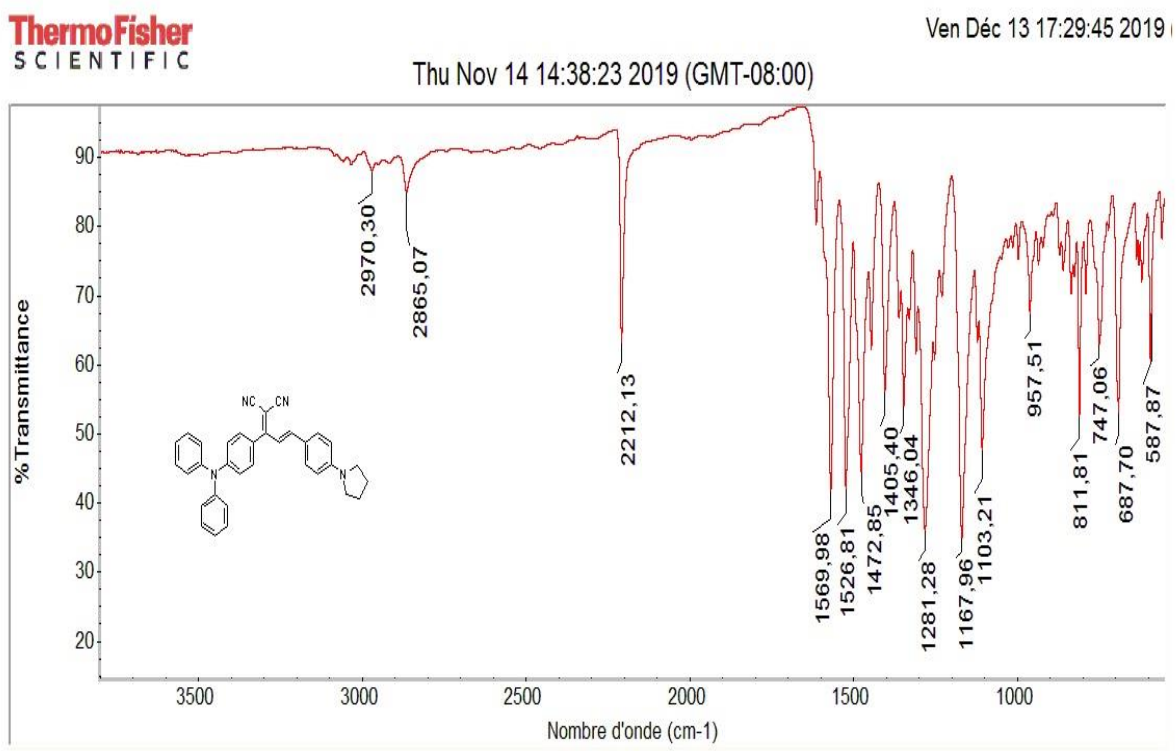

Figure 1.12. FT-IR spectra of 3d

Annex-1. (Cont.) FT-IR, ^{1}H-NMR, ^{13}C-NMR, and HR-MS spectra of compound 3a-d

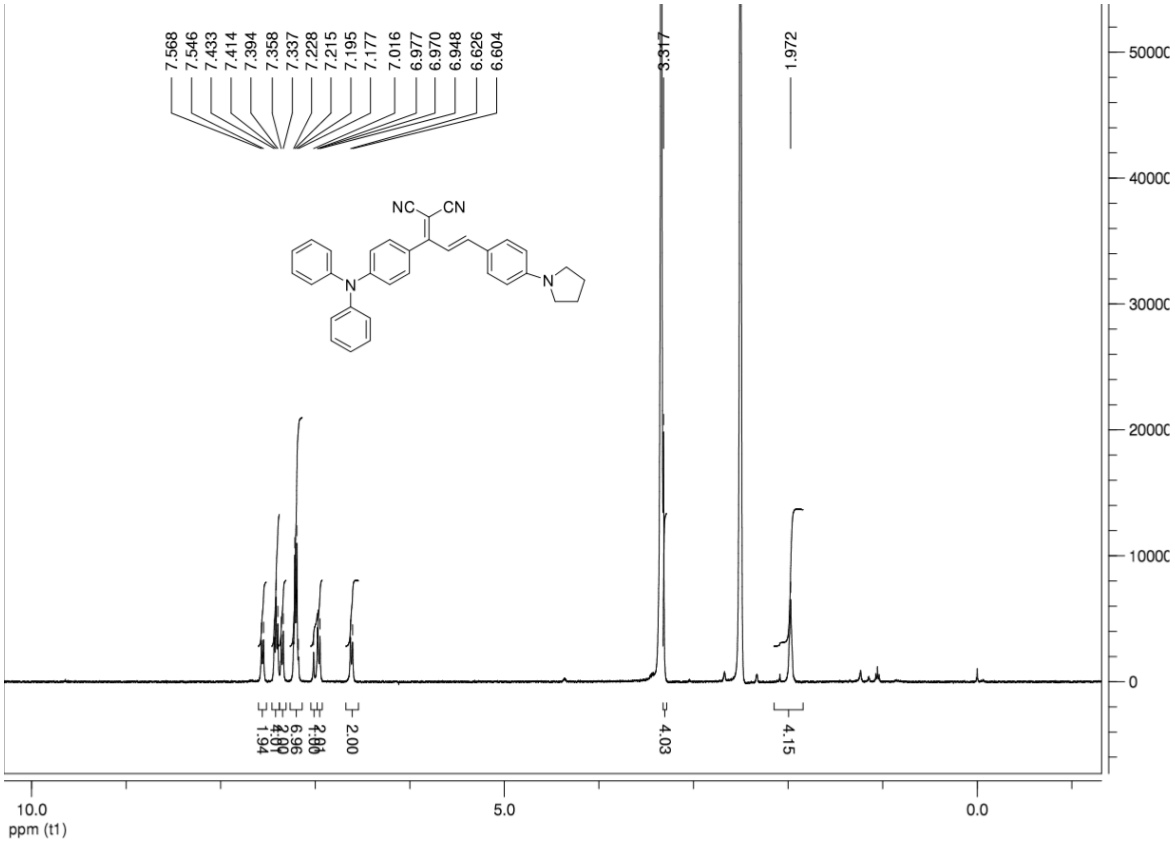

Figure 1.13.^{1}H-NMR spectra of 3d in DMSO-d_6

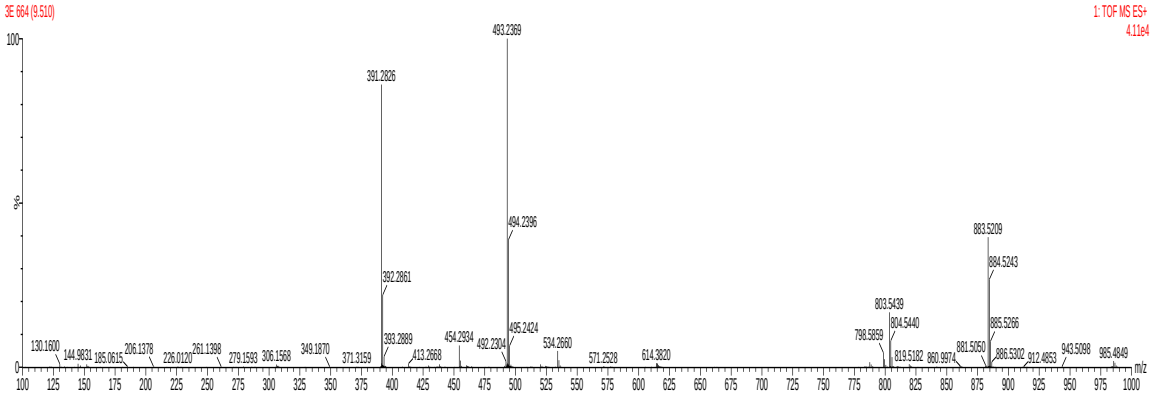

Figure 1.14. HRMS spectra of 3d

Annex-2. FT-IR, ^{1}H-NMR, ^{13}C-NMR, and HR-MS spectra of compound 6a-f

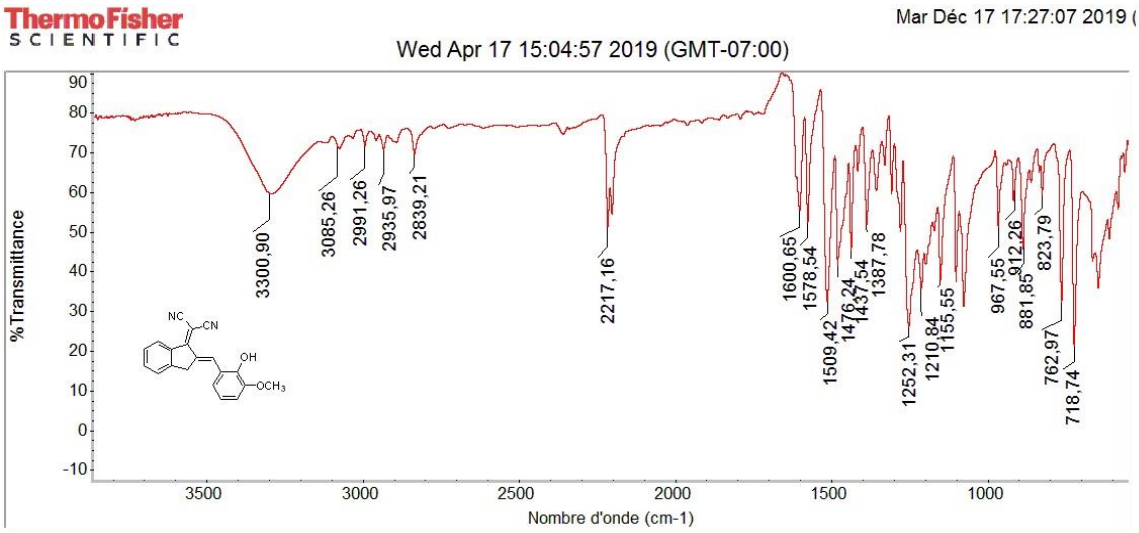

Figure 2.1. FT-IR spectra of compound 6a

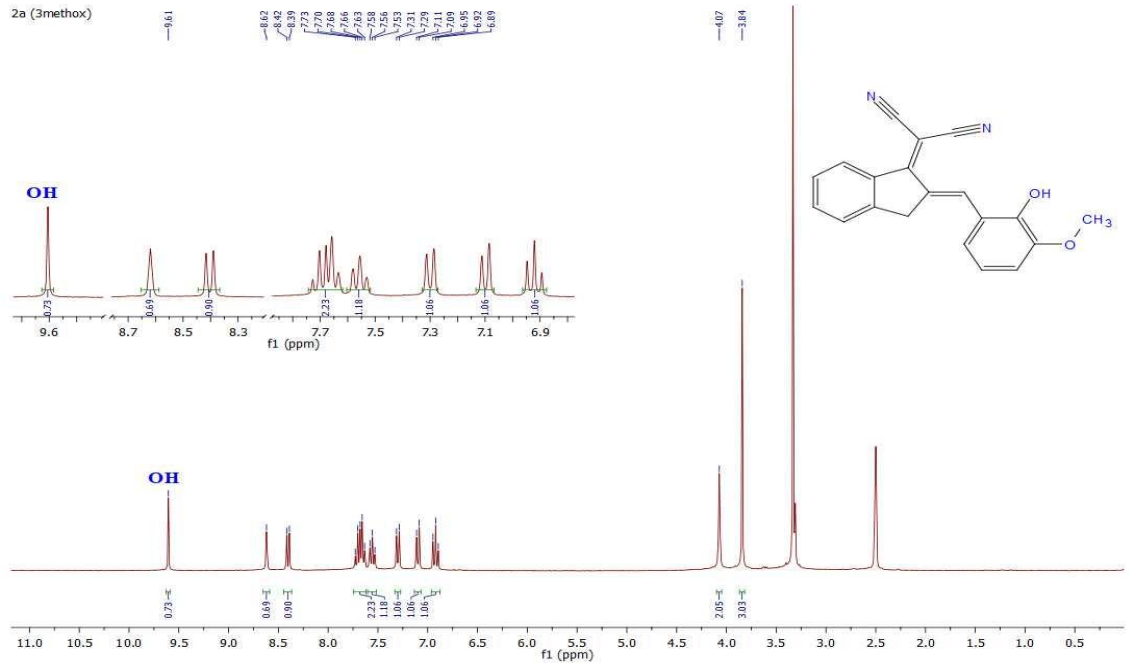

Figure 2.2. ^{1}H-NMR spectra of compound 6a in DMSO-d_6

Annex-2. (Cont.) FT-IR, ^{1}H-NMR, ^{13}C-NMR, and HR-MS spectra of compound 6a-f

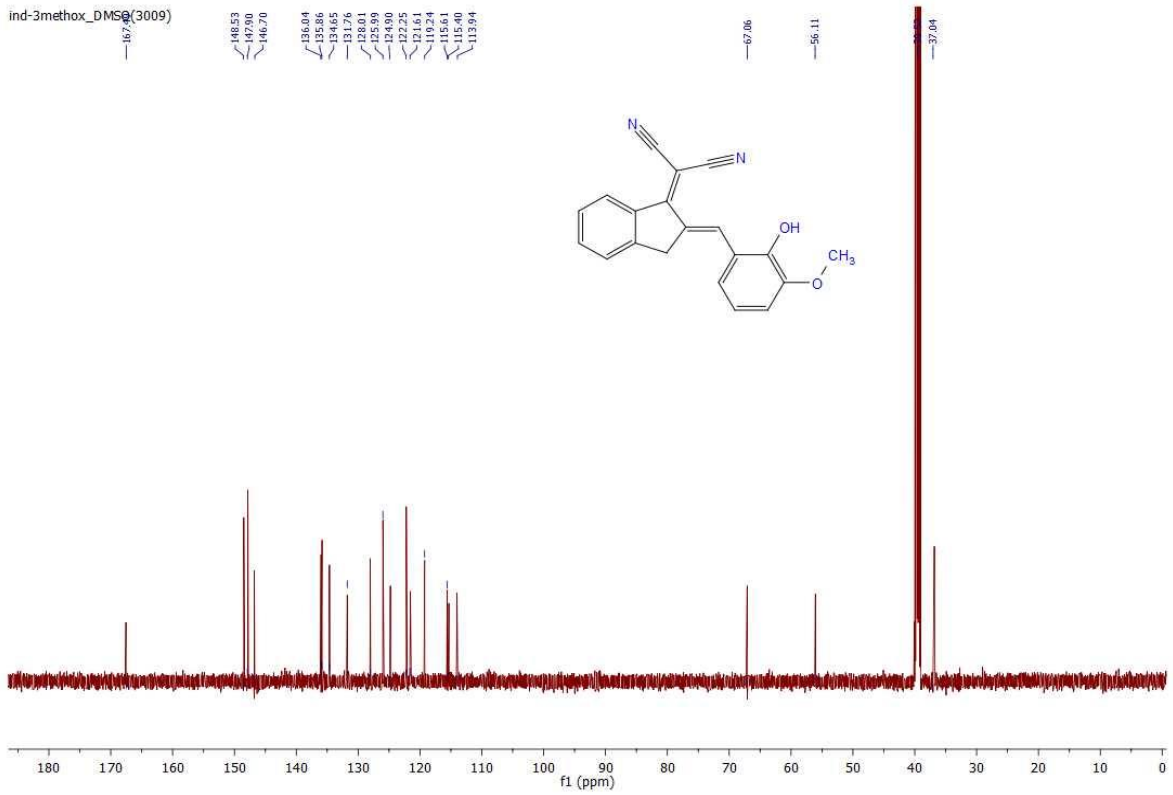

Figure 2.3. ^{13}C-NMR spectra of compound 6a in DMSO-d_6

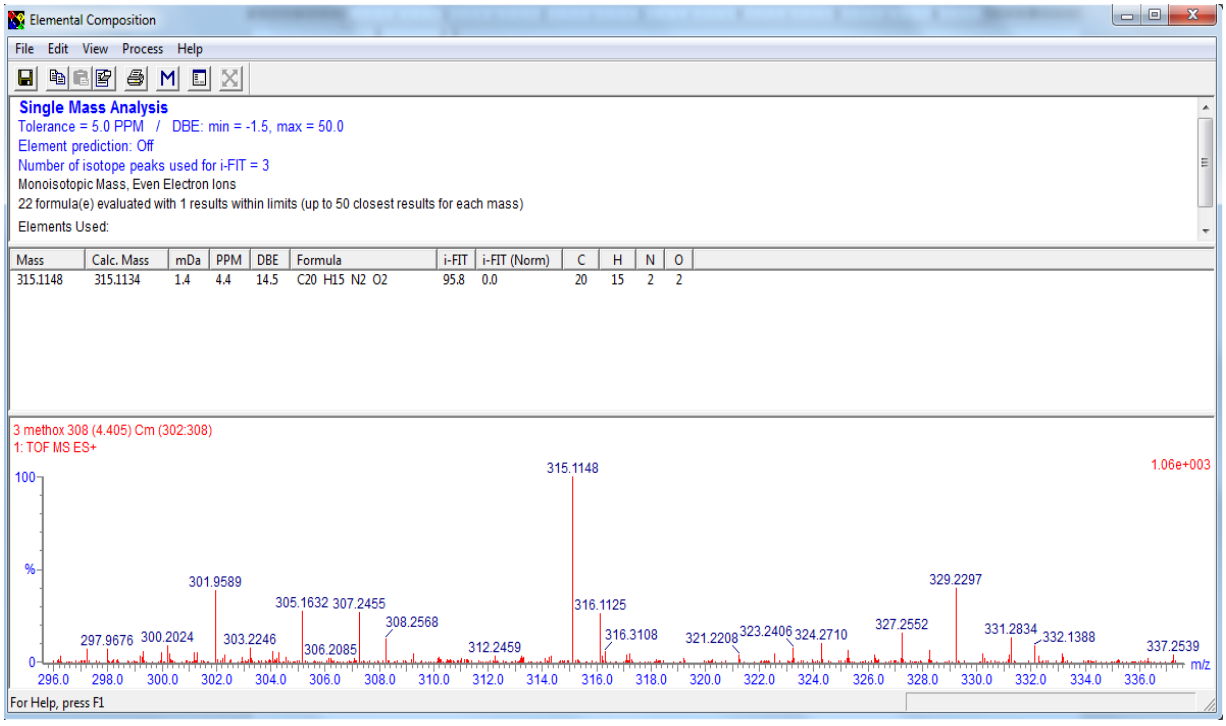

Figure 2.4. HRMS spectra of compound 6a

Annex-2. (Cont.) FT-IR, ^{1}H-NMR, ^{13}C-NMR, and HR-MS spectra of compound 6a-f

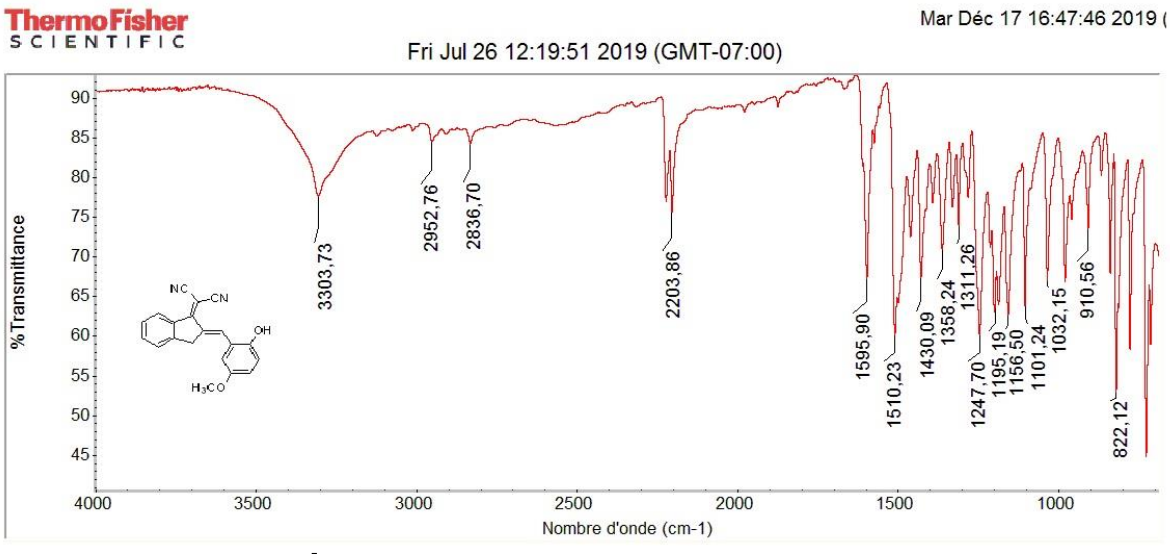

Figure 2.5. FT-IR spectra of compound 6b

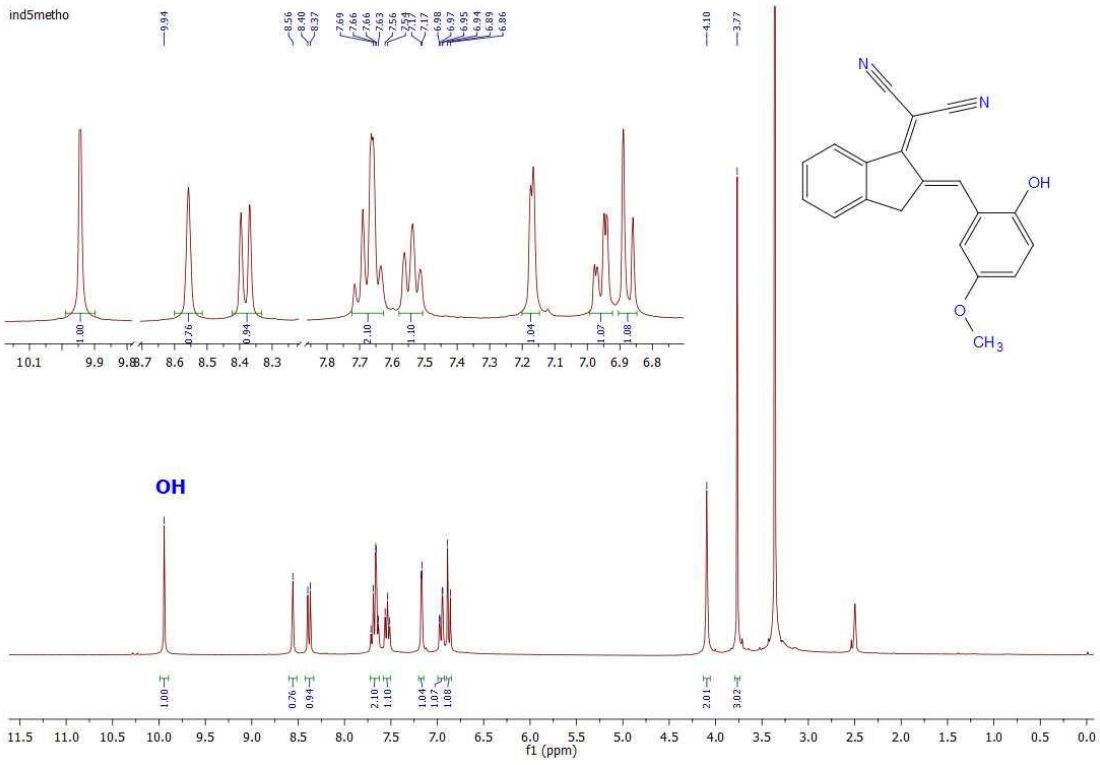

Figure 2.6. ^{1}H-NMR spectra of compound 6b in DMSO-d_6

Annex-2. (Cont.) FT-IR, ^{1}H-NMR, ^{13}C-NMR, and HR-MS spectra of compound 6a-f

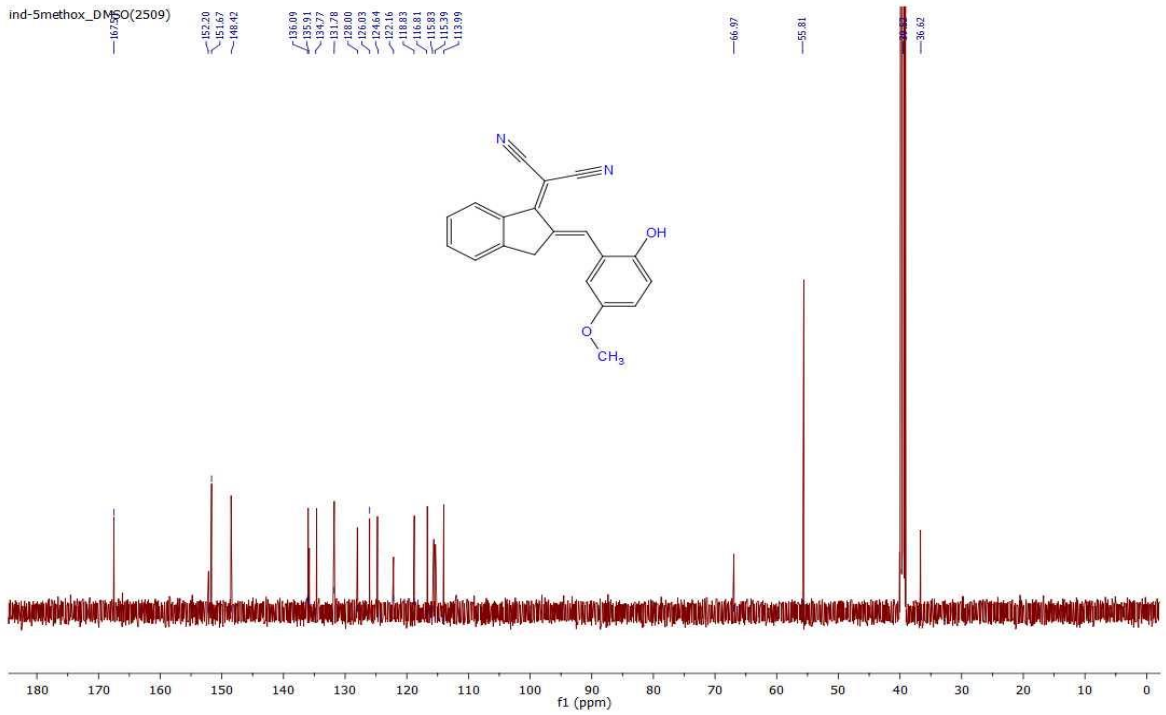

Figure 2.7.^{13}C-NMR spectra of compound 6b in DMSO-d_6

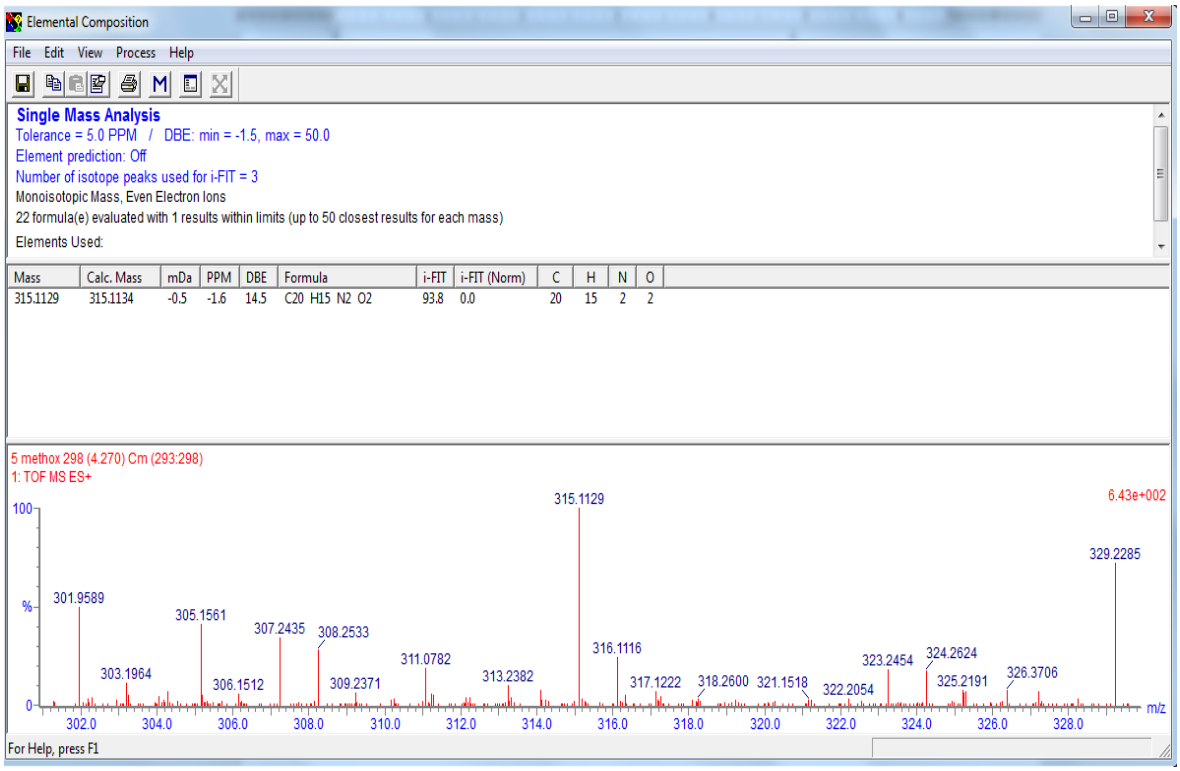

Figure 2.8. HRMS spectra of compound 6b

Annex-2. (Cont.) FT-IR, ^{1}H-NMR, ^{13}C-NMR, and HR-MS spectra of compound 6a-f

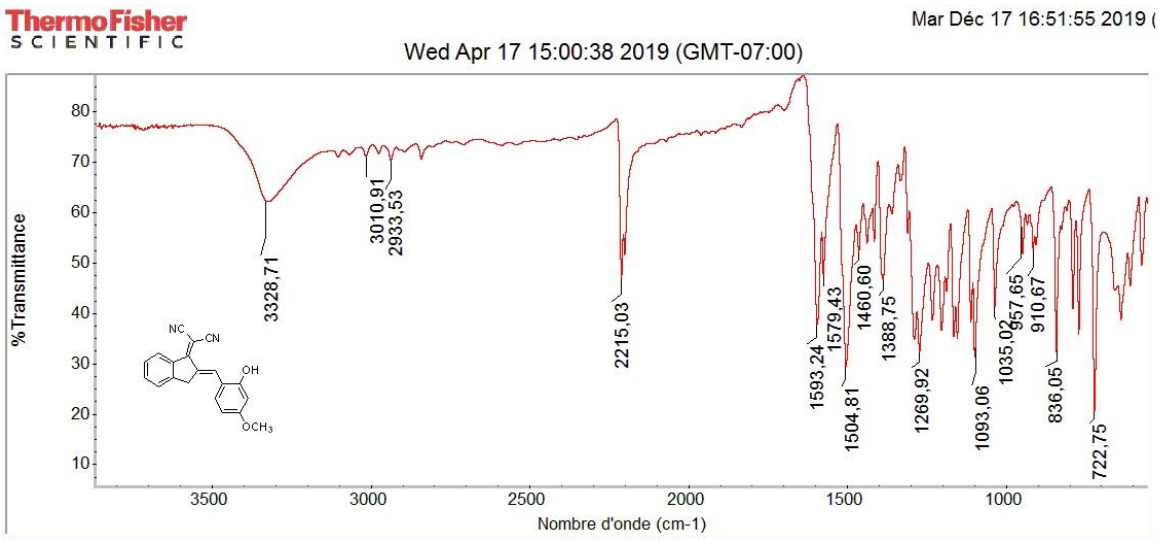

Figure 2.9. FT-IR spectra of compound 6c

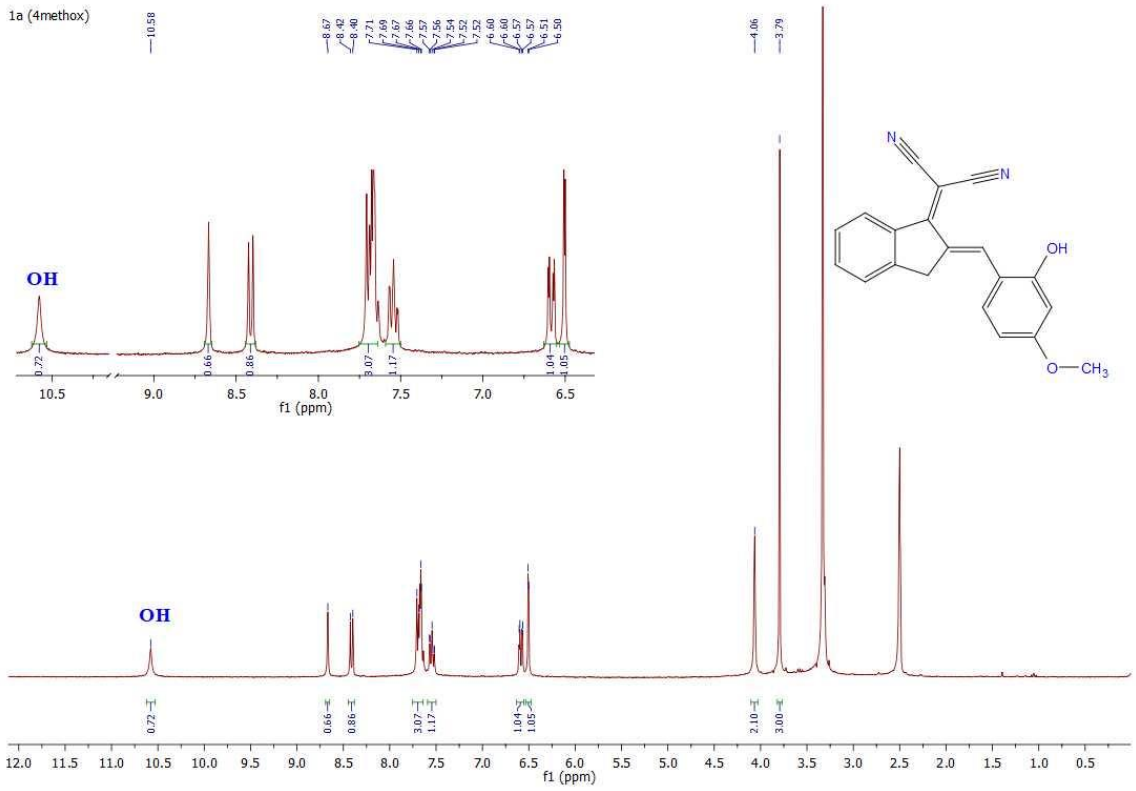

Figure 2.10.^{1}H-NMR spectra of compound 6c in DMSO-d_6

Annex-2. (Cont.) FT-IR, ^{1}H-NMR, ^{13}C-NMR, and HR-MS spectra of compound 6a-f

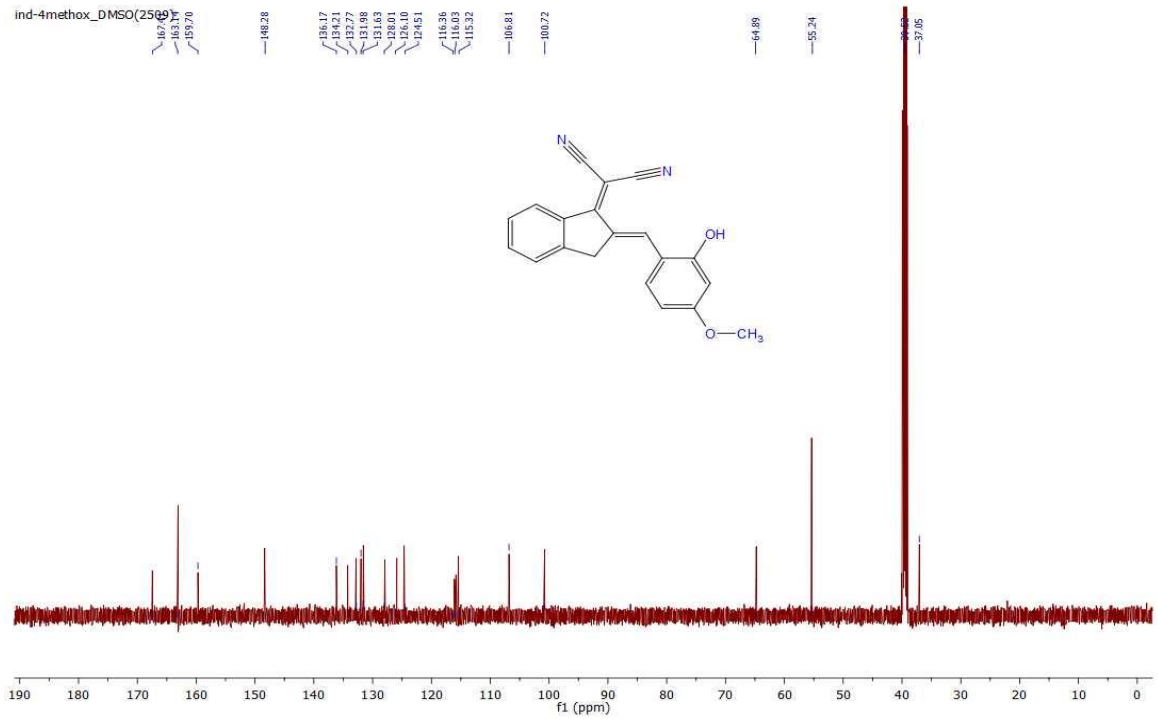

Figure 2.11. ^{13}C-NMR spectra of compound 6c in DMSO-d_6

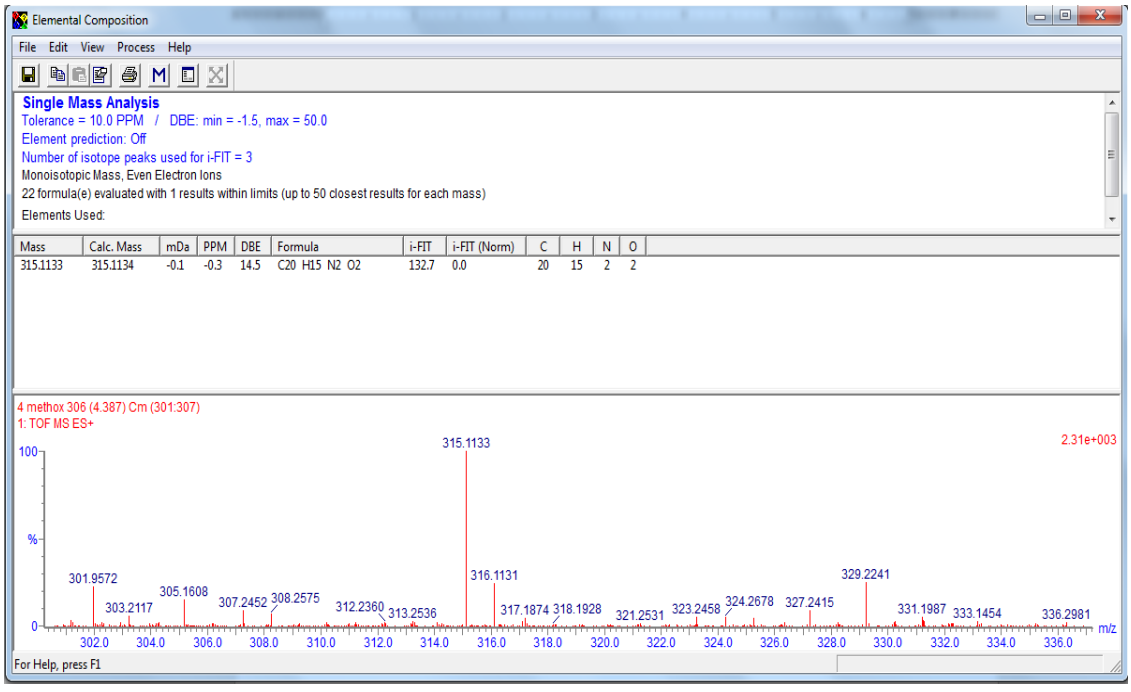

Figure 2.12. HRMS spectra of compound 6c

Annex-2. (Cont.) FT-IR, ^{1}H-NMR, ^{13}C-NMR, and HR-MS spectra of compound 6a-f

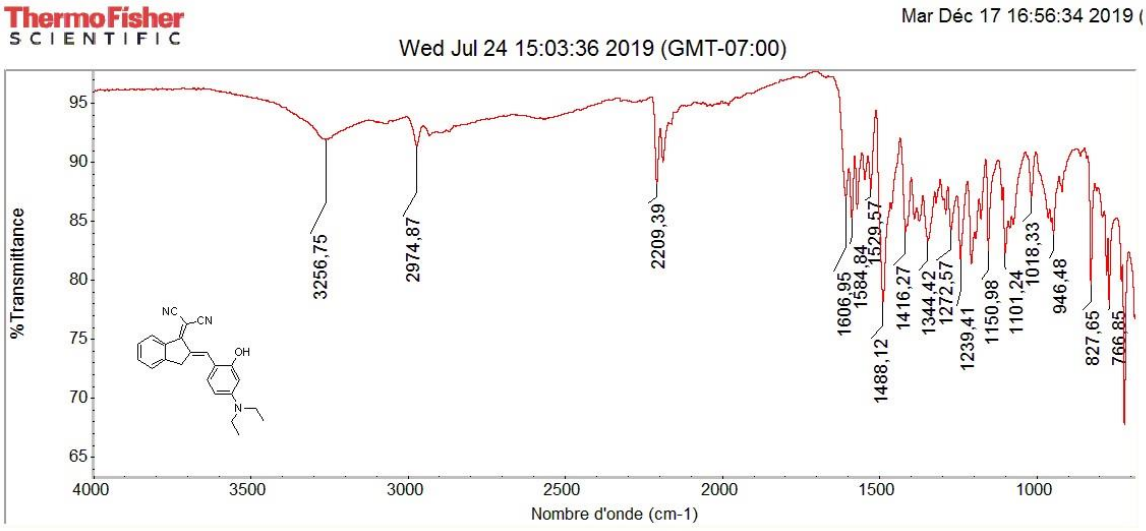

Figure 2.13. FT-IR spectra of compound 6d

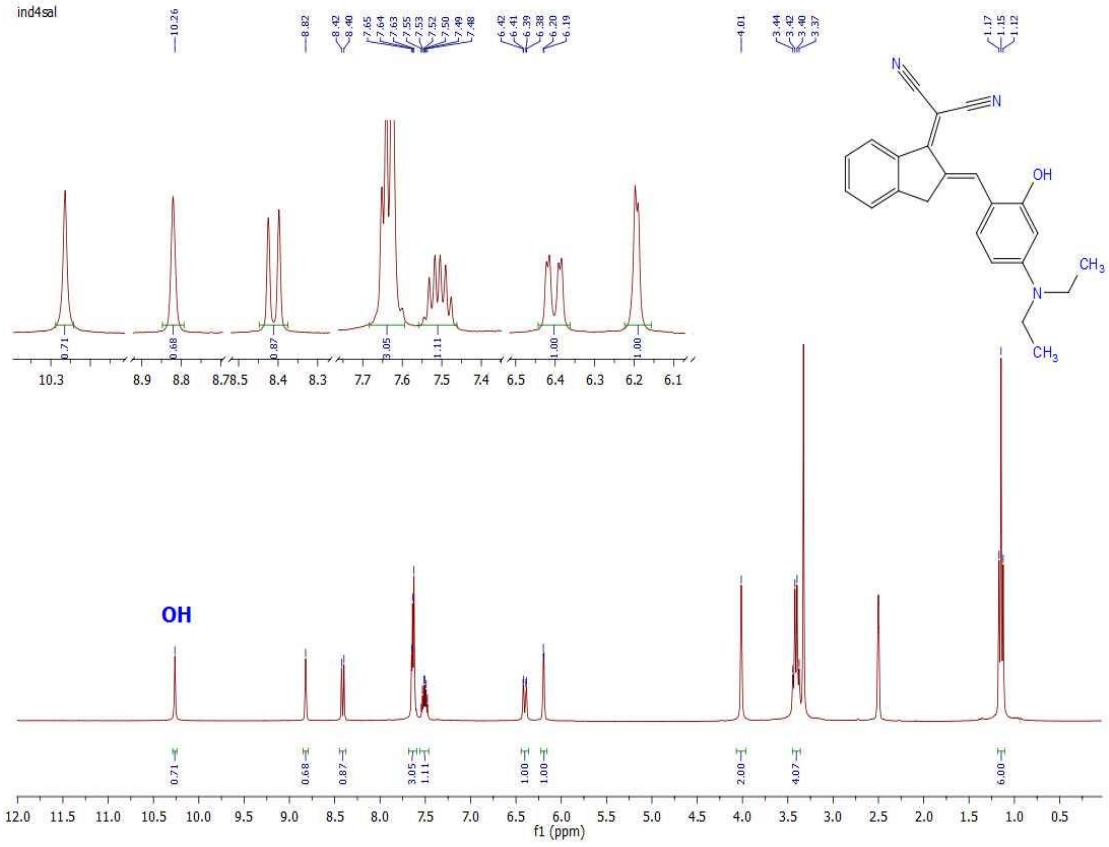

Figure 2.14.^{1}H-NMR spectra of compound 6d in DMSO-d_6

Annex-2. (Cont.) FT-IR, ^{1}H-NMR, ^{13}C-NMR, and HR-MS spectra of compound 6a-f

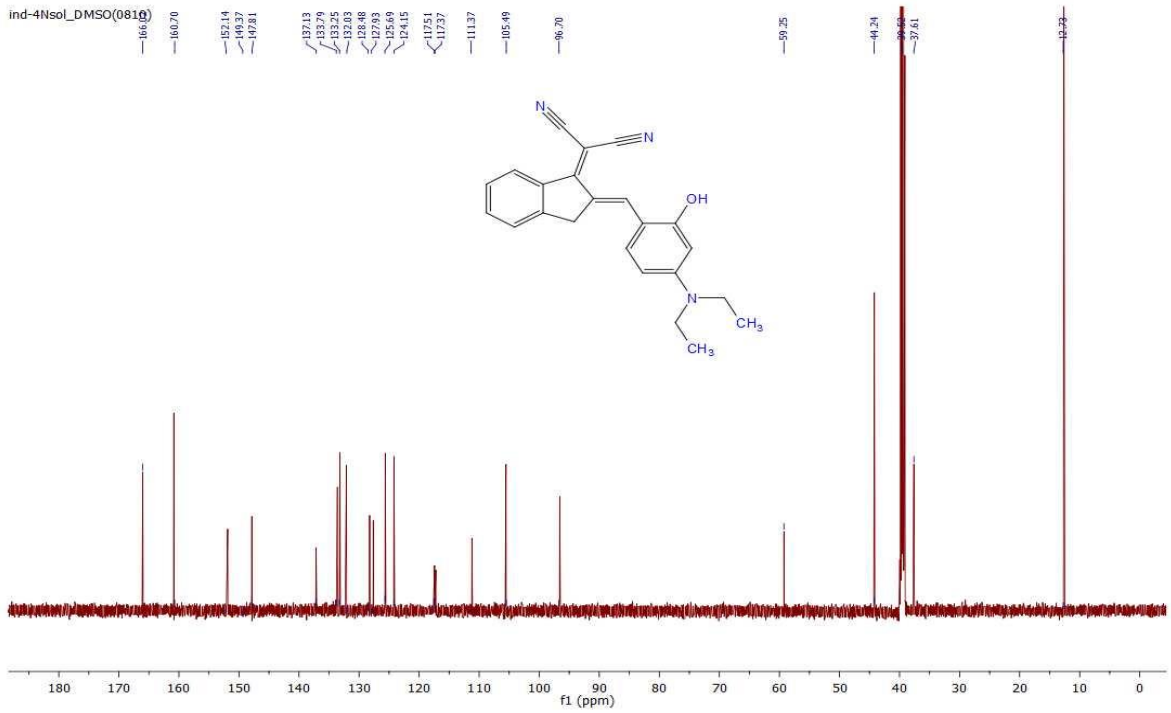

Figure 2.15.^{13}C-NMR spectra of compound 6d in DMSO-d_6

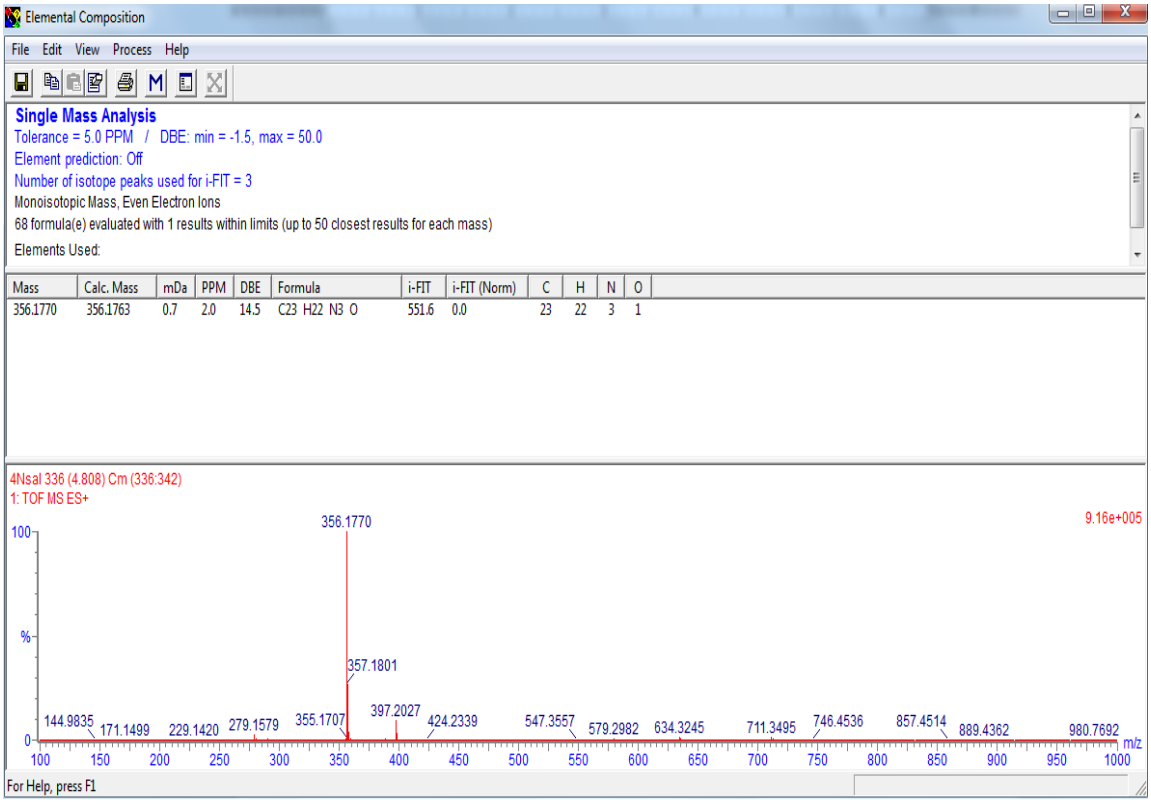

Figure 2.16. HRMS spectra of compound 6d

Annex-2. (Cont.) FT-IR, ^{1}H-NMR, ^{13}C-NMR, and HR-MS spectra of compound 6a-f

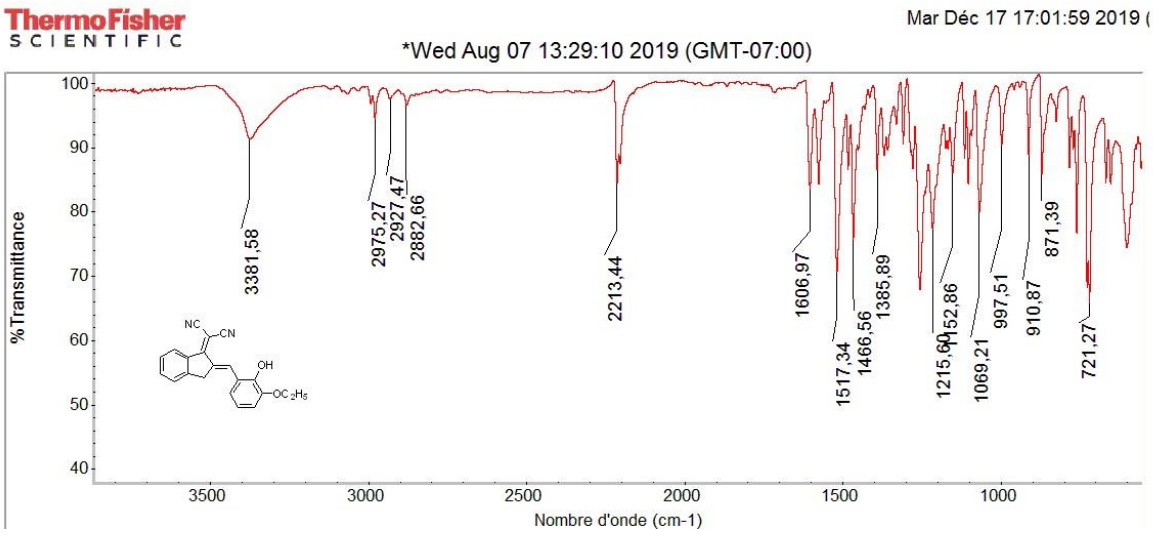

Figure 2.17. FT-IR spectra of compound 6e

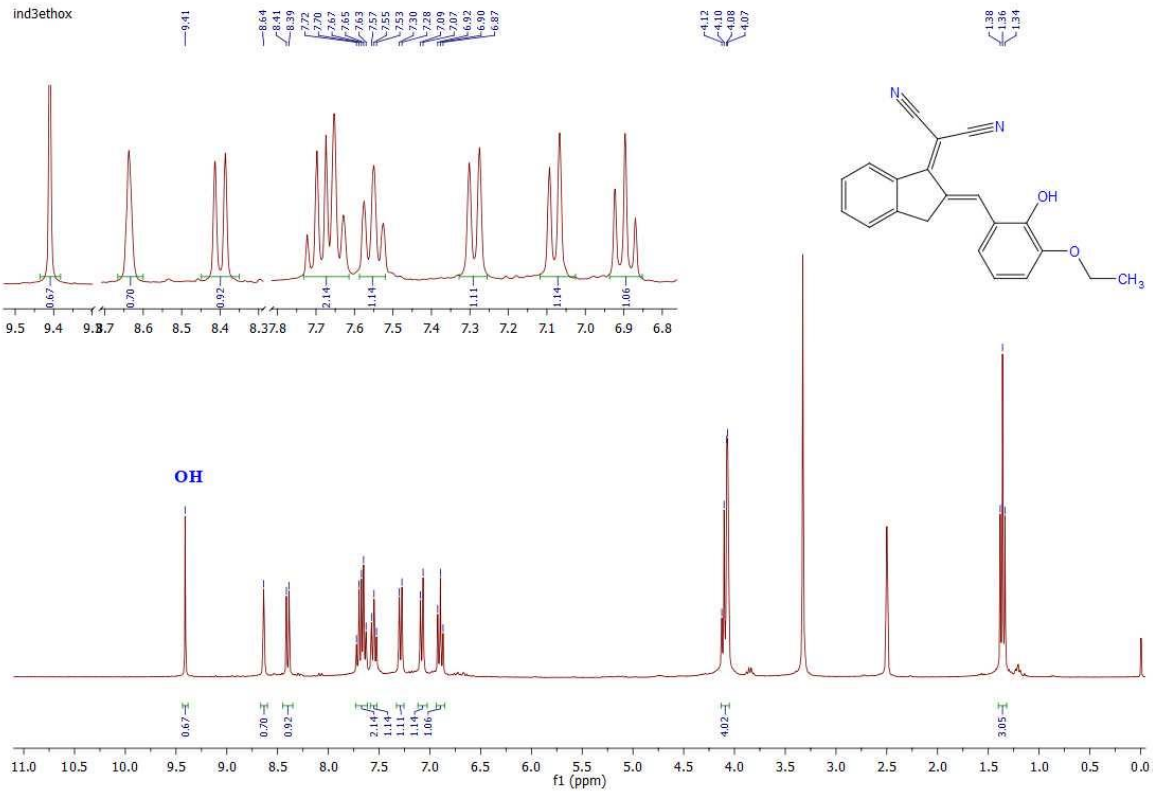

Figure 2.18.^{1}H-NMR spectra of compound 6e in DMSO-d_6

Annex-2. (Cont.) FT-IR, ^{1}H-NMR, ^{13}C-NMR, and HR-MS spectra of compound 6a-f

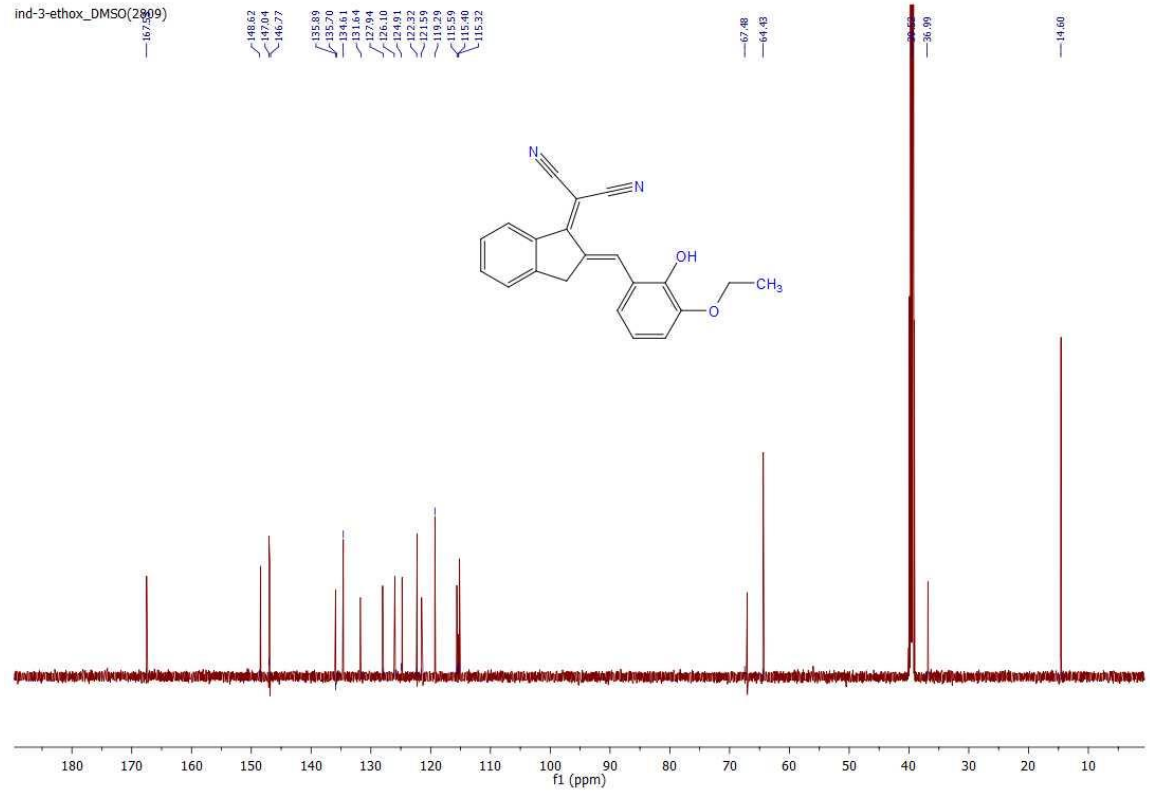

Figure 2.19.^{13}C-NMR spectra of compound 6e in DMSO-d_6

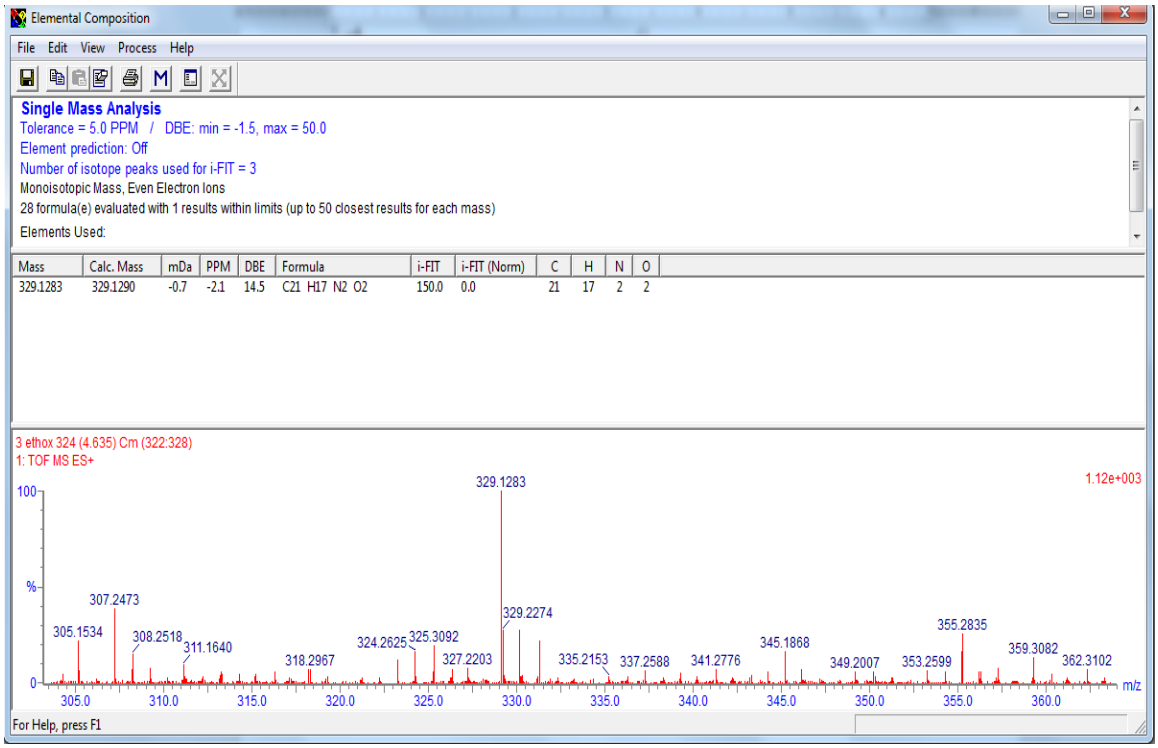

Figure 2.20. HRMS spectra of compound 6e

Annex-2. (Cont.) FT-IR, ^{1}H-NMR, ^{13}C-NMR, and HR-MS spectra of compound 6a-f

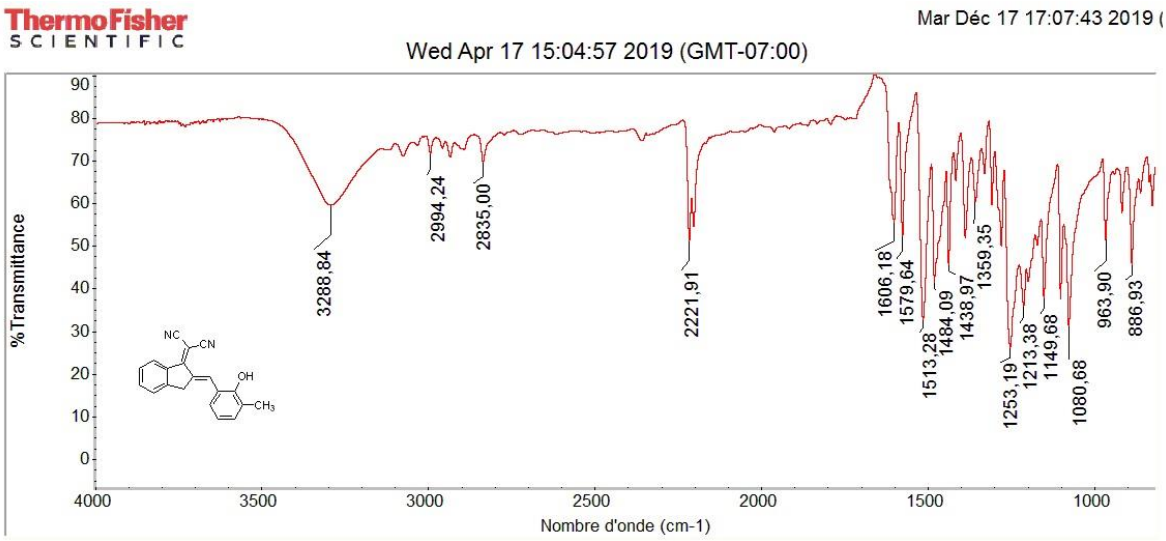

Figure 2.21. FT-IR spectra of compound 6f

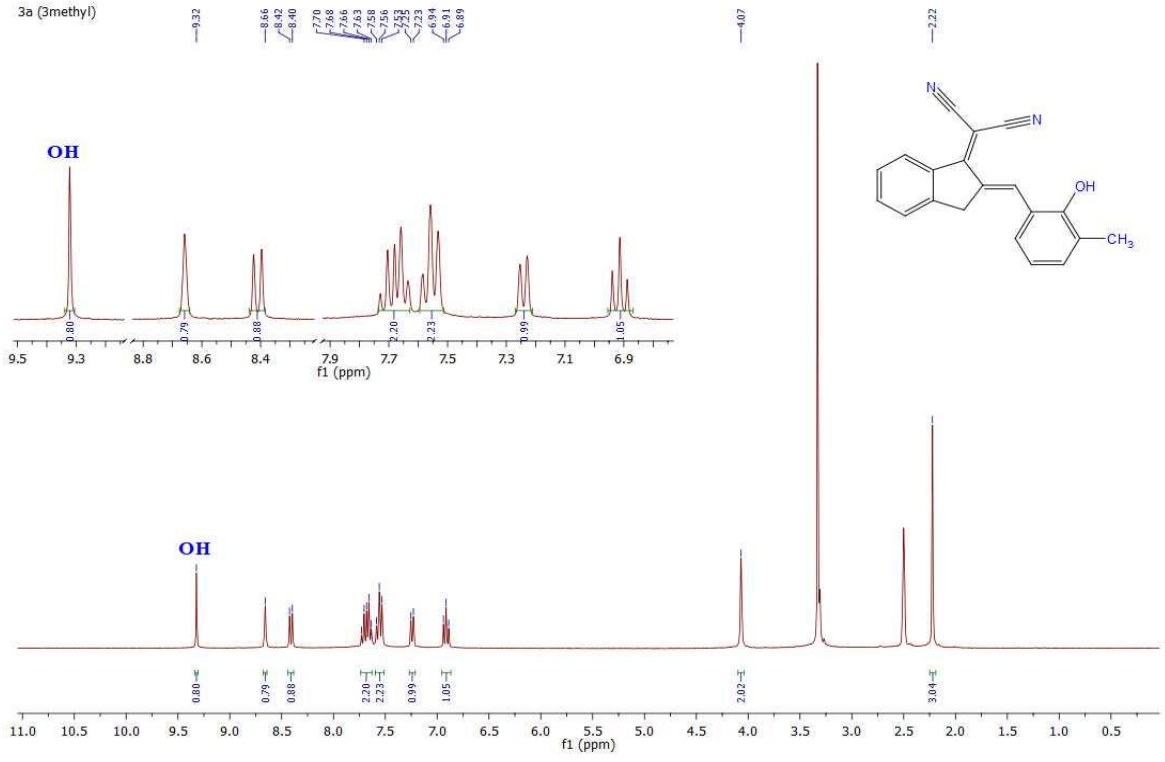

Figure 2.22. ^{1}H-NMR spectra of compound 6f in DMSO-d_6

Annex-2. (Cont.) FT-IR, ^{1}H-NMR, ^{13}C-NMR, and HR-MS spectra of compound 6a-f

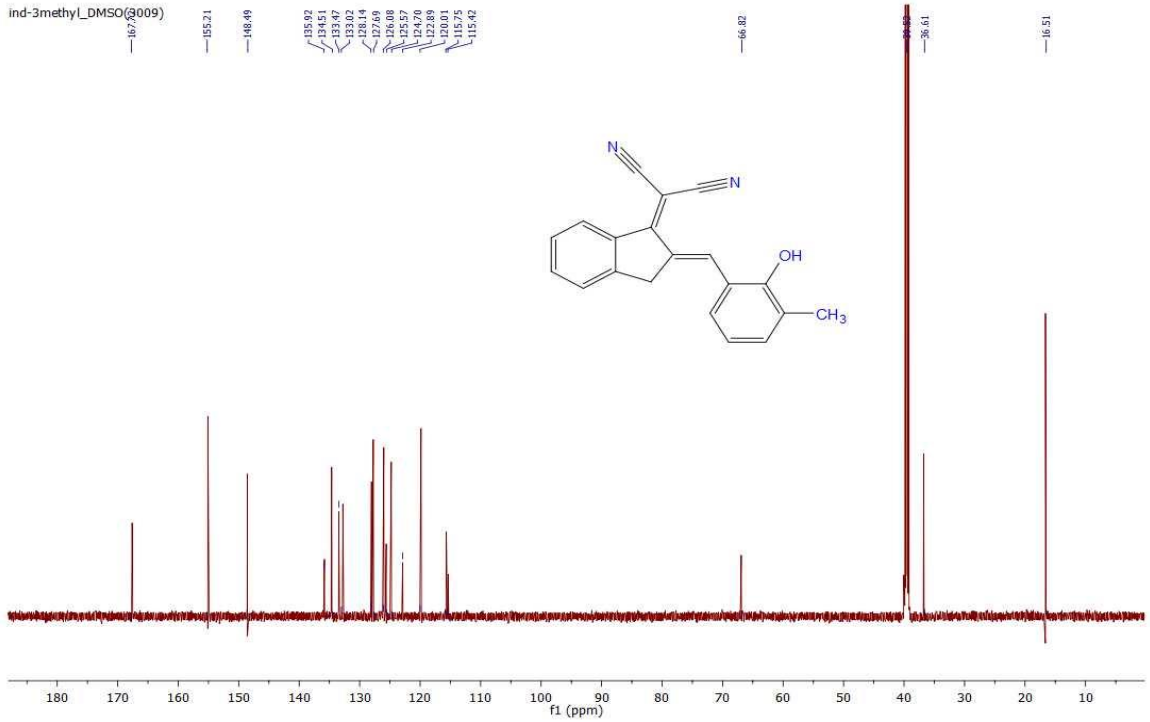

Figure 2.23.^{13}C-NMR spectra of compound 6f in DMSO-d_6

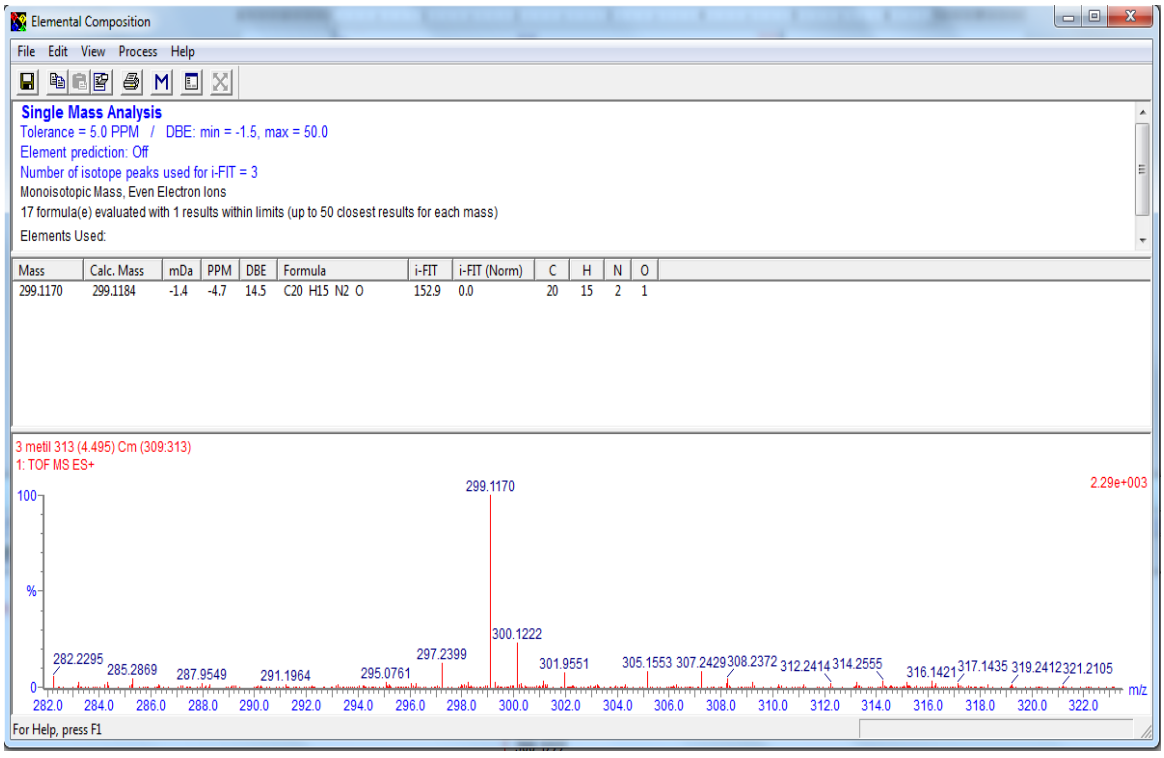

Figure 2.24. HRMS spectra of compound 6f

Annex-2. (Cont.) FT-IR, ^{1}H-NMR, ^{13}C-NMR, and HR-MS spectra of compound 6a-f

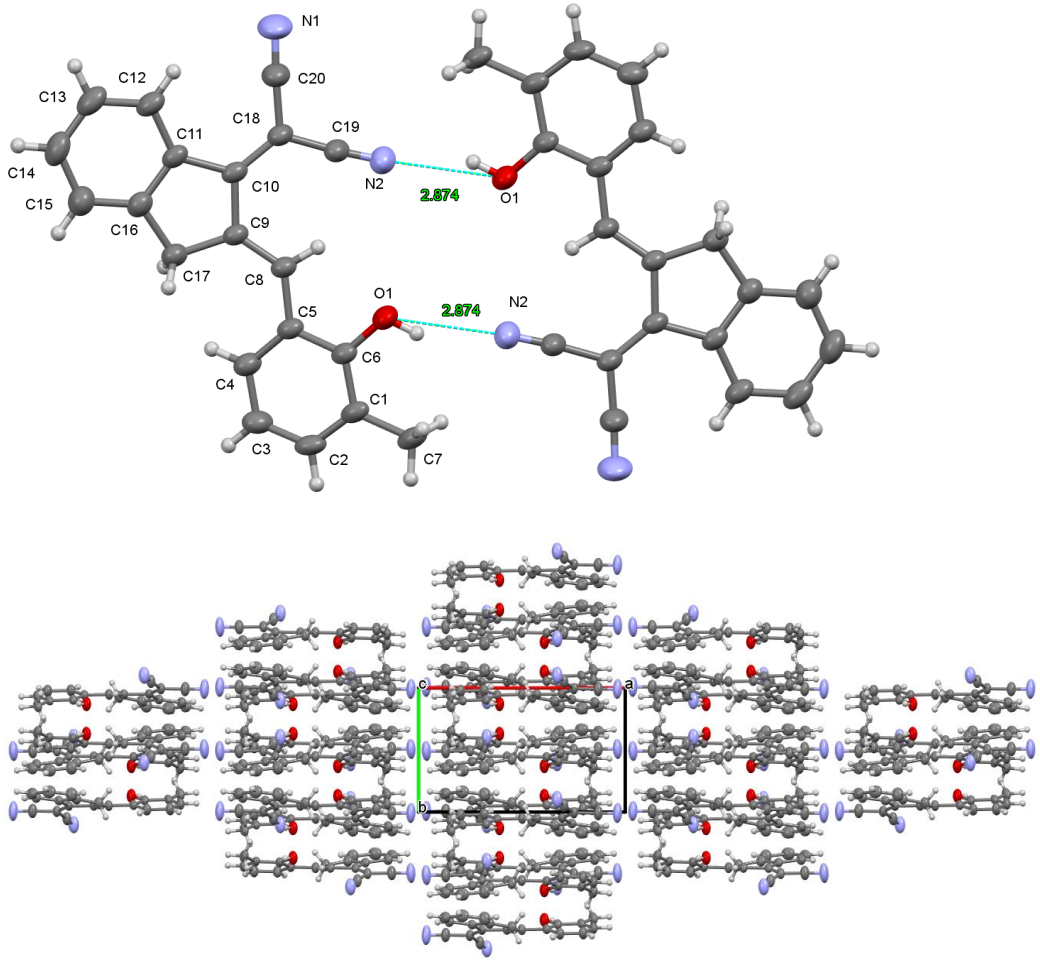

Figure 2.25. (Top) Molecular structure of 6f (asymmetric unit). Thermal ellipsoids are drawn at the 40% probability level

Annex-3. FT-IR, ^{1}H-NMR, ^{13}C-NMR, and HR-MS spectra of compounds 7a-c and 8a-c

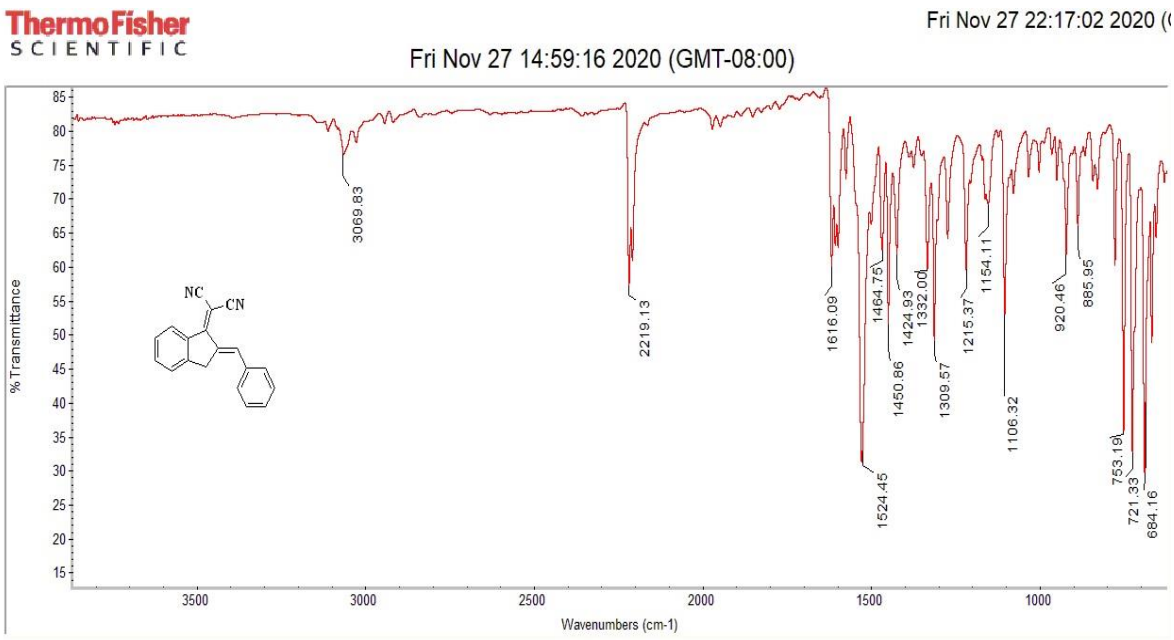

Figure 3.1. FT-IR spectrum of Compound 7a.

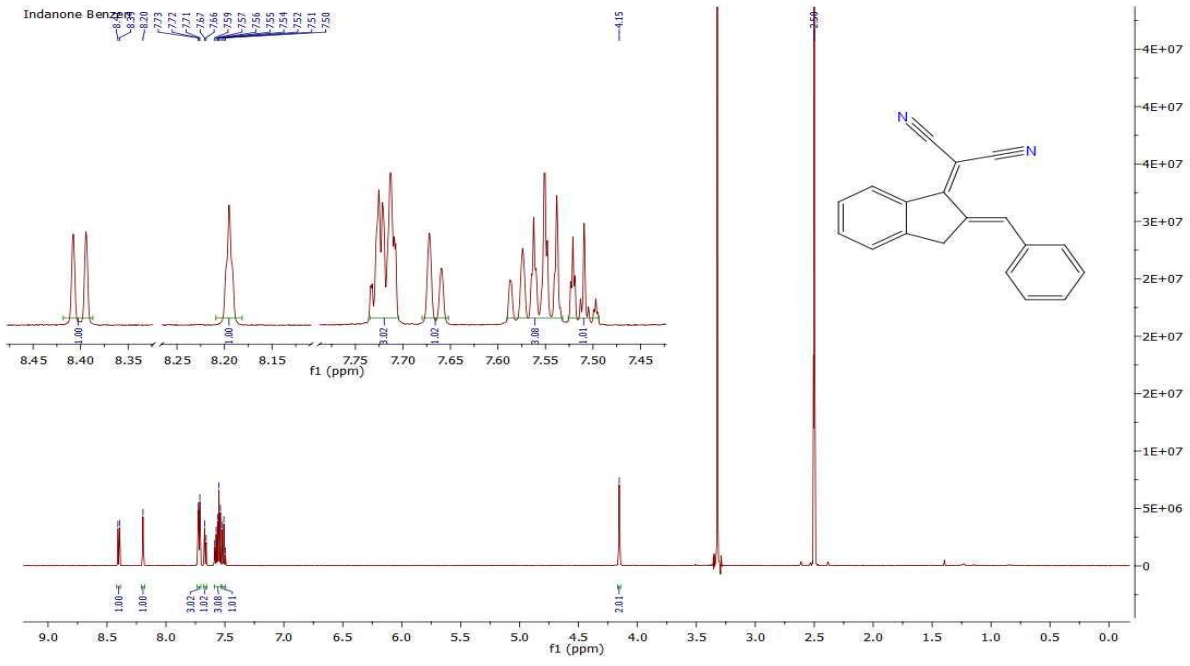

Figure 3.2. ^{1}H-NMR spectrum of Compound 7a in DMSO-d_6.

Annex-3. (Cont.) FT-IR, ^{1}H-NMR, ^{13}C-NMR, and HR-MS spectra of compounds 7a-c and 8a-c

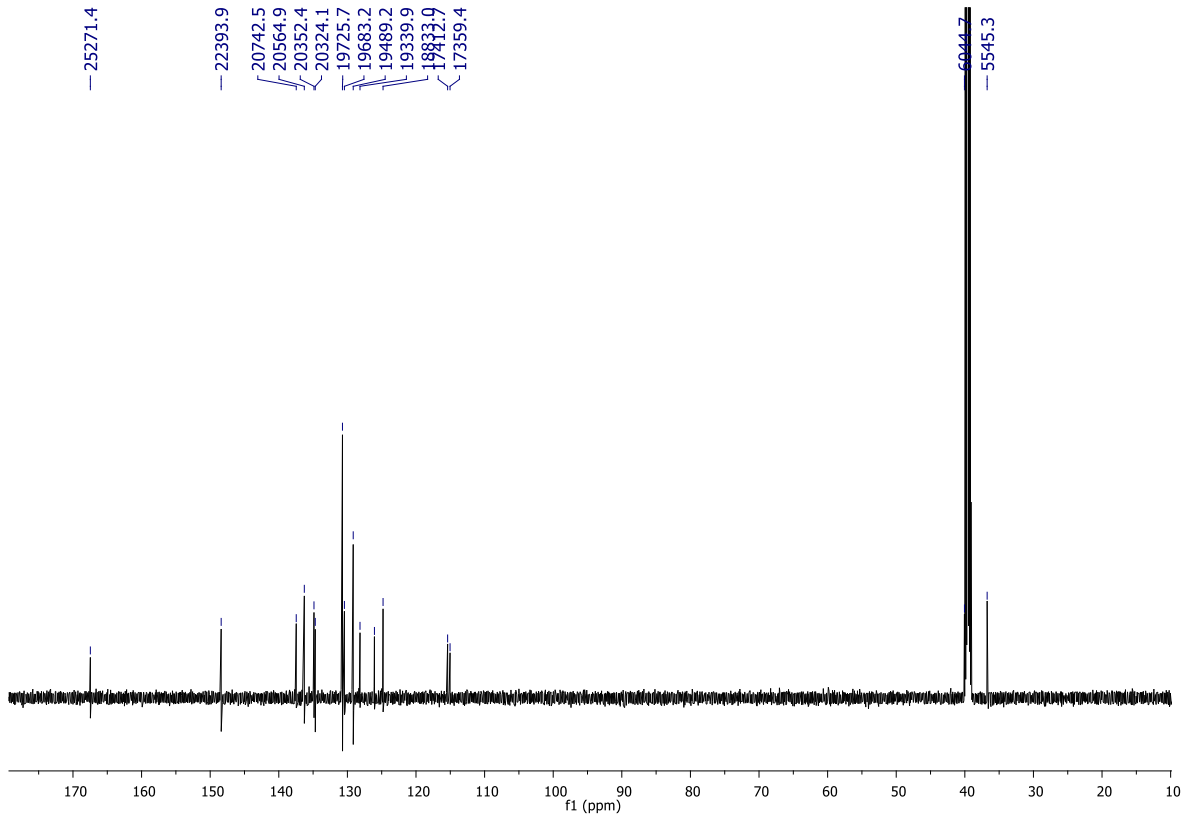

Figure 3.3. ^{13}C-NMR spectrum of Compound 7a in DMSO-d_6.

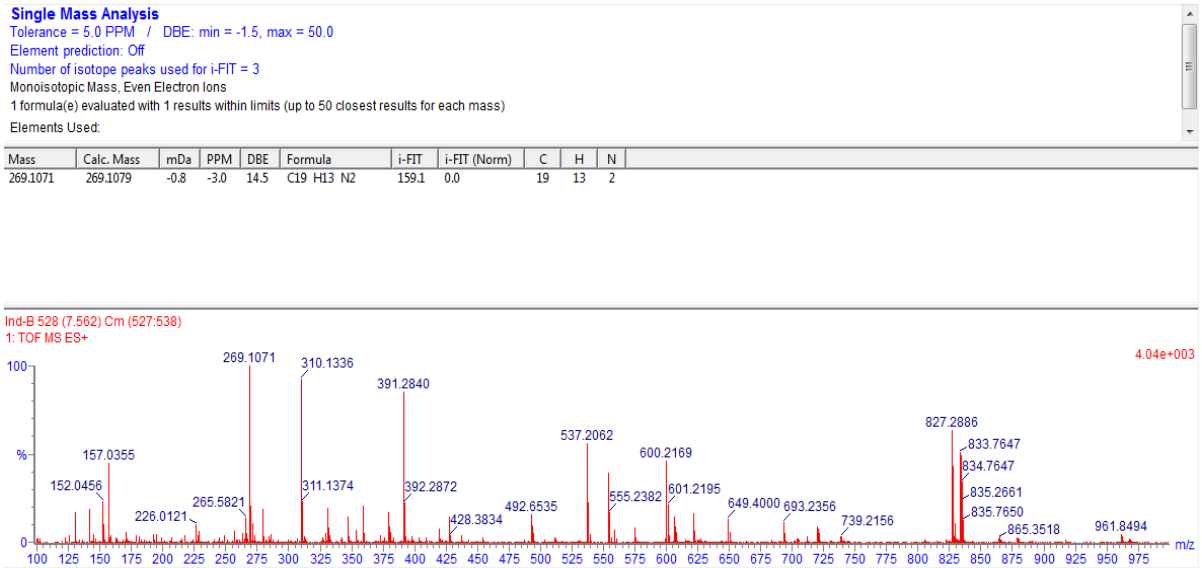

Figure 3.4. Mass spectrum of Compound 7a.

Annex-3. (Cont.) FT-IR, ^{1}H-NMR, ^{13}C-NMR, and HR-MS spectra of compounds 7a-c and 8a-c

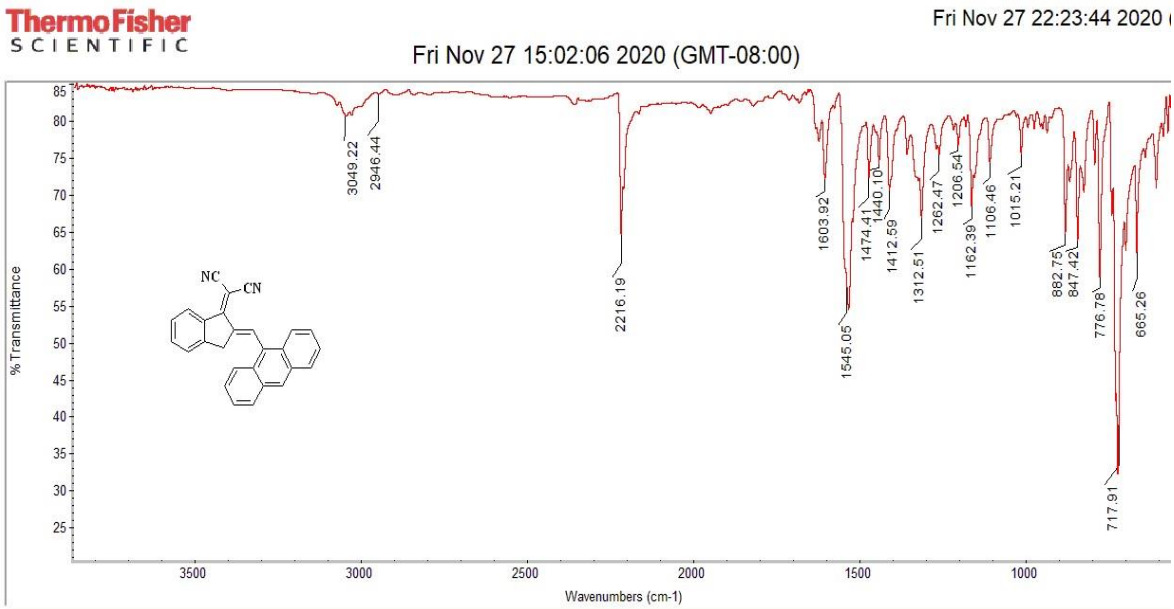

Figure 3.5. FT-IR spectrum of Compound 7b.

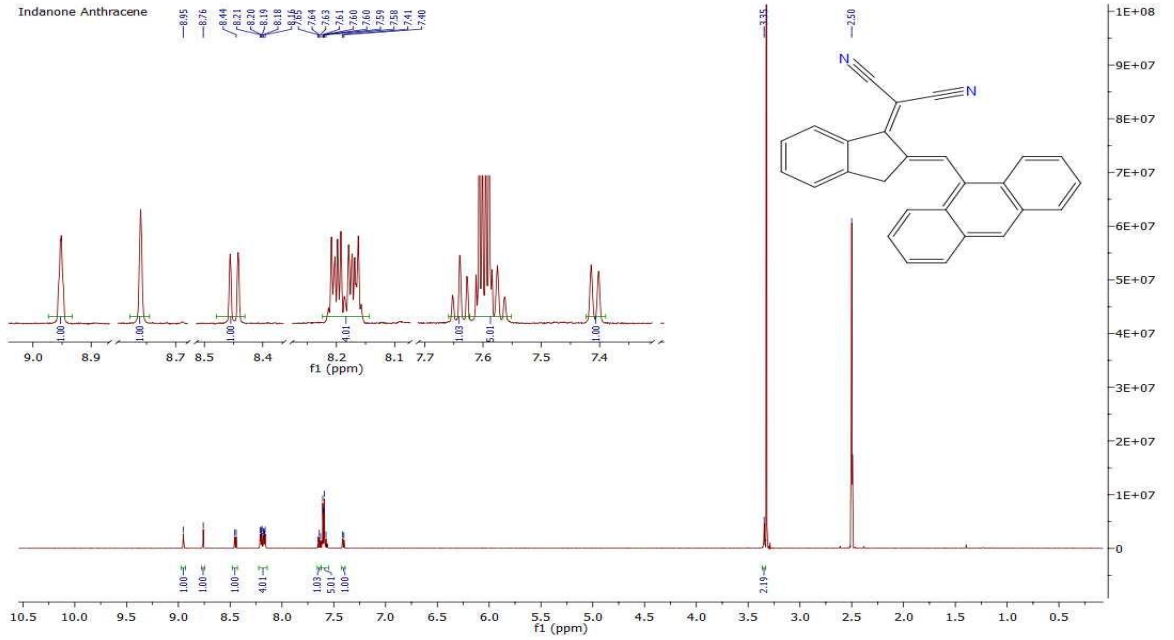

Figure 3.6. ^{1}H-NMR spectrum of Compound 7b in DMSO-d_6.

Annex-3. (Cont.) FT-IR, ^{1}H-NMR, ^{13}C-NMR, and HR-MS spectra of compounds 7a-c and 8a-c

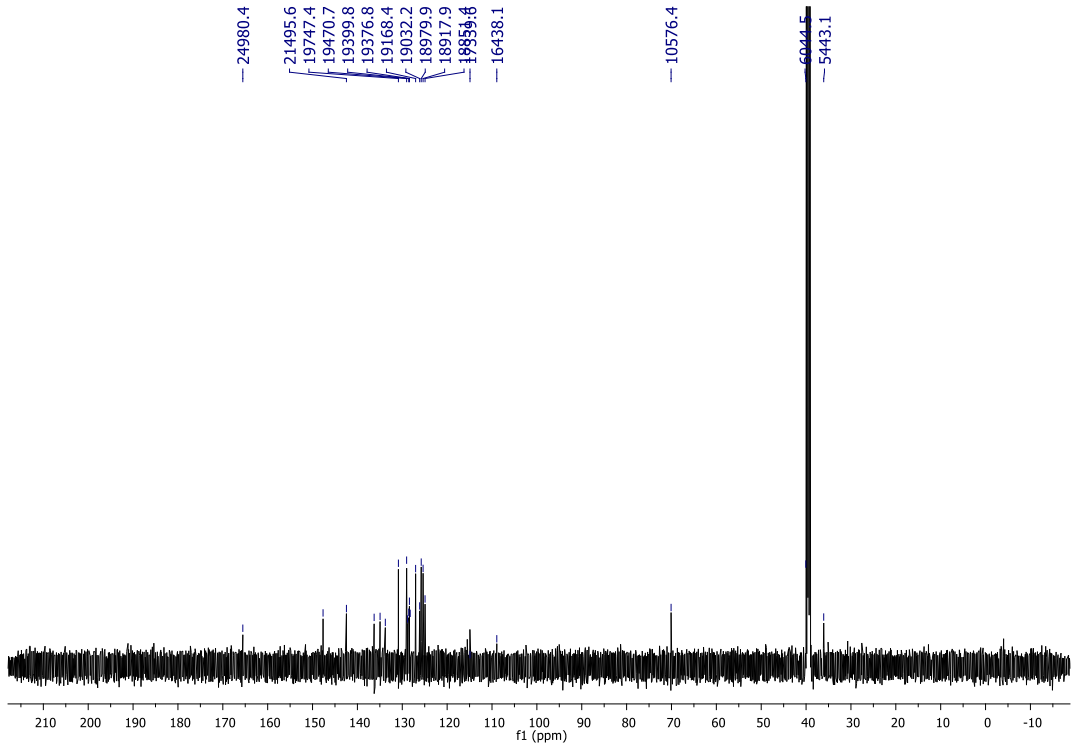

Figure 3.7.^{13}C-NMR spectrum of Compound 7b in DMSO-d_6.

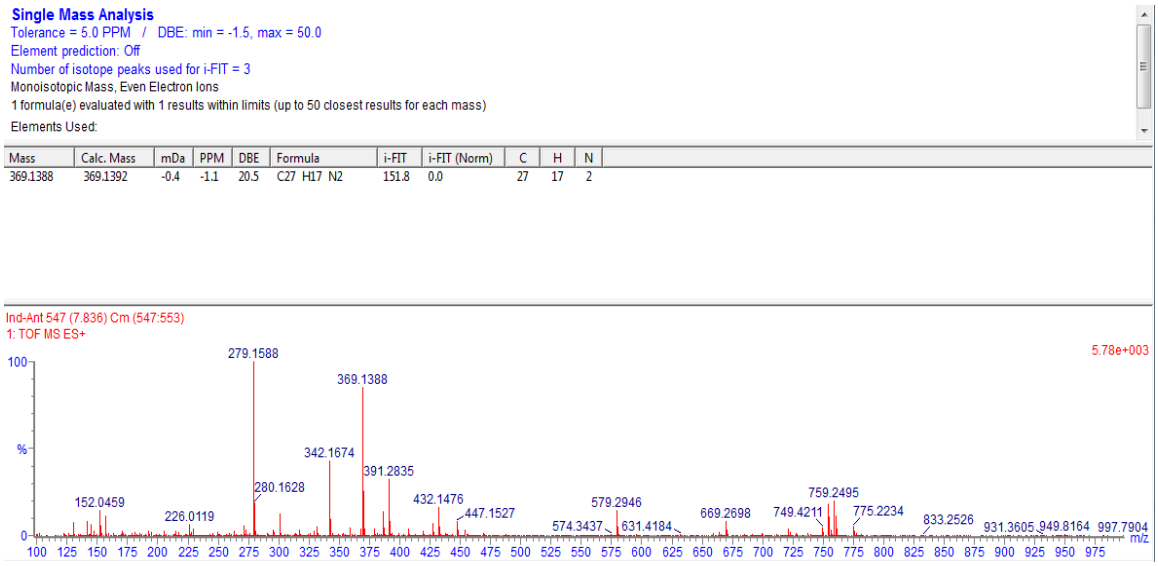

Figure 3.8. Mass spectrum of Compound 7b.

Annex-3. (Cont.) FT-IR, ^{1}H-NMR, ^{13}C-NMR, and HR-MS spectra of compounds 7a-c and 8a-c

The structure of {2-[(anthracen-9-yl)methylidene]-2,3-dihydro-1H-inden-1-ylidene}propanedinitrile (7b) was characterized by single-crystal X-ray diffraction analysis. The suitable crystal for X-ray analysis was obtained by slow crystallization from toluene solution. The plot shown in Figure 59 confirmed the proposed molecular structure, particularly the E stereoisomery of the exocyclic double bond. Compound 7b crystallized as red prisms and was solved in the monoclinic space group P21/n with four molecules in the unit cell. The structure has cyano and anthracenyl groups linked with the C=C double bonds (C17=C25, 1.360 Å, and C15=C16, 1.319 Å) to the indan core. The average C≡N bond length is 1.143 (3) Å, and the average C−C single bond length is 1.435 (4) Å in the malononitrile group. The anthracene and indan rings are almost planar. The dihedral angle between these planes is 77.2 degrees. Deviation from the planarity of the molecule is due to significant steric effects and intermolecular interactions. The crystal packing shows (Figure 59 Bottom) molecules are connected by slight C-H···N [D···A = 3.28-3.54 Å] interactions. The π-π stacking interactions between the delocalized π-electrons of the anthracenyl and indanyl groups are relatively weak. The distance between the ring centroids is in the range of 3.69–5.43 Å.

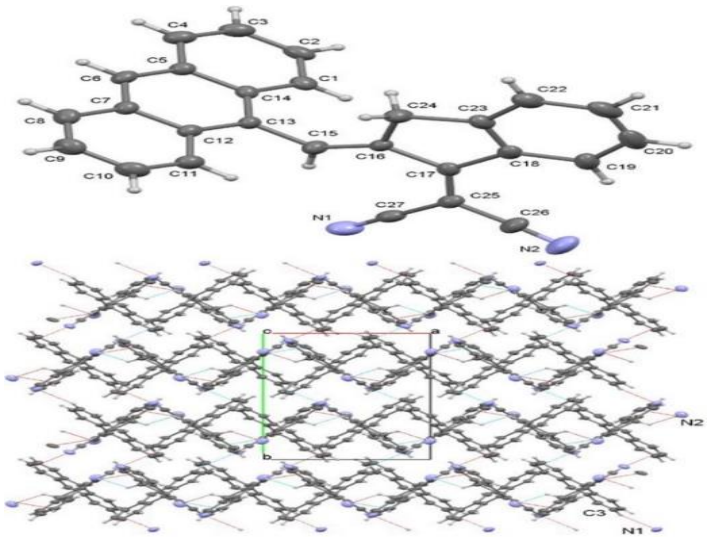

Figure 3.9. Molecular structure of 7b (asymmetric unit). Thermal ellipsoids are drawn at the 40% probability level. (Bottom) Stacking motif with the unit cell viewed down along the c-axis. Dashed lines indicate C-H···N interactions

Annex-3. (Cont.) FT-IR, ^{1}H-NMR, ^{13}C-NMR, and HR-MS spectra of compounds 7a-c and 8a-c

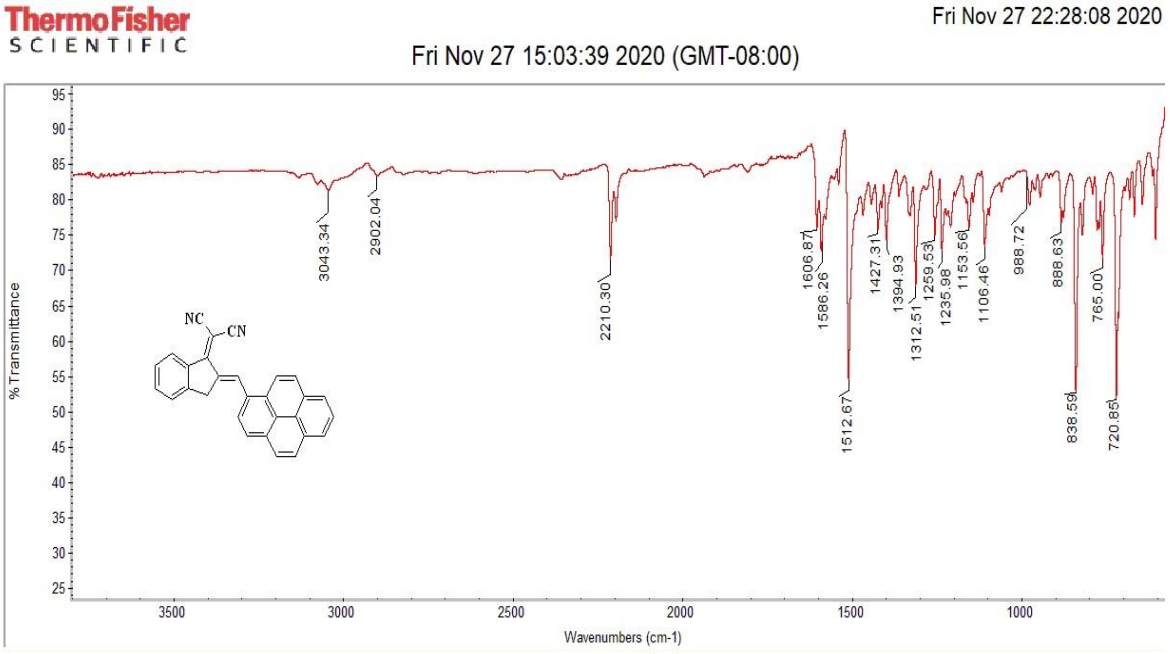

Figure 3.10. FT-IR spectrum of Compound 7c.

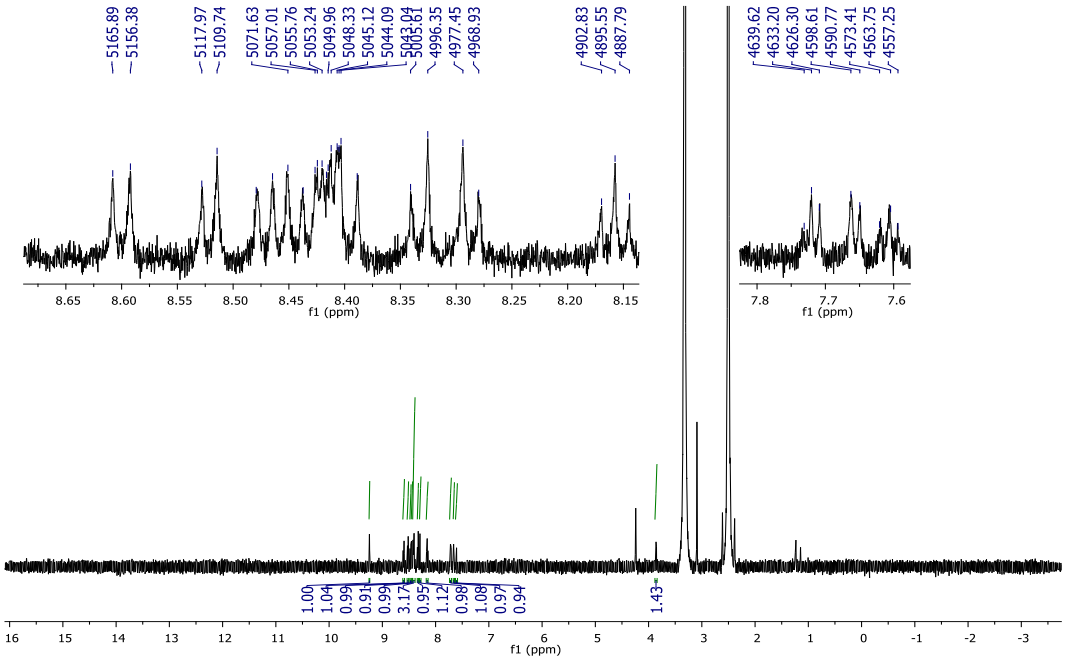

Figure 3.11.^{1}H-NMR spectrum of Compound 7c in DMSO-d_6.

Annex-3. (Cont.) FT-IR, ^{1}H-NMR, ^{13}C-NMR, and HR-MS spectra of compounds 7a-c and 8a-c

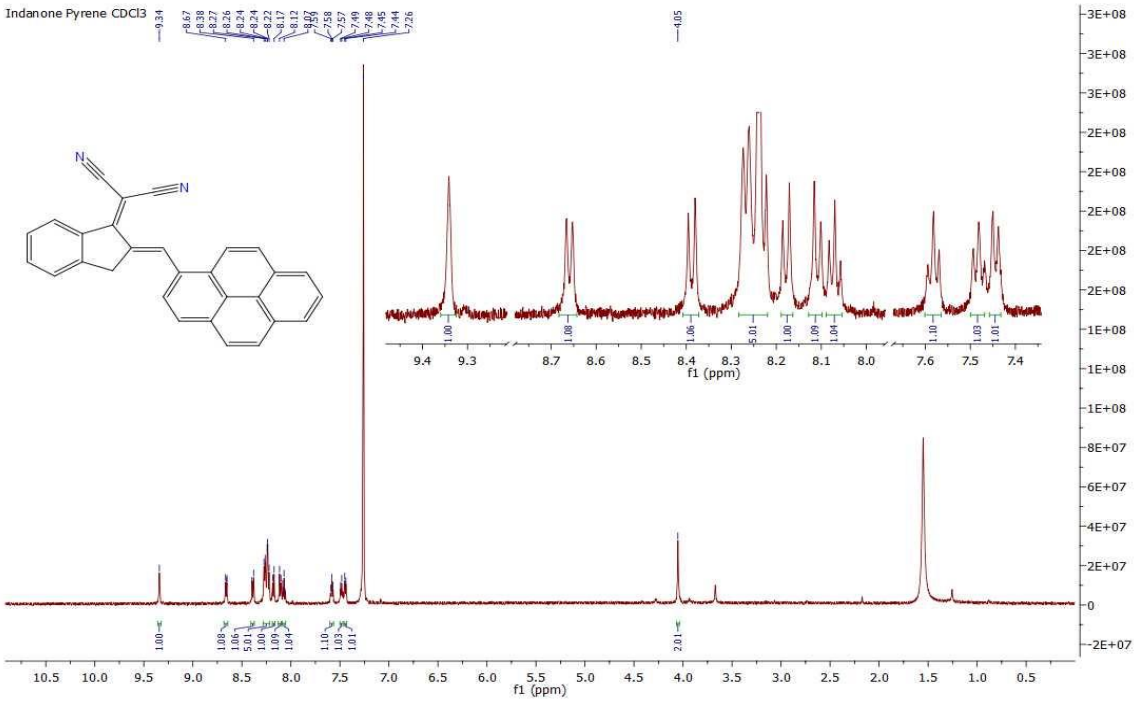

Figure 3.12.^{1}H-NMR spectrum of Compound 7c in $CDCl_3$.

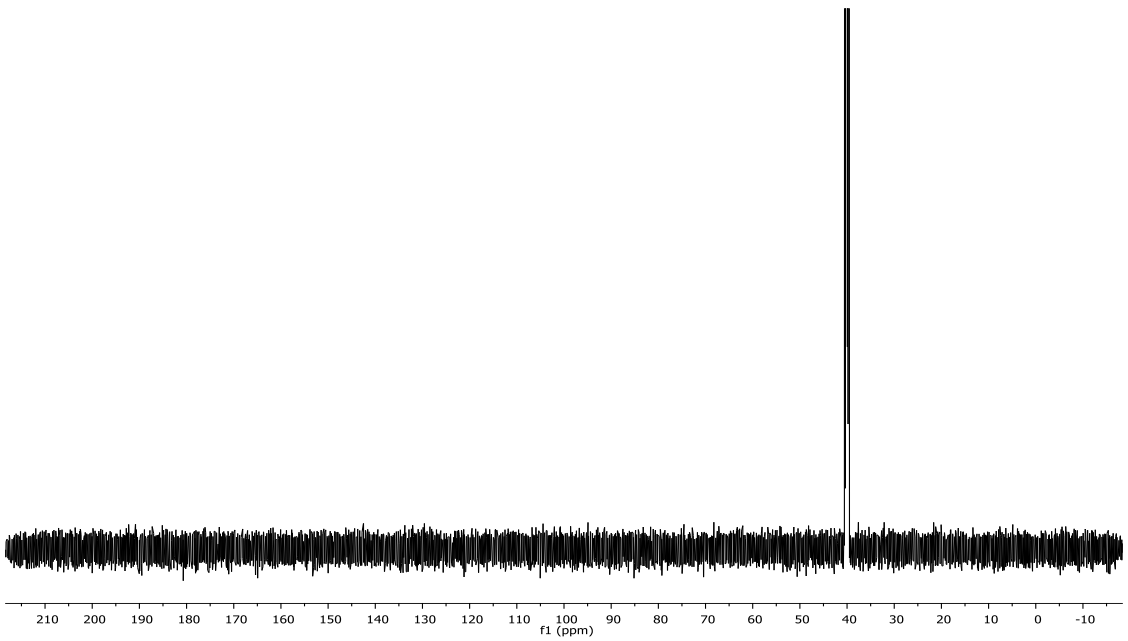

Figure 3.13.^{13}C-NMR spectrum of Compound 7c in DMSO-d_6.

Annex-3. (Cont.) FT-IR, ^{1}H-NMR, ^{13}C-NMR, and HR-MS spectra of compounds 7a-c and 8a-c

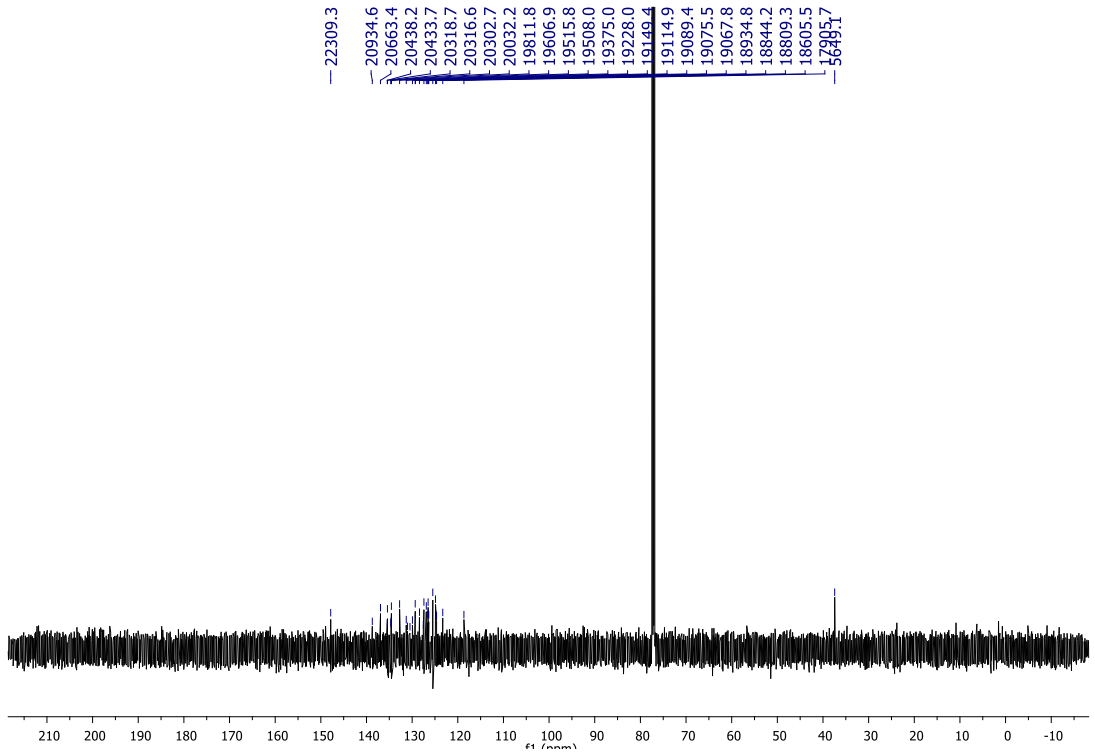

Figure 3.14. ^{13}C-NMR spectrum of Compound 7c in $CDCl_3$.

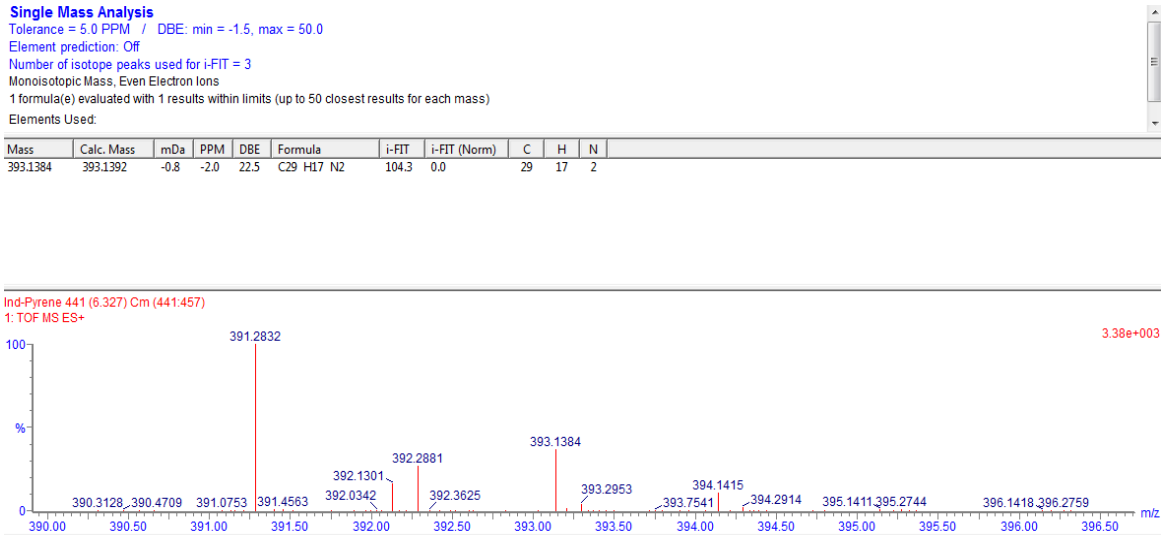

Figure 3.15. Mass spectrum of Compound 7c.

Annex-3. (Cont.) FT-IR, ^{1}H-NMR, ^{13}C-NMR, and HR-MS spectra of compounds 7a-c and 8a-c

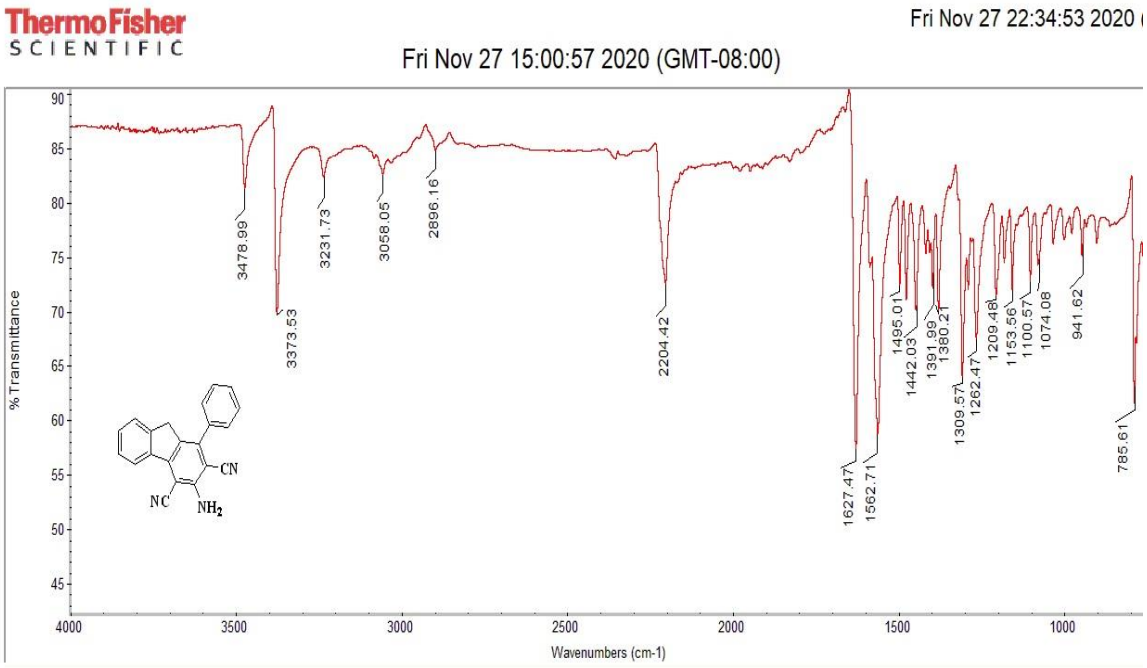

Figure 3.16. FT-IR spectrum of Compound 8a.

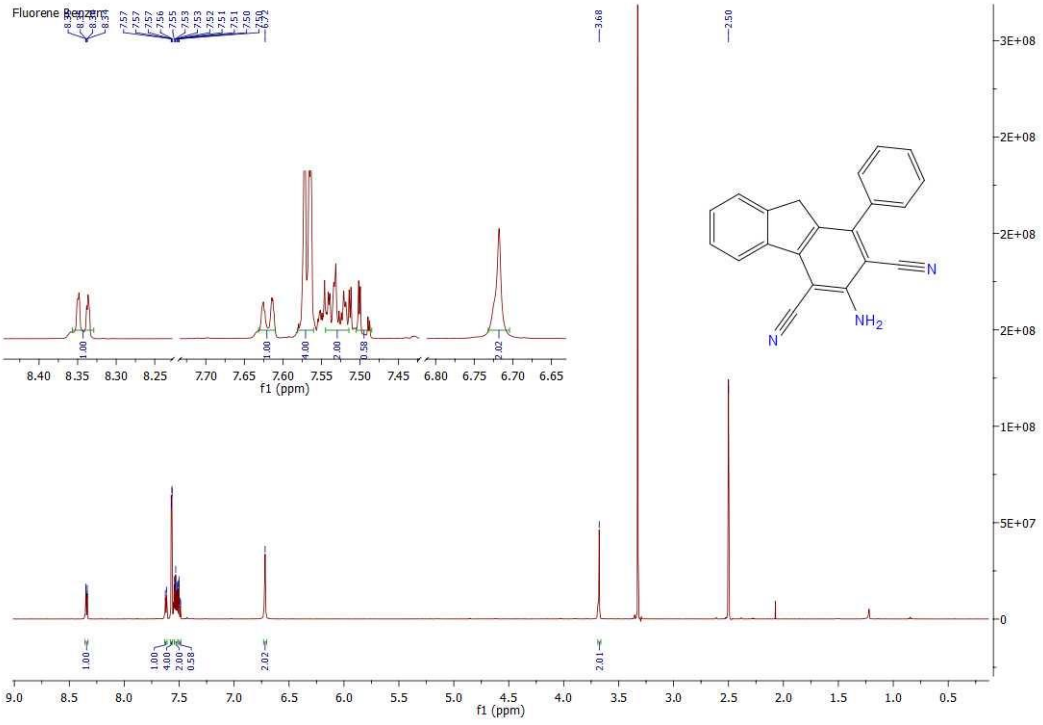

Figure 3.17.^{1}H-NMR spectrum of Compound 8a in DMSO-d_6.

Annex-3. (Cont.) FT-IR, ^{1}H-NMR, ^{13}C-NMR, and HR-MS spectra of compounds 7a-c and 8a-c

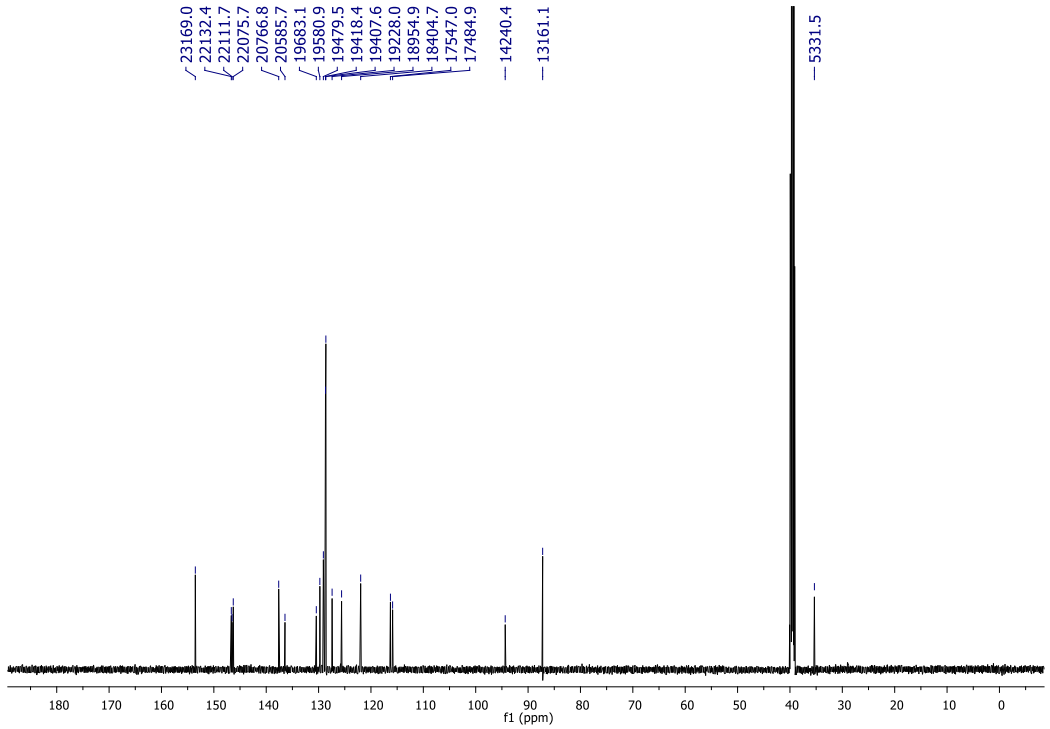

Figure 3.15.^{13}C-NMR spectrum of Compound 8a in DMSO-d_6.

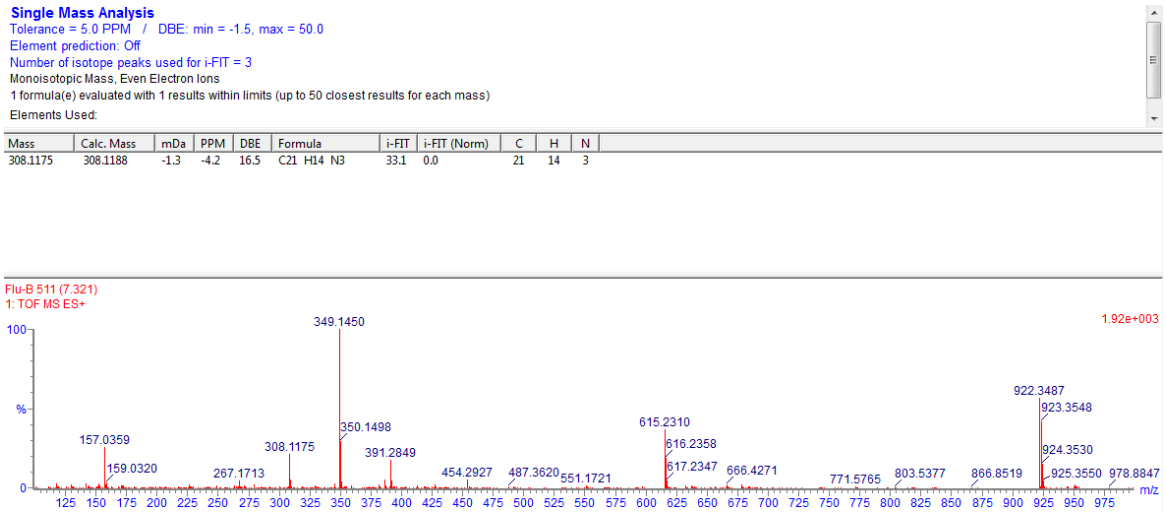

Figure 3.19. Mass spectrum of Compound 8a.

Annex-3. (Cont.) FT-IR, ^{1}H-NMR, ^{13}C-NMR, and HR-MS spectra of compounds 7a-c and 8a-c

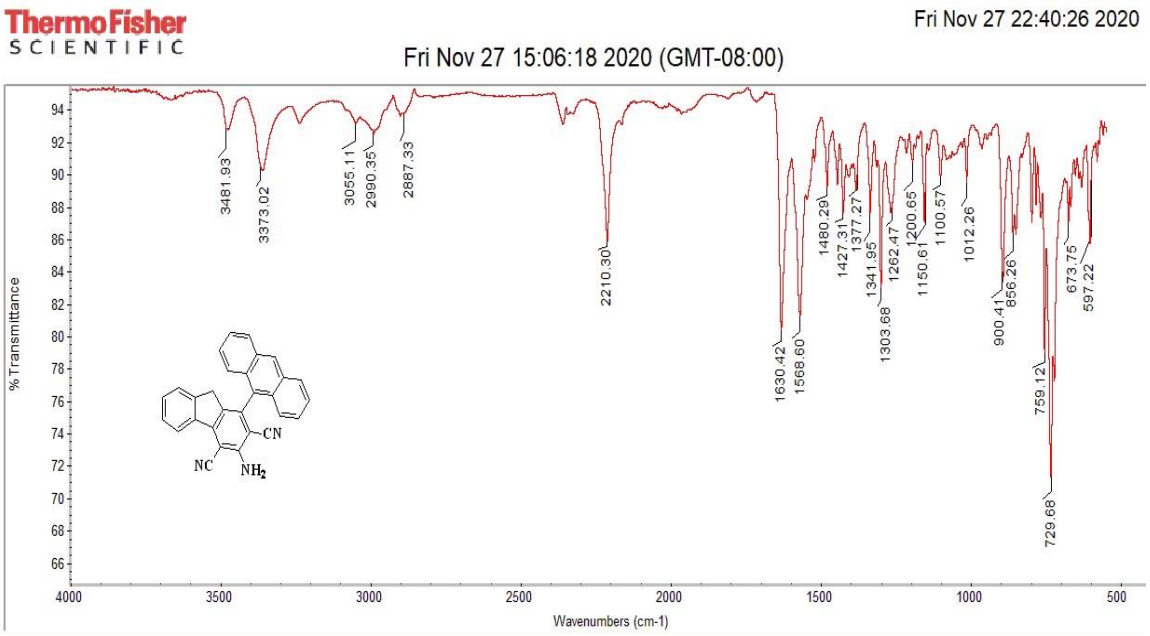

Figure 3.2016. FT-IR spectrum of Compound 8b.

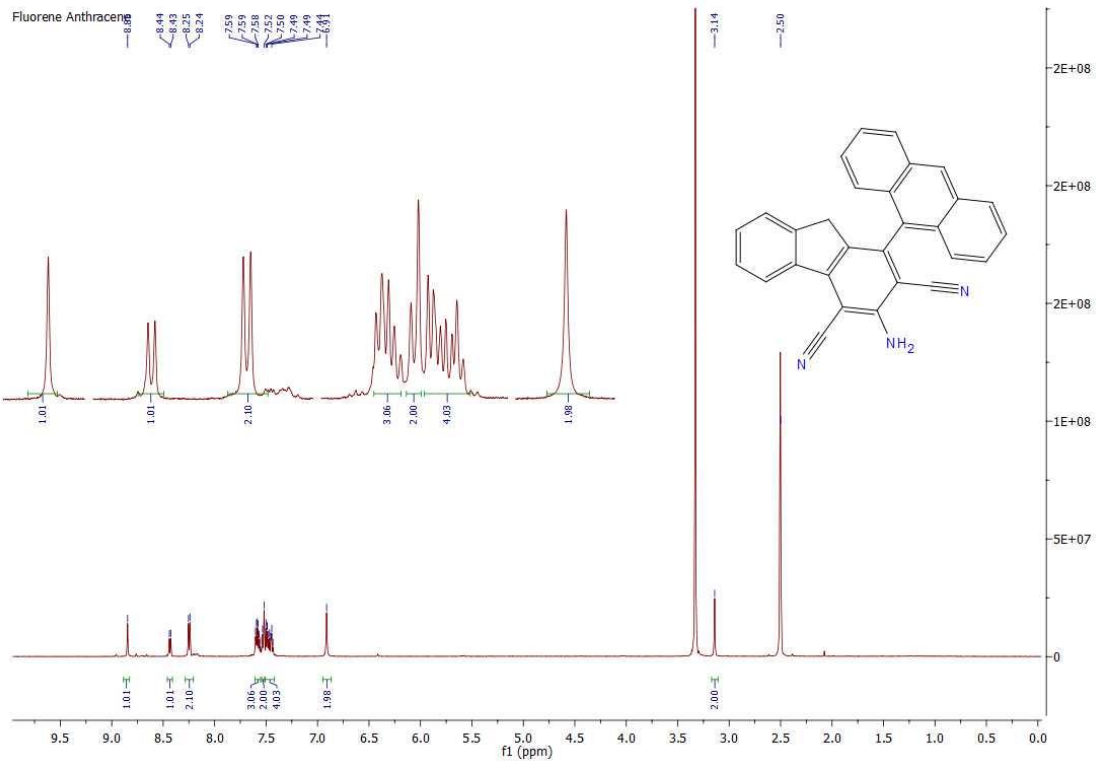

Figure 3.21.^{1}H-NMR spectrum of Compound 8b in DMSO-d_6.

Annex-3. (Cont.) FT-IR, ^{1}H-NMR, ^{13}C-NMR, and HR-MS spectra of compounds 7a-c and 8a-c

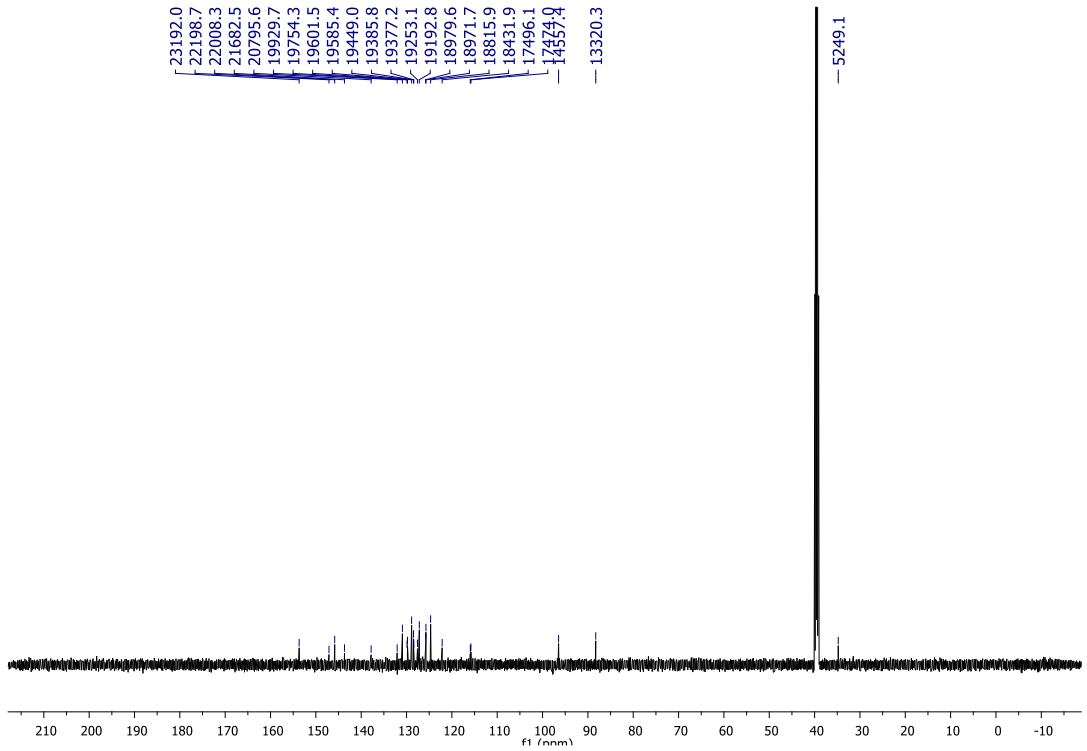

Figure 3.22. ^{13}C-NMR spectrum of Compound 8b in DMSO-d_6.

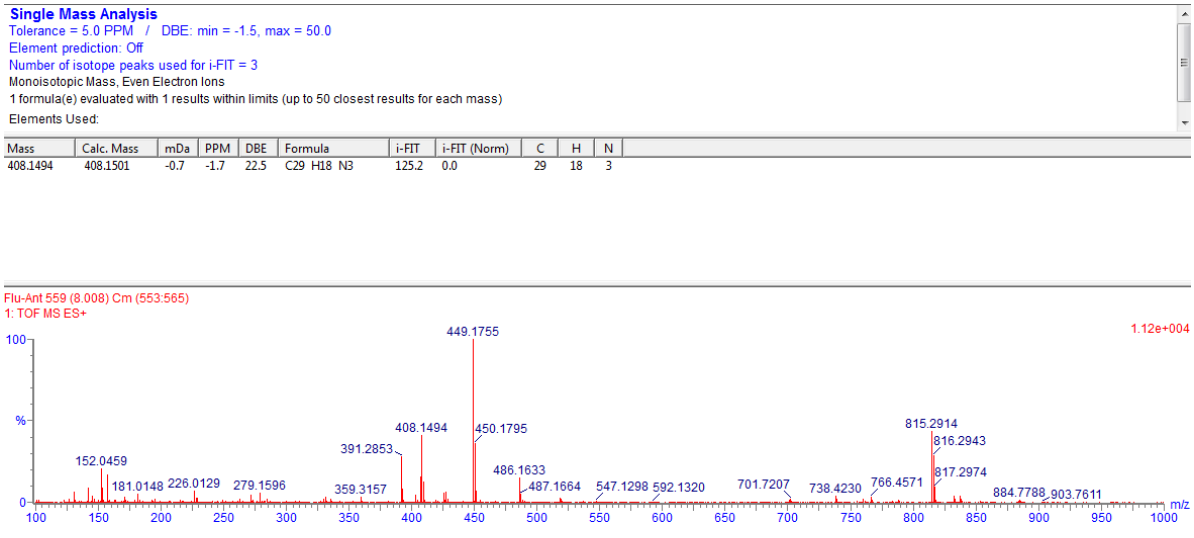

Figure 3.23. Mass spectrum of Compound 8b.

Annex-3. (Cont.) FT-IR, ^{1}H-NMR, ^{13}C-NMR, and HR-MS spectra of compounds 7a-c and 8a-c

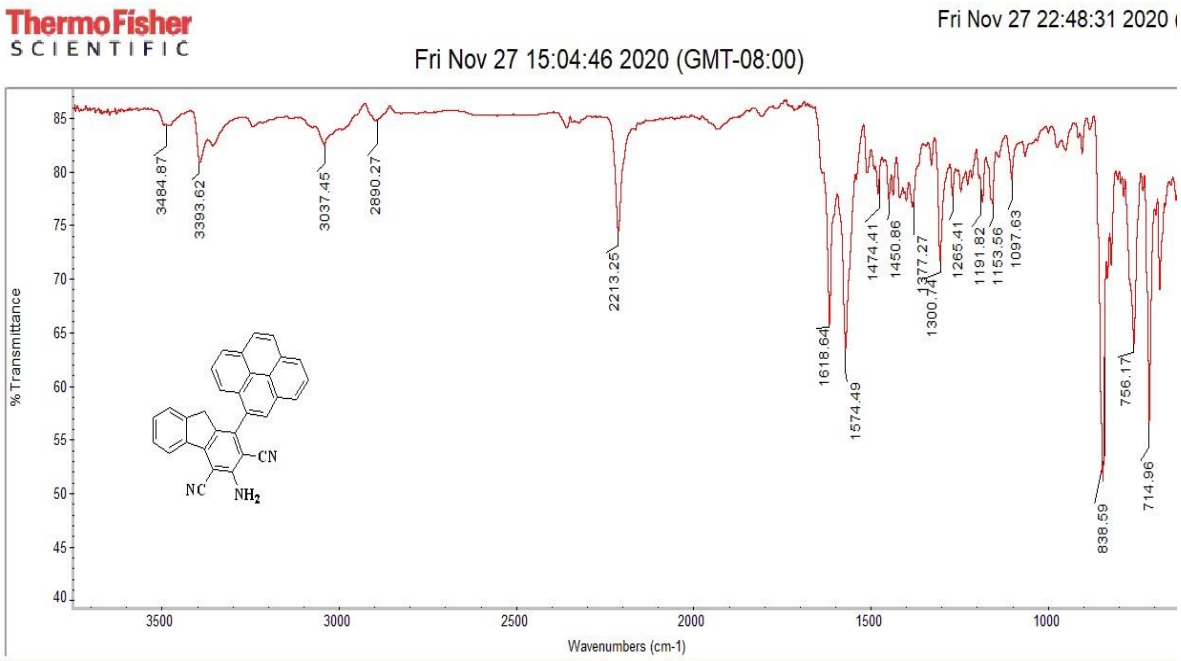

Figure 3. 24. FT-IR spectrum of Compound 8c.

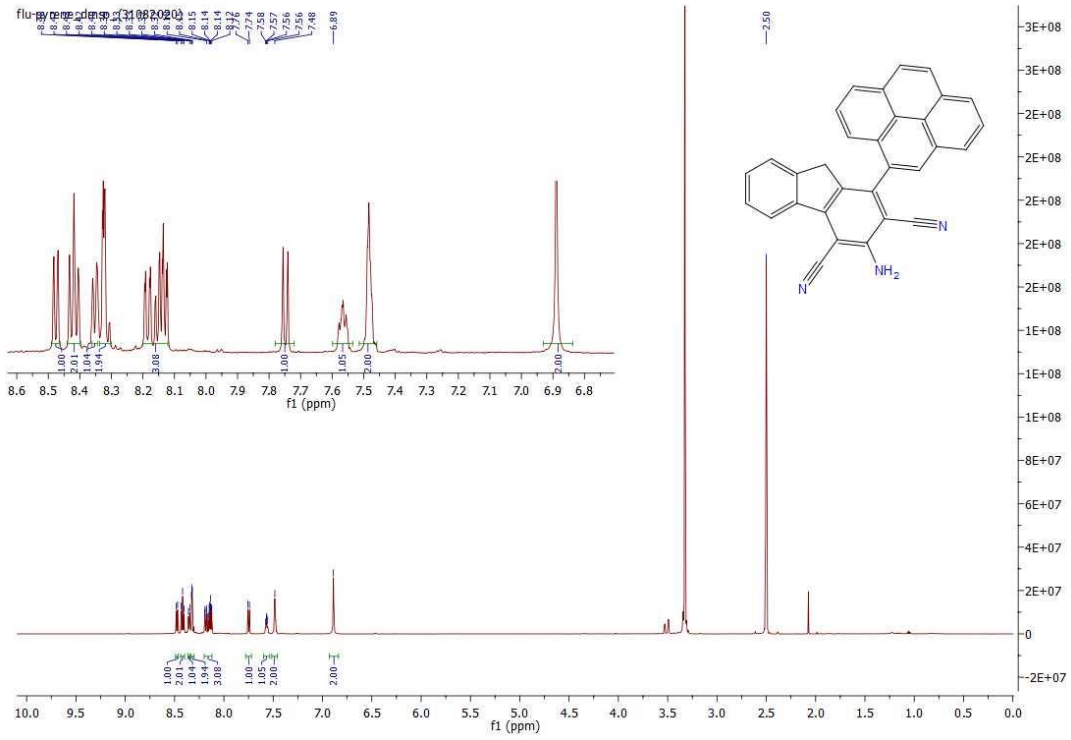

Figure 3.25. ^{1}H-NMR spectrum of Compound 8c in DMSO-d_6.

Annex-3. (Cont.) FT-IR, ^{1}H-NMR, ^{13}C-NMR, and HR-MS spectra of compounds 7a-c and 8a-c

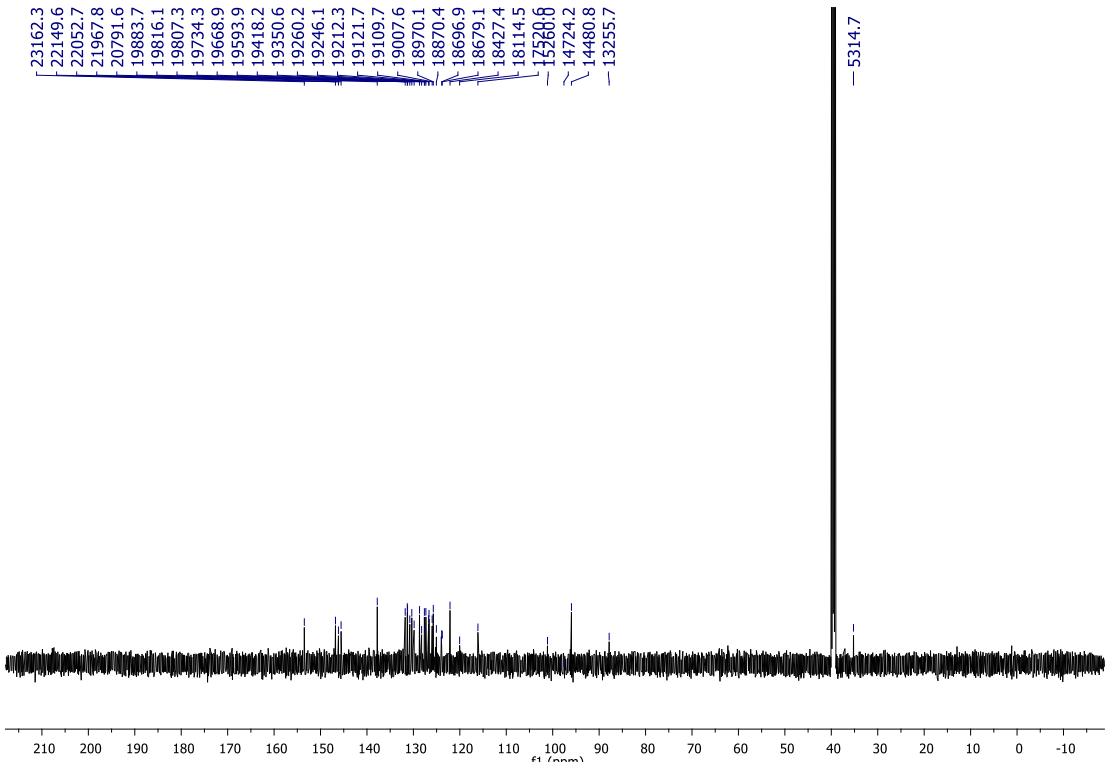

Figure 3. 26.^{13}C-NMR spectrum of Compound 8c in DMSO-d_6.

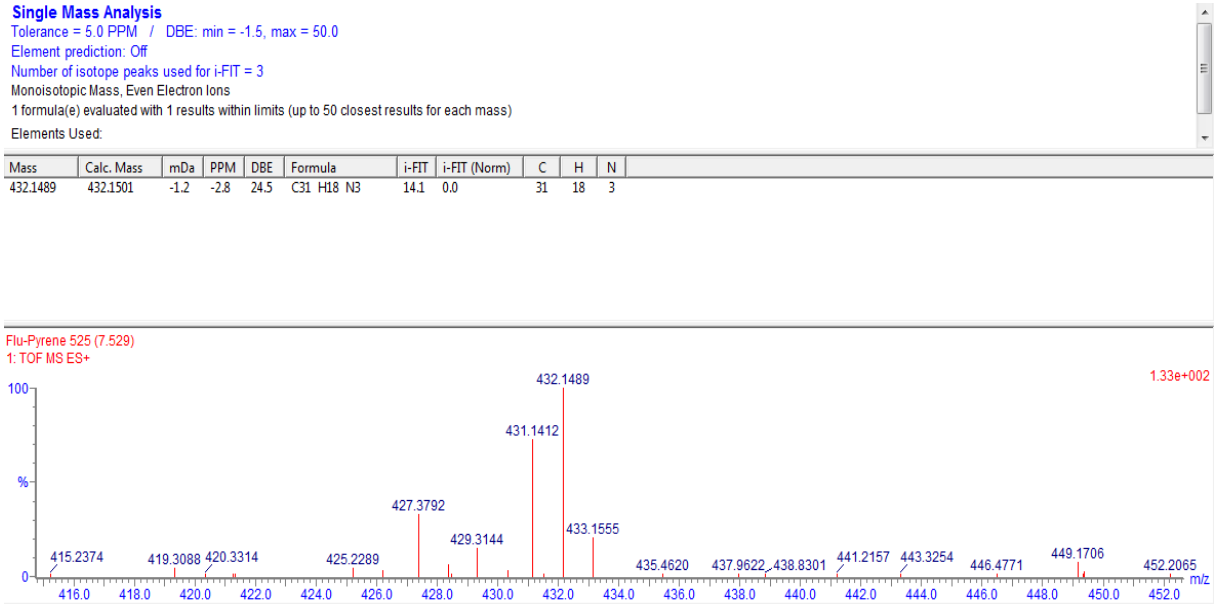

Figure 3.27. Mass spectrum of Compound 8c.

Annex-4. Calibration curve of [CN^-] for 6a-f

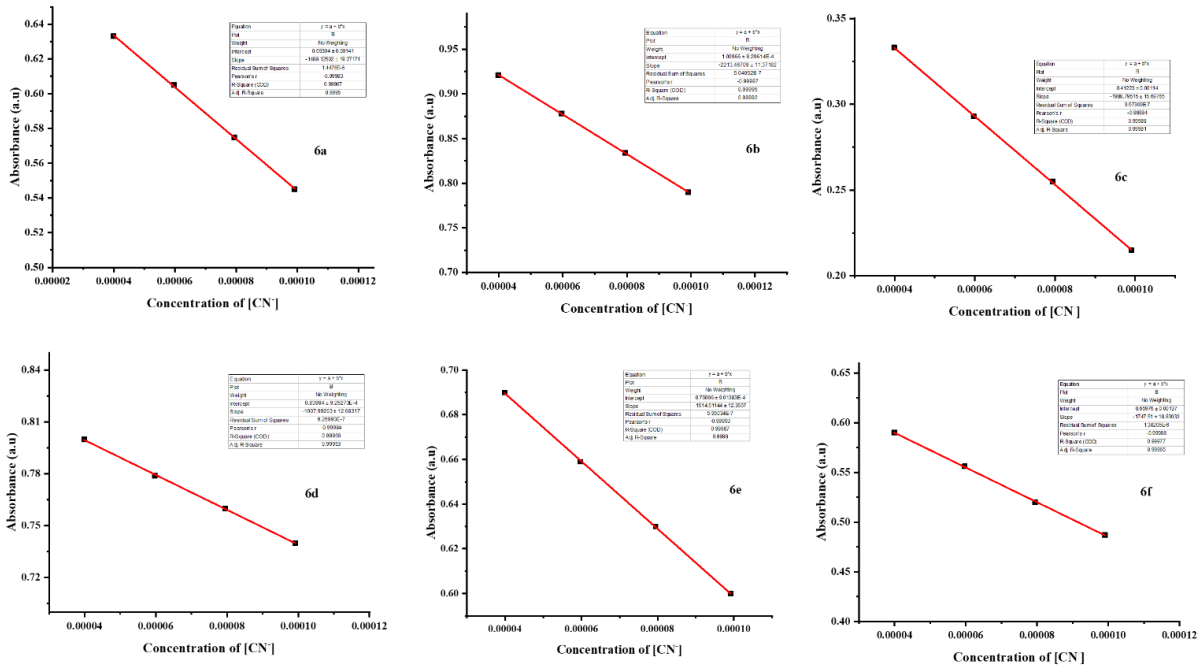

Figure 4.1. The absorbance calibration curve of [CN^-] for 6a-f in DMSO

GAZİ GELECEKTİR..